



Norwegian University of
Science and Technology

Field and Laboratory Investigations to Evaluate the Coefficient of Earth Pressure at Rest

NGTS Flotten Quick Clay Test Site

Anders Lindgård
Christian Strømme Ofstad

Civil and Environmental Engineering

Submission date: June 2017

Supervisor: Steinar Nordal, IBM

Co-supervisor: Jean-Sébastien L'Heureux, NGI
Arnfinn Emdal, IBM

Norwegian University of Science and Technology
Department of Civil and Environmental Engineering



Report Title: Field and laboratory investigations to evaluate the coefficient of earth pressure at rest. NGTS Flotten quick clay test site.	Date: 09.06.2017			
	Number of pages (incl. appendices): 274			
	Master's thesis	X	Project thesis	
Name: Anders Lindgård and Christian Strømme Ofstad				
Professor in charge/supervisor: Steinar Nordal (NTNU)				
Other external professional contacts/supervisors: Arnfinn Emdal (NTNU), Jean-Sébastien L'Heureux (NGI)				

Abstract:

The coefficient of earth pressure at rest is a key geotechnical parameter, required in almost any investigation of material behaviour. A review of literature on the in situ and laboratory determination of K_0' has been carried out. It shows that a generally accepted method for the estimation of K_0' is yet to come. In addition, it demonstrates the effect of stress history and time effects on the evolution of K_0' .

Extensive testing with Glötzl earth pressure cells between 5 and 10 m depth at the "Norwegian Geo-Test Sites" (NGTS) Flotten quick clay test site outside Trondheim has been carried out. It suggests that installation and evaluation of results is challenging. A dilatometer test and an oedotriaxial test have also been performed. The field vane and work criterion in oedometer approaches have been tested. Scattered data material makes a unique determination of K_0' challenging, from both in situ, laboratory and correlation methods.

Additionally, a general site classification through in situ, index, oedometer and triaxial testing is presented. The testing indicates a plastic clay layer above a layer of quick clay from around 7 - 8 m depth. The clay appears to be overconsolidated, decreasing with depth. Various time effects and Quaternary geological history may explain this.

Keywords:

1. Earth pressure at rest
2. Earth pressure cell
3. In situ testing
4. Laboratory testing

Anders Lindgård

Christian Ofstad

(sign.)

MSc Thesis**TBA4900 – Geotechnical Engineering**

Spring 2017

Anders Lindgård and Christian Strømme Ofstad

Field and laboratory investigations to evaluate the coefficient of earth pressure at rest. NGTS Flotten quick clay test site.**BACKGROUND**

In geotechnical engineering it is essential to know the in situ stress state for planning laboratory tests as well as for performing geotechnical calculations and design. The ratio between the effective in situ horizontal and the effective vertical stress is referred to as K_0' . The vertical stress state is given by the overburden pressure, while the horizontal stress may be hard to determine. The topic for this master's thesis is determination of K_0' . The topic was originally proposed by Jean-Sébastien L'Heureux at NGI as part of the research project "Norwegian Geo-Test Sites", NGTS.

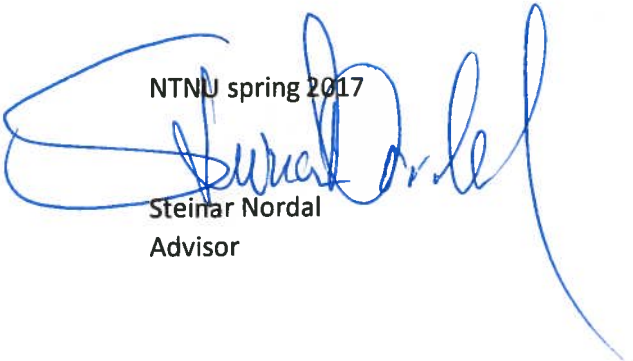
PROBLEM FORMULATION

The thesis should include a literature study on the determination of K_0' by in situ, laboratory and correlation methods. The effects of previous geologic processes at a site should be addressed. Considerations on grain or micro- scale level and effects of time may also be included.

The main focus should be on in situ measurements providing K_0' at the "Norwegian Geo-Test Site" Flotten close to Tiller outside Trondheim. At Flotten there is clay that is quick from about 7 m depth. This MSc thesis will require participation in practical field work. It is planned to install earth pressure cells (Glötzl push in cells) to measure horizontal total stress and pore pressure. Plans for this is to be made. It is further planned to do a dilatometer test. Since there is limited experience available from previous field testing of this kind on sensitive soils it is important to focus on installation procedures and critically evaluate test results, discuss them and consider possible sources of errors.

In addition to field testing it is suggested to do laboratory work to characterise the material and determine the overconsolidation level. Both oedometer and triaxial testing is of interest. Oedotriaxial testing may be performed to determine the lateral stress ratio. The work on characterising the material shall be coordinated and shared with MSc student Konjit Paulos Gella, who in parallel is working on material from the same site.

NTNU spring 2017


Steinar Nordal
AdvisorArnfinn Emdal
Co-advisor

Preface

This master's thesis in geotechnical engineering is written as part of the MSc in Civil and Environmental Engineering at the Norwegian University of Science and Technology during the spring of 2017.

The original idea for this master's thesis was proposed by co-supervisor Dr. Jean-Sébastien L'Heureux at NGI. This report represents a careful selection of ideas suggested by the authors, supervisor Professor Steinar Nordal and co-supervisors Assistant Professor Arnfinn Emdal and Dr. Jean-Sébastien L'Heureux.

Please note that a zip-file was delivered along with this thesis in DAIM, containing raw data and also some processed data for the performed field and laboratory tests.

Trondheim, 2017-06-09



Anders Lindgård



Christian Strømme Ofstad

Acknowledgment

We would like to thank supervisor Professor Steinar Nordal and co-supervisors Assistant Professor Arnfinn Emdal at NTNU as well as Dr. Jean-Sébastien L'Heureux at NGI for valuable discussions and ideas during the work with this thesis.

Next, we would like to thank NTNU engineers Espen Andersen and Karl Ivar Volden Kvisvik for their skilled help with equipment installation at Flotten. Their great efforts and good spirit have been crucial for this master's thesis.

Parallel to our master thesis, fellow MSc student Konjit Paulos Gella conducted a general site classification of the test site at Flotten, running index, oedometer and triaxial testing on samples from depths between 2 and 12 m. We would like to express our sincere gratitude for the ability to use these results to gain a better understanding of the soil conditions at Flotten.

We would also like to thank fellow MSc student Kathrine Buene Gangenes for many valuable and educational discussions throughout the work with this thesis. Your time and patience is hugely appreciated.

Finally, we would like to thank Zeynep Ozkul at NGI for processing of the dilatometer data and Samson Degago at the Norwegian Public Roads Administration for help in acquiring previously developed field equipment.

AL & CSO

Summary and Conclusions

Any laboratory test or computational modelling procedure in geotechnical engineering relies on accurate determination of soil parameters and the in situ stress state. The vertical effective stress state is well defined by the overburden pressure, while determination of the horizontal effective stress has proved more challenging. Despite several investigations, the factors influencing the evolution of the coefficient of earth pressure at rest, K'_0 remain unresolved. In addition, in situ and laboratory measurements tend to alter the stress situation, and thus the measured horizontal stress is not the true in situ stress. This thesis has looked into field and laboratory methods to determine the coefficient at earth pressure at rest, as well as the geological evolution of K'_0 .

One of the key findings in the literature on the geological evolution of K'_0 is that the stress history of the deposit is crucial. Also, time effects can explain the change in apparent preconsolidation and K'_0 with time.

The repeatability, reliability and ease of use varies a lot between the many different approaches to determine K'_0 in situ. Some methods have a great need for empirical factors to relate in situ data to K'_0 . These factors may have limited value between different sites and soil properties. In much literature, the three direct measurement methods of earth pressure cells, hydraulic fracturing and self-boring pressuremeter stand out as reference methods.

Some laboratory methods, like the split-ring oedometer and the oedotriaxial procedure seem to give reliable results.

Jaky's equation $K'_{0nc} = 1 - \sin \phi'$ is repeatedly validated by both laboratory and in situ studies. There is more uncertainty and spread in the calculations of K'_{0oc} , and the complexity of the correlation methods for overconsolidated soils is varying. The results presented support that the spread in calculations of K'_{0nc} is small compared to K'_{0oc} . Also, the dependency on correct OCR input is discussed.

A general site classification is presented, based on soundings, index testing and Quaternary geology information. At Flotten there is a 2 m dry crust overlaying a quite homogeneous plastic clay layer extending to 7 m depth. A transition zone lies between the plastic clay and the quick clay starting at 8 m depth. Below approximately 20 m depth coarser materials act as draining layers. This is the cause of the under-hydrostatic pore pressure with depth.

Earth pressure cells have been installed to the desired final depth 11 times, to measure horizontal total stress and pore pressure. The resulting K'_0 values are presented along with other utilized methods. Installations at 5 m gave a huge scatter in the calculated values of K'_0 . Consequently, several different installation procedures have been tested and evaluated. Some have proven more successful than others. In general, the results are

scattered. The influence of the installation procedure on the in situ stress conditions is thoroughly discussed. The possibility to produce a protective cover has been evaluated.

The dilatometer test performed at Flotten gives quite reasonable, albeit slightly high estimates of K'_0 compared to both earth pressure cells and correlation methods. This is to be expected based on similar findings in the literature, and this is further discussed. However, when used in highly sensitive clays, the validity of the dilatometer parameters and the amount of disturbance remain open questions.

The field vane approach combining field vane results with a triaxial compression test gave low estimates of K'_0 compared to the other methods at 8.4 and 9.4 m depth. The most reasonable field vane value of K'_0 is at 10.4 m depth, where consolidation of the corresponding triaxial test was closest to the in situ conditions. The limited amount of data suggest that the chosen parameters for the triaxial test is determining for the calculated K'_0 , but it is not possible to conclude on this matter based on the limited data available and the amount of sample disturbance. Also, the input undrained shear strengths found from the field vane are probably too low compared to in situ. The theoretical foundation of the field vane approach has some weaknesses, which have been addressed.

A total of 17 oedometer tests performed on Flotten clay have given quite scattered results, probably linked to disturbance of the 54 mm samples. The general trend in the interpreted preconsolidation profile is a quite overconsolidated deposit at shallow depth, with a decreasing overconsolidation with depth. As the geological history of the site is not able to explain the observed overconsolidation, the possible influence of various time effects is discussed.

The theoretical background for determining in situ stresses from the work criterion has some weaknesses. An unambiguous determination appears to be difficult in practice. Also, the determination of p'_c using the work criterion seems to be of limited value.

Based on a total of 19 triaxial tests performed both by the authors of this thesis and Konjit Paulos Gella, estimates of key strength parameters for the Flotten clay have been determined. The triaxial testing supports the idea of a transition from plastic to quick clay at a depth of about 7 to 8 m.

The manual oedotriaxial test compares rather well to estimates based on both in situ and correlation methods to determine K'_0 . However, to ensure a drained test the utilized procedure requires the test to run for a substantial amount of time.

Sammendrag og konklusjoner

Enhver laboratorietest eller datamodelleringsprosedyre innenfor geoteknikk avhenger av at jordparametre og in situ spenningssituasjon er bestemt så nøyaktig som mulig. Den vertikale spenningssituasjonen er tydelig definert ut fra overlagingen, mens bestemmelse av den effektive horisontalspenningen har vist seg å være mer utfordrende. Til tross for en rekke undersøkelser mangler fortsatt et helhetlig bilde av hvilke faktorer som påvirker hviletrykkskoeffisienten, K'_0 . I tillegg vil både in situ og laboratorieundersøkelser endre spenningssituasjonen, slik at de målte horisontalspenningene ikke er like de faktiske in situ spenningene. Denne oppgaven har tatt for seg felt- og laboratoriemetoder for å undersøke hviletrykkskoeffisienten, i tillegg til den geologiske utviklingen av K'_0 .

Et av de viktigste funnene i litteraturen om den geologiske utviklingen av K'_0 har vært at spenningshistorien spiller en avgjørende rolle. I tillegg kan ulike tidseffekter være med på å forklare endringer i tilsynelatende prekonsolidering og K'_0 over tid.

Repeterbarheten, påliteligheten og brukervennligheten varierer mye mellom de ulike metodene for å bestemme K'_0 in situ. Noen metoder er avhengig av empiriske sammenhenger for å knytte sammen målinger in situ og K'_0 . Slike sammenhenger har typisk begrenset verdi mellom ulike områder med ulike materialegenskaper. Direkte målemetoder som jordtrykksceller, hydraulisk frakturering og selvborende jordtrykksmåler trekkes ofte frem som referansemetoder i mye av litteraturen.

Noen laboratoriemetoder, som for eksempel splittet ring ødometer og ødotreaksprosedyren, ser også ut til å gi pålitelige resultater.

Jakys likning $K'_{0nc} = 1 - \sin \phi'$ har gjentatte ganger blitt bekreftet gjennom både laboratorie- og in situ målinger. Det er mer usikkerhet og variasjon knyttet til beregninger av K'_{0oc} . Ulike korrelasjonsmetoder av varierende kompleksitet har blitt foreslått for overkonsolidert leire. De presenterte resultatene bekrefter at det er mindre spredning i beregningen av K'_{0nc} sammenliknet med K'_{0oc} . I tillegg har sammenhengen med OCR blitt diskutert.

Basert på sonderinger, indekstester og kvartærgeologi har det blitt gitt en generell beskrivelse av testområdet på Flotten. Under en omtrent 2 m tykk tørrskorpe finnes et plastisk leirlag ned til rundt 7 m dybde. Rundt 8 m går materialet over til kvikkleire, før grovere materialer fungerer som drenerende lag fra omkring 20 m dybde. Dette er med på å forklare den underhydrostatisk poretrykksfordelingen.

Jordtrykksceller har blitt installert til ønsket dybde totalt 11 ganger, for å måle horisontale totalspenninger og poretrykk. De resulterende verdiene av K'_0 presenteres sammen med en rekke andre anvendte metoder for å estimere K'_0 . Det er stor spredning i målingene tatt på 5 m dybde. En rekke andre installasjonsmetoder har også blitt testet og evaluert, noen mer vellykket enn andre. Spredningen i målingene er generelt stor og kon-

sekvenser av ulike installasjonsprosedyrer har derfor blitt diskutert grundig. Muligheten for å konstruere et beskyttende futteral til ei jordtrykkscelle har blitt vurdert.

Målinger med et dilatometer på Flotten har gitt fornuftige, men noe høye verdier av K'_0 sammenliknet med både jordtrykkscellene og ulike korrelasjonsmetoder. Dette er i samsvar med liknende funn i litteraturen. Det hersker noe usikkerhet rundt både mengden forstyrrelse ved bruk av dilatometeret samt ved gyldigheten til korrelasjonene i kvikke leirer. Dette har blitt diskutert nærmere.

Estimater av K'_0 basert på å kombinere vingeormmålinger med treaksiale kompresjonsforsøk har generelt gitt lave verdier for 8,4 og 9,4 m dybde. Den mest fornuftige verdien av K'_0 fra vingebor ble funnet for målinger på 10,4 m dybde, der konsolideringen av den sammenhørende treaksialprøven er antatt å være nærmest den korrekte in situ spenningssituasjonen. Testene indikerer at hvilke parametre som velges for treaksialforsøk er avgjørende for den endelig verdien av K'_0 . Det kan imidlertid ikke konkluderes entydig grunnet begrenset informasjonsmengde og prøveforstyrrelse. I tillegg er trolig skjæstyrken bestemt fra vingeborforsøkene for lave. Enkelte teoretiske svakheter ved metoden har blitt diskutert nærmere.

Totalt har det blitt gjennomført 17 ødometerforsøk på leirprøver fra Flotten. Resultatene har stor spredning, noe som trolig skyldes bruken av forstyrrede 54 mm prøver. Generelt fremstår jordavsetningen som ganske overkonsolidert i grunne dybder. Overkonsolideringen avtar med dybden. Fordi den geologiske historien til området ikke forklarer disse funnene, har påvirkningen fra ulike tidseffekter blitt diskutert.

Den teoretiske bakgrunnen for å bruke et arbeidskriterium for å bestemme in situ spenninger har flere svakheter. En entydig bestemmelse synes å være vanskelig i praksis. En tolkning av prekonsolideringsspenningen fra samme metode virker også å ha begrenset verdi.

Totalt 19 treaksforsøk gjennomført av både forfatterne og Konjit Paulos Gella har blitt lagt til grunn for å bestemme styrkeparametre for leire på Flotten. Disse forsøkene støtter overgangen fra plastisk leire til kvikkleire rundt 7 til 8 m.

En manuell ødotreakstest har gitt resultater som samsvarer ganske godt med både in situ og korrelasjonsmetoder for å bestemme K'_0 . Det krever at testen kjøres over et lengre tidsrom for å oppnå en drenert test.

Contents

Preface	i
Acknowledgment	iii
Summary and Conclusions	v
Sammendrag og Konklusjoner	vii
List of Figures	xv
List of Tables	xix
List of Symbols and Abbreviations	xxvi
1 Introduction	1
1.1 Background	1
1.1.1 Problem Formulation	1
1.1.2 Literature Survey	2
1.1.3 What Remains to be Done?	3
1.2 Objectives	3
1.3 Limitations	4
1.4 Approach	4
1.5 Structure of the Report	5
2 Background	7
2.1 Definition of K'_0	7
2.2 Geological Processes Governing the Evolution of K'_0	8
2.2.1 Effect of Stress History	8
2.2.2 Time Effects	9
2.2.3 Chemical Changes	10
2.2.4 Drying	12
2.2.5 Secondary Compression	12
2.2.6 Force Chains	15
2.2.7 Quaternary Geology	18

2.3	Introduction to Methods for Determining K'_0	19
2.4	In Situ Methods	20
2.4.1	Earth Pressure Cell	20
2.4.2	Seismic and Ordinary Dilatometer	24
2.4.3	Hydraulic Fracturing	27
2.4.4	Stepped Blade	30
2.4.5	Cone Penetration Tests	31
2.4.6	Self-boring Pressuremeter	32
2.4.7	Shear Wave Measurements	34
2.4.8	Field Vane	35
2.5	Laboratory Methods	38
2.5.1	Work Criterion in Oedometer	39
2.5.2	Oedotriaxial	40
2.5.3	Split-ring Oedometer	41
2.5.4	K'_0 From Ratio of Preconsolidation Stresses	42
2.6	Correlation Methods	42
2.6.1	Normally Consolidated Soils	42
2.6.2	Overconsolidated Soils	44
3	In Situ Investigations	47
3.1	Initial Evaluations of the Test Site	47
3.2	Piezometers	50
3.3	Earth Pressure Cells	50
3.3.1	First Installations at 5 m	51
3.3.2	Installation at 6 m	52
3.3.3	Installation at 7 m	53
3.3.4	Installation at 8 m	53
3.3.5	Installation at 9 m	57
3.3.6	Installations at 10 m	57
3.3.7	Last Installation at 5 m	58
3.4	Earth Pressure Cell with Protective Cover	60
3.5	Dilatometer	63
3.6	Field Vane	63
4	Laboratory Investigations	65
4.1	Index Testing	65
4.1.1	Water Content	65
4.1.2	Atterberg Limits	66

4.1.3	Falling Cone	66
4.1.4	Density	66
4.2	Oedometer	66
4.3	Work Criterion in Oedometer	69
4.4	Triaxial Testing	69
4.5	Oedotriaxial	71
5	Results	75
5.1	In Situ Methods	75
5.1.1	Soundings	75
5.1.2	Pore Pressure Distribution	75
5.1.3	Earth Pressure Cells	76
5.1.4	Dilatometer	78
5.1.5	Field Vane	78
5.2	Laboratory Methods	78
5.2.1	Index Testing	78
5.2.1.1	Water Content	79
5.2.1.2	Atterberg Limits	79
5.2.1.3	Falling Cone	79
5.2.1.4	Density	79
5.2.2	Oedometer	79
5.2.3	Work Criterion in Oedometer	83
5.2.4	Triaxial Testing	83
5.2.5	Oedotriaxial	85
5.3	Correlation Methods	85
5.4	Comparison of all Methods	86
6	Discussion	89
6.1	Quaternary Geology	89
6.2	In Situ Methods	90
6.2.1	Soundings	90
6.2.2	Pore Pressure at Flotten	91
6.2.3	Earth Pressure Cells	93
6.2.3.1	Stress Conditions	94
6.2.3.2	Pore Pressure from Earth Pressure Cells	97
6.2.3.3	Equipment Errors	98
6.2.3.4	First Installations at 5 m	102
6.2.3.5	Installation at 6 m	103

6.2.3.6	Installation at 7 m	104
6.2.3.7	Installations at 8 m	104
6.2.3.8	Installation at 9 m	105
6.2.3.9	Installations at 10 m	106
6.2.3.10	Last Installation at 5 m	106
6.2.3.11	Installation at 5 m at Onsøy	107
6.2.3.12	Possible Corrections	107
6.2.4	Dilatometer	108
6.2.5	Field Vane	112
6.2.6	In Situ Methods not Tested	114
6.3	Laboratory Methods	115
6.3.1	Index Testing	115
6.3.1.1	Water Content	115
6.3.1.2	Atterberg Limits	116
6.3.1.3	Falling Cone	116
6.3.1.4	Density	117
6.3.2	Oedometer and Preconsolidation	118
6.3.3	Work Criterion in Oedometer	121
6.3.4	Triaxial Testing	123
6.3.5	Oedotriaxial	126
6.4	Correlation Methods	128
7	Summary and Further Work	133
7.1	Summary and Conclusions	133
7.2	Recommendations for Further Work	135
	Bibliography	137
	Appendix A Soundings	147
	Appendix B Pore Pressure Measurements	163
	Appendix C Earth Pressure Cells	169
	Appendix D Dilatometer	183
	Appendix E Field Vane	185
	Appendix F Index Properties	187
	Appendix G Oedometer Testing	191

<i>CONTENTS</i>	xiii
Appendix H Work Criterion in Oedometer	213
Appendix I Triaxial Testing	217
Appendix J Oedotriaxial Test	243

List of Figures

- 2.1 Vertical and horizontal pressures are affected by loading and unloading. 9
- 2.2 Idealized force chain with lines indicating the direction of the major principal stress. 16
- 2.3 Force chains in photoelastic disk experiment 16
- 2.4 Force chains after indentation. 17
- 2.5 Quaternary geology map of the Flotten test site. 18
- 2.6 Detailed Quaternary geology map of the Flotten test site. 19
- 2.7 Earth pressure cell equipment. 21
- 2.8 Comparison of Camkometer self-boring pressuremeter, Camkometer self-boring load cell, earth pressure cell and laboratory investigations. 23
- 2.9 Over-read of earth pressure cell. 24
- 2.10 The Marchetti dilatometer. 25
- 2.11 Equipment used for hydraulic fracturing. 28
- 2.12 Typical results from hydraulic fracturing test. 29
- 2.13 Results from fall cone tests close to piezometer location. 30
- 2.14 The stepped blade. 31
- 2.15 Schematic overview of the lateral stress seismic piezocone. 32
- 2.16 The Cambridge self-boring pressuremeter. 33
- 2.17 Equipment used for shear wave measurements. 35
- 2.18 Principal stress situation for vane test. 36
- 2.19 Illustration of active, direct and passive state. 37
- 2.20 Graphical construction to determine K'_0 from field vane test. 38
- 2.21 Cumulated work per unit volume plotted against effective stress for oedometer test. 39

- 3.1 Overview and closer look at the Flotten test site. 49
- 3.2 Cell damaged during penetration to 6 m. 53
- 3.3 Cells damaged during penetration to 8 m depth. 55
- 3.4 Rings to guide cells through casings. 56

3.5	Cell damaged during penetration to 10 m.	58
3.6	Equipment used to evaluate clay in casing.	59
3.7	Old cell and most promising protective cover from Veglaboratoriet.	61
3.8	New cell fitted in old protective cover.	62
4.1	Idealized graphs to determine p'_c by the Janbu method.	69
5.1	Overview of approximate preconsolidation from oedometer testing on 54 mm samples from Flotten.	82
5.2	Comparison of different approaches to K'_0	87
6.1	An elevation profile from the test site to the river Nidelva.	93
6.2	Close-up of the test setup for quantifying the effect of elastic bending.	99
6.3	Permanent misalignment of the earth pressure membranes due to bending.	100
A.1	Map indicating the location of the test site.	149
A.2	Overview map of boreholes.	150
A.3	Detailed map of boreholes.	151
A.4	Presentation of rotary pressure soundings in borehole DRT1.	152
A.5	Presentation of rotary pressure soundings in borehole DRT2.	153
A.6	Presentation of rotary pressure soundings in borehole DRT3.	154
A.7	Presentation of rotary pressure soundings in borehole DRT4.	155
A.8	Presentation of rotary pressure soundings in borehole DRT5.	156
A.9	Presentation of rotary pressure soundings in borehole DRT6.	157
A.10	Presentation of rotary pressure soundings in borehole DRT7.	158
A.11	Presentation of rotary pressure soundings in borehole DRT8.	159
A.12	Presentation of rotary pressure soundings in borehole DRT9.	160
A.13	Presentation of rotary pressure soundings in borehole DRT10.	161
A.14	Presentation of CPTu soundings in borehole CPTU1.	162
B.1	Overview of pore pressure measurements taken at Flotten.	166
B.2	Overview of potential with depth.	167
B.3	Pore pressure measurements with time at Flotten.	168
C.1	Stress and pore pressure versus logarithmic time.	170
D.1	Presentation of key parameters from dilatometer test at Flotten.	184
E.1	Undrained shear strength with time from field vane measurements.	186
F.1	Overview of key index parameters for the Flotten clay.	188

G.1	Presentation of CRS-results from depths 4 to 8 m.	194
G.2	Presentation of CRS-results from depths 9 to 11 m.	195
G.3	Presentation of CRS-results from depth 4.50 m.	196
G.4	Presentation of CRS-results from depth 5.10 m.	197
G.5	Presentation of CRS-results from depth 5.50 m.	198
G.6	Presentation of CRS-results from depth 5.50 m.	199
G.7	Presentation of CRS-results from depth 5.70 m.	200
G.8	Presentation of CRS-results from depth 6.50 m.	201
G.9	Presentation of CRS-results from depth 6.50 m.	202
G.10	Presentation of CRS-results from depth 7.50 m.	203
G.11	Presentation of CRS-results from depth 7.50 m.	204
G.12	Presentation of CRS-results from depth 9.40 m.	205
G.13	Presentation of CRS-results from depth 9.40 m.	206
G.14	Presentation of CRS-results from depth 9.50 m.	207
G.15	Presentation of CRS-results from depth 10.20 m.	208
G.16	Presentation of CRS-results from depth 10.20 m.	209
G.17	Presentation of CRS-results from depth 10.40 m.	210
G.18	Presentation of CRS-results from depth 10.40 m.	211
G.19	Presentation of CRS-results from depth 10.60 m.	212
H.1	Work criterion calculation based on oedometer test CRS0510.	214
H.2	Work criterion calculation based on oedometer test CRS0940-2.	215
H.3	Work criterion calculation based on oedometer test CRS0950.	216
I.1	Presentation of all CAUc-results from depths 3 to 8 m.	220
I.2	Presentation of all CAUc-results from depths 8 to 12 m.	221
I.3	Presentation of all CIUc-results from depths 3 to 8 m.	222
I.4	Presentation of all CIUc-results from depths 8 to 12 m.	223
I.5	Presentation of CAUc-results from depth 3.40 m.	224
I.6	Presentation of CAUc-results from depth 4.40 m.	225
I.7	Presentation of CAUc-results from depth 5.40 m.	226
I.8	Presentation of CAUc-results from depth 6.40 m.	227
I.9	Presentation of CAUc-results from depth 7.40 m.	228
I.10	Presentation of CAUc-results from depth 9.34 m.	229
I.11	Presentation of CAUc-results from depth 9.40 m.	230
I.12	Presentation of CAUc-results from depth 10.15 m.	231
I.13	Presentation of CAUc-results from depth 10.36 m.	232
I.14	Presentation of CAUc-results from depth 10.40 m.	233

I.15	Presentation of CAUc-results from depth 10.56 m.	234
I.16	Presentation of CAUc-results from depth 11.53 m.	235
I.17	Presentation of CIUc-results from depth 5.26 m.	236
I.18	Presentation of CIUc-results from depth 5.40 m.	237
I.19	Presentation of CIUc-results from depth 6.26 m.	238
I.20	Presentation of CIUc-results from depth 7.26 m.	239
I.21	Presentation of CIUc-results from depth 9.26 m.	240
I.22	Presentation of CIUc-results from depth 10.26 m.	241
I.23	Presentation of CIUc-results from depth 11.42 m.	242
J.1	Presentation of oedotriaxial results from depth 9.2 m.	244

List of Tables

- 4.1 Sample quality evaluation based on $\Delta e/e_0$ 67
- 4.2 Sample quality evaluation based on volumetric strain during the consolidation phase. 71
- 4.3 First day of oedotriaxial testing. 73
- 4.4 Subsequent days of oedotriaxial testing. 74

- 5.1 Overview of earth pressure cell testing at Flotten. 77
- 5.2 K'_0 from field vane tests. 78
- 5.3 Overview of oedometer tests performed by the authors. 80
- 5.4 Overview of selected oedometer tests performed by Konjit Paulos Gella. . . 80
- 5.5 Estimates of OCR with depth 81
- 5.6 Comparison of p'_c interpreted by the Janbu method and the work criterion method 83
- 5.7 Overview of CAUc triaxial tests performed by the authors. 83
- 5.8 Overview of triaxial tests performed by Gella 84
- 5.9 Overview of CIUc triaxial tests performed by Gella. 84
- 5.10 Strength parameters as determined from triaxial testing. 84
- 5.11 Input parameters used in correlation methods. 85
- 5.12 A summary of correlation methods. 86

- 6.1 Change in σ_h from screwdriver test. 99
- 6.2 Comparison of zero readings taken both in the field and at NTNU 102
- 6.3 Change in air pressure, measured total horizontal stress and measured pore pressure for three subsequent days. 107

- A.1 Coordinates of bore holes at Flotten 148

- B.1 Overview of Geotech PVT piezometers at Flotten. 163
- B.2 Individual pore pressure measurements taken at Flotten. 164
- B.3 Final pore pressure measurements taken from earth pressure cells. 165
- B.4 Pore pressure measurements used in assumed distribution. 165

E.1	Table for calculation of K'_0	185
E.2	Triaxial tests used as input for field vane calculations of K'_0	185
F.1	Results of cylinder and small ring density measurements with depth.	189
F.2	Results of oedometer ring density measurements with depth.	189
F.3	Results of particle density measurements with depth.	190

List of Symbols and Abbreviations

Acronyms

Symbol	Description	Units
<i>AnL</i>	Operator Anders Lindgård	
<i>CAUc</i>	Anisotropic consolidation undrained triaxial compression test	
<i>CIUc</i>	Isotropical consolidated undrained triaxial compression test	
<i>CPTu</i>	Cone Penetration Test with pore pressure measurement	
<i>CRS</i>	Constant Rate of Strain Oedometer test	
<i>CSO</i>	Operator Christian Strømme Ofstad	
<i>DMT</i>	Dilatometer	
<i>EA</i>	Operator Espen Andersen	
<i>KPG</i>	Operator Konjit Paulos Gella	
<i>MSc</i>	Master of Science	
<i>NGF</i>	Norwegian Geotechnical Society	
<i>NGI</i>	Norwegian Geotechnical Institute	
<i>NGTS</i>	Norwegian Geo-Test Sites	
<i>NPRA</i>	Norwegian Public Roads Administration	
<i>NTNU</i>	Norwegian University of Science and Technology	
<i>OCR</i>	Overconsolidation Ratio	
<i>SCPT</i>	Seismic Cone Penetration Test	
<i>SDMT</i>	Seismic Dilatometer	

UNIS The University Centre in Svalbard

Greek Symbols

Symbol	Description	Units
α	Slope parameter	-
β_k	Soil type parameter, dilatometer	-
χ	Modified Cam-Clay slope ratio parameter	-
δ	Deformation	mm
$\Delta\sigma'_1$	Incremental change in vertical effective stress	kPa
$\Delta\sigma'_3$	Incremental change in radial effective stress	kPa
$\Delta\varepsilon_1$	Incremental vertical strain	-
δ_i	Deformation at the in situ stress	mm
Δe	Change in void ratio	-
ΔV	Change in triaxial specimen volume during consolidation phase	cm^3
η	Anisotropic elastic stiffness parameter	-
γ	Unit weight	kN/m^3
γ_s	Particle unit weight	kN/m^3
ϕ'	Effective friction angle	°
ρ	Mobilized friction angle	°
ρ_s	Particle density	g/cm^3
σ'_1	Major principal effective stress	kPa
σ'_2	Middle principal effective stress	kPa
σ'_3	Minor principal effective stress	kPa
σ_h	Total horizontal stress	kPa
σ'_h	Effective horizontal stress	kPa

σ_r	Radial total stress	kPa
σ_v	Total vertical stress	kPa
σ'_v	Effective vertical stress	kPa
σ'_{10}	Major principal effective in situ stress	kPa
σ'_{30}	Minor principal effective in situ stress	kPa
σ'_{3f}	Minor principal effective stress at failure	kPa
σ_{cell}	Cell pressure	kPa
σ'_{h0}	Effective horizontal overburden stress	kPa
σ'_{ph}	Horizontal preconsolidation pressure	kPa
σ'_{pv}	Vertical preconsolidation pressure	kPa
σ'_{v0}	Effective vertical overburden stress	kPa
τ	Shear stress	kPa
ε	Strain	-
ε_a	Axial strain	-
ε_v	Vertical strain	-
ε_{vol}	Volumetric strain	-

Roman Symbols

Symbol	Description	Units
$[K_0]_p$	Coefficient of earth pressure after primary consolidation	-
a	Attraction	kPa
A_0	Original triaxial specimen area	cm^2
A_a	Adjusted area after consolidation	cm^2
A_s	Area during shearing corrected for axial strain	cm^2
c	Cohesion	kPa

c_v	Coefficient of consolidation	$m^2/year$
C_α	Secondary compression index	-
C_c	Compression index	-
C_r	Recompression index	-
e	Void ratio	-
e_0	Initial void ratio	-
E_D	Dilatometer modulus	kPa
$EE_{measured}$	Measured total earth pressure	mA
EE_{sens}	Mean sensitivity of cell	mA/bar
F	Piston force	N
f	Mobilization	-
g	Gravitational constant	m/s^2
h_0	Original specimen height	cm
I_D	Material index, dilatometer	-
I_P	Plasticity index	%
K_0	Coefficient of earth pressure at rest for total stresses	-
K'_0	Coefficient of earth pressure at rest for effective stresses	-
K_D	Lateral stress index, dilatometer	-
K_P	Coefficient of passive earth pressure	-
K'_{0nc}	Coefficient of earth pressure at rest, normally consolidated soil	-
K'_{0oc}	Coefficient of earth pressure at rest, over-consolidated soil	-
M	Oedometer stiffness modulus	kPa
m	Soil type parameter, dilatometer	-

m_1	Weight of cup and wet sample	g
m_2	Weight of cup and dry sample	g
m_c	Weight of cup	g
m_s	Dry weight of sample	g
m_w	Weight of water in sample	g
OCR_{DMT}	Overconsolidation ratio, dilatometer	-
p_0	Initial pressure value, dilatometer	kPa
p_1	Inflated pressure value, dilatometer	kPa
p_2	Deflated pressure value, dilatometer	kPa
p'_c	Effective vertical preconsolidation pressure	kPa
pV	Calibration factor for pre-excitation due to welding of the blade	mA
PWD_0	Current at atmospheric pressure	mA
$PWD_{measured}$	Measured pore pressure	mA
PWD_{sens}	Mean sensitivity of cell	mA/bar
q	Deviatoric stress	kPa
S	Slope inclination	-
S_0	At rest slope inclination	-
S_t	Sensitivity	-
s_u	Undrained shear strength	kPa
s_r	Remoulded shear strength	kPa
s_{uv}	Undrained shear strength, field vane	kPa
s'_{uv}	Remoulded shear strength, field vane	kPa
t_p	Time elapsed after primary consolidation	h
t_p	Time for primary consolidation	h

u	Pore pressure	-
u_0	Initial pore pressure	kPa
u_1	Front pore pressure measurement, CPTu	kPa
u_2	Rear pore pressure measurement, CPTu	kPa
u_b	Base pore pressure	kPa
V_0	Original specimen volume	cm^3
V_s	Volume of solids	cm^3
w	Water content	%
w_L	Liquid limit	%

Chapter 1

Introduction

1.1 Background

1.1.1 Problem Formulation

In geotechnical engineering problems it is crucial to know the in situ stress state. The quality of results from laboratory tests which aim to recreate the in situ stress state depend on the chosen stress state. For instance, triaxial test results will be most valuable if the in situ stress state is recreated (Watabe, Tanaka, Tanaka, & Tsuchida, 2003).

Also hand calculations and finite element analyses depend on knowledge of the in situ stress state. Hand calculations of retaining structures will be affected by the initial stresses in the ground. Finite element analyses of retaining structures rely on the correctness of the user specified in situ stress state (Watabe et al., 2003; Sivakumar, Doran, Graham, & Navaneethan, 2002). For a finite element program to predict the deformations of tunnels, slopes, retaining walls, piles, dams and excavations, input of the correct in situ stress state is important (Sivakumar et al., 2002).

The in situ stress state is often divided into a horizontal and a vertical stress component, and the ratio of these is referred to as K'_0 . The vertical stress state is assumed to be well defined by the overburden pressure alone (Massarsch, 1975; Lefebvre, Bozozuk, Philibert, & Hornych, 1991; Sivakumar et al., 2002). This may be determined by subtracting the pore pressure from the depth multiplied by the density of the overburden material (Lefebvre et al., 1991). On the other hand, the determination of the horizontal stress state has proven challenging, as it is affected by several quite complicated factors (Hamouche, Leroueil, Roy, & Lutenegger, 1995; Fioravante, Jamilokowski, Lo Presti, Manfredini, & Pedroni, 1998).

The uncertainties linked to determining the horizontal stress state may be divided into two main parts. First, the understanding of the factors that affect the in situ horizontal

stress state is not satisfactory. Despite several investigations, the factors influencing the evolution of K'_0 remains unresolved. Second, in situ and laboratory measurements tend to alter the stress situation, and thus the measured horizontal stress is not the true in situ stress (Hamouche et al., 1995; Fioravante et al., 1998).

The in situ determination of the horizontal stress is one of the topics in a recently launched research project, "Norwegian Geo-Test Sites" (NGTS). As a cooperation between NGI, NTNU, SINTEF, UNIS and the Norwegian Public Roads Administration, the project features four test sites across mainland Norway as well as a test site in Longyearbyen at Svalbard. The goal of the project is to use the five test sites to evaluate and develop methods for soil investigation. This master's thesis is part of the NGTS research project and the NGTS quick clay test site at Flotten will be used for performing field investigations.

1.1.2 Literature Survey

In Chapter 2 the result of a literature study on K'_0 is presented. The main findings in the literature study may be divided into four main parts.

First, the geological evolution of K'_0 is affected by both mechanical and chemical processes. The mechanical processes include secondary compression (Jamiolkowski, Ladd, Germaine, & Lancellotta, 1985; Mesri & Castro, 1987; Schmertmann, 1991; Bjerrum, 1967), unloading due to erosion (Bjerrum, 1967) and other factors reducing the overburden pressure, as well as force chain formation and buckling (J. Peters, Muthuswamy, Wibowo, & Tordesillas, 2005). The chemical processes include among others chemical bonding and thixotropy (Jamiolkowski et al., 1985; Mesri & Castro, 1987; Fioravante et al., 1998).

Second, many different methods have been proposed to measure K'_0 in situ. To a varying degree the methods impose stress changes during measuring (Fioravante et al., 1998; Hamouche et al., 1995). The repeatability of the methods is also varying. Three methods stand out in the literature as reference methods. These are earth pressure cells, hydraulic fracturing and the Camkometer self-boring pressuremeter (Ku & Mayne, 2013).

Third, several laboratory methods to determine K'_0 have been proposed. Running triaxial tests under oedometer conditions has given quite good results (Watabe et al., 2003). On the other hand, methods like calculating K'_0 from the ratio of horizontal and vertical preconsolidation stresses has been proved wrong (Hamouche et al., 1995).

Last, there are numerous equations of varying complexity correlating parameters like friction angle and OCR to K'_0 . The simplest and probably the most recognized is the Jaky's equation for normally consolidated soils (Hamouche et al., 1995; P. W. Mayne & Kulhawy, 1982; Diaz-Rodriguez, Leroueil, & Aleman, 1992). Brooker and Ireland (1965) found that the stress history is of great importance for the value of K'_0 . Work by

Sivakumar, Navaneethan, Hughes, and Gallagher (2009), trying to include the effects of anisotropy, stress history and the structure of the material, yielded a substantially more intricate equation.

1.1.3 What Remains to be Done?

There is presently no in situ, laboratory or correlation method which has been proven to correctly determine the horizontal stress needed to calculate K'_0 in every soil deposit. Gaining an understanding of the factors influencing the geological evolution of K'_0 and finding a method which is able to measure the correct horizontal stress in any soil deposit is what remains to be done on this topic.

1.2 Objectives

Since extensive amount of work remains on the topic of K'_0 , the objectives for this master's thesis are more limited. The objectives are presented below:

1. Review literature on the geological evolution of K'_0
2. Study methods to measure K'_0 in situ and in the laboratory
3. Install and evaluate earth pressure cell tests at Flotten
4. Perform and evaluate a dilatometer test at Flotten
5. Evaluate the possibility to make a protective cover for an earth pressure cell
6. Perform oedometer tests on Flotten clay samples in order to find preconsolidation
7. Perform undrained triaxial tests to investigate material properties. Use results as input for the field vane approach to evaluate K'_0
8. Present a general site classification of the Flotten test site
9. Run an oedotriaxial test
10. Compare K'_0 values from field and laboratory methods, as well as correlation methods, and discuss the results

1.3 Limitations

There have mainly been two types of limitations to this master's thesis. First, the field investigations have been limited by the fact that only equipment already available at NTNU or through the NGTS project have been utilized. Thus, recognized methods like hydraulic fracturing and the Camkometer self-boring pressuremeter have not been tested. Equipment available through the NGTS research project is primarily based on Lunne and L'Heureux (2016). In general, methods recommended in Lunne and L'Heureux (2016) is also supported by findings presented in Chapter 2.

The second limitation has been time. Since a master's thesis should be performed during a limited amount of time, the authors have made choices regarding which methods to dedicate the most time. The earth pressure cells have been granted the most time of any single methods, since it is the only one of the three in situ reference methods which the authors had access to. Also, a lot of time has been spent in the laboratory to gain a reasonable understanding of the soil conditions at Flotten and investigating laboratory methods for the determination of K'_0 .

1.4 Approach

The approach for objectives 1 and 2 is to extend and partially revise the literature study performed as part of the authors' project thesis in the autumn semester of 2016. More articles should be found and reviewed.

Objectives 3 and 4 will be approached by performing and evaluating field investigations at the NGTS Flotten test site.

The approach for objective 5 is to gain access to protective covers which are briefly described in Vaslestad (1989), and use them as inspiration for the design of a new protective cover, compatible with the current Glötzl earth pressure cells. Subsequently, an evaluation of the effect of such a cover is required before the final production is initiated.

Objectives 6 and 7 may be met by performing laboratory investigations. For objective 7 there is an additional need for field vane test results.

Extensive amounts of information may be used for interpreting the soil conditions at Flotten and fulfilling objective 8. The field and laboratory studies by the authors may supplement soundings performed by NTNU engineers and laboratory tests performed by Konjit Paulos Gella.

To meet objective 9 it is necessary to find an effective and sound procedure for running an oedotriaxial test using the available triaxial testing equipment in the geotechnical laboratories at NTNU.

Finally, with a subsequent comparison of all acquired estimates of K'_0 , objective 10 will be accomplished.

1.5 Structure of the Report

The remaining part of this thesis is divided into six chapters. Chapter 2 treats literature on the geological evolution of K'_0 and methods to measure K'_0 in situ and in the laboratory. Chapter 3 describes the performed in situ testing at the Flotten test site. Chapter 4 deals with the performed laboratory testing. In Chapter 5 the results of the field and laboratory investigations are presented, as well as results from correlation methods. Chapter 6 presents a thorough discussion of the results. A summary of key findings and experiences as well as recommendations for further work are given in Chapter 7.

Chapter 2

Background

A theoretical foundation is required for the evaluation and discussion of methods to investigate the horizontal stress state and K'_0 . This chapter gives a thorough presentation of the definition and geological evolution of K'_0 , before a selection of methods for investigating K'_0 is given.

The material presented herein represents a further development of the literature survey presented as part of the project thesis written during the autumn of 2016 (Lindgård & Ofstad, 2016). The original material has been expanded with new sections. These new sections include the work criterion approach suggested by Becker, Crooks, Been, and Jefferies (1987) as well as the vast majority of sections on geological processes governing the evolution of K'_0 . The sections about the field vane approach suggested by Aas, Lacasse, Lunne, and Hoeg (1986) and oedotriaxial testing have been elaborated. Additionally, the remaining sections have partially been condensed and rewritten.

2.1 Definition of K'_0

The relationship between the in situ horizontal and vertical stress is usually expressed by a factor called the coefficient of earth pressure at rest (Sivakumar et al., 2002). The relationship in Equation 2.1 was first proposed by A.D. Donath in his 1891-paper for total stresses (Hamouche et al., 1995; Brooker & Ireland, 1965).

$$K_0 = \frac{\sigma_h}{\sigma_v} \quad (2.1)$$

To obtain a relationship between the horizontal and vertical effective stresses, the effect of the pore pressure u is subtracted. The resulting expression for K'_0 , as seen in Equation 2.2, is the one that will be used in this report as the coefficient of earth pressure at rest. Please note that some authors use the term K'_0 in when actually referring to K_0

as defined in Equation 2.2 (Mesri & Hayat, 1993; Mesri & Castro, 1987; Schmertmann, 1983).

$$K'_0 = \frac{\sigma'_h}{\sigma'_v} \quad (2.2)$$

K'_0 is defined as the ratio in Equation 2.2, under the conditions of vertical loading and no lateral deformation (Mesri & Hayat, 1993). The oedometer resembles the K'_0 condition.

2.2 Geological Processes Governing the Evolution of K'_0

Much research and development during the last decades has centered around field and laboratory investigations of K'_0 , making it clear that the value of K'_0 is affected by both the material properties of the soil as well as the stress history (Shin & Santamarina, 2009). Hence, many researchers have tried to find ways to explain the creation and evolution of K'_0 (Brooker & Ireland, 1965; Shin & Santamarina, 2009; Schmertmann, 1983). This topic will be treated in greater detail below.

2.2.1 Effect of Stress History

First of all, it is clear that the horizontal stress is affected by the loading history of the deposit investigated (Hamouche et al., 1995; Brooker & Ireland, 1965; Lefebvre et al., 1991; Sivakumar et al., 2002; Shin & Santamarina, 2009). Clay that has only experienced primary loading is often referred to as normally consolidated, while truly overconsolidated clays have a preconsolidation pressure higher than the present overburden pressure due to unloading (Aas et al., 1986). Other authors name clays with any preconsolidation pressure higher than the present overburden pressure as overconsolidated, regardless of what has caused the preconsolidation pressure (Sivakumar et al., 2002). Sivakumar et al. (2009) stated that the value of K'_0 is constant during first loading, as an increase in vertical loading also affects the horizontal stress proportionally. However, in succeeding unloading of the material, the proportionality between the vertical and horizontal stress is no longer valid. The vertical stress will reduce more than the horizontal, as a result of interparticle locking conserving more of the horizontal stress than the vertical stress. This is particularly evident in frictional granular materials (Shin & Santamarina, 2009).

The difference in response for loading and unloading is illustrated in Figure 2.1. For soil deposits with high overconsolidation values, that is where the preconsolidation pressure is much higher than the current loading, the horizontal stress is likely to be greater than

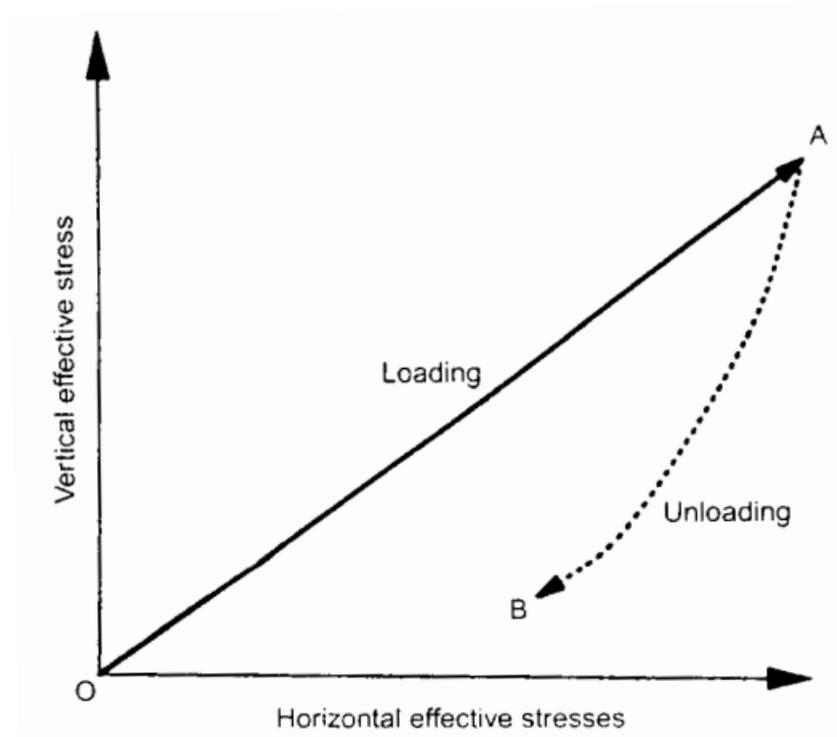


Figure 2.1: Vertical and horizontal pressures are affected by loading and unloading. Figure from Sivakumar, Doran, Graham, and Navaneethan (2002).

the vertical stress. Hence, the K'_0 -value tend to increase with the overconsolidation ratio, OCR (Sivakumar et al., 2009; Hanzawa & Kishida, 1981). This has also been confirmed experimentally (see for instance Hamouche et al., 1995; Brooker & Ireland, 1965; Lefebvre et al., 1991). OCR is defined in Equation 2.3.

$$OCR = \frac{p'_c}{\sigma'_{v0}} \quad (2.3)$$

where p'_c is the effective vertical preconsolidation pressure and σ'_{v0} is the current effective overburden pressure (P. W. Mayne & Kulhawy, 1982).

One straightforward example of such overconsolidated materials are clays deposited towards the end of the last ice age in Norway (Gylland, Long, Emdal, & Sandven, 2013; Bjerrum, 1967). As the ice melted and the land began to rise, the clays deposited at the seabed were brought up to dry land. Subsequent erosion resulted in unloading of the overburden pressure and therefore overconsolidated clay materials were formed (Bjerrum, 1967).

2.2.2 Time Effects

The rather clear link between K'_0 and OCR has been pointed out in several articles (see for instance Brooker & Ireland, 1965; Sivakumar et al., 2009; P. W. Mayne & Kulhawy, 1982).

Hence, it is of great interest to investigate other mechanisms that could result in a preconsolidation pressure higher than the current overburden load. Aas et al. (1986) pointed out the importance of differentiating between mechanical overconsolidation and other forms of overconsolidation. The authors argued that only mechanical overconsolidation could be considered true overconsolidation. Apparent overconsolidation gives an increase in the preconsolidation pressure, but the soil is still to be considered as normally consolidated. Apparent overconsolidation is caused by other effects that will be more closely discussed below. Since both mechanical and other effects may cause overconsolidation, Aas et al. (1986) argued that differentiating only between normally and overconsolidated soils does not provide the entire picture of how soils behave. Since time effects, and thus the age of the deposit, is crucial for the behaviour, one should in addition describe soils as "young" or "aged" (Aas et al., 1986).

It is important to note that the effects discussed in this sections is a selection of mechanisms often categorized in the literature as either time effects or aging. For the remaining of this section, these mechanisms will be referred to as time effects. In an article by Jamiolkowski et al. (1985) this categorization was used about effects like the influence of strain rate on material behaviour, different kinds of creep as well as relaxation. The importance of these effects is recognized through an extensive amount of research and discussions throughout the last decades (see for instance Shin & Santamarina, 2009; Schmertmann, 1983; Jamiolkowski et al., 1985; Kavazanjian Jr & Mitchell, 1984; Hanzawa & Kishida, 1981). In the discussion below, several mechanisms known to affect the apparent preconsolidation will first be briefly presented. Next, special attention will be given to the behaviour and effect of secondary compression, named by Mesri and Castro (1987) as an important mechanism that could also cause a direct change in the value of K'_0 . Last, the concept of force chains and their connection to K'_0 is presented.

2.2.3 Chemical Changes

First, various types of chemical bonding as well as thixotropy are said to influence the apparent preconsolidation pressure (Jamiolkowski et al., 1985; Mesri & Castro, 1987; Fioravante et al., 1998). Bjerrum (1967) listed exchange of cations and cementation as the most important chemical bonding effects in the relatively young Norwegian clays. Exchange of cations is a direct consequence of rainwater entering the clay. The negatively charged clay minerals are typically balanced by Na^+ -ions as the clay deposits rises above sea level. The rainwater containing O_2 and CO_2 will gradually lower the pH-value, eventually leading to the precipitation of Na^+ -ions. These ions may be replaced by for instance K^+ -ions released from clay minerals as a consequence of the lowered pH-value.

Bjerrum (1967) investigated these exchange effects for the Drammen clay. First, the

seepage effect of rainwater is assumed to be reduced with increasing depth. Consequently, by measuring the types of ions absorbed by the clay, Bjerrum (1967) found the exchange effect to be most pronounced in depths just below the dry crust, decreasing to an almost unaltered clay at about 6 to 7 meters. After consolidating clay samples beyond the previous overburden pressure in the laboratory, the author passed water rich in K^+ -ions through the clay. Consequent loading in small steps indicated that the preconsolidation had increased by almost 50 %, due to the increased concentration of K^+ -ions in the clay (Bjerrum, 1967).

Fischer, Andersen, and Moum (1978) investigated the process of cementation, in which sediments eventually develop from soils into rock under high pressure, also known as lithification. In clays exposed to this process, there exists additional chemical bonding in addition to the friction and cohesion found in uncemented clays (Fischer et al., 1978). Fischer et al. (1978) inquired the possibility of invoking cementation in two normally consolidated samples of Drammen clay. The authors found that the strength of a normally consolidated clay increased with about 35 - 40 % as a consequence of the cementation process. Finally, Fischer et al. (1978) stated that for a stiff clay the change in engineering properties was essentially the same regardless of whether the preconsolidation originated from mechanical overconsolidation or cementation.

Thixotropy is a strength increasing process due to reversible changes in viscosity (Schmertmann, 1991). Materials showing thixotropic behaviour are able to stiffen with a great increase in strength over a short period of time and thereafter lose most of its strength and become a viscous fluid when exposed to some mechanical disturbance. Schmertmann (1991) argued that the process is the result of a dispersion-flocculation process occurring for instance during the deposition of sediments. Even when exposed to almost no effective stresses, particles will tend to accumulate due to attractive forces. Because of the low stress level, it takes almost no disturbance for the particles to break apart (Schmertmann, 1991).

Schmertmann (1991) also reviewed published literature regarding different mechanisms related to the fact that soils age. The author used the term pure aging to describe effects only involving the passage of time. Herein, this is referred to as time effects. Consequently, the author differentiated between chemical time effects like thixotrophy and mechanical time effects that included secondary compression and some other effects. Schmertmann (1991) argued that both types of time effects resulted in an increased strength of the material and that both involve the flocculation and dispersion of particles. On the other hand, thixotrophy is most likely to occur during very low effective stresses whilst mechanical time effects will dominate under higher stresses. Hence, the mechanical time effects will be much more pronounced from an engineering point of view.

2.2.4 Drying

Drying, as in evaporation or freezing, is mentioned as a mechanism able to influence the preconsolidation pressure (Jamiolkowski et al., 1985). When a material experiences drying, the loss of pore water will generate suction (Shin & Santamarina, 2009). During repeated wet and dry cycles, very fine soils may experience very high effective stresses due to the suction. The effect of drying is likely to mainly affect the first few meters of a soil deposit, where the existing preconsolidation due to overburden load is quite small. Hence, these stresses may easily induce a new, higher preconsolidation pressure for the clay (Tomás, Domenech, Mira, Cuenca, & Delgado, 2007).

Mahar and O'Neill (1983) investigated the geotechnical properties of dried clays and suggested that the suction process may generate cracks in the material. These cracks will lead to variability in suction force, resulting in high variability in both preconsolidation pressure and undrained shear strength over the deposit.

2.2.5 Secondary Compression

After loading a material, secondary compression, also referred to as secondary consolidation, is the more slow process of drained creep under constant vertical load following the primary consolidation stage (Jamiolkowski et al., 1985; Mesri & Castro, 1987; Schmertmann, 1991; Bjerrum, 1967). The process is characterized by the rearrangement of particles to achieve a more stable equilibrium state (Mesri & Castro, 1987). To replicate the in situ consolidation process, the process of secondary compression is often investigated by performing one-dimensional loading of soil specimens, as in the oedometer (Jamiolkowski et al., 1985). The oedometer-condition resembles the gradual loading during deposition of a natural soft clay (Mesri & Castro, 1987).

For completeness, it is interesting to note that secondary compression also takes place after isotropic loading of a soil sample (de Jong & Verruijt, 1965). Based on this observation, Mesri and Castro (1987) pointed out that secondary compression is not uniquely linked to the K'_0 -condition itself.

Clearly, it is of great importance to be able to quantify the change in K'_0 as a consequence of secondary compression. Secondary compression is often modelled by the C_α/C_c -concept, first proposed by Mesri and Godlewski (1977). This model is based on the relationship between two constants, called the secondary compression index, C_α , and the compression index, C_c . These are defined as follows:

$$C_\alpha = \frac{\partial e}{\partial \log t} \quad (2.4)$$

$$C_c = \frac{\partial e}{\partial \log \sigma'_v} \quad (2.5)$$

where e is void ratio, t is time and σ'_v is effective vertical stress. ∂ indicates partial derivatives. The value of the C_α/C_c -ratio is thereafter determined based on compression curves for three different consolidation pressures in an oedometer. The C_α/C_c -concept will not be further utilized for calculations within this thesis, and will consequently not be treated in greater detail here. A more thorough presentation is given in articles by Mesri and Godlewski (1977) and Mesri and Castro (1987). Since the original proposal, the concept has been used for predicting the secondary compression behaviour in several different kinds of soil materials (Mesri & Castro, 1987; Mesri & Choi, 1984). One of the primary advantages with this concept, is that the value of the C_α/C_c -constant shows incredible small variations between different types of soil (Mesri & Castro, 1987).

In an article by Schmertmann (1983), the author demonstrated that there existed no common opinion regarding the connection between secondary compression and changes of K'_0 with time. The author simply asked how K'_0 would change with time, for a normally consolidated cohesive soil material, during secondary compression (Schmertmann, 1983; Jamiolkowski et al., 1985). Based on different assumptions regarding soil behaviour, Schmertmann (1983) presented a total of three different outcomes.

First, one may assume that cohesive soils are made up of particles separated by bound layers of water. The behaviour of these layers is regarded as viscous, so as time pass by the cohesive material will approach an increasingly homogeneous stress state where the shear stresses that once existed in the soil have vanished due to slow rearrangement of the soil. The cohesive material is in this case regarded as a time-softening material. Since the shear stresses decrease with time, one would expect K'_0 to increase with time for normally consolidated soils (Schmertmann, 1983; Kavazanjian Jr & Mitchell, 1984).

On the other hand, both Bjerrum (1967) and Hanzawa and Kishida (1981) argued that the strength of a cohesive material will increase with time as a consequence of various chemical bonding between particles as discussed previously. The soil is treated as a time-hardening material. A cohesive material which has higher strength needs less lateral support to support the same overburden pressure. This suggests that K'_0 will decrease with time (Schmertmann, 1983).

Finally, one could also argue that K'_0 would not change with time. If the cohesive soil is assumed to be an elastic material which does not change considerably with time, the Poisson's ratio is constant and therefore K'_0 is unchanged (Schmertmann, 1983).

As a survey of 40 geotechnical engineers gave all three kinds of answers, Schmertmann (1983) concluded that more research would be of great importance in order to better understand the evolution of K'_0 .

As a consequence of the article by Schmertmann (1983), several other authors investigated the effect of secondary compression on K'_0 . Kavazanjian Jr and Mitchell (1984) reviewed some recent laboratory work on San Francisco Bay mud and kaolinite, suggesting an increase in K'_0 for normally consolidated clays during secondary compression. By combining this with both a theoretical analysis and some behavioural reasoning, the authors concluded that the value of K'_0 would either increase or decrease towards $K'_0 = 1.0$ as a consequence of secondary compression. The authors argued that the soil would develop towards the isotropic consolidation state with no shear stresses present. σ'_1 is kept constant during secondary compression. Hence, σ'_3 must increase for a normally consolidated soil to reach $K'_0 = 1.0$. For an overconsolidated soil, with K'_0 values above 1.0, σ'_3 must decrease in order to reduce the shear stresses and approach $K'_0 = 1.0$ (Kavazanjian Jr & Mitchell, 1984).

The proposal that K'_0 approaches 1 with time was later questioned in several other articles (see for instance Jamiolkowski et al., 1985; Mesri & Castro, 1987; Kavazanjian Jr & Mitchell, 1985). As part of a general evaluation of new developments in laboratory and field investigations, Jamiolkowski et al. (1985) conducted secondary compression tests in an oedometer. No changes in K'_0 was found when testing Panigaglia clay, whilst a fairly clear, albeit small increase in K'_0 was observed when testing organic silty clays. Even as much as ten cycles of loading allowing for secondary compression and subsequent unloading only led to an increase in K'_0 of about 0.1. The authors hence concluded that the practical implications of the increase in K'_0 during secondary compression was rather small. Similarly, this was also supported by Holtz, Jamiolkowski, and Lancellotta (1986), investigating the change in K'_0 during secondary compression in a special odometer test on hand-carved block samples of a highly plastic, Italian clay.

Mesri and Castro (1987) used the C_α/C_c -concept to investigate the possible change in the degree of overconsolidation as a consequence of secondary compression. By combining the K'_0 -OCR-relationship in Equation 2.29 originally proposed by P. W. Mayne and Kulhawy (1982) with the C_α/C_c -concept, the authors proposed the following equation for estimating the increase in K'_0 during secondary compression.

$$K'_0 = [K_0]_p \left(\frac{t}{t_p} \right)^{[(C_\alpha/C_c)/(1-C_r/C_c)] \cdot \sin \phi'} \quad (2.6)$$

Where $[K_0]_p$ is the value of K'_0 at the end of the primary consolidation, t is the time elapsed since the end of primary consolidation, t_p is the time required for primary consolidation, C_r is the recompression index and C_c is the compression index. As for both C_α and C_c , the determination of C_r is given in more detail in Mesri and Castro (1987).

Using Equation 2.6, Mesri and Castro (1987) predicted a slight increase in K'_0 for five lightly overconsolidated natural soft clays. Such an increase was also supported by the

majority of research for normally consolidated clays reviewed by Mesri and Castro (1987). Based on the results, Mesri and Castro (1987) also investigated the value of $\frac{t}{t_p}$ required in order to reach a value of $K'_0 = 1.0$, which was suggested by Kavazanjian Jr and Mitchell (1984) as the final equilibrium state. Mesri and Castro (1987) found that time periods in the range of 10^{12} to 10^{24} multiplied by the time required for primary consolidation were necessary to reach $K'_0 = 1.0$ in Equation 2.6. These calculations may suggest that the final equilibrium state of $K'_0 = 1.0$ is of no engineering interest. This conclusion was also reached by Jamiolkowski et al. (1985).

Kavazanjian Jr and Mitchell (1984) later acknowledged that their original proposal that K'_0 goes towards 1.0 with time was to be considered preliminary, due to the rather limited amount of experimental data the proposal was based on (Kavazanjian Jr & Mitchell, 1985). The authors also expressed their support to the findings by Kavazanjian Jr and Mitchell (1984) and Mesri and Castro (1987), namely that the value of K'_0 show a small increase with time, but for any practical engineering purpose, the in situ value of K'_0 may be considered constant over the life time of buildings (Kavazanjian Jr & Mitchell, 1985).

Kavazanjian Jr and Mitchell (1985) raised an important question of whether or not short time laboratory tests may resemble the in situ behaviour of soils that have experienced secondary compression for thousands of years. Indeed, a soil specimen have been unloaded during sampling and then loaded as part of laboratory testing. The process of consolidation starts over, and the specimen will most likely not experience secondary compression due to the limited time frame (Kavazanjian Jr & Mitchell, 1984). This will affect the measured value of K'_0 compared to the in situ value (Mesri & Castro, 1987), considering that the typical age of a soft clay deposit in Norway may be taken as about 10 000 years (Reite, Sveian, & Erichsen, 1999). Similarly, Kavazanjian Jr and Mitchell (1984) argued that in situ loading of a soil deposit will lead to primary and secondary consolidation starting over again, and thus making the deposit "young".

2.2.6 Force Chains

Force chains is a physical phenomenon which has been investigated quite a lot over the past decades (J. Peters et al., 2005). The basic idea is that in granular materials the majority of the load is carried by chains of particles resembling a network of columns. Imagine the particles in a granular material as ping pong balls put on top of each other into one column. This resembles a force chain in a granular material. The column of balls will not be able to stand by itself. The amount of lateral support needed to keep the column in place depends strongly on how much it deviates from a straight column. Increasing non-linearity will increase the need for lateral support. An idealized force chain with lines indicating the direction of the major principal stress is shown in Figure 2.2.

The particles which are not part of the force chain act as lateral supports for the chain (J. Peters et al., 2005).

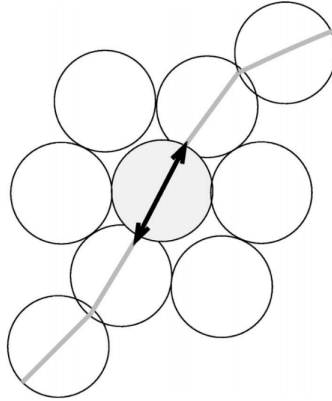


Figure 2.2: Idealized force chain with lines indicating the direction of the major principal stress. Figure from J. Peters, Muthuswamy, Wibowo, and Tordesillas (2005).

Despite lots of research has been made, there is no general agreement on a definition of force chains (J. Peters et al., 2005). A reasonable definition may be that force chains are heavily loaded networks of particles that support the majority of the force applied to a static or slowly moving granular material (Campbell, 2003). Numerical simulations like in Figure 2.4 and experiments with photoelastic disks as in Figure 2.3 show that the direction of the force chains coincide more or less with the direction of the major principal compressive stress (Muthuswamy, Peters, & Tordesillas, 2006).

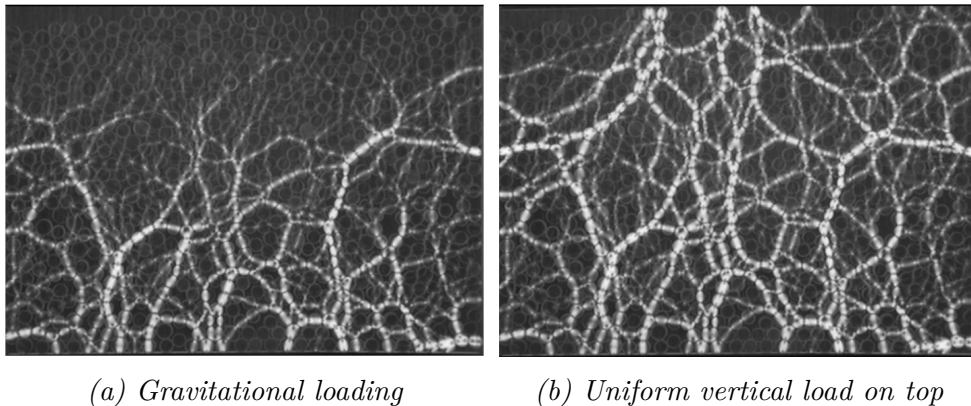


Figure 2.3: Force chains in photoelastic disk experiment. Figure from Muthuswamy, Peters, and Tordesillas (2006).

The particles in an assembly may be divided into two types of networks with distinct behaviour (Radjai, Wolf, Jean, & Moreau, 1998). These are the strong and the weak network, and must not be confused with the network of force chains described earlier. Only about half of the particles in the strong network constitute a part of force chains. Rajai et al. (1998) defined the strong network to be those particles carrying above the

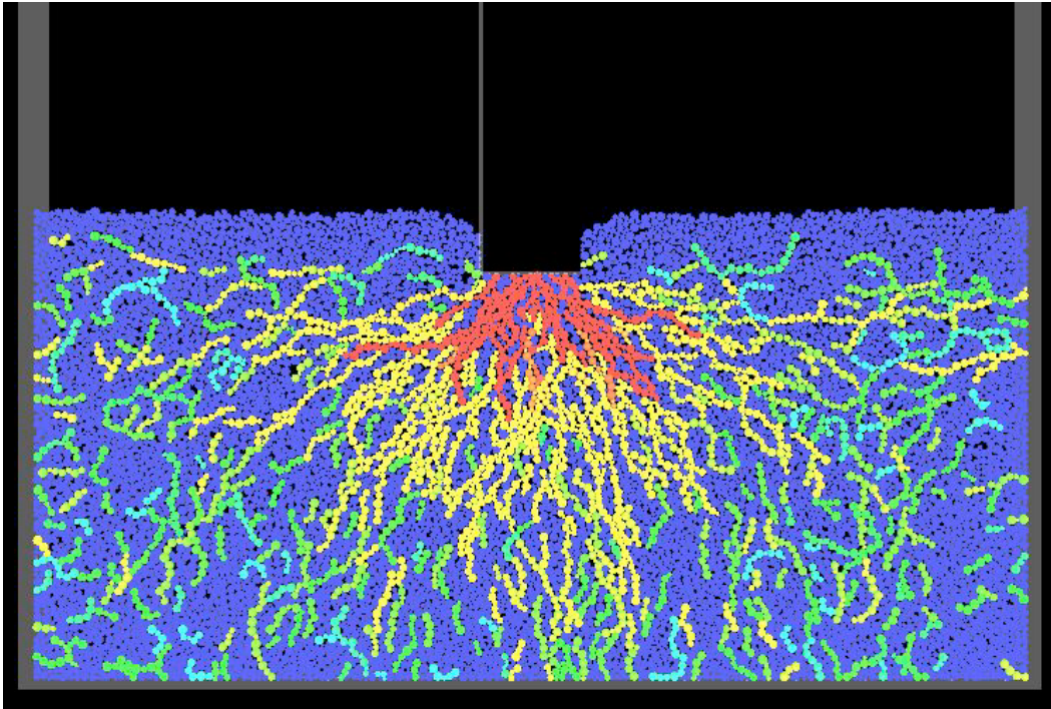


Figure 2.4: Force chains after indentation. Figure from Muthuswamy, Peters, and Tordesillas (2006).

average stress of all the particles. The strong network typically consists of less than approximately 40 % of the particles. A distinct feature of particle assemblies is that as the stresses increase, the number of particles carrying above the average stress decreases. This may be illustrated by Figure 2.4, where a limited number of force chains carry the majority of the load.

Tordesillas, Zhang, and Behringer (2009) stated that rolling friction is probably the most important energy transfer mode when force chains in granular materials buckle. When a force chain buckles, energy is transferred to the surrounding particles. The buckling of force chains is closely connected with the micromechanical formation of shear bands (Oda, Takemura, & Takahashi, 2004). In the weak network, sliding friction is the major energy transfer mode (Tordesillas et al., 2009).

In the case of in situ flat terrain that is not too overconsolidated, the major principal stress direction is vertical. Thus the directions of the force chains will be mainly vertical (Muthuswamy et al., 2006). In this case the in situ horizontal earth pressure at rest will depend on the need for lateral support of the force chains (J. Peters et al., 2005). In this way, the formation and stability of force chains in granular materials will be determining for the value of K'_0 .

No literature on force chain behaviour in pure clays have been found, but the subject of force chains is included herein for completeness. J. F. Peters and Berney IV (2009) treated the formation of force chains in mixtures of sand and clay. One of the key findings

was that with between 45 % and 48 % sand content by mass, the behaviour is distinctly changing from clay dominated behaviour to sand dominated behaviour. The authors argued that this was evidence of force chains carrying the majority of the load when the material exhibits sand dominated behaviour. When force chains carry the main part of the load, the function of the clay is to give lateral support to the force chains as part of the weak network (J. F. Peters & Berney IV, 2009).

2.2.7 Quaternary Geology

Reite et al. (1999) treats the Quaternary geological evolution of the area around Trondheim. The Flotten test site is situated within an area with thick marine deposits, as indicated with blue colours in Figure 2.5. Marine deposits often consist of silty clay or clayey silt material (Reite et al., 1999).

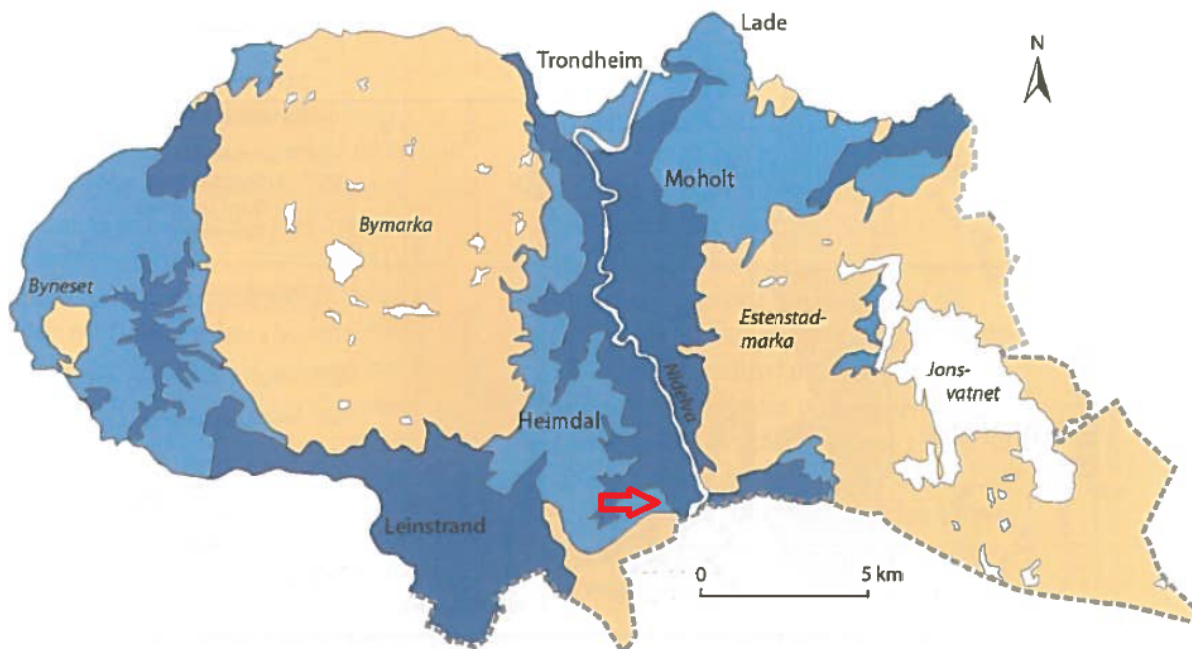


Figure 2.5: Quaternary geology map. Light blue colour is old seabed; darker blue colour is eroded marine deposits. The red arrow indicates the location of the Flotten test site. Figure from Reite, Sveian, and Erichsen (1999).

As it may be seen from Figure 2.5, the test site is located in an light blue area, which are areas where the old sea floor is basically intact. The darker blue colour indicates areas which are more affected by erosion caused by landslides and river erosion. The test site is located not far from areas with dark blue colour. These eroded areas may be seen as slopes down towards Nidelva in Figure A.1. Some of the slopes towards Nidelva are known to be results of quick clay landslides, like for instance the Tiller landslide which happened in 1816 a bit downstream from the test site (Reite et al., 1999). Reite et al.

(1999) also suggest that there may have been an ice shelf covering the marine deposits at the test site. This could have led to mechanical overconsolidation.

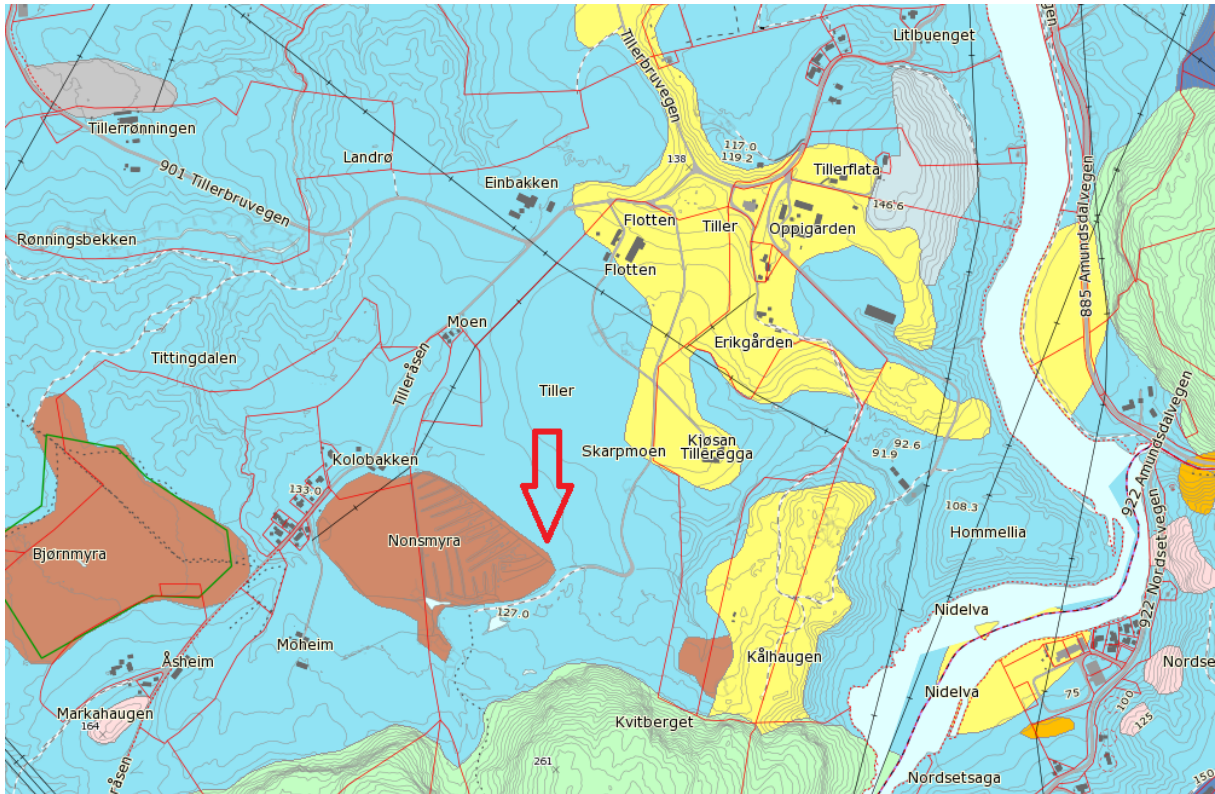


Figure 2.6: Detailed Quaternary geology map. Light blue colour is thick marine deposits, yellow is fluvial deposits and brown is peat and swamp. The red arrow indicates the location of the Flotten test site. Figure from NGU (geo.ngu.no/kart/losmasse/).

The more detailed Quaternary geological map in Figure 2.6 show fluvial deposits situated to the east of the test site. The deposits have most likely been placed there by the river Nidelva at some point in the last 9800 years. At that time, Nidelva changed river course from running west from the lake Selbusjøen, to running north along a new course similar to the present (Reite et al., 1999).

2.3 Introduction to Methods for Determining K'_0

The importance of knowledge regarding the horizontal stress situation in several common geotechnical engineering problems has already been addressed. This importance has led to a vast amount of research and development, resulting in a wide range of proposed methods and correlations.

When developing new equipment and methods to determine the horizontal stress state and thus K'_0 , the ability to compare results between methods and materials is crucial. This requires a thorough understanding of the different methods, as well as both advantages

and weaknesses of the different approaches to K'_0 . Consequently, this part will give a rather extensive review of key trends within this area.

In comparing different ways of determining K'_0 it is convenient to divide the methods into three categories. Both in situ and laboratory methods are based on measurements of material properties, and some assumptions and theory is required in order to determine K'_0 . The third category of methods is based on correlations between K'_0 and parameters acquired in situ or in the laboratory (Hamouche et al., 1995; Fioravante et al., 1998).

2.4 In Situ Methods

By now it is quite clear that several different factors as well as even small horizontal strains are likely to alter the horizontal stress state (Fioravante et al., 1998; Hamouche et al., 1995; Ryley & Carder, 1995). Consequently, any equipment installation where soil is displaced may alter the horizontal stress state, making in situ measurements of the horizontal stress rather challenging (Hamouche et al., 1995; Lefebvre et al., 1991). Hence, the in situ methods are typically classified based on the amount of disturbance associated with implementing the method (Hamouche et al., 1995; Fioravante et al., 1998). The majority of the in situ methods are intrusive, where equipment is penetrated into the soil. This is likely to alter the stress state and may also give a local rise in pore pressure. The importance of this disturbance on the measurements is often hard to predict. On the other hand, the self-boring pressuremeter (presented in section 2.4.6) is the most discussed example of a less intrusive method, reducing the amount of disturbance imposed on the soil (Hamouche et al., 1995; Fahey & Randolph, 1984; Law & Eden, 1980). This section is devoted to a selection of in situ methods to determine K'_0 .

2.4.1 Earth Pressure Cell

The earth pressure cell is a thin spade-shaped cell able to measure the total stress perpendicular to the bore hole direction as well as the pore pressure. The older versions did not have an integrated pore pressure measuring device, and therefore the pore pressure had to be measured by a piezometer in the vicinity of the earth pressure cell (Massarsch, 1975). When the horizontal effective stress is calculated from the measurements with the earth pressure cell, K'_0 can be determined if the overburden pressure is known from the density of the overburden soil.

The earth pressure cell is a sealed hydraulic system filled with oil. The oil pressure depends on the total stress acting on the cell. In the old models, there is a valve in the cell that opens when the applied pressure from a hose running to terrain level equals the pressure in the oil. A manometer connected to the pressurized hose measures the

pressure in the oil (Lunne & L'Heureux, 2016). In newer models, there is a vibrating wire sensor which reads the oil pressure (Lunne & L'Heureux, 2016) and the pore pressure (see Appendix C). Figure 2.7 shows the test setup for an old earth pressure cell without vibrating wire sensors.

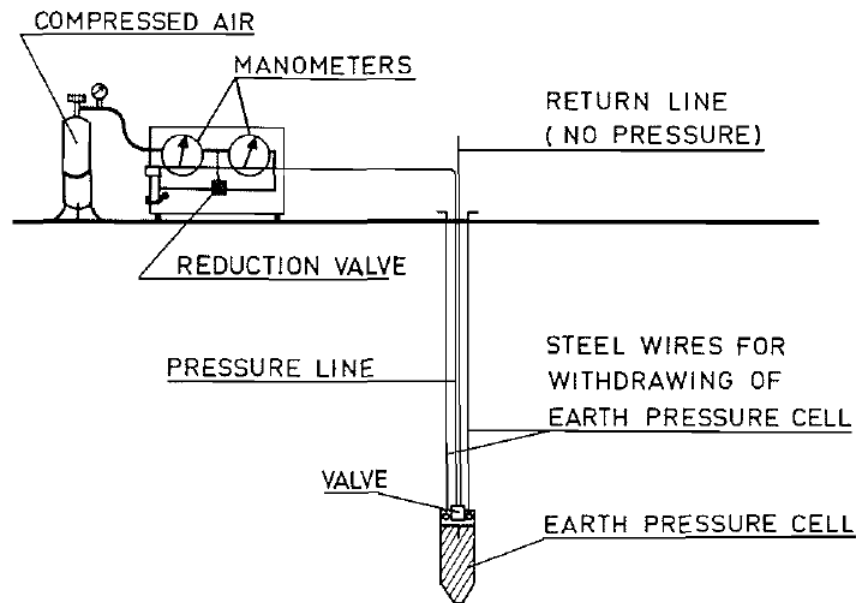


Figure 2.7: Example of old earth pressure cell equipment without vibrating wire sensors. Figure from Ryley and Carder (1995).

There exist several different earth pressure cell models with various geometries. For instance, Massarsch (1975) used a Glötzl cell with dimensions 200 mm x 100 mm x 4 mm. In Vaslestad (1989) a smaller cell with dimensions 140 mm x 70 mm x 4 mm is tested. There are also models with thicknesses of 5 mm (Tedd & Charles, 1981) and 6 mm (Ryley & Carder, 1995). It is desirable to make the cell as thin as possible, since the insertion of the cell into the soil causes disturbance. There is a tendency that the cells over-read due to the compaction of the adjacent soil during installation (Ryley & Carder, 1995), and this effect will be elaborated in a later paragraph. Vaslestad (1989) reported that miniature cells developed in England had given promising results with less over-read than the ordinary size cells.

The earth pressure cell is pushed into the ground by for instance a drill rig. It is possible to pre-drill a hole to avoid pushing the cell a long way, at least through firm layers (Ryley & Carder, 1995). Tedd and Charles (1981) showed that it is possible to push cells through 0.5 m of stiff London clay. Some of the models feature a protective cover, allowing the cell to be pushed even through soft silt or loose sand (Massarsch, 1975) without pre-drilling. If a hole is pre-drilled or a protective cover is used, it is important that the cell alone is pushed into undisturbed soil. There are different procedures suggested. In Tedd and Charles (1981) and Ryley and Carder (1995) the cell is pushed 0.5 m into the bottom of

the bore hole. Massarsch (1975) suggested that the cell should be pushed 0.3 m without the protective cover.

Next, some time is required in order to let increased pore pressure due to soil compaction around the cell dissipate (Hamouche et al., 1995). Massarsch (1975) found that after installation about a week was needed to dissipate the increased pore pressure caused by installation in soft clay. In stiff to very stiff London clay the measurements had almost stabilized after a month, but there were still a few minor changes during the next month in the deepest cells (Ryley & Carder, 1995). Tedd and Charles (1981) reported stable values in London clay down to 12 m depth after about a month. Since modern versions of the earth pressure cell often incorporate both total stress and pore pressure measurements in one unit, the changes caused by dissipation of excess pore pressure may be monitored continuously. An example of pressure versus time curves is given in Figure C.1 in Appendix C.

Tedd and Charles (1981) compared results obtained by earth pressure cells to Camkometer self-boring pressuremeter and Camkometer self-boring load cell for a London clay underlying Claygate beds, which is alternating clay and sand. In general, the earth pressure cells measured the highest total horizontal stress and the Camkometer self-boring load cell the lowest. The Camkometer self-boring pressuremeter measured on average something in between the other two. Tedd and Charles (1981) concluded that if the average of the measurements from both the Camkometers is assumed to be the true value of the horizontal stress, then the earth pressure cells tend to over-read. This is as one should expect from a push-in method causing compression of the soil around the cell. However, the reproducibility of the results from the earth pressure cell was greater than for the two Camkometers (Tedd & Charles, 1981).

In Tedd and Charles (1982) a laboratory study was conducted on the same Essex clay as in Tedd and Charles (1981). The results of both the in situ and laboratory studies are presented in Figure 2.8. When calculating the horizontal stress in the London clay, both an input value for an isotropic elastic material and a typical value for London clay was used. The laboratory results were within the scatter of the measurements made by the Camkometer self-boring pressuremeter for both the input values. The laboratory results supported the conclusions and measurements in Tedd and Charles (1981). If a correction for sampling disturbance had been made, this would have given a bit lower values of the horizontal stresses measured in the laboratory. This would bring the laboratory results a bit further away from the values of the horizontal stress measured by the earth pressure cells.

Some studies have investigated the amount of over-reading in the earth pressure cell measurements. Tedd and Charles (1983) suggested that the over-read could be taken as

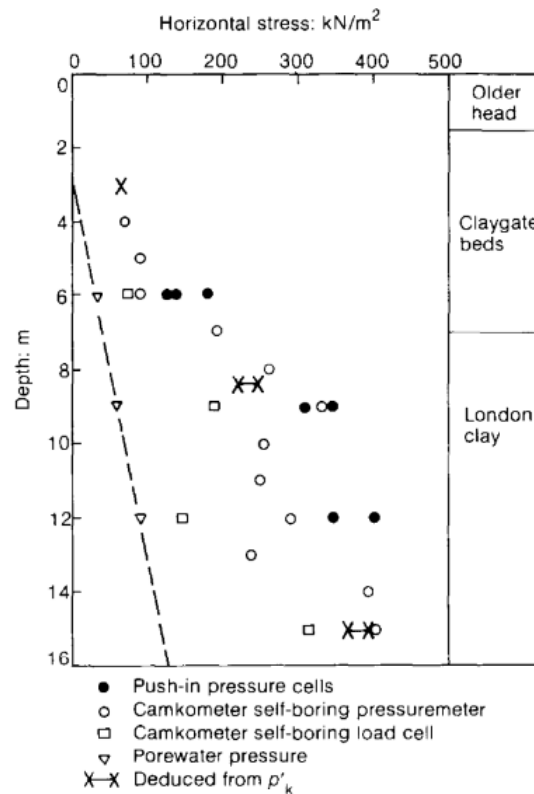


Figure 2.8: Comparison of the results from earth pressure cells, Camkometer self-boring pressuremeter, Camkometer self-boring load cell and laboratory investigations. Figure from Tedd and Charles (1982).

$0.5 \cdot s_u$. Carder and Symons (1989) reported that the over-read may be even larger for very stiff clays with $s_u > 150$ kPa. This conclusion was found by comparing earth pressure cell readings to the Camkometer self-boring pressuremeter and the dilatometer (presented in section 2.4.2).

Ryley and Carder (1995) performed a study of the over-read for the earth pressure cell when the stress measured was the well-defined overburden pressure. Six cells were installed horizontally at different depths from within the Heathrow Express trial tunnel. The cells were placed so far from the tunnel that the vertical pressure measured would be the actual well-defined overburden pressure. The unit weight of the soil above the cells was determined by laboratory tests.

Ryley and Carder (1995) concluded that for firm to stiff clays with s_u in the range of 40 to 150 kPa, the best fit of the over-read was $0.8 \cdot s_u$. For design purposes $0.5 \cdot s_u$ would be a more conservative value to use, while for research purposes $0.8 \cdot s_u$ would probably be better. For very stiff clay with $s_u > 150$ kPa the best fit would give an over-read significantly higher than $0.8 \cdot s_u$. The best fit line for very stiff clay is reported to be $4 \cdot (s_u - 120 \text{ kPa})$. The best fit lines for the over-read versus undrained shear strength are shown in Figure 2.9.

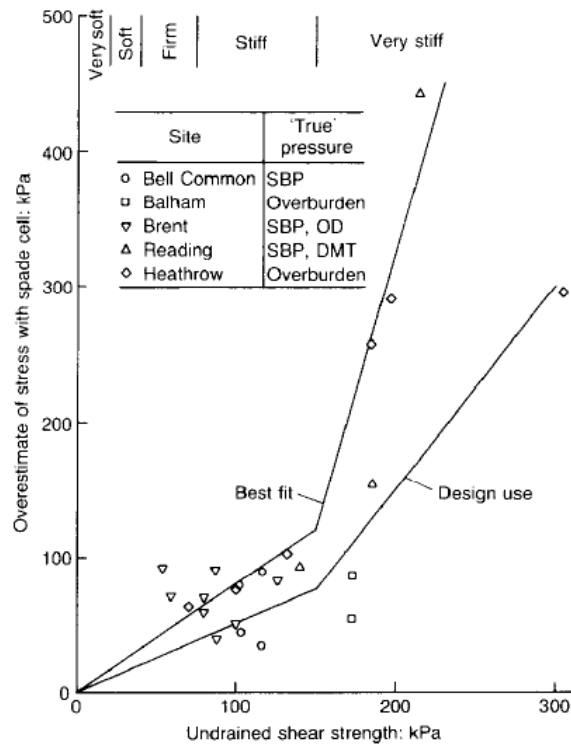


Figure 2.9: Over-read of earth pressure cell versus undrained shear strength with best-fit lines. Figure from Ryley and Carder (1995).

2.4.2 Seismic and Ordinary Dilatometer

The flat dilatometer was first introduced by Marchetti in 1980 (Marchetti, 1980). The dilatometer is shown in Figure 2.10a and features a circular membrane, which by the use of for instance compressed nitrogen may be inflated after penetrating the equipment to the desired depth. A more detailed view of the working principle is shown in Figure 2.10b. An audible signal is used to provide the operator with information about the inflation level of the disc (Marchetti, 1980). One pressure reading is taken before the membrane is inflated, called p_0 ; another called p_1 is taken after the membrane is extended 1.1 mm from the base (Marchetti, 1980). An additional pressure reading called p_2 may be taken when the membrane has moved back to the same position as p_0 is taken (Marchetti, Monaco, Totani, & Calabrese, 2006). For sands p_2 will be close to the equilibrium pore pressure, while for clays it will be somewhat higher (Campanella & Robertson, 1991). The different states are shown in Figure 2.10a. The dilatometer is typically penetrated another 20 cm before a new reading is taken. Based on the measured pressures, three key parameters may be determined: the material index I_D , the dilatometer modulus E_D and the lateral stress index K_D . An example of figures for these three key parameters registered at Flotten is given in Appendix D.

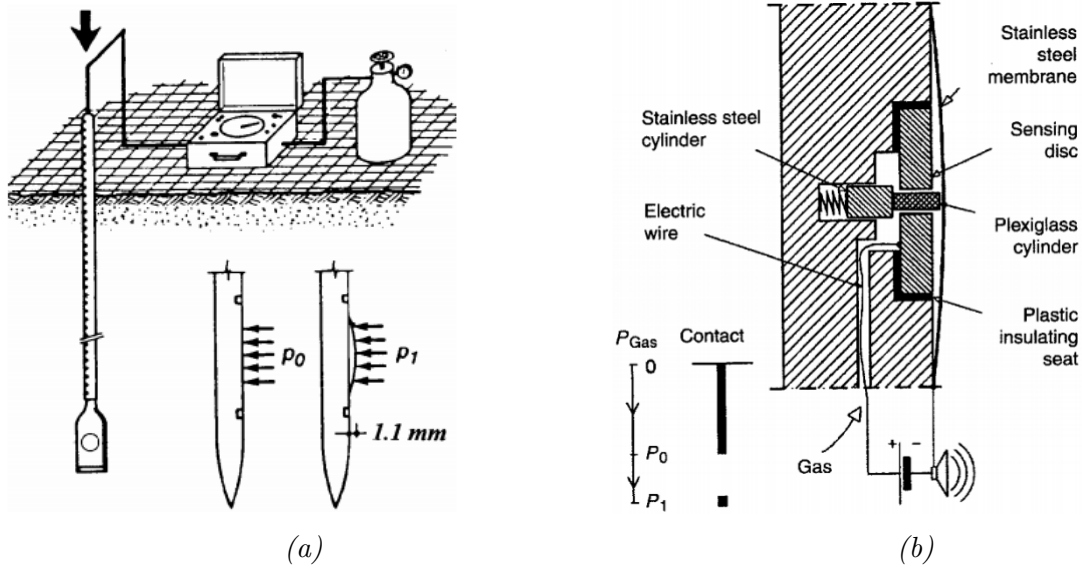


Figure 2.10: (a) The Marchetti dilatometer with equipment. (b) A more detailed view of the working principle of the measuring membrane. Figures from Marchetti, Monaco, Totani, and Calabrese (2006).

$$I_D = \frac{p_1 - p_0}{p_0 - u_0} \quad (2.7)$$

where u_0 is the initial pore pressure.

$$E_D = 34.7(p_1 - p_0) \quad (2.8)$$

$$K_D = \frac{p_0 - u_0}{\sigma'_{v0}} \quad (2.9)$$

where σ'_{v0} is the effective overburden pressure.

Based on values from Equation 2.9, the original Equation 2.10 relating the lateral stress index to the coefficient of earth pressure at rest is given below (Marchetti, 1980). This equation was originally meant for sand, but may also be used to give an approximate value of K'_0 in clay (Marchetti, 2015).

$$K'_0 = \left(\frac{K_D}{\beta_k} \right)^{0.47} - 0.6 \quad (2.10)$$

where β_k may vary between 3 and 0.9. The value of 1.5 was originally proposed by Marchetti (1980) and may be used for intact insensitive clays (Hamouche et al., 1995). Later Hamouche et al. (1995) used the value 2 for intact sensitive clays.

Furthermore, based on several field and lab investigations at different NGI sites, Lacasse and Lunne (1989) stated that the original relationship proposed by Marchetti (given in Equation 2.10) tends to overestimate the K'_0 value. The authors proposed Equation

2.11 below for Norwegian clays, with $m = 0.44$ for highly plastic clays and $m = 0.64$ for low plastic clays (Lacasse & Lunne, 1989).

$$K'_0 = 0.34(K_D)^m \quad (2.11)$$

Additionally, Marchetti et al. (2006) suggested the Equation 2.12 as a way to estimate OCR based on the K_D -parameter obtained from a dilatometer test.

$$OCR_{DMT} = (0.5K_D)^{1.25} \quad (2.12)$$

Since the first introduction of the dilatometer, much research has centered around finding general correlations to relate dilatometer test results with other index properties (P. Mayne & Martin, 1998). Despite this, the major drawback of the dilatometer continues to be the use of uncertain empirical correlations to determine material properties and stress states (Lacasse & Lunne, 1989). As several investigations have found, the correlations have limited value across different sites (Ku & Mayne, 2013) and may be dependant on the geological history of the deposit investigated (Roque, Janbu, & Senneset, 1988). Despite this apparent lack of consistency, Marchetti has kept his original correlation given in Equation 2.10 (Lunne & L'Heureux, 2016). Also, in P. Mayne and Martin (1998), the self-boring pressuremeter, total stress cell or hydraulic fracturing is recommended instead of the dilatometer to determine K'_0 as these methods represents a more direct approach without relying on empirical correlations. Some authors (see for example P. Mayne and Martin (1998)) have also indicated that the dilatometer is best suited for usage in softer clays, as a slight over-read is apparent when used in stiffer clays (P. Mayne & Martin, 1998; Lunne & L'Heureux, 2016).

On the other hand, several investigations have found a quite good fit when comparing values of K'_0 obtained from the dilatometer with values obtained with other test equipment. Hamouche et al. (1995) found a good fit between results obtained with the dilatometer and the self-boring pressuremeter (Hamouche et al., 1995; F. H. Kulhawy & Mayne, 1990).

P. Mayne and Martin (1998) stated that the flat dilatometer must be considered a rather exploratory tool, which should be used with site-specific calibrations. The results should preferably be compared to results gained from for example the self-boring pressuremeter. Lutenegger (1990) proposed that the dilatometer may be used as a total stress cell after being installed at a desired depth. The pressure reading p_0 may be taken as the pressure required to overcome the horizontal stresses in the soil. One challenge is that the thickness of the dilatometer may lead to an increased pore pressure dissipation period after installation (P. Mayne & Martin, 1998).

The amount of disturbance and excess pore pressure generated have also been investigated in several papers. Lacasse and Lunne (1989) stated that a flat dilatometer blade is likely to cause less disturbance compared to that created by a cylindrical probe. Comparing the dilatometer with a piezometer used for hydraulic fracturing (see section 2.4.3), Hughes and Robertson (1985) stated that a cylindrical piezometer tip will create a cylinder of compacted soil around the tip. This complicate measurements of an undisturbed horizontal total stress due to disturbance of the soil, as well as arching effects which may result in too low radial stresses acting on the piezometer. Arching effects are closer described in section 6.2.3.1.

Furthermore, Roque et al. (1988) determined that insertion of a dilatometer blade causes soil disturbance in a distance of up to 7 mm from the blade itself. The authors also pointed out the generation of excess pore pressure and hence reduction in effective stresses in saturated soils (Roque et al., 1988). The effect of this stress change is unknown, as it may lead to elastic deformation, failure or something in between.

The combination of the flat dilatometer and the ability to measure shear wave velocities was first proposed by Hepton in 1988 (Marchetti, Monaco, Totani, & Marchetti, 2008). The equipment resembles the flat dilatometer in shape and appearance, but the probe shaft is slightly elongated, making room for two seismic receivers with an individual distance of 500 mm. The working principle of the equipment resembles the seismic cone (SCPT) (Marchetti et al., 2008), as described in section 2.4.7, and makes it possible to combine dilatometer and shear wave measurements as the probe is advanced into the ground.

2.4.3 Hydraulic Fracturing

The method of hydraulic fracturing has proven a rather versatile method, suitable both for rock and soil application (Andersen, Rawlings, Lunne, & By, 1994; Bjerrum & Anderson, 1972). Through several investigations, the method has gained reputation as one of the more reliable methods for determining K'_0 , especially in soft clays (Lunne & L'Heureux, 2016).

The technical background for the hydraulic fracturing method is rather simple. By injecting water into a borehole, the pressure inside the borehole will increase until a crack is generated (Bjerrum & Anderson, 1972; Andersen et al., 1994). For the crack to open, the water pressure has to overcome the tensile strength of the soil and be larger than the horizontal total stress. If conditions below ground water is assumed, the total horizontal stress consists of both the horizontal effective stress and the pore pressure. Both pressures will counteract the pressure resulting from water injected into the borehole. It should however be noted that, the test material must have a limited permeability in order for

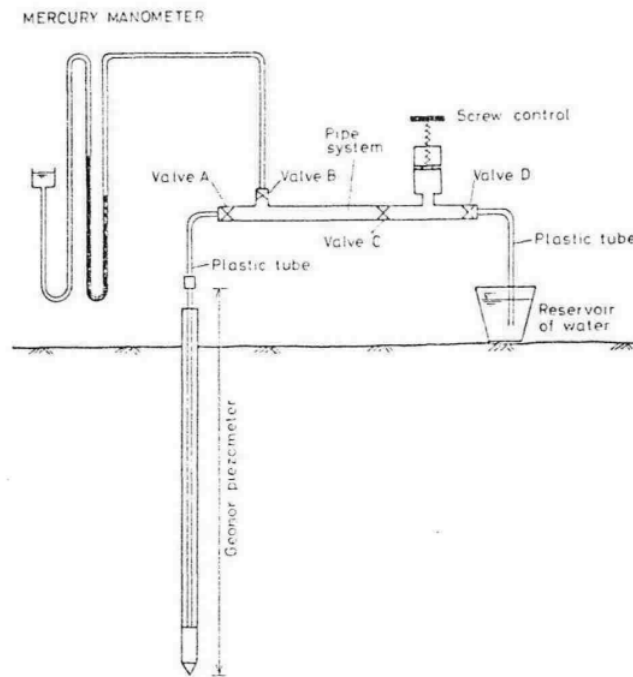


Figure 2.11: Equipment used for hydraulic fracturing. Figure from Bjerrum and Anderson (1972).

fractures to open. This limits the method to use in fine-grained materials. In coarser material, the injected water will tend to drain away from the tip without causing any defined crack (Lefebvre et al., 1991; Bjerrum & Anderson, 1972).

Initial testing with hydraulic fracturing as a way of determining the in situ horizontal stress state was performed by Bjerrum and Anderson (1972), by using a piezometer to inject and pressurize fluid inside a borehole. Similarly as for the earth pressure cells, the piezometer should be left in the ground for a time period before measurements are taken, in order for any excess pore pressure caused by installation to dissipate (Bjerrum & Anderson, 1972; Lefebvre et al., 1991). The equipment used by Bjerrum and Anderson (1972) is shown in Figure 2.11. First, by increasing the water pressure, a crack is generated. This will greatly increase the water flow and the pressure is reduced until the fracture closes. Based on continuous measurements of both water flow and the water pressure inside the borehole, the pressure may be determined both when a crack opens and closes (Bjerrum & Anderson, 1972). A typical pressure against time curve is shown in Figure 2.12. To reduce the effect of disturbance caused by the piezometer installation, Bjerrum and Anderson (1972) proposed the closing pressure as a more reliable indication of the horizontal total stress state.

The original mechanism believed to explain hydraulic fracturing is that an increase in pore pressure inside the borehole will reduce both the minor and major stress equally (Panah & Yanagisawa, 1989; Lefebvre et al., 1991; Bjerrum & Anderson, 1972). As

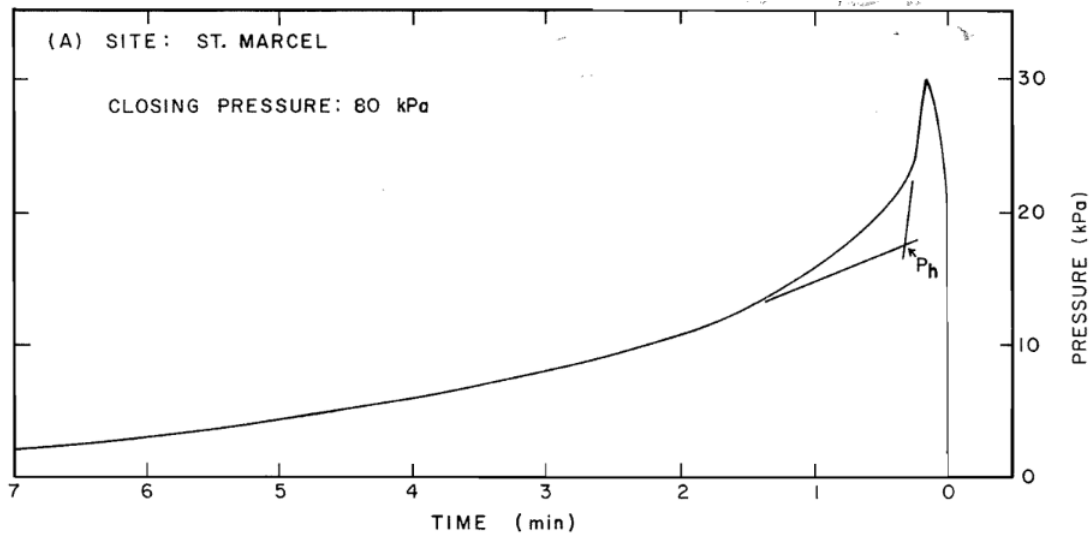


Figure 2.12: Typical pressure against time curve. Please note the direction of the horizontal axis. Figure from Lefebvre, Bozozuk, Philibert, and Hornych (1991).

the minor principal stress will be the first to become tensile, the cracks will emerge perpendicular to the minor principal stress direction. For an approximately normally consolidated uniform soil deposit in flat terrain, the minor principal stress direction will be the horizontal direction.

The method has been closer examined in several articles. Lefebvre et al. (1991) determined K'_0 values as high as 4.0 at the five sites tested. This supported their proposal that higher OCR would give K'_0 values above one. To further investigate both fracturing direction and the effect of disturbance, Lefebvre et al. (1991) also recovered the soil material in which the piezometer tip was penetrated, by using a Sherbrooke block sampler. During these examinations, the authors observed vertical fractures in samples from all testing sites (Lefebvre et al., 1991).

The discovery of vertical fissures in combination with values of K'_0 larger than one, contradicts the fundamental hypothesis of the hydraulic fracturing method, where the fracture direction is directly linked to the minor principal stress direction (Bjerrum & Anderson, 1972). However, as the findings in Lefebvre et al. (1991) suggest, the minor principal stress direction may not be the determining factor of the directions of the fissures.

Consequently, Haimson (1978) stated that in rock mechanics, a long cylindrical borehole will always result in initial vertical fracturing, independent of the major and minor stress directions. Similarly, by using cavity expansion theory, Massarsch (1978) proposed that hydraulic fracturing in clays could be viewed as an expansion of an infinitely long cylindrical cavity. Thus, the increase in pressure caused by injected water will try to expand the vertical borehole and hence create vertical fractures, independent of the minor and major stress directions. In addition, this new proposal is also able to explain one of

the findings made in the article by Lefebvre et al. (1991), namely an apparent dependency between the fracturing direction and the length of the piezometer tips. Shorter tips gave a combination of both vertical and horizontal fractures, while longer tip lengths gave mostly vertical cracks. As the short tip lengths will tend to concentrate the water pressure over a shorter vertical distance, a horizontal crack is more likely to occur with a short tip length compared to a longer tip.

The amount of disturbance caused by installation of the measuring equipment is a key topic. Hence, Lefebvre et al. (1991) performed fall cone tests on the retrieved block samples mentioned earlier, see Figure 2.13, to get an indication of how far away from the tip of the measuring equipment the soil had been disturbed. These tests demonstrated that the fractures had extended into less disturbed soil, further away from the tip of the equipment (Lefebvre et al., 1991).

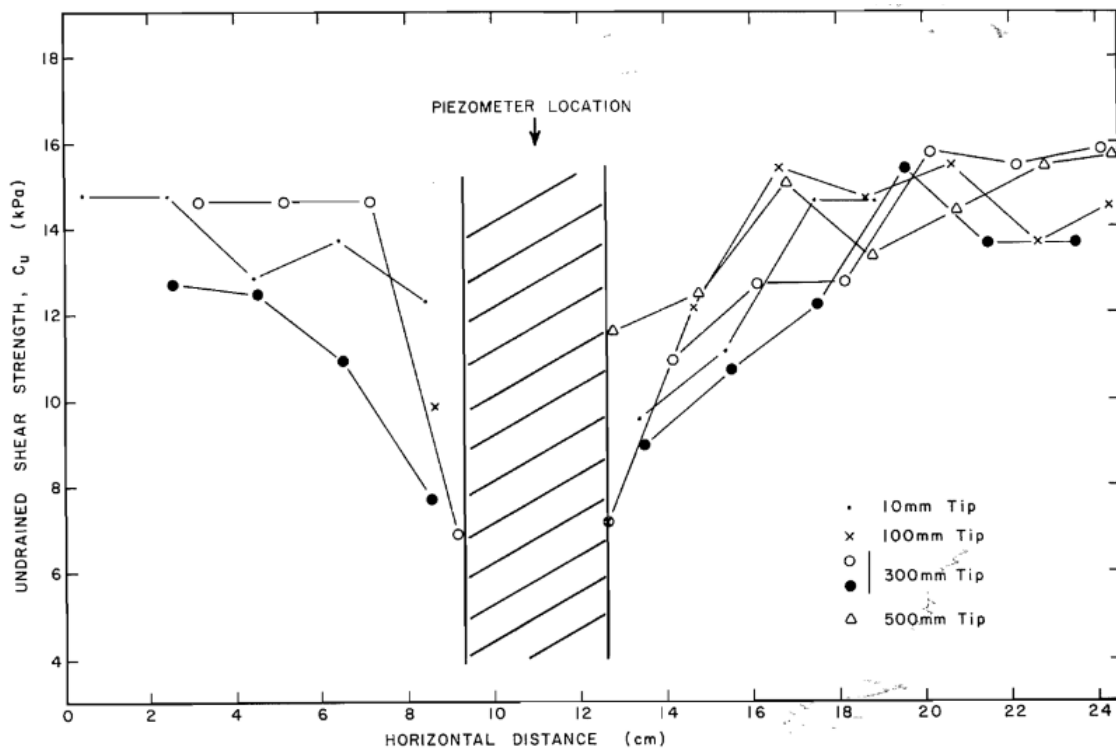


Figure 2.13: Results from fall cone tests close to piezometer location, Canadian clay. Figure from Lefebvre, Bozozuk, Philibert, and Hornych (1991).

2.4.4 Stepped Blade

A concept sharing some similarities with the earth pressure cell, is the Iowa Stepped Blade, first introduced by Richard Handy in the 1980s (Lunne & L'Heureux, 2016). The tool consists of a long blade with varying thickness. Each thickness level contains a membrane, which measures the pressure, just as for the earth pressure cell (Vaslestad, 1989). Extrapolation is used to find the stress at an imagined zero blade thickness, see

Figure 2.14. This stress is assumed to represent the in situ total horizontal earth pressure (Hamouche et al., 1995; Handy, Mings, Retz, & Eichner, 1990). Some articles have found that the extrapolation prohibits a clearly defined zero value, making the horizontal stress determination difficult (Lunne & L'Heureux, 2016). Although it is argued by Handy et al. (1990) that the blade is suitable for use both in clay, silt and sand, others report that the blade has proven to be quite easily damaged during testing (Lutenegger & Timian, 1986).

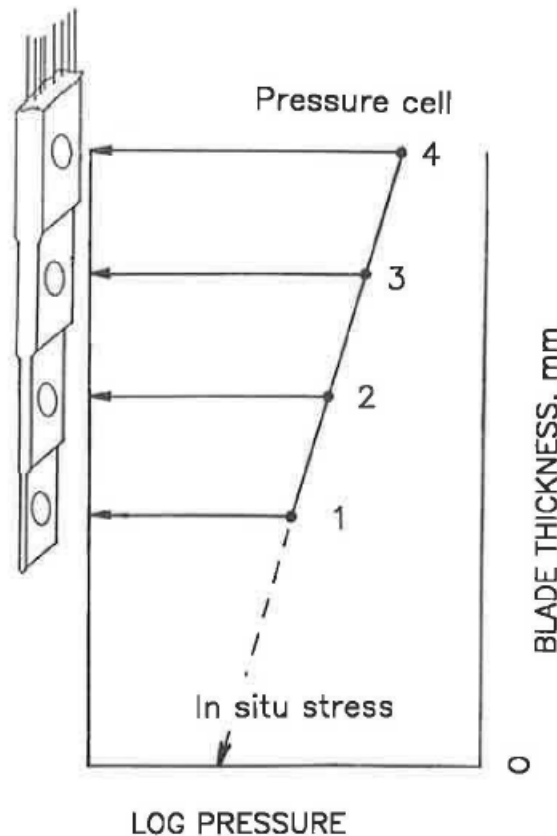


Figure 2.14: The stepped blade equipment and the extrapolation used to determine in situ horizontal stress. Figure from Handy, Mings, Retz, and Eichner (1990).

2.4.5 Cone Penetration Tests

Several attempts were made in the 1980s to correlate lateral stress measured on a friction sleeve of a CPT probe to K'_0 (Lunne, Lacasse, Rad, & Decourt, 1990). None of the attempts were successful enough to be in use today (Lunne & L'Heureux, 2016). In 2014, researchers at University of British Columbia presented a lateral stress seismic piezocone. A schematic overview of the equipment is shown in Figure 2.15. The equipment features a "button" sensor for measurement of lateral stress. Although the researchers believe that the method may give reliable values of the lateral stress, a lot of testing is required before it can be concluded whether or not the measured lateral stress can be correlated to K'_0 in a satisfactory way (Lunne & L'Heureux, 2016).

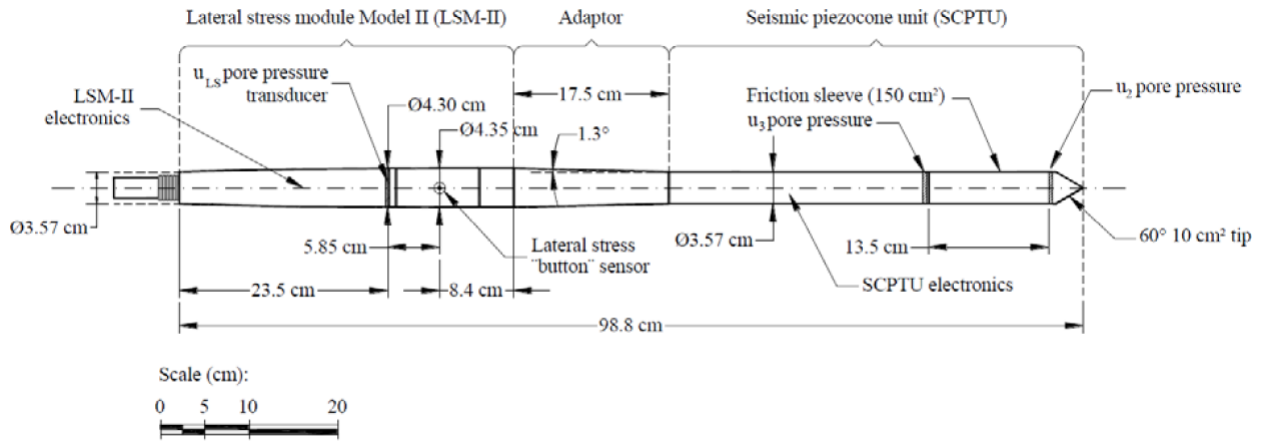


Figure 2.15: Schematic overview of the lateral stress seismic piezocone. Figure from Lunne and L'Heureux (2016).

Sully and Campanella (1991) investigated the possibility of correlating K'_0 to the measured change in pore pressure from the tip u_1 to behind the tip u_2 , normalized by the initial effective overburden stress σ'_{v0} . Sully and Campanella (1991) concluded that for a specific site there seems to be a linear relationship between K'_0 and $\frac{u_1 - u_2}{\sigma'_{v0}}$. However, the scatter in the measurements between different sites was too large to conclude with a universally valid linear relationship (Sully & Campanella, 1991).

2.4.6 Self-boring Pressuremeter

Another approach to the challenges of in situ stress measurements is taken by the pressuremeter, and more recently the self-boring pressuremeter. A probe containing three inflatable rubber membranes located with even distance around the probe cylinder is penetrated into the ground. At the desired depth, the membranes are inflated with the use of nitrogen. The expansion of the membranes is measured by three expandable strain arms (Fahey & Randolph, 1984). The horizontal stress state may be taken as the pressure required for the initial expansion of the membranes (Hamouche et al., 1995; Ku & Mayne, 2013). The idea to use expanding membranes to measure horizontal stress is similar to the dilatometer.

The installation of the pressuremeter is often complicated by the soil conditions, as the equipment and membranes are quite fragile. As pre-drilling will disturb the soil to some extent (Vaslestad, 1989), the self-boring pressuremeter was developed, see Figure 2.16. In addition to the pressuremeter measuring system, a cutting shoe encasing a rotating cutter bit is mounted at the far end of the probe. As the probe is lowered, the cutter bit removes material; the material is brought to the surface by a water flushing system (Fahey & Randolph, 1984).

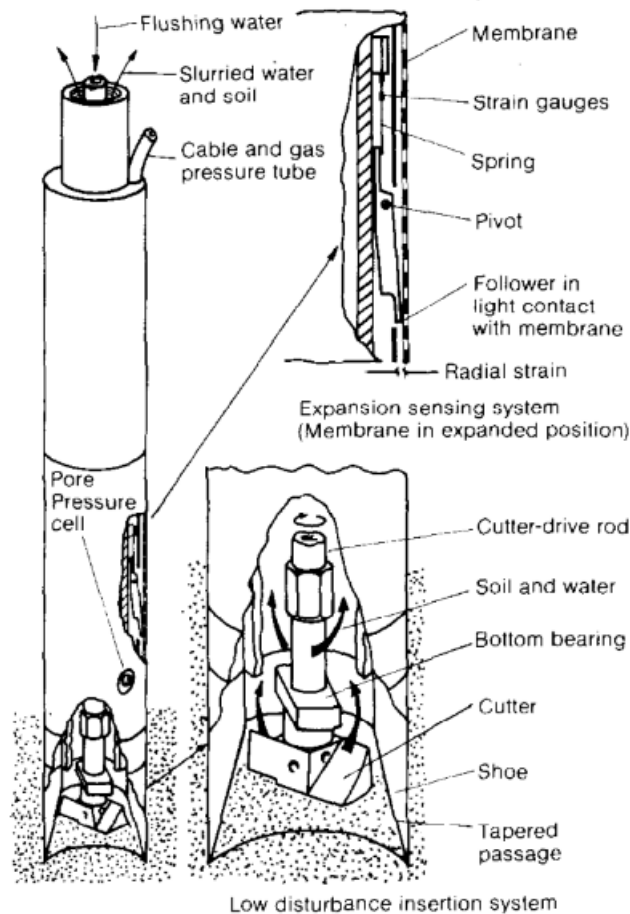


Figure 2.16: Detailed view of the Cambridge self-boring pressuremeter. Figure from Fahey and Randolph (1984).

Since the first introduction, the self-boring pressuremeter has been utilized in several different investigations and materials. Hamouche et al. (1995) argue that the method represents a less intrusive way of measuring the horizontal stress state, as the self-boring ability means less soil disturbance; the soil is removed rather than being compacted by the installation of the probe. However, some authors have argued that the process of removing the soil during installation modifies the stress field around the probe, and hence causes disturbances of unknown magnitude (Ghionna, Jamiolkowski, & Lancellotta, 1982).

Hamouche et al. (1995) used the Camkometer in combination with hydraulic fracturing and a dilatometer at different clay sites in Eastern Canada. Despite a rather large variation in the data material, Hamouche et al. (1995) found that for an OCR below 4, the three different methods gave quite similar results.

The large variation in the data acquired from self-boring pressuremeters has also been observed by others (see for example Tedd and Charles (1981)), and have by some authors been linked to natural variations of the soil material (Hamouche et al., 1995). These variations were also observed by W. F. Anderson and Pyrah (1991), when using the equipment in artificially consolidated clay under isotropic conditions in the laboratory.

W. F. Anderson and Pyrah (1991) proposed individual differences in membrane stiffnesses as a possible explanation. Furthermore, Hughes and Robertson (1985) stated that the quality of the results is highly dependant on the operator performing the test.

Despite some variation in the obtained results, the self-boring pressuremeter is often mentioned together with earth pressure cells and hydraulic fracturing as one of the more reliable ways of determining the horizontal stress state (P. Mayne & Martin, 1998; Ku & Mayne, 2015, 2013). For testing at a site with OCR above 5, the values gained from hydraulic fracturing and the self-boring pressuremeter deviated with about 20 %. This was explained by changes in fracture direction in such overconsolidated clays (Hamouche et al., 1995).

2.4.7 Shear Wave Measurements

For the methods presented so far, the amount of disturbance caused by penetrating the equipment into the material has been questioned (see for instance Tedd & Charles, 1981; Fioravante et al., 1998). Fioravante et al. (1998) found a general lack of consistency when comparing results obtained with the different intrusive field methods for measuring the horizontal stress state. Consequently, some methods not requiring penetration into the soil materials have been proposed (Fioravante et al., 1998; Ku & Mayne, 2013).

One that has gained quite some attention is the use of shear wave velocity measurements. The method is based on seismic waves and rely on the connection between the wave velocity and the stress state of the soil (Fioravante et al., 1998). Such measurements may be carried out by the use of a seismic cone penetrometer (SCPT) or seismic dilatometer (Ku & Mayne, 2013). This equipment is quite similar to the original CPTu and dilatometer, but is additionally fitted with one or two shear wave receivers (Sully & Campanella, 1995). When the probe is at the desired depth, a hammer and anvil at the surface is used to generate the shear waves. The time necessary for the waves to reach the seismic receiver in the ground is registered by a data acquisition system that is activated when the hammer strikes the anvil. Subsequent measurements at different depths makes the generation of a shear wave profile possible (Sully & Campanella, 1995). A typical view of the test equipment is shown in Figure 2.17. Shear wave velocity tests are divided into two types. These are vertical downhole tests, like for instance the seismic dilatometer test, and horizontal crosshole tests where the shear waves move between different boreholes (Ku & Mayne, 2013).

Previous research has indicated that the shear wave velocity is dependent on the effective stress state in the soil, hence Fioravante et al. (1998) proposed that the value of K'_0 may be determined by comparing the shear wave velocity in the vertical and horizontal direction. This was also supported by Ku and Mayne (2013). Furthermore, Ku and

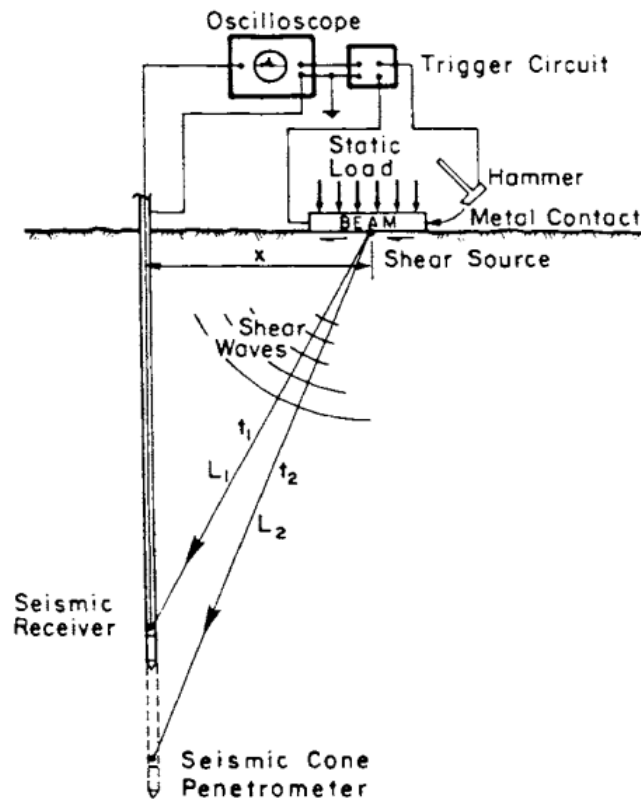


Figure 2.17: Example of equipment used for shear wave measurements. Slightly modified figure from Campanella and Stewart (1992).

Mayne (2015) proposed a method for determining the OCR of a soil deposit (Lunne & L'Heureux, 2016). With the OCR known, Equation 2.29 may be utilized as a method for determining the value of K'_0 . On the other hand, Fioravante et al. (1998) pointed out that the final value of K'_0 is easily affected by even small errors in the shear wave velocity determination. The authors also argued that the method is less suited for layered deposits, as wave reflections may make a unique determination of shear wave velocity impossible.

2.4.8 Field Vane

Combining a field vane test with a triaxial CAUc test, the value of K'_0 for a clay may be found (Aas et al., 1986). Since the minor principal effective stress at failure σ'_{3f} is horizontal in both tests, σ'_{3f} found from the two methods may according to Aas et al. (1986) be assumed to be equal.

In the triaxial cell the sample is consolidated to the assumed in situ stress situation. From the shearing phase, the effective stress path is plotted and the minor principal effective stress at failure σ'_{3f} is determined.

The in situ stress situation before performing the field vane test is as in Figure 2.18 (a), assuming that insertion does not alter the stress situation. During rotation of the field

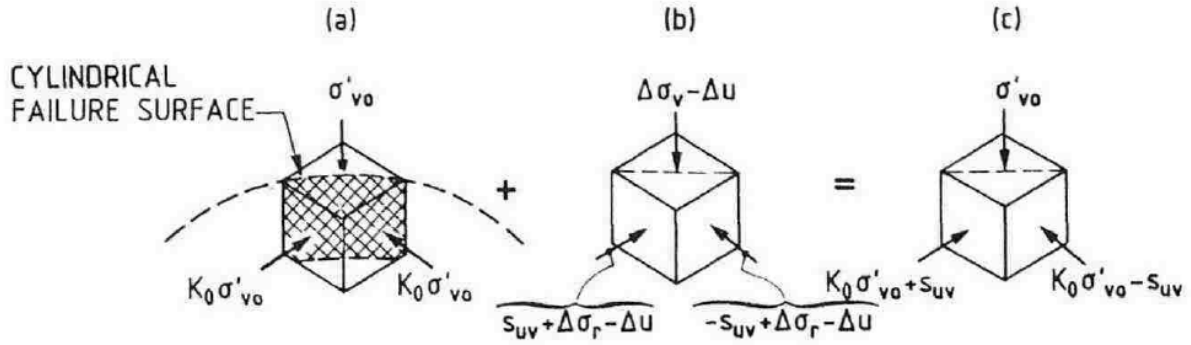


Figure 2.18: Principal stress situation before vane test (a), additional stresses during test (b) and resulting failure stresses (c). Figure from Aas, Lacasse, Lunne, and Hoeg (1986).

vane, additional normal stresses on planes at $\pm 45^\circ$ angles from the vertical cylindrical failure plane are changed vertical total stress $\Delta\sigma_v - \Delta u$, changed radial total stress $\Delta\sigma_r - \Delta u$ and undrained shear strength s_{uv} as in Figure 2.18 (b). If the clay has a residual strength s'_{uv} after failure, this will add to the undrained shear strength to give the stress situation after remoulding. The clay is assumed to behave undrained during vane rotation.

From geometrical considerations, it is assumed that the height and diameter of the failure zone is constant during the vane test. This implies that the thickness of the failure zone is constant, and the stress situation is similar to that in a direct shear test. This assumption is supported by Kimura and Saitoh (1983), which took radiographs of plastic clay during vane rotation in the laboratory. Under direct shear the effective stresses remain unchanged, and therefore $\Delta\sigma_v - \Delta u = 0$ and $\Delta\sigma_r - \Delta u = 0$. The resulting effective stress condition at failure in field vane testing is therefore as in Figure 2.18 (c). After remoulding, s'_{uv} must be added to the stress situation if the clay has residual strength. This means that the minor principal stress after remoulding is given by Equation 2.13.

$$\sigma'_{3f} = K'_0 \sigma'_{v0} - s_{uv} + s'_{uv} \quad (2.13)$$

By rearranging Equation 2.13 and substituting σ'_{3f} by the minor principal effective stress at failure from triaxial testing, K'_0 may be determined by Equation 2.14.

$$K'_0 = \frac{\sigma'_{3f}}{\sigma'_{v0}} + \frac{(s_{uv} - s'_{uv})}{\sigma'_{v0}} \quad (2.14)$$

Determination of K'_0 by Equation 2.14 can be illustrated graphically in a $\frac{\sigma'_v - \sigma'_h}{2\sigma'_{v0}}$ versus $\frac{\sigma'_v + \sigma'_h}{2\sigma'_{v0}}$ plot, as shown in Figure 2.20. For quick clay there is almost no residual strength, and therefore $s'_{uv} = 0$ in the upper figure.

The development in geotechnical engineering since Aas et al. (1986) was published raises doubt about the method presented in this section. In more recent years it is quite

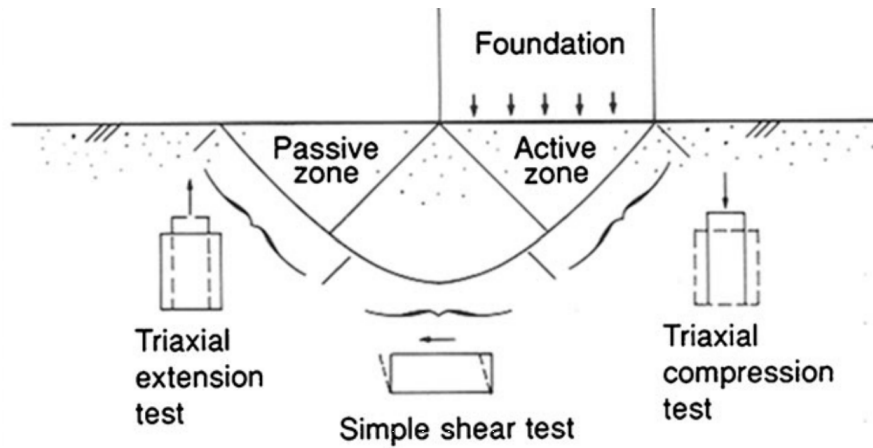


Figure 2.19: Illustration of active, direct and passive state. Figure from Grimstad, Andresen, and Jostad (2012).

common to distinguish between undrained shear strength in active, direct and passive state. Active state resembles a triaxial compression test, while passive state resembles a triaxial extension test. Direct state is found in shear box experiments (Grimstad, Andresen, & Jostad, 2012). This is illustrated in Figure 2.19. The failure mechanism around the field vane in situ is quite similar to that in a shear box experiment (Gylland, Jostad, Nordal, & Emdal, 2013). This means that instead of comparing the field vane to a triaxial compression test, it would be more correct to compare it to the minor principal stress σ'_{3f} from a shear box experiment performed with shear strains in the horizontal plane. The lack of considering different undrained shear strengths under different strain conditions suggests that the reasoning by Aas et al. (1986) for the field vane method is outdated.

The assumption by Aas et al. (1986) that the failure surface around the field vane is circular and has a clearly defined geometry is questioned by Roy and Leblanc (1988) for soft clay and more recently by Gylland, Jostad, et al. (2013) for sensitive clay. These authors found that the failure surface is not circular at the peak strength, which is the stress state that defines s_{uv} in Equation 2.14. The failure surface was found to be more like a rounded square at the peak strength Gylland, Jostad, et al. (2013). Also, the thickness of the shear zone is not necessarily constant during shearing, due to the non-smooth shear surface (Gylland, Jostad, et al., 2013). The above aspects of the failure geometry suggest that the assumptions made by Aas et al. (1986) need modifications, at least for sensitive clays.

The minor principal stress σ'_{3f} found from a triaxial test is according to Aas et al. (1986) totally dependent on the stress history and the consolidation stresses. This means that the consolidation parameters chosen for the consolidation of the triaxial test will influence the resulting σ'_{3f} . This is a weakness of the method presented in this section.

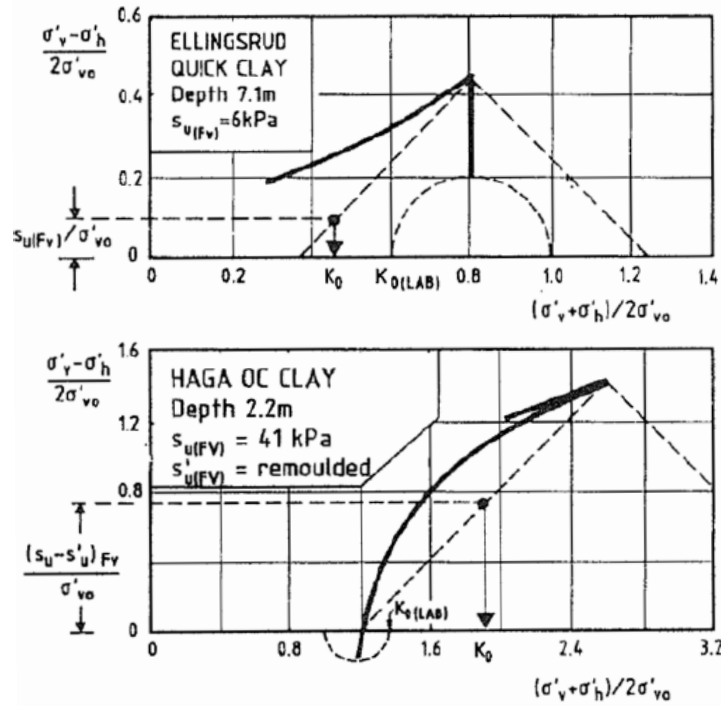


Figure 2.20: Graphical construction to determine K'_0 from field vane test. Figure from Aas, Lacasse, Lunne, and Hoeg (1986).

Aas et al. (1986) compared field vane tests with hydraulic fracturing, dilatometer and self-boring pressuremeter tests for clay under the weathered zone at Onsøy and Haga, and found a very good fit between the different methods for determining K'_0 . Even though the method have proven to produce good results at Onsøy and Haga, new knowledge questions the validity of the method. Since the assumptions that the method depends on are somewhat questionable, the results obtained with the method should be treated with care.

s_{uv}

2.5 Laboratory Methods

Several methods to determine the value of K'_0 in geotechnical laboratories have been developed (Ku & Mayne, 2015). This section will primarily focus on the split-ring oedometer, the oedotriaxial procedure as well as two different techniques proposed by Tavenas, Blanchette, Leroueil, Roy, and Rochelle (1975) and Becker et al. (1987).

To be able to use laboratory methods to predict the in situ K'_0 value, the stress state of the samples should be as undisturbed as possible (Ku & Mayne, 2015). This often calls for both time consuming and expensive sampling equipment (Fioravante et al., 1998; Ku & Mayne, 2015) like the block sampler, which is known to reduce the influence of

sample distribution (Watabe et al., 2003; Karlsrud & Hernandez-Martinez, 2013). In addition, the samples are vulnerable to disturbance during transport between the site and the laboratory (Ku & Mayne, 2015).

2.5.1 Work Criterion in Oedometer

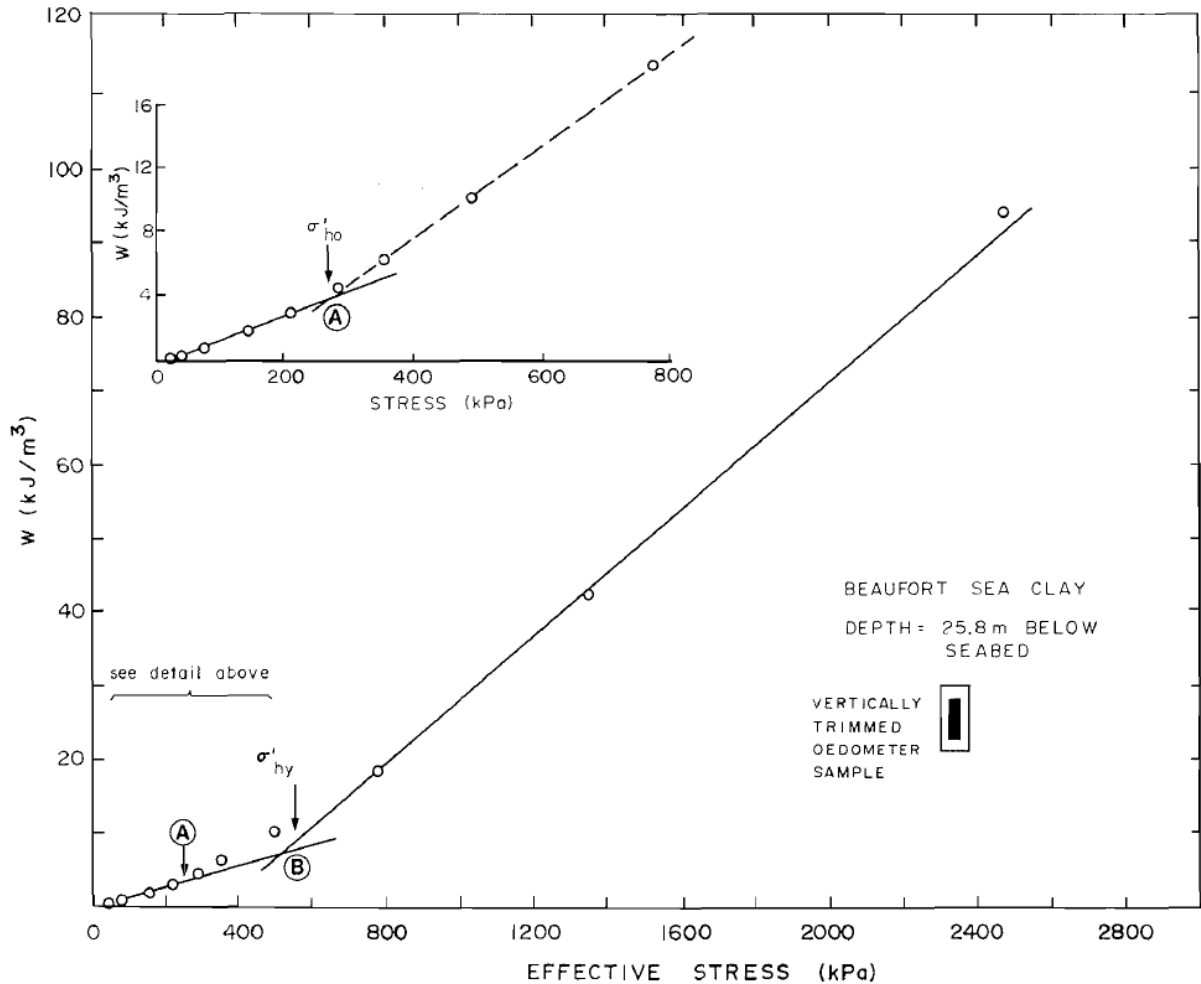


Figure 2.21: Cumulated work per unit volume plotted against effective stress for oedometer test. Figure from Becker, Crooks, Been, and Jefferies (1987).

Becker et al. (1987) suggested a method to determine in situ and yield stresses based on a work criterion applied to oedometer tests. If the in situ effective horizontal stress may be calculated from this method, K'_0 may be calculated when the overburden pressure is known. In the method, cumulated work per unit volume is plotted against effective stress as shown in Figure 2.21. The increments of work are calculated from Equation 2.15 where σ'_i and σ'_{i+1} are the effective stresses and ε_i and ε_{i+1} are incremented natural strains at the beginning and end of the increment, respectively.

$$\Delta W_{oed} = \frac{\sigma'_i + \sigma'_{i+1}}{2} (\varepsilon_{i+1} - \varepsilon_i) \quad (2.15)$$

In Figure 2.21 the curve has been approximated as three linear lines. The first line segment is from the beginning of the test and up to the in situ stress. The second dotted line segment is where the test results start deviating from the approximated linear relationship in the beginning. The intersection of the two line segments is taken as the in situ stress. The authors argue that the in situ stress may be found in this way because the test will show a stiffer response below the in situ stress due to changes in stress condition and sample disturbance. This statement will be discussed in section 6.3.3.

Above p'_c the test data are represented by a different linear line segment. p'_c is interpreted as the intersection between the first and the last line segment. The authors argue that the intersection represent the transition from small strain to large strain response, which is a way to view p'_c . This way of thinking is in accordance with the Cam-Clay model, which uses two different stiffnesses above and below p'_c (Schofield & Wroth, 1968).

2.5.2 Oedotriaxial

The triaxial test apparatus can be run with a K'_0 consolidation procedure (Watabe et al., 2003; Janbu & Senneset, 1995). During the consolidation phase, the cross-sectional area is kept constant like in an oedometer by increasing the cell pressure. The cell pressure is adjusted so that the amount of pore water expelled is equal to the volume change caused only by the vertical strain. Equation 2.16 gives the relation between expelled pore water ΔV and the vertical strain ε_v . The cross-sectional area of the sample is taken as 2.29 cm^2 (see also Equation 4.7), and the value of the vertical strain in percent and deformation in mm will be the same since the sample height is 10 cm. Equation 2.16 is only true if the sample is fully saturated at the beginning of the test. If not, the compressible air in the sample will affect the test results.

$$\Delta V = 2.29 \varepsilon_v \quad (2.16)$$

The inclination of the test graph in the weight versus ε_{axial} diagram may be used to assess whether the test has been run under oedometer conditions. Under the assumption of fully saturated sample from the beginning of the test, the oedotriaxial test is performed under oedometer conditions if the inclination of the graph is in accordance with Equation 2.16.

Since the consolidation phase is drained, the cell pressure is equal to the horizontal effective stress in the sample and the sum of the piston force and the cell pressure equals the vertical effective stress. From the measured values of the piston force and cell pressure a value of K'_0 can be calculated from Equation 2.17 (Janbu & Senneset, 1995).

$$K'_0 = \frac{\sigma'_{30} + a}{\sigma'_{10} + a} = \frac{1}{1 + 2S_0} \quad (2.17)$$

where S_0 is the inclination of the oedotriaxial stress path in the NTNU plot, a is attraction, and σ'_{10} and σ'_{30} are vertical and radial effective stresses, respectively. The S_0 line should according to the above equation pass through $-a$ on the σ'_3 axis in the NTNU plot (Janbu & Senneset, 1995). Note that the above definition of K'_0 is not the same as the definition K'_0 presented in Equation 2.2 used in the rest of this thesis. The implications of this will be addressed in section 6.3.5.

In addition, the oedometer stiffness modulus M may be calculated from Equation 2.18 (Janbu, 1991). Plotting M against vertical effective stress σ'_1 will give the possibility to determine a value for p'_c (Janbu, 1970).

$$M = \frac{\Delta\sigma'_1}{\Delta\varepsilon_1} \quad (2.18)$$

By utilizing the oedotriaxial procedure described above, Watabe et al. (2003) investigated the K'_0 values of marine clays from several different locations around the world. The results were compared to values based on a K'_0 -OCR-relationship and from dilatometer tests. The authors found quite comparable values of K'_0 when comparing laboratory tests on overconsolidated samples and results from the dilatometer tests performed in the field (Watabe et al., 2003).

2.5.3 Split-ring Oedometer

The split-ring oedometer test is a modified oedometer test developed at NTH (now NTNU) during the 1980's (Senneset, 1989). The sample is cut and placed in the apparatus as for an ordinary oedometer test, but the ring ensuring zero lateral strain in an ordinary oedometer test is replaced by three ring segments. The ring segments feature steel membranes which will ensure a closed ring around the sample. The steel membranes are equipped with high precision strain gauges. When the oedometer test is carried out, the strain in the steel membranes can be correlated to the horizontal total stress in the sample. The vertical total stress is known from a load cell on the load piston. If the test is run as a CRS experiment with a constant rate of strain, the pore pressure at the bottom of the sample is measured in order to calculate the effective stresses from the measured total stresses. From the effective horizontal and vertical stresses the value of K'_0 can be calculated (Senneset, 1989). Senneset and Janbu (1994) achieved reasonable results using the split ring oedometer to investigate several clays from the Trondheim area.

2.5.4 K'_0 From Ratio of Preconsolidation Stresses

Tavenas et al. (1975) suggest that K'_0 can be calculated as the ratio of the preconsolidation stresses in the horizontal and the vertical direction as in Equation 2.19. The preconsolidation stresses can be found from oedometer tests performed on samples trimmed so that the longitudinal axis correspond to either the vertical or the horizontal direction in situ. Following the proposal by Tavenas et al. (1975), the method has been utilized by other authors (Jamiołkowski et al., 1985; Mesri & Castro, 1987).

$$K'_0 = \frac{\sigma'_{ph}}{\sigma'_{pv}} \quad (2.19)$$

Hamouche et al. (1995) stated that the method proposed by Tavenas et al. (1975) was wrong. In situ measurements show values of K'_0 increasing with increasing OCR , whereas the ratio in Equation 2.19 seem to be approximately the same regardless of changes in the overconsolidation ratio. This suggests that there is no significant correlation between K'_0 and $\frac{\sigma'_{ph}}{\sigma'_{pv}}$, contradicting the original proposal by Tavenas et al. (1975)

2.6 Correlation Methods

As in situ and laboratory testing is undoubtedly both difficult and costly (Lunne, Lacasse, & Rad, 1992), the horizontal stress state in soil deposits is frequently approximated using theoretical or empirical equations alone (Ku & Mayne, 2015). Several formulas of varying complexity have been proposed for calculating K'_0 . Some of the formulas are used for normally consolidated soils, while others try to account for the effect of stress history.

2.6.1 Normally Consolidated Soils

One of the simplest equations was originally proposed by Jaky in 1944 (Jaky, 1944), and simplified in 1948 (Jaky, 1948). Equation 2.20 states that K'_{0nc} for a normally consolidated soil depends only on the effective friction angle ϕ' .

$$K'_{0nc} = 1 - \sin\phi' \quad (2.20)$$

The validity of Equation 2.20 has been investigated both in the laboratory and in situ. For laboratory conditions the work by P. W. Mayne and Kulhawy (1982), Diaz-Rodriguez et al. (1992) and Watabe et al. (2003) validated the equation. Based on in situ measurements at Berthierville, Hamouche et al. (1995) suggested that the equation is also a good approximation for K'_0 when the clay has an OCR close to 1. The equation

has gained great popularity and is widely used for calculating K'_{0nc} , for instance in the finite element program Plaxis.

However, several studies have resulted in slightly modified versions of Equation 2.20. Brooker and Ireland (1965) suggested that Equation 2.21 gave a better fit to results for cohesive soils, but the scatter was quite significant and the amount of samples limited.

$$K'_{0nc} = 0.95 - \sin\phi' \quad (2.21)$$

$$K'_{0nc} = \frac{1 - \sin(\phi' - 11.5)}{1 + \sin(\phi' - 11.5)} \quad (2.22)$$

$$K'_{0nc} = \frac{\sqrt{2} - \sin\phi'}{\sqrt{2} + \sin\phi'} \quad (2.23)$$

Furthermore, Bolton (1991) proposed Equation 2.22 and Simpson (1992) suggested Equation 2.23. The difference between the estimates of K'_{0nc} are relatively small with all the above equations (Sivakumar et al., 2002). P. W. Mayne and Kulhawy (1982) report that with only small changes made to the original Jaky's equation it would fit well with 121 samples of clays and sands tested. The modified equation from P. W. Mayne and Kulhawy (1982) is Equation 2.24.

$$K'_{0nc} = 1 - 1.003\sin\phi' \quad (2.24)$$

P. W. Mayne and Kulhawy (1982) reported that many attempts have been made to correlate K'_{0nc} with index properties such as plasticity index, liquid limit, void ratio, clay fraction and others.

Larsson (1977) stated that for Scandinavian inorganic clays many tests had shown a relationship between the plasticity index I_P and K'_{0nc} , alternatively between the liquid limit w_L and K'_{0nc} . The correlations presented by Larsson (1977) are given in equations 2.25 and 2.26. An apparent relationship between I_P and K'_{0nc} was also suggested by Brooker and Ireland (1965).

$$K'_{0nc} = 0.31 + 0.71(w_L - 0.2) \quad (2.25)$$

$$K'_{0nc} = 0.315 + 0.77I_P \quad (2.26)$$

However, the test results from more than 170 samples of clays and sands in P. W. Mayne and Kulhawy (1982) supported none of the correlation between index properties and K'_{0nc} . Also P. W. Mayne and Kulhawy (1982) indicated that for 130 clay samples the

scatter was too large to find any useful correlations between K'_0 and such index properties.

2.6.2 Overconsolidated Soils

Brooker and Ireland (1965) stated that the value of K'_0 depends heavily on the stress history of the soil. This is supported by many studies, including Sivakumar et al. (2002) and P. W. Mayne and Kulhawy (1982). In a well-known article, Brooker and Ireland (1965) investigated the relationship between the earth pressure at rest and stress history. By doing high-pressure one-dimensional compression tests on five cohesive soils, the authors found that the stress history of a soil deposit is the primary factor influencing the coefficient of earth pressure at rest. As OCR increases, the value of K'_{0oc} should theoretically approach the coefficient of passive earth pressure, K_P (Brooker & Ireland, 1965).

Schmidt (1966) proposed Equation 2.27 taking into account the effect of overconsolidation for soils experiencing first unloading.

$$K'_{0oc} = K'_{0nc} OCR^\alpha \quad (2.27)$$

where α is the slope of the curve when $\log K'_{0oc}$ is plotted against $\log OCR$. In order to utilize this relationship, laboratory investigations to determine the preconsolidation pressure is required (Fioravante et al., 1998). P. W. Mayne and Kulhawy (1982) used the relationship between K'_{0oc} and OCR for more than 170 samples of clays and sands in order to state that

$$\alpha = \sin\phi' \quad (2.28)$$

Combining Equation 2.28 with Equations 2.20 and 2.27 gives Equation 2.29

$$K'_{0oc} = (1 - \sin\phi') OCR^{\sin\phi'} \quad (2.29)$$

The results reported by Hamouche et al. (1995) suggest that Equation 2.28 does not fit well with findings on sensitive clays in Eastern Canada. Based on in situ tests using the dilatometer, hydraulic fracturing and the Cambridge self-boring pressuremeter, higher values than those predicted by Equation 2.29 were found. The values of K'_{0oc} found from the three in situ methods were quite similar, and corresponded to values of α in the range of 0.75 to 1.15. Additionally, Hamouche et al. (1995), presented the results from a number of other authors. Those results supports that the value of α can vary between a lower limit equal to $\sin\phi'$ and values above one. Hamouche et al. (1995) also suggested that the value of α tend to increase with increased sensitivity.

Moreover, Sivakumar et al. (2009) made an evaluation of the existing theoretical approaches to estimating the coefficient of earth pressure for overconsolidated clays. In agreement with Sivakumar et al. (2002), Sivakumar et al. (2009) stated that the different estimates of K'_{0oc} which are primarily based on the angle of internal friction and OCR show rather large variations (F. H. Kulhawy & Mayne, 1990).

For completeness, two rather advanced methods for determining K'_0 are presented in the following, even though the laboratory testing required to use these methods is not further pursued in this thesis.

Sivakumar et al. (2002) performed a thorough theoretical approach based on the modified Cam-Clay model in order to find the relation between K'_{0oc} and OCR given in Equation 2.30, taking anisotropic in situ stresses into account.

$$OCR = \frac{\sigma'_{pv}}{\sigma'_{v0}} = \left[\frac{1 - \chi K'_{0oc}}{1 - \chi K'_{0nc}} \right]^{\frac{1}{\chi}} \quad (2.30)$$

χ is the ratio between the slopes of the unloading-reloading curves used in the modified Cam-Clay model for 1D and isotropic loading conditions (Sivakumar et al., 2002). K'_{0nc} can be found for instance from Equation 2.20 (Sivakumar et al., 2002). Experiments reported in Sivakumar et al. (2009) confirm that the relation in Equation 2.30 manages to take into account the effect of anisotropic in situ stresses.

Sivakumar et al. (2009) tried to relate K'_{0oc} not only to the stress history of the clay, but also to the structure of the material. The background for the proposed Equation 2.31 is the modified Cam-Clay model, as for Equation 2.30.

$$K'_{0oc} = \frac{1}{\eta} [1 - (1 - \eta K'_{0nc}) OCR^{(1-\chi)}] \quad (2.31)$$

η describes the anisotropic elastic stiffness behaviour of the clay within the yield locus. If $\eta = -2$ the material is assumed to be isotropically elastic, and a higher value of η indicates that the anisotropy is increasing. χ is as for Equation 2.30. Theoretically the ratio χ should be equal to 1 for linearly elastic materials, while it is found through laboratory experiments to typically be around 0.8 (Sivakumar et al., 2009). K'_{0nc} can be found for instance from Equation 2.20 (Sivakumar et al., 2009).

The challenge with using equations 2.30 and 2.31 for predicting K'_{0oc} is the need for several laboratory tests (Sivakumar et al., 2002, 2009).

Hamouche et al. (1995) concluded that it is hard to determine K'_{0oc} from correlations, and therefore pointed out the need for in situ measurements if an accurate value of K'_{0oc} is required. This is especially true as the value of α in Equation 2.23 tends to vary substantially, and showing increasing values with increasing sensitivity (Hamouche et al., 1995). This is also supported by Ku and Mayne (2015), stating that the most accurate

values of K'_0 are found from direct in situ measurements. Even though the correlation methods are increasing in complexity and ability to account for different soil behaviour effects, it seems like the conclusion in Hamouche et al. (1995) is still valid.

Chapter 3

In Situ Investigations

This chapter presents details regarding the in situ testing conducted as part of this master's thesis. All tests were performed at the NGTS quick clay test site at Flotten, close to Trondheim. The site is located in close proximity to the Tiller test site, used by NTNU (formerly NTH) for more than three decades (Gylland, Long, et al., 2013). Several maps of the test site are presented in Appendix A. A map indicating the location of the site in relation to Trondheim city center is shown in Figure A.1.

3.1 Initial Evaluations of the Test Site

As an early assessment of soil conditions at Flotten, both rotary pressure soundings as well as a cone penetration test (CPTu) were conducted by technical operators from NTNU in the period between 24 and 27 January 2017. The locations of these soundings are indicated in Figure A.2. These initial soundings indicate a dry crust extending down to about 2 m depth. Next, two rather homogeneous clay layers are evident between 2 and 20 m depth, before the soundings indicate several layers containing coarser materials at depth below 20 m. A quite clear change in material behaviour is evident at 7 to 8 m depth. The clay above 7 m depth is plastic and less sensitive, while the clay below 8 m depth is quick clay. The soundings will be further discussed in Chapter 6.

The area surrounding the Flotten test site is shown in Figure 3.1a. Note the yellow drill rig standing at the test site in the middle of the figure, indicated by a red arrow. It may be seen that the area is generally flat, which is in accordance with the assumption in section 2.2.7 that the test site is almost unaltered clay sea bed that has risen above the sea level. Figure 3.1b offers a closer look at the test site. This figure may be studied alongside the map in Figure A.3. The four piezometers at the test site and the casing used for the last installation attempts in borehole EPC006 can be seen. The earth pressure cells in boreholes EPC001 to EPC005 were situated on a line between the drill rig and

the orange pole in the left of the picture. A small recession running parallel to the earth pressure cell locations lies just to the left of the low vegetation in the far left of the figure.



(a) Overview of area surrounding the Flotten test site.



(b) Closer look at the test site.

Figure 3.1: Overview and closer look at the Flotten test site.

3.2 Piezometers

A total of six GEOTECH PVT piezometers are currently installed at or near the Flotten research site. A closer description of the location of the different piezometers is given in Appendix B. See also the map of soundings in Appendix A. Two piezometers with serial number 4362 and 4363 were installed in connection with another nearby project. Next, two piezometers with serial number 6081 and 6082 were installed by NTNU engineers in early January 2017 at the Flotten research site. It is assumed that the installation procedures for these piezometers comply with recommendations given in NGF Melding 6 (NGF, 1989a).

Finally, the piezometers with serial number 11360 and 11361 were installed by a NTNU engineer and the authors of this thesis on 15 May 2017. The upper crust was pre-drilled using total sounding equipment, before the filter of the piezometer was saturated. The piezometer was consequently penetrated to the desired installation depth while the NAUTIZ x7 handheld computer was used to monitor that the pressure limit of the equipment was not exceeded.

3.3 Earth Pressure Cells

A field test program has been carried out with a total of eleven earth pressure cell installations at the desired final depth. Five cells were installed at 5 m depth in order to compare the spread in the results at the same depth. One of the cells at 5 m was left in place for the entire field test period to monitor changes with time. From 6 to 9 m, one cell has been installed at each depth, while at 10 m depth two cells have been installed. The authors of this thesis have participated in the installation of all the cells, except for the second cell installed at 10 m on 11 April. Also, the installations of the casings itself on 16 March, 29 March and 4 April were performed by NTNU engineer Espen Andersen. The rest of this section should preferably be read together with Table 5.1, since the table summarizes the tests performed. The location of the boreholes is given in the map in Appendix A. Note the approximately three meters deep recession running parallel to the boreholes EPC001 to EPC005, indicated in Figure 3.1. The cells at depths 5 to 9 m were installed with the blade perpendicular to the direction of the recession. The cells at 10 m were both installed with the blade parallel to the recession.

Zero readings of the measured total earth pressure and pore pressure were made shortly before installation of all the cells. Zero readings were also made for several cells after extraction from the ground. The zero values are given in Table 5.1.

The filters of the pore pressure measuring system of the earth pressure cells were

saturated in the lab before installation at the test site. The filters were submerged in deionized water, before an exicator and a vacuum pump was used to remove any trapped air. This process continued for as long as air bubbles emerged from the filters. At the test site, the pore pressure measuring system were filled with a mixture of antifreeze solution and deionized water to prepare the cells in the field. The preparation was done in accordance with the instruction manual in Appendix C.

During penetration of the cells, the readings of total horizontal earth pressure were continuously monitored. In order to capture the initial dissipation of pore pressure and hence change in effective horizontal stress, frequent measurements of both earth pressure and pore pressure were taken in the first 30.5 minutes after arriving at the final installation depth. Curves showing the change in measurements with time are given in Figure C.1.

All of the cells were pushed through 30 cm of undisturbed soil. This installation procedure was chosen based on literature describing the installation procedure of cells pushed through either 30 cm (Massarsch, 1975) or 50 cm (Tedd & Charles, 1981; Ryley & Carder, 1995) of undisturbed soil. The shortest distance used in the literature was selected, due to the cell damaged during push-in installation as described in the project thesis by the authors (Lindgård & Ofstad, 2016).

The blades of the cells have dimensions 70 x 140 mm. The thickness is 4 mm.

3.3.1 First Installations at 5 m

The first two cells were installed on the 15th of February. For the first cell, in borehole EPC001, an auger with a diameter of approximately 85 mm was used for pre-drilling before installation of the earth pressure cell. This method was primarily used to avoid damage to the earth pressure cell during insertion, which had proven rather fragile in previous pilot experiments conducted in quite similar soil conditions (Lindgård & Ofstad, 2016). The first cell installed had a measuring range of 0-4 bar, and proved to be quite difficult to install, as the output value exceeded the measuring range even during penetration in the pre-augered part of the borehole. For the final 30 cm into undisturbed soils, the cell was pushed 2-3 cm at a time, followed by a pause of about 10 minutes. Due to the difficulties during penetration of the first cell, it was left in the ground until 15 May to monitor the changes with time.

Between the installation of the first and second cell, some minor adjustments were made to the procedure. Instead of the original auger, a total sounding drillbit with a diameter of 77 mm was used without flushing for pre-drilling borehole EPC002 down to 4.70 m depth. This change was made both because this drill bit was believed to help create a more open bore hole, as well as to increase the efficiency of the operation. The drill bit was penetrated back into the bore hole after the first drilling, in order to remove

excess soil. The second cell installed had a measuring range of 0-7 bar and proved more rigid than the first. The measuring range was not exceeded during penetration, not even when penetrating the cell into undisturbed soils. This proved that the total sounding drill bit was a suitable way of pre-drilling before installing the cells. As the first cell had proven so difficult and time-demanding to penetrate, only two cells were installed this day.

Subsequently, three more cells were installed in boreholes EPC003, EPC004 and EPC005 on the 17th of February. All of these cells had a measuring range of 0-7 bar, and total sounding equipment was used for pre-drilling as described in the procedure for the second cell. The installation went by without any major issues. These three cells were retracted from the ground 27 February when they had been stable for quite some time.

3.3.2 Installation at 6 m

To further investigate the robustness of the cells, the cell at 5 m depth in borehole EPC002 with measuring range 0-7 bar was pushed directly from 5 to 6 m depth without extracting the cell to the surface on 27 February. During penetration the cell gave very high read-out values. Consequently, the penetration was conducted as slow as possible using the drill rig. Upon extraction from the ground 15 May it was evident that the cell was permanently damaged, as may be seen from Figure 3.2.



Figure 3.2: Cell damaged during penetration to 6 m. Earth pressure sensor EE24694.

3.3.3 Installation at 7 m

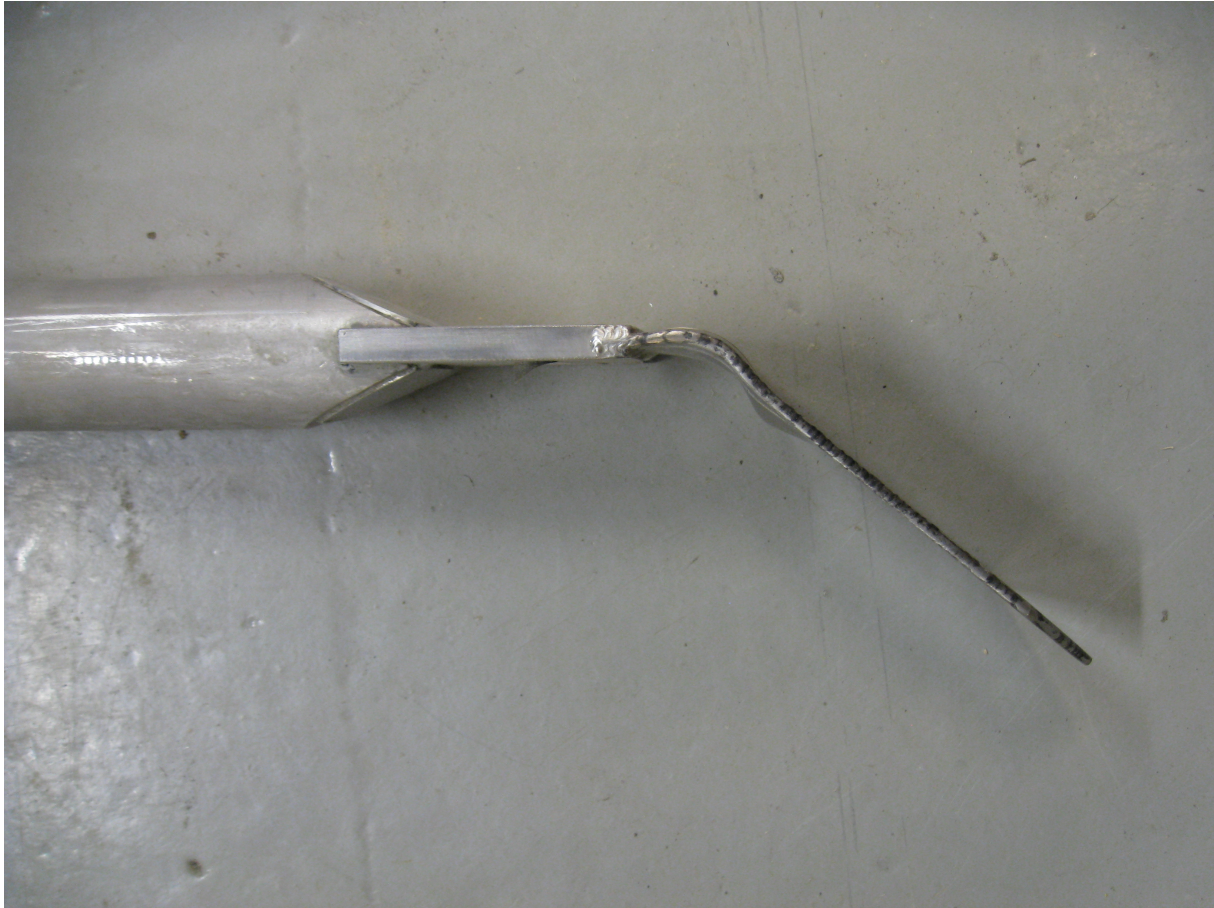
A cell with measuring range 0-7 bar was installed 27 February at a depth of 7 m in borehole EPC003 after pre-drilling to about 6.70 m with a total sounding drill bit, as described for the last four cells at 5 m depth. There were no special issues during the installation. The cell was retracted on 4 April.

3.3.4 Installation at 8 m

Borehole EPC004 was on 27 February pre-drilled with a total sounding drill bit to a depth of 7.70 m. A cell with measuring range 0-7 bar was first used. During penetration of the cell, at an approximate depth of 7.3 m, a sudden drop followed by a steady decline in the earth pressure readings was observed. The values continued to decrease, even below the original zero readings taken at the surface. Penetration into undisturbed soil did not alter this development. Withdrawn to the surface, the cell was clearly bent as seen in Figure 3.3a.

The installation at 8 m depth was attempted again the same day using another cell

with measuring range 0-7 bar in borehole EPC005. The hole was once more pre-drilled to a depth of 7.70 m, and the total sounding drill bit was penetrated several times to ensure an as open bore hole as possible. Despite these precautions, the same sudden decrease in pressure readings was observed once more, this time at a depth between 6 and 7 m. The damaged cell is shown in Figure 3.3b.



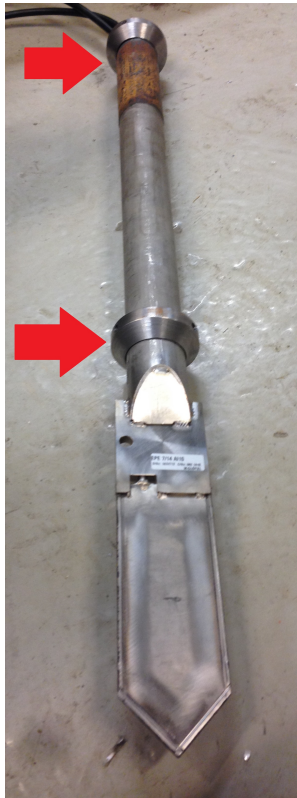
(a) First cell damaged during penetration to 8 m. Earth pressure sensor EE24696.



(b) Second cell damaged during penetration to 8 m. Earth pressure sensor EE24692.

Figure 3.3: Cells damaged during penetration to 8 m depth.

Consequently, installation of an earth pressure cell through ODEX casings was conducted. The casings have inner diameter 78 mm, outer diameter 90 mm and length 1.22 m. The cell was fitted with two metal rings as shown in Figure 3.4a to guide the cell through the casings. The rings were rounded to ensure that the rings would not get stuck on the way back into the casings after readings were finished. Guiding rings were used as the cells feature a sharp angle at the transition to the rods, which could obstruct the retraction of the cell back into the casing.



(a) Solid rings.



(b) Rings with three pieces cut off.

Figure 3.4: Rings to guide cells through casings.

The first installation with casings was performed in borehole EPC004 to a desired final depth of 8 m. For this test a cell with a measuring range 0-10 bar was used. On 16 March an auger with diameter of approximately 85 mm was used to remove excess soil down to 7.50 m depth. Then the ODEX casings, which have a slightly larger diameter than the auger, were installed down to 7.50 m and the casings were filled with water. The next day, pre-drilling was performed with a 57 mm drill bit down to 7.70 m. Upon retracting the pre-drilling rods from the ground, clay sticking to the final meter of the rods was observed. This indicate that the deepest ODEX casing contained quite a bit of clay. The cell was pushed down to the desired final depth of 8 m. When the force applied by the drill rig on the rods was removed, the rods moved some centimetres upwards. The rods were pushed back down to the desired final depth and the force was maintained for three

minutes. Upon unloading of the rig, the rods moved 3 cm upwards. The cell and rods were left at a final depth of 7.97 m and the readings started soon after the unloading. One minute into the readings, the casing was filled with water. The cell was retracted on 29 March.

3.3.5 Installation at 9 m

The second installation with casings was conducted in hole EPC004 to a final depth of 9 m with a cell with a measuring range 0-10 bar. Solid metal rings as shown in Figure 3.4a were still fitted to the cell. On 29 March augering with the approximately 85 mm auger was conducted down to 8.50 m in an effort to remove excess soil, and casings were installed to the same depth. The casings were filled with water after installation. The next day a 57 mm drill bit was used for pre-drilling to 8.70 m. The cell was installed at the final depth of 9.00 m and the measurements were started immediately after the cell arrived at the final depth. The pushing force from the rig was not removed until the cell had stayed at the final depth for 12 minutes. Upon unloading, no upwards movement was observed. The cell was retrieved on 4 April.

3.3.6 Installations at 10 m

The casing in borehole EPC004 was extended and pushed further down to a total depth of about 9.70 m on 4 April. Total sounding equipment with water flushing was used all the way to the bottom of the casings to make a water and clay based slurry inside. The casings were left over night, before the earth pressure cell with measuring range 0-10 bar was installed on 5 April. The area of the metal rings had been reduced to let the clay pass the cell, due to the upwards movement observed at installation through casings at 8 m depth. The cell had to be pushed with the drill rig for approximately the last 1.5 m down to the final depth. Possibly because three parts of the rings on the cell were cut off as shown in Figure 3.4b, the cell did not move upwards upon unloading. The unloading happened soon after the cell arrived at the final depth. No problems were encountered during installation of the first cell at 10 m depth. The cell was retracted on 11 April.

The same cell with metal rings as shown in Figure 3.4b was installed at 10 m depth in borehole EPC003 on 11 April. The casings were pushed down to 9.70 m depth on the 11 April. The hole had been pre-drilled to about 6.70 m depth at the installation to 7 m depth on 27 February. Total sounding equipment with water flushing was as for the other cell at 10 m depth used all the way to the bottom of the casings to make a water and clay based slurry inside. The cell was then installed to the final depth of 10 m. The installation seemingly went by without any trouble. When the cell was extracted from

the ground 12 May the cell was clearly bent, as shown in Figure 3.5.



Figure 3.5: Cell damaged during penetration to 10 m. Earth pressure sensor EE24712.

3.3.7 Last Installation at 5 m

Since the last cell installed at 10 m depth was clearly damaged, and the effect of the flushing during pre-drilling on the in situ stress was unknown, it was decided to attempt a more cautious installation at 5 m depth.

12 May the auger with approximate diameter 85 mm was used to try to remove the soil down to 4.95 m depth. At this depth the auger was rotated several times and then brought up to the surface and wiped off. This procedure was repeated one more time. Then casings were installed down to 4.95 m depth. A metal rod fitted to a rope, as shown in Figure 3.6a, was lowered into the casing to find out if the auger had really removed the excess soil down to 4.95 m. At depth 2.09 m the metal rod hit the soil inside the casing. A piece of timber was attached to thin field vane rods and lowered to approximately 4 m into the casings. The setup is shown in Figure 3.6b. Upon rotating the rods and the piece of timber there was almost no resistance from the remoulded soil inside the casings. Since the soil inside the casing seemed to be sufficiently remoulded, a cell with measuring range 0-7 bar fitted with the reduced metal rings was attempted to be installed by using only

body weight and hand force. This proved unsuccessful, as the cell got stuck after passing through some of the soil inside the casing. Due to this, the attempts of installation were terminated.



(a) Metal rod and rope.

(b) Timber and vane rods.

Figure 3.6: Equipment used to evaluate clay in casing

A last attempt to perform a cautious installation was attempted 15 May. The same cell and casings as 12 May were used. First, the casings were pushed down to 5.05 m depth. Then approximately three liters of water was added inside the casings. The idea was that the added water would make a less viscous fluid inside the casings when total sounding equipment without flushing was used inside the casings down to 5.05 m depth. The total sounding equipment was rotated up and down inside the casings several times. The cell was then attempted to be pushed down through the casing. To be extra careful with the cell it was decided that the middle of the cell should not be pushed more than 20 cm out of the casings, meaning 10 cm less than what had been tried earlier. However, the cell never came that far, since it stopped 48 cm before the intended installation depth. The cell was at this point pushed down by a sum of body weight and hand force equal to approximately 100 kg. The attempts to install the cell by the use of total sounding equipment without flushing was consequently terminated.

3.4 Earth Pressure Cell with Protective Cover

To avoid spending time on pre-drilling beyond the dry crust, the earth pressure cell may be fitted inside a protective cover during most of the penetration. Close to the final depth the cell is pushed out of the protective cover to reach the final depth, much like the field vane equipment.

Tor Helge Johansen at the Norwegian Public Road Administration did upon request find and ship two different models of protective covers developed at Veglaboratoriet as partially described in Vaslestad (1989), together with some old earth pressure cells. The covers were used as inspiration when evaluating the possibility to create a new protective cover for a modern Glötzl earth pressure cell.

The most promising protective cover is shown along with an old earth pressure cell in figure 3.7, both pushed out and retracted into the cover. The two pieces of the cover are held together by screws. Note the slot that guides the cell in and out of the cover. Also, note the metal pieces which keep soil from entering the cover during penetration. The equipment is operated with a double rod system, like a field vane. The outer rod is fitted to the cover, while the inner rod pushing the cell out of the cover is fitted to the end of the cell itself.



(a) Retracted cell.



(b) Pushed out cell.

Figure 3.7: Old cell and most promising protective cover from Veglaboratoriet.

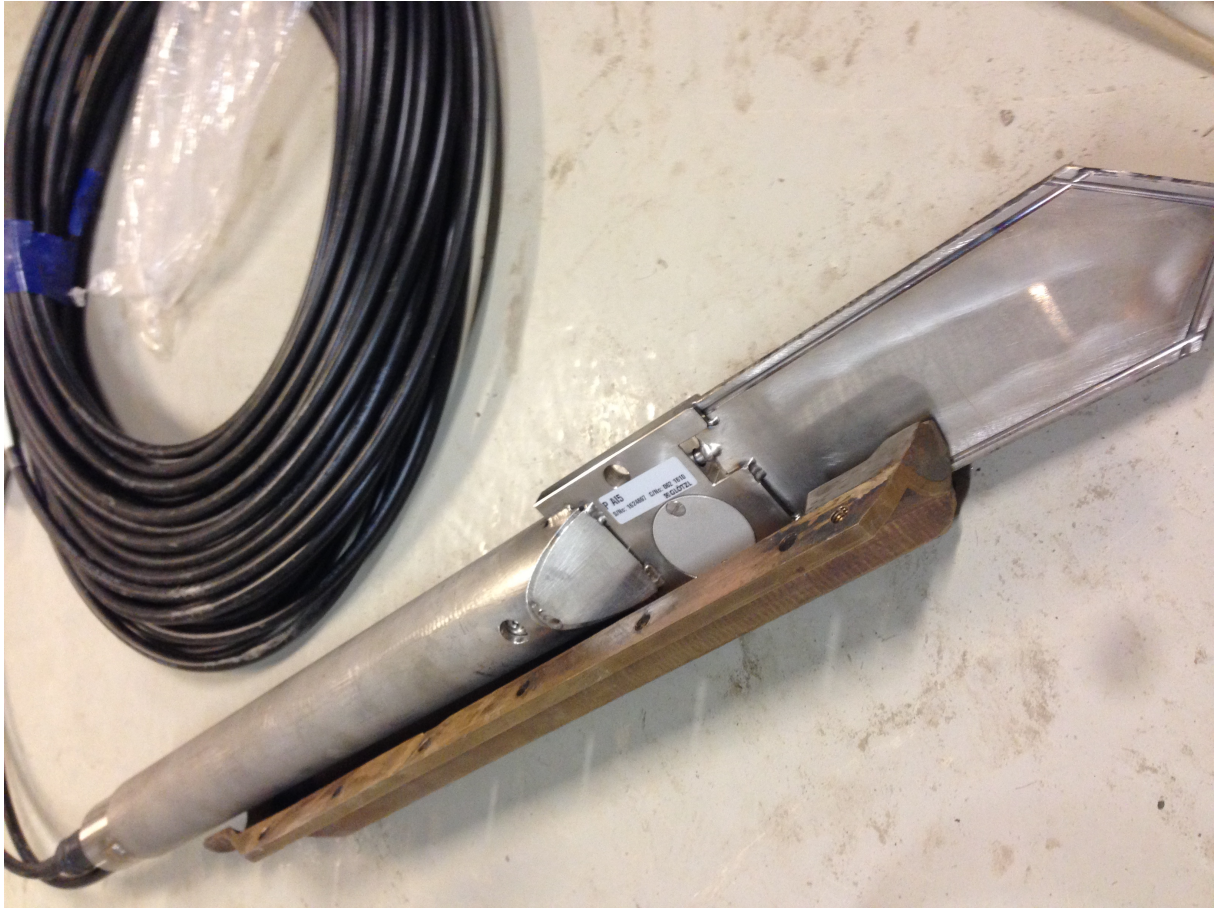


Figure 3.8: New cell fitted in old protective cover.

Figure 3.8 shows the new cell fitted in the old protective cover. It is evident that a new cover needs to be longer. Also, the metal pieces keeping soil from entering the cover during penetration would obstruct the cell from being pushed out of the cover, and therefore a new protective cover should be made without these metal pieces. To avoid filling the cover with very compacted soil, the cover could have notches which allow the soil to exit. The diameter of the cover should also be larger at the bottom than where the notches are placed, so that the soil would more easily exit from the cover.

The old protective cover does not allow the entire cell to be pushed out from the cover and into the soil. A new cover should allow for pushing the entire cell out at least 30 cm into the soil in order to install it in less disturbed soil.

A metal cone with holes for the wires to pass through the back end of the new cell, similar to the one found on the old cell in Figure 3.7, should be attached in order to have a proper place to fit the threading for the inner rods.

The old cover is made of brass, avoiding corrosion problems. The new protective cover would be easier to produce if brass is used, but material costs for a steel cover are lower.

The amount of disturbance caused by pushing the protective cover into the soil is unknown. Therefore, the results in which the earth pressure cell with protective cover

can obtain may be of questionable quality. Since the production of a protective cover is both time demanding and costly, it has been decided not to pursue this issue any further within the scope of this master's thesis.

3.5 Dilatometer

A dilatometer test with seismic measurements was conducted on 14 February using the Marchetti SDMT equipment. The location of the bore hole used is indicated with SDMT001 in the map in Appendix A. The test was performed in cooperation with NTNU engineers, as well as Zeynep Ozkul at NGI. A and B readings were taken every 20 cm, while seismic readings were taken every 50 cm. The A and B readings were taken continuously from 1.80 m to 20.60 m depth. The seismic measurements were taken continuously from 4.50 m to 20.00 m depth. At shallow depths poor signal quality prohibited useful readings. Description of the test procedure is given in section 2.4.2.

The raw data was processed by Zeynep Ozkul to obtain corrected A and B readings. The rest of the processing was done by the authors. Since an average unit weight of $\gamma = 17.5 \text{ kN/m}^3$ for all depths is the best estimate used in this thesis, this was used along with the assumed pore pressure distribution in section 6.2.2 to calculate the overburden pressure. Plots indicating the key parameters I_d , K_d and E_d with depth, along with OCR with depth, is presented in Appendix D. A total of four different interpretations of K'_0 , as presented in section 2.4.2, is included in Figure 5.2, which compares different approaches to K'_0 .

More information about the testing procedures as well as an entire view of the raw data is presented in Ozkul and L'Heureux (2017).

3.6 Field Vane

The field vane test has become a both popular and widely used method for the determination of the undrained shear strength of clays (Chandler, 1988; Blight, 1968). Field vane experiments were conducted by technical operators from NGI in cooperation with the Swedish geotechnical field equipment company Geotech AB on the 21 February 2017. A tapered end vane with height 110 mm and width 65 mm was used. Measurements of both undisturbed as well as remoulded shear strength were taken at depths 8.4 m, 9.4 m and 10.4 m. The registered raw data processed by the authors of this thesis. The acquired data has been used for exploring the correlation method proposed by Aas et al. (1986).

Chapter 4

Laboratory Investigations

This chapter treats the performed laboratory investigations. The tests were primarily performed by the authors and Konjit Paulos Gella. In addition, one oedometer test was run by NTNU engineer Espen Andersen.

4.1 Index Testing

As part of the general classification of the soil material, several index tests were performed. Some parameters from index tests are used as input for correlation methods to calculate K'_0 . The majority of such index tests were performed just after the opening and cutting of clay cylinders. A brief summary of the performed index tests are given below. Testing by both the authors as well as Gella is combined in the subsequent section 5.2.1 and Appendix F. The majority of the water contents, falling cone tests and average cylinder densities were performed by Gella, while the Atterberg limits, grain density tests and densities of small ring were performed exclusively by Gella. Please note that it is assumed that testing by Paulos Gella was performed mostly in accordance with relevant standards and recommendations. Details regarding the exact testing procedures utilized is found in the master's thesis by Gella.

4.1.1 Water Content

The water content of the clay samples were determined in accordance with ISO 17892-1 (ISO, 2014a). Small specimens of clay were dried in porcelain cups over night using an oven maintaining a temperature of about 105° . The cups were weighed before and after drying and the water content was hence determined using Equation 4.1

$$w = \frac{m_1 - m_2}{m_2 - m_c} \cdot 100 \% = \frac{m_w}{m_s} \cdot 100 \% \quad (4.1)$$

where w is the water content, m_1 is the weight of the cup and wet sample, m_2 is the weight of the cup and dry sample, m_c is the weight of the cup, m_w is the weight of the water in the sample and m_s is the dry weight of the sample.

4.1.2 Atterberg Limits

The liquid limit was determined both by the Casagrande method as well as by the fall cone method. As ISO17892-12 recommends utilizing the fall cone method instead of the Casagrande method (ISO, 2004a), results obtained by the fall cone method are presented in Figure F.1.

The plastic limit of the Flotten clay was determined in accordance with ISO17892-12 (ISO, 2004a). The specimens were kept in small glass cylinders during drying over night.

4.1.3 Falling Cone

The undrained shear strength, s_u of the Flotten clay was determined using the fall cone test. The testing by Gella was performed in accordance with recommendations given in Håndbok 014 Laboratorieundersøkelser by the National Road Administration of Norway (SVV, 1997). For the testing by the authors of this thesis, clay specimens taken from the outer, disturbed parts of the 54 mm cylinder were often used for determining the remoulded strength, as these are less suited for other tests.

4.1.4 Density

Before every sample extrusion, the average cylinder density was calculated based on the weight of the entire sample, the length of the sample and the known area of the 54 mm piston sample tube. In addition, the density of two smaller specimens were determined through the use of a small ring. The testing was conducted in accordance with section 4.5.1 in ISO 17892-2 (ISO, 2014b).

A pycnometer was used to determine the grain density of the clay samples, making the calculation of γ_s possible. The testing was conducted in accordance with ISO 17892-3 (ISO, 2015).

4.2 Oedometer

Several oedometer tests have been conducted as a part of the investigations of the Flotten clay. Oedometer tests are performed to establish both stiffness and consolidation

properties of the material. As some important theoretical correlations for the determination of K'_0 relies on OCR, an important goal of running oedometer tests was also the determination of preconsolidation stress, p'_c .

The testing was performed using oedometers in the geotechnical laboratories at NTNU. Samples from between 5 to 12 m depth were tested. A ring with height 20 mm and inner area of 20 cm^2 was used. The testing was mostly conducted in accordance with the Norwegian Standard NS8018 (NBR, 1993). In the standard, a strain rate between 0.25 %/h and 0.75 %/h is recommended for clay. For the samples from a depth of about 5 m, a strain rate of 1 %/h was used. When testing samples from depths 9 to 11 meters, a strain rate of 0.5%/h was used. Some tests were initially conducted at 0.25 %/h until a sufficient vertical stress resulted in a pore pressure ratio below the 10 % requirement given in NS8018.

To gain a better understanding of the preconsolidation at Flotten, Appendix G also contains several CRS oedometer tests conducted by fellow master student Konjit Paulos Gella. More information regarding assumptions made in relation to these tests are found in Appendix G.

After performing the oedometer tests, the sample quality for all the tests with the required parameters available was evaluated using the $\Delta e/e_0$ -criterion suggested by Lunne, Berre, and Strandvik (1997), given in Table 4.1.

Table 4.1: Sample quality evaluation based on $\Delta e/e_0$. Table from Lunne, Berre, and Strandvik (1997).

OCR [–]	Depth [m]	Very good to excellent quality $\Delta e/e_0 <$	Good to fair quality $< \Delta e/e_0 <$	Poor quality $< \Delta e/e_0 <$	Very poor quality $\Delta e/e_0 >$
1-2	0-10	0.04	0.04-0.07	0.07-0.14	0.14
2-4	0-10	0.03	0.03-0.05	0.05-0.10	0.10

The initial void ratio e_0 was calculated using Equation 4.2.

$$e_0 = \frac{\gamma_s(1+w)}{\gamma} - 1 \quad (4.2)$$

Where γ_s is the particle unit weight, w is water content and γ is the unit weight.

The value of γ_s was taken from index test results, see section 5.2.1. An average $\gamma_s = 27.8 \text{ kN}/m^3$ was used for all samples tested. The procedures of weighing the sample before and after testing varied between the tests. The water content was mainly determined based on the weight of the oedometer specimen before and after testing. For some tests, the water content was determined from spare clay after trimming the

sample. For some other tests, the wet and dry weight of oedometer test specimen were not determined. For these tests, the $\Delta e/e_0$ -criterion has not been evaluated.

An approximation of the in situ vertical effective stress σ'_{v0} was calculated using an average $\gamma = 17.5 \text{ kN/m}^3$ and pore pressure measurements from piezometers installed at Flotten. Next, for a one-dimensional stress state as in the oedometer, the volumetric strain equals the vertical strain. Based on the calculated in situ stress, the associated deformation was retrieved from the oedometer raw data file and Equation 4.3 was used to determine the volumetric strains at the in situ stress level.

$$\varepsilon_{vol} = \varepsilon_v = \frac{\delta_i}{h_0} \quad (4.3)$$

where δ_i is the deformation at the in situ stress and h_0 is the initial height of the specimen. h_0 is equal to 20 mm for all specimens tested.

Next, change in void ratio Δe may be determined from Equation 4.4.

$$\Delta e = \frac{V_0 \cdot \varepsilon_{vol}}{V_s} \quad (4.4)$$

where $V_0 = 40 \text{ cm}^3$ is the original volume of the oedometer test specimen, ε_{vol} is the volumetric strain at the in situ stress level, as calculated from Equation 4.3, and V_s is the volume of solids calculated from Equation 4.5.

$$V_s = \frac{m_s \cdot g}{\gamma_s} \quad (4.5)$$

where m_s is the dry mass of the oedometer test specimen after testing, $g = 9.81 \text{ m/s}^2$ is the gravity of Earth and γ_s is the unit weight of solids.

Details regarding the assumed values of σ'_{v0} and pore pressure, as well as the axial strain at in situ stress level is indicated for each test in Appendix G.

The determination of p'_c in this thesis is based on Janbu (1970). The author finds $p'_c = \sigma'_c$ to be only slightly to the left of the minimum of the test curve in the modulus M versus vertical stress σ'_v diagram as shown in Figure 4.1. The minimum of the modulus diagram coincides with the greatest curvature of the test graph in the vertical strain ε_1 versus vertical stress σ'_v diagram. In this thesis the above determination of p'_c is referred to as the Janbu determination.

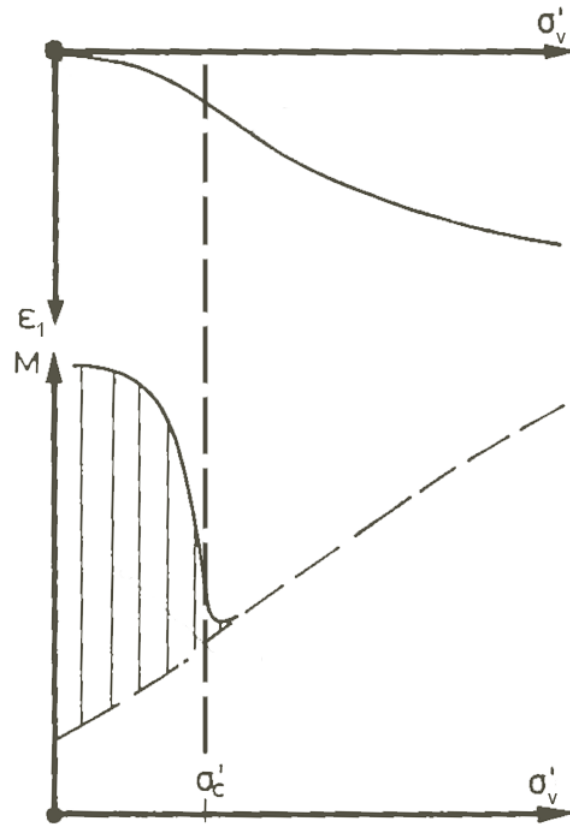


Figure 4.1: Idealized graphs to determine p'_c by the Janbu method. Modification of figure from Janbu (1970).

4.3 Work Criterion in Oedometer

The work criterion in oedometer tests was applied to three oedometer tests performed on Flotten clay. The interpretations of p'_c and in situ stress according to section 2.5.1 are shown in Figures H.1, H.2 and H.3 in Appendix H. The raw data was processed in Excel according to the description in section 2.5.1.

4.4 Triaxial Testing

Triaxial testing was conducted in order to achieve estimates of material strength properties like attraction and friction angle for the Flotten clay. The parameters are needed as input for the correlation methods to calculate K'_0 . Additionally, there is a need for triaxial compression tests to use the field vane approach suggested by Aas et al. (1986), see section 2.4.8.

A total of four Consolidated Anisotropically Undrained compression (CAUc) triaxial tests were performed by the authors using a triaxial cell without back pressure in the geotechnical laboratories at NTNU. The testing was mostly conducted in accordance

with ISO 17892-9 (ISO, 2004b) on specimens from between 9 and 11 m depth. The specimens were consolidated to a best estimate of the in situ stress state, using primarily pore pressures from the earth pressure cells. As the triaxial testing was conducted over the course of about eight weeks, the values of both K'_0 as well as the in situ pore pressure used in calculating the consolidation pressures were slightly changed between the different tests. For the initial testing, measurements of pore pressure and total earth pressure from the same depth were still not available. Hence, measurements from depth of about 5 to 6 m was used, and the value of K'_0 to use for consolidation was found by the K'_0 -OCR-relationship proposed by P. W. Mayne and Kulhawy (1982).

As presented in section 3.1, initial soundings and sampling at Flotten indicated two rather homogeneous clay layers between 2 and 20 m. Initial cylinder density calculations suggested an average unit weight of 18 kN/m^3 for the clay layers. Consequently, an average unit weight of 18 kN/m^3 was assumed for the entire depth for all but one triaxial test. For test CAUc-0934 a unit weight of 17 kN/m^3 was assumed for the upper 2 meters of dry crust. Please note that this deviates from the final average unit weight of 17.5 kN/m^3 , based on all index testing performed during the semester. Piezometers installed at Flotten (see appendix B) indicated an approximate pore pressure of about 40 kPa at 10 m depth. For all but the first test CAUc-0934, the most recent value taken from the piezometers was used. For the first test CAUc-0934, performed on a specimen from depth 9.34 m, an assumed hydrostatic distribution of pore pressure from 2 m below surface was erroneously used.

The specimens were consolidated in steps, adding approximately 10 kPa cell pressure every second hour. The vertical anisotropy was added in steps of about 5 kPa as the cell pressure was increased. The samples was sheared at a strain rate of 0.75 % /hour in accordance with recommendations given in Berre (1981). The shearing was automatically stopped after reaching a total deformation of 30 mm.

Please note that information about the assumed overburden and pore pressure, K'_0 as well as other key information is presented together with each set of test results, in Appendix I. The appendix also includes details regarding the processing of the raw data files from each test. To gain a better understanding of the soil conditions at Flotten and to determine input parameters to the correlation methods for calculating K'_0 , the appendix also contains several CAUc and CIUc triaxial tests conducted by fellow master student Konjit Paulos Gella.

After completing the triaxial testing, the sample quality was evaluated by examining the volumetric strains during the consolidation phase. Based on the Table 4.2, the samples were classified as of perfect, acceptable or disturbed quality. The results of this evaluation is presented in the Section 5.2.4.

Table 4.2: Sample quality evaluation based on volumetric strain during the consolidation phase. Table from Andresen and Kolstad (1979).

OCR [–]	Depth [m]	Perfect quality $\varepsilon_{vol} <$	Acceptable quality $< \varepsilon_{vol} <$	Disturbed quality $\varepsilon_{vol} >$
1-1.2	0-10	3.0	3.0-5.0	5.0
1.2-1.5	0-10	2.0	2.0-4.0	4.0
1-5-2	0-10	1.5	1.5-3.5	3.5
2-3	0-10	1.0	1.0-3.0	3.0
3-8	0-10	0.5	0.5-1.0	1.0

The volumetric strains ε_{vol} were evaluated by using Equation 4.6.

$$\varepsilon_{vol} = \frac{\Delta V}{V_0} \quad (4.6)$$

where ΔV is the change in volume during the consolidation phase and V_0 is the original volume of the sample.

During the consolidation phase, a scale was used to keep track of the amount of water expelled from the sample. Subsequently, the total amount of water expelled during the consolidation phase is taken as ΔV , under the assumption that the sample is fully saturated. The sample area of a 54 mm steel piston sample is given in Equation 4.7.

$$A_0 = \pi \cdot \left(\frac{5.4 \text{ cm}}{2} \right)^2 = 22.9 \text{ cm}^2 \quad (4.7)$$

Where A_0 is the specimen area. With a specimen height h_0 of 10 cm, V_0 equals 229 cm^3 .

Finally, collective plots including all triaxial test results were generated and linear curves were fitted to interpret approximate values of the attraction and friction angle of the clay. The preliminary soundings at Flotten (see Appendix A) indicate that the transition zone between plastic and quick clay is at about 7 to 8 m depth. Based on this observation combined with the triaxial test result, two pairs of values of attraction and friction angle were chosen, one for depth 2 to 8 m, and another for depths 8 to 12 m.

4.5 Oedotriaxial

Two oedotriaxial tests were started, but only one was finished as an oedotriaxial test. A general description of the oedotriaxial test is given in section 2.5.2. The graphs for the first oedotriaxial test is shown in Figure J.1 in Appendix J, along with the raw data. The data for the second oedotriaxial test is presented as part of the ordinary triaxial tests since it was not fully performed as an oedotriaxial test.

In the first oedotriaxial test the sample was mounted and the consolidation started on 2 March. The sample was consolidated to cell pressure 10 kPa and vertical stress 12.5 kPa, which corresponds to an assumed K'_0 value of 0.8. This K'_0 value is probably a bit too high, but a slightly lower K'_0 used for consolidation would probably not change the oedotriaxial test results that much. The next day, the oedotriaxial part of the test was run in the shear phase module of the triaxial apparatus to keep the rate of deformation constant. The test was performed with manual adjustment of the cell pressure to keep the cross-sectional area constant. A manually run test facilitates understanding of how to perform a good test. The measuring glass was partially covered with adhesive tape to reduce the effect of evaporation. Brief summaries of the testing conditions of the first oedotriaxial test are given in Table 4.3 and Table 4.4. Please note that there is a weekend between test day 1 and 2.

A key aspect is to run the test at a rate of deformation which ensures an approximately drained situation. To start out after consolidation, the shear phase was run on the 3 March at a rate of deformation of 1 mm/h for 27 minutes. 3 March is referred to as day 1 of shearing in Table 4.4. Then the cell pressure and deformation was kept unchanged for 32 minutes. The test was then continued at 1 mm/h deformation rate for 22 minutes, and then a break was made for 24 minutes. During this break 0.37 g of water was expelled, indicating that the test was run too fast to drain completely. Therefore the test was run at a rate of deformation of 0.5 mm/h for 27 minutes. During a subsequent break lasting 23 minutes 0.16 g of water was expelled. For the next 48 minutes the test was run at a rate of deformation of 0.3 mm/h. 0.10 g of water was expelled in the following 29 minutes break. Then the test was run at 0.3 mm/h for 6 minutes and then at 0.25 mm/h for 2 hours and 50 minutes. 0.25 mm/h rate of deformation was assumed to be close to a drained situation. At this point the cell pressure had reached 39 kPa.

The sample was left over the weekend under conditions of constant cell pressure and constant vertical deformation. On Monday 6 March, referred to as day 2 in Table 4.4, the hose from the valve block to the scale was filled with water from a syringe, since water in the hose had dried out during the weekend. The deformation was continued at a rate of 0.25 mm/h. The reference cross-sectional area that was supposed to be kept constant had to be determined. It was taken as the area when the vertical stress was the same as when the test was paused before the weekend. At this point water was expelled to the scale, indicating that the hose was fully saturated and water was squeezed out of the sample. The test was continued up to cell pressure 83 kPa this Monday.

Day 3 the test was continued at a rate of deformation of 0.25 mm/h up to cell pressure 133 kPa.

Day 4 the test was started at a rate of deformation of 0.25 mm/h up to cell pressure

145 kPa. From 145 kPa to 158 kPa the test was run at 0.20 mm/h. From 158 kPa to 163 kPa the test was continued at 0.15 mm/h. The reason for changing the rate of deformation was that during breaks at 145 kPa and 158 kPa, too much water continued to come out of the sample after the deformation has been paused.

Day 5 the test was continued at 0.15 mm/h deformation rate up to cell pressure 171 kPa. After a break where water continued to be expelled, the rate of deformation was reduced to 0.10 mm/h. The test was then continued up to cell pressure 176 kPa.

Day 6, Friday, the rate of deformation of 0.10 mm/h was kept constant up to cell pressure 193 kPa. A break in the middle of the day was made to check if the rate of deformation was too high, but it seemed to be sufficiently low for the water to dissipate out of the sample.

The sample was left over the weekend under the same conditions as the previous weekend. On Monday 13 March the test was run for 62 minutes, and then terminated. The main reasons for termination was that the test had given sufficient results in order to be able to determine a value of K'_0 , and also much information on how slow the test had to be run in order to be assumed to be drained. An additional reason for termination was that the test would have to be run at a decreasing rate of deformation as the sample densified during compression, and thus the time required to continue the test would be too long compared to the possible outcome of continuing the test.

Table 4.3: First day of oedotriaxial testing.

Rate of strain [mm/h]	Time period [min]	Water expelled [g]
1	27	-
0 (break)	32	No measurement
1	22	-
0 (break)	24	0.37
0.5	27	-
0 (break)	23	0.16
0.3	48 -	
0 (break)	29	0.10
0.3	6	-
0.25	170	-

Table 4.4: Subsequent days of oedotriaxial testing.

Day [-]	Cell pressure range [kPa]	Rate of strain [mm/h]
2	39 - 83	0.25
3	83 - 133	0.25
4	133 - 145	0.25
4	145 - 158	0.20
4	158 - 163	0.15
5	163 - 171	0.15
5	171 - 176	0.10
6	176 - 193	0.10

A second oedotriaxial test was consolidated overnight from 13 March. The cell pressure was 10.4 kPa and the vertical stress was 17.3 kPa, corresponding to $K'_0 = 0.60$, which was close to $K'_0 = 0.58$ found in the first oedotriaxial test. Before consolidation, additional adhesive tape was added to the measuring glass to reduce evaporation. The only opening in the tape was a square with area less than 1 cm^2 . The new solution seemed to work better than the tape solution in the first oedotriaxial test, since a drop of water was still hanging from the hose above the scale after a night of consolidation. Another explanation for the drop still hanging there is that the test was not performed sufficiently drained, and hence water continued to be expelled through the night.

The oedotriaxial part of the test was run at a rate of deformation of 0.25 mm/h up to a cell pressure of 20.1 kPa. During a pause of deformation of 3 hours and 49 minutes, 1.07 g of water was expelled. This indicated that the sample was far from drained, even though the test was run at a rate of deformation which had been suitable for the first oedotriaxial test. Since the test would have to be run at a rate of deformation much lower than the first oedotriaxial test, and thus possibly taking several weeks to complete, the sample was instead consolidated further and a standard CAUc test was performed. The test has test identity CAUc-1015.

Chapter 5

Results

In this chapter the results from the field, laboratory and correlation methods will be presented. The results are presented in the same order as the methods were presented in Chapter 2, 3 and 4. At the end of this chapter, results from the different methods will be compared.

5.1 In Situ Methods

5.1.1 Soundings

The results from ten rotary pressure soundings and the CPTU performed are given as graphs in Appendix A. In addition, the map showing the locations of the field investigations is given in the same appendix.

5.1.2 Pore Pressure Distribution

Several figures regarding pore pressure measurements and the assumed pore pressure distribution is presented in Appendix B.

First, Figure B.1 shows the pore pressure measured by the piezometers and earth pressure cells corrected for air pressure. The trend line is the assumed pore pressure distribution at Flotten, which will be more thoroughly addressed in section 6.2.2. The pore pressure values from the piezometers are the values measured 22 May, while the dates for the pore pressure measurements of the earth pressure cells are given in Table B.3.

Second, Figure B.2 is the calculated potential with depth based on the same pore pressures from piezometers and earth pressure cells corrected for air pressure as for Figure B.1. The trend line is potential based on the assumed pore pressure distribution at Flotten. The

Last, Figure B.3 shows the development of the pore pressures with time. This graph has not been corrected for air pressure.

5.1.3 Earth Pressure Cells

Table 5.1 gives an overview of the results from the earth pressure cell tests performed at Flotten. EE and PDW are the identities of the total earth pressure and pore pressure measuring devices, respectively. σ_{h0} is the stable total horizontal pressure not corrected for air pressure or seasonal variations in pore pressure. u is the stable pore pressure measured the same day as the corresponding σ_{h0} . σ'_{h0} is found from the two previous parameters. σ'_{v0} is the best estimate of the vertical effective stress. K'_0 is found from the ratio of σ'_{h0} and σ'_{v0} . In addition, zero readings, taken in air before and after the tests are presented if available, along with some comments. The zero measurements were generally taken in the field soon after extracting the earth pressure cells to the surface.

The development of σ_{h0} and u with time after installation is presented in Figure C.1. The straight lines in the beginning are due to lack of data points to draw the lines through.

The raw data was processed as described in Appendix C.

The values of K'_0 are presented graphically together with the other methods in Figure 5.2.

Table 5.1: Overview of earth pressure cell testing at Flotten. Zero readings are relative to pressure 100 kPa.

Depth [m]	Date	EE	PWD	Borehole	σ_{h0} [kPa]	u [kPa]	σ'_{h0} [kPa]	σ'_{v0} [kPa]	K'_0 [-]	Zero readings			Comments	
										EE		PWD		
							Before [kPa]	After [kPa]	Before [kPa]	After [kPa]				
5.0	15.02.17	24708	24707	EPC001	90	32	58	57	1.02	-4.6	-8.4**	4.1	-3.7	Auger
5.0	15.02.17	24694	24693	EPC002	82	32	50	57	0.88	-4.2	-	4.4	-	Total sounding
5.0	17.02.17	24702	24701	EPC003	87	28	59	57	1.04	-8.9	-11.1	2.1	-2.3	Total sounding
5.0	17.02.17	24696	24695	EPC004	72	26	46	57	0.81	-2.8	-11.6	-0.3	-8.0	Total sounding
5.0	17.02.17	24692	24691	EPC005	68	32	36	57	0.63	-4.2	-12.6	3.0	-2.3	Total sounding
6.0	27.02.17	24694	24693	EPC002	210	39	171	71	(2.41)	-	-36.1	-	-4.3	Pushed, broken
7.0	27.02.17	24702	24701	EPC003	107	44	63	86	0.73	-10.4	-5.0	-1.4	2.4	Total sounding
8.0	27.02.17	24692	24691	EPC005	-	-	-	-	-	-12.1	-151.9**	-1.4	2.5**	Broken*
8.0	27.02.17	24696	24695	EPC004	-	-	-	-	-	-10.9	-219.9**	-6.1	0.6**	Broken*
8.0	17.03.17	24712	24711	EPC004	81	47	34	102	0.33	-9.5	-	-1.7	-	Casing
9.0	30.03.17	24712	24711	EPC004	107	49	58	118	0.49	-6.6	-7.4	1.9	-10.6	Casing
10.0	05.04.17	24712	24711	EPC004	124	47	77	134	0.57	-9	-	0.5	-	Casing
10.0	11.04.17	24712	24711	EPC003	201	45	156	134	(1.16)	-27.3	-204.9	2.6	2.2	Casing, broken

*The cell was broken during installation.

**Measurements were taken outside NTNU 30 May.

5.1.4 Dilatometer

The graphs showing the key parameters I_D , K_D and E_D with depth are presented in Appendix D. The appendix also includes an estimate of OCR with depth, based on Equation 2.12. All the raw data is presented in detail in Ozkul and L'Heureux (2017).

The values of K'_0 estimated by the dilatometer are presented along with the other methods in Figure 5.2. Two of the K'_0 lines are calculated from Equation 2.10 proposed by Marchetti (1980). The use of β_k values of 1.5 for intact insensitive clays and 2 for intact sensitive clays was proposed by Hamouche et al. (1995), as described in section 2.4.2. The other two lines are based on Equation 2.11, which is proposed for Norwegian clays by Lacasse and Lunne (1989). The authors suggested $m = 0.44$ for highly plastic clays and $m = 0.64$ for low plastic clays, and the lines resulting from these two values of m are plotted in the comparison figure.

5.1.5 Field Vane

The raw data and interpretations of the field vane tests are given in Appendix E. The appendix also includes Figure E.1 illustrating development in the measured undrained shear strength with time for the three tests performed.

The K'_0 values calculated for the three test depths are given in Table 5.2, as a summary of Table E.1 in Appendix E. The values of K'_0 are also presented together with the other methods in Figure 5.2.

Table 5.2: K'_0 from field vane tests.

Depth [m]	Calculated K'_0 [-]
8.4	0.38
9.4	0.36
10.4	0.53

5.2 Laboratory Methods

5.2.1 Index Testing

In order to gain the best possible understanding of the soil conditions at Flotten, data from testing both by the authors as well as by Gella is combined in all subsequent index test results. All index test results are presented together in Appendix F.

5.2.1.1 Water Content

A plot indicating the water content with depth is presented in figure F.1.

5.2.1.2 Atterberg Limits

A plot indicating the Atterberg limits with depth is given in Figure F.1. The plot indicates the plastic limit w_P , the liquid limit w_L as well as the water content of a nearby specimen of the same cylinder.

5.2.1.3 Falling Cone

A plot indicating the undrained shear strength with depth as determined by the method of falling cone is given in figure F.1. A plot with the change in sensitivity with depth is also given.

5.2.1.4 Density

During index testing, the density of the samples has primarily been determined by dividing the weight of the entire sample by the known volume of the sample tube, as well as by the use of a small ring. Results of cylinder and small ring measurements is given in the Table F.1. In addition, density calculations have also been performed on oedometer samples, before testing, as indicated in the Table F.2 Based on all these measurements, an average unit weight of 17.5 kN/m^3 has been assumed between 0 and 12 m depth.

Results of particle density measurements through the use of a pycnometer is indicated in Table F.3. The test results show a quite small variation with depth, hence an average particle density of $\rho_s = 2.83 \text{ g/cm}^3$, resulting in $\gamma_s = 27.8 \text{ kN/m}^3$ was assumed for depth from 2 to 12 m.

5.2.2 Oedometer

The results of extensive oedometer testing both by the authors as well as Konjit Paulos Gella is presented in Appendix G. The tests have been given name according to the type of test and depth of the specimen tested. The test CRS-0510 is a CRS oedometer test conducted with a specimen from a depth of 5.10 m. An overview of the tests performed by the authors is given in Table 5.3, while Table 5.4 shows an overview of the tests performed by Gella and one test performed by Espen Andersen. All tests performed by either Gella or Andersen are equipped with a name prefix, indicating the operator of the test. Please note that further details regarding testing procedures used by Gella will not be reviewed in great detail here.

Table 5.3: Overview of oedometer tests performed by the authors of this master thesis.

Test id.	Depth [m]	Strain rate [%/hr]	p'_c [kPa]	OCR [-]	$\Delta e/e_0$ [-]	Figure no.
CRS-0510	5.10	1	280	4.8	0.09	G.4
CRS-0570	5.70	1	260	3.9	0.06	G.7
CRS-0940-1	9.40	1	120	0.96	0.19	G.12
CRS-0940-2	9.40	1	230	1.8	-	G.13
CRS-0950	9.50	0.5	170	1.4	0.12	G.14
CRS-1020-1	10.20	0.5	140	1.0	0.20	G.15
CRS-1020-2	10.20	0.5	180	1.3	0.13	G.16
CRS-1040-1	10.40	0.5	230	1.6	-	G.17
CRS-1040-2	10.40	0.5	190	1.5	-	G.18

Table 5.4: Overview of selected oedometer tests performed by Konjit Paulos Gella. Additionally one test performed by Espen Andersen is included. Please note that ε_{a0} is given as a rough sample quality estimate.

Test id.	Operator	Depth [m]	Strain rate [%/hr]	σ'_c [kPa]	OCR [-]	ε_{a0} [%]	Figure no.
KPG-CRS-0450	KPG	4.50	1	320	6.2	2.2	G.3
KPG-CRS-0550-1	KPG	5.50	1.5	330	5.2	1.9	G.5
KPG-CRS-0550-2	KPG	5.50	1	300	4.7	2.1	G.6
KPG-CRS-0650-1	KPG	6.50	1	330	4.2	3.5	G.8
KPG-CRS-0650-2	KPG	6.50	1	340	4.4	4.1	G.9
KPG-CRS-0750-1	KPG	7.50	1	290	3.1	4.8	G.10
KPG-CRS-0750-2	KPG	7.50	1	280	3.2	4.5	G.11
EA-CRS-1060	EA	10.60	1	200	1.4	6.4	G.19

Figure 5.1 indicates a very high variation in the interpreted values of the preconsolidation pressure between the performed tests. As a direct consequence, OCR has only been determined for depths of 5, 7.5 and 10 m. This evaluation was based on the resulting plots from each individual oedometer test and assessments of sample quality through the $\Delta e/e_0$ -criterion. Generally, tests indicating the best sample quality were used. Please note that most of the specimens tested are of poor quality. Table 5.5 presents the sample quality, assumptions regarding the overburden and pore pressure as well as the subsequent value of OCR for four selected oedometer tests. Details regarding the pore pressure distribution is given in Appendix B. These values of OCR are used when estimating K'_0 from correlation methods, see section 5.3. Collective and detailed plots of all oedometer

tests are presented in Appendix G.

Table 5.5: Estimates of OCR with depth. Sample quality based on the $\Delta e/e_0$ -criterion. $\gamma = 17.5 \text{ kN/m}^3$ assumed for all depths.

Depth [m]	Sample quality [-]	p'_c [kPa]	Pore pressure [kPa]	σ'_{v0} [kPa]	OCR [-]
5.1	0.06	280	31	58	4.8
5.7	0.09	260	33	67	3.9
7.5	-	290	38	93	3.1
9.5	0.13	170	40	126	1.4
10.2	0.13	180	41	137.4	1.3

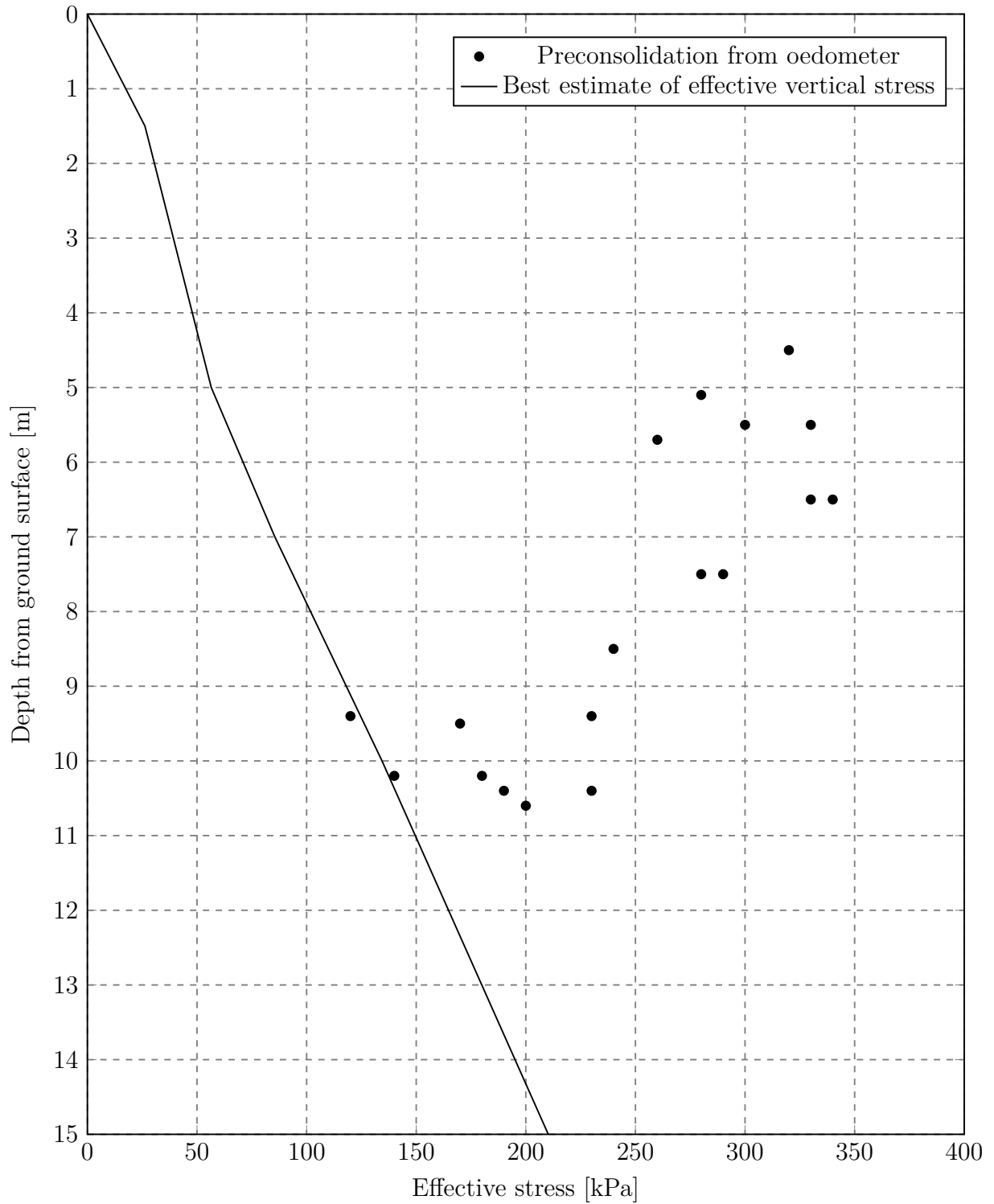


Figure 5.1: Overview of approximate preconsolidation from oedometer testing on 54 mm samples from Flotten. The black line indicates an assumed vertical effective stress profile. $\gamma = 17.5 \text{ kN/m}^3$ assumed for the entire depth. Details regarding the pore pressure distribution assumed is given in Appendix B.

5.2.3 Work Criterion in Oedometer

Becker et al. (1987) presented a way to determine in situ and yield stresses from oedometer tests. Figures H.1, H.2 and H.3 in Appendix H show the cumulated work per unit volume plotted against effective stress for three oedometer test. The tests are regarded as relatively good based on the shapes of the curves in the ε versus σ'_m and the M versus σ'_m plots, as given in Appendix G. However, Table 5.6 shows that the sample quality of two of the samples is characterized as poor. The third test lacks data for calculating $\Delta e/e_0$. Equation 2.15 was applied to unsmoothed oedometer raw data to produce the graphs.

Table 5.6 shows the sample quality, the values of p'_c interpreted by the Janbu method as described in section 4.2 and the values of p'_c interpreted by the work criterion method.

Table 5.6: Sample quality and p'_c interpreted by the Janbu method and the work criterion method

Depth [m]	Test id.	$\Delta e/e_0$ [-]	Sample quality	p'_c Janbu [kPa]	p'_c Work criterion [kPa]
5.1	CRS0510	0.09	Poor quality	280	230
9.4	CRS0940-2	-	-	230	170
9.5	CRS0950	0.13	Poor quality	170	130

5.2.4 Triaxial Testing

An overview of the triaxial tests performed by the authors is given in Table 5.7. The tests have been named according to the same procedure used for the oedometer testing, as closer described in 5.2.2.

Table 5.7: Overview of triaxial tests performed by the authors. Strain rate 0.75 %/hr used for all tests.

Test id.	Depth [m]	σ'_{v0} [kPa]	K'_0 [-]	u [kPa]	ε_{vol} [%]	Figure no.
CAUc-0934	9.34	93	0.74	73.4	-	I.10
CAUc-1015	10.15	146	0.74	34.7	7.9	I.12
CAUc-1036	10.36	148	0.79	38.1	8.1	I.13
CAUc-1056	10.56	152	0.79	38.1	6.6	I.15

In Table 5.8 and 5.9 below, a brief overview of tests performed by Gella is presented. Further details regarding testing procedures by Gella is presented in Appendix I.

Table 5.8: Overview of CAUc triaxial tests performed by Gella. $K'_0 = 0.7$ assumed for all tests.

Test id.	Depth [m]	σ'_{v0} [kPa]	u [kPa]	Strain rate [%/hr]	ε_{vol} [%]	Figure no.
KPG-CAUc-0340	3.40	47.2	14	3	-	I.5
KPG-CAUc-0440	4.40	55.3	24	3	1.1	I.6
KPG-CAUc-0540	5.40	63.1	34	2	1.3	I.7
KPG-CAUc-0640	6.40	70.0	44	2	1.5	I.8
KPG-CAUc-0740	7.40	77.7	54	2	2.0	I.9
KPG-CAUc-0940	9.40	92.4	74	1.2	4.6	I.11
KPG-CAUc-1040	10.40	99.6	84	1.2	3.7	I.14
KPG-CAUc-1153	11.53	108.1	95.3	1.2	3.9	I.16

Table 5.9: Overview of CIUc triaxial tests performed by Gella.

Test id.	Depth [m]	σ'_{v0} [kPa]	u [kPa]	Strain rate [%/hr]	ε_{vol} [%]	Figure no.
KPG-CIUc-0526	5.26	69.4	32.6	2	1.2	I.17
KPG-CIUc-0540	5.40	46.5	34.0	3	1.2	I.18
KPG-CIUc-0626	6.26	55.3	42.6	2	8.1	I.19
KPG-CIUc-0726	7.26	56.4	52.6	2	1.8	I.20
KPG-CIUc-0926	9.26	74.5	72.6	1.2	4.2	I.21
KPG-CIUc-1026	10.26	89.0	82.6	1.2	4.3	I.22
KPG-CIUc-1142	11.42	86	94.2	1.2	3.9	I.23

Based on the triaxial testing performed by the authors as well as Gella, the strength parameters indicated in Table 5.10 have been determined based on curve fitting on collective plots in Figures I.1 to I.4. The transition from plastic to quick clay is believed to be at about 7 - 8 m depth, see section 6.2.1 for details. Indeed, a rather clear change in soil behaviour is evident when comparing triaxial test results on samples from above and below this depth. Consequently, a different set of attraction and friction angle is selected for the clay below a depth of 8 m.

Table 5.10: Strength parameters as determined from triaxial testing.

Depth [m]	Attraction [kPa]	Friction angle [°]
2-8	20	31
8-12	18	28

Collective NTNU and stress-strain plots of the triaxial tests conducted by the authors of this thesis as well as selected tests by Gella is presented in Appendix I. In addition, detailed plots of each test is also presented in Appendix I. Failure lines based on the parameters specified in Table 5.10 is indicated in all plots.

5.2.5 Oedotriaxial

The fitted line in the NTNU plot in Figure J.1 in Appendix J has an inclination of $S_0 = 0.31$. Inserting this into Equation 2.17 gives $K'_0 = 0.62$. By rearranging Equation 2.17 and inserting the assumed in situ overburden stress and attraction, $K'_0 = \frac{\sigma'_h}{\sigma'_v} = 0.58$ is calculated. The latter K'_0 value is comparable to the other values in this thesis, and is therefore presented together with the other methods in Figure 5.2.

5.3 Correlation Methods

Based on the input parameters summarized in Table 5.11, estimates of K'_0 from a selection of correlations methods is given in Table 5.12.

Table 5.11: Input parameters used in correlation methods.

Depth [m]	Friction angle [°]	OCR [-]	w_l [%]	I_p [%]	η [-]	χ [-]
5	31	4.4	52	28	-2	0.8
7.5	31	3.1	36	20	-2	0.8
10	28	1.3	37	19	-2	0.8

Table 5.12: A summary of equations, input parameters and results from the correlation methods.

Equation	Formula	Depth [m]	K'_0 [-]
Jaky original		5	0.49
2.20	$K'_{0nc} = 1 - \sin\phi'$	7.5	0.49
		10	0.53
Jaky cohesion		5	0.44
2.21	$K'_{0nc} = 0.95 - \sin\phi'$	7.5	0.44
		10	0.48
Bolton		5	0.50
2.22	$K'_{0nc} = \frac{1 - \sin(\phi' - 11.5)}{1 + \sin(\phi' - 11.5)}$	7.5	0.50
		10	0.56
Simpson		5	0.47
2.23	$K'_{0nc} = \frac{\sqrt{2} - \sin\phi'}{\sqrt{2} + \sin\phi'}$	7.5	0.47
		10	0.50
Mayne		5	0.48
2.24	$K'_{0nc} = 1 - 1.003\sin\phi'$	7.5	0.48
		10	0.53
Larsson for w_l		5	0.54
2.25	$K'_{0nc} = 0.31 + 0.71(w_L - 0.2)$	7.5	0.42
		10	0.43
Larsson for I_p		5	0.53
2.26	$K'_{0nc} = 0.315 + 0.77I_P$	7.5	0.47
		10	0.46
Modified Jaky		5	1.0
2.29	$K'_{0oc} = (1 - \sin\phi')OCR^{\sin\phi'}$	7.5	0.87
		10	0.61
Sivakumar		5	0.82
2.31	$K'_{0oc} = \frac{1}{\eta}[1 - (1 - \eta K'_{0nc})OCR^{(1-\chi)}]$	7.5	0.74
		10	0.59

5.4 Comparison of all Methods

A comparison of both in situ, field and correlation approaches to K'_0 is presented in Figure 5.2.

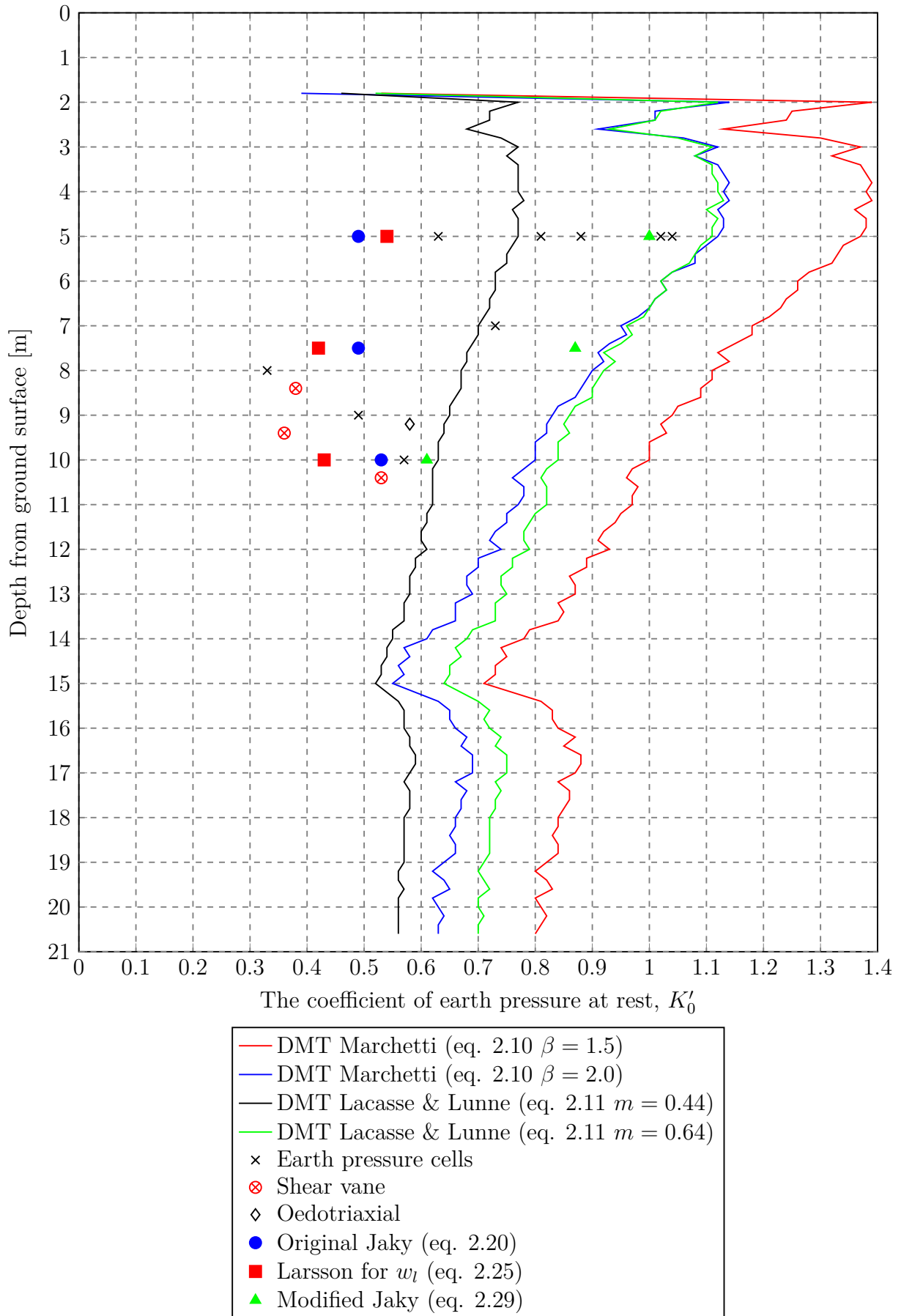


Figure 5.2: Comparison of different approaches to K'_0 . $\gamma = 17.5\text{kN/m}^3$ assumed for all depths.

Chapter 6

Discussion

In the beginning of this chapter, Quaternary geology at Flotten will be briefly discussed. Then in situ methods for investigating the horizontal stress state and K'_0 will be discussed. The main focus of this part is to discuss and learn from the in situ testing conducted during the work with this master's thesis. In addition, there is a small section discussing other approaches to in situ evaluation of K'_0 . This small section represents some key findings from the project thesis written in the autumn of 2016 (Lindgård & Ofstad, 2016). In the next parts of this chapter, laboratory and correlation approaches to estimating K'_0 will be discussed. Also these parts focus on methods utilized as part of this thesis.

6.1 Quaternary Geology

A key question is whether or not the fluvial deposits east of the test site could have covered the test site at some point. Fluvial deposits including sand are more easily eroded than clay (Wan & Fell, 2004), suggesting that Nidelva could possibly have eroded the fluvial deposits away from the top of the clay which is seen at the test site today. For the river to erode away the sand at the test site and not the fluvial deposits seen in Figure 2.6, it demands that the river course of Nidelva at some point went on the west side of the green hills in the lower parts of the figure. Reite et al. (1999) state that Nidelva has for the last 9800 years been running to the east of the hills. As long as the river course has only been to the east of the hills, there is no logical explanation to how Nidelva could have eroded away fluvial deposits at the test site without removing the fluvial deposits in Figure 2.6 as well.

The section above and the Quaternary geological information in section 2.2.7 does not present a final answer to the properties of the Flotten test site. Since it is basically intact old sea floor, it could be normally consolidated if the ice shelf covering it has not affected the clay due to buoyancy. On the other hand, the clay could be mechanically

overconsolidated to some degree due to the ice shelf cover. The material may in any case be overconsolidated due to various time effects (see section 2.2.1). Also, one may expect to find either silty clay or clayey silt material. Quick clay is present at least in the nearby area (Reite et al., 1999).

6.2 In Situ Methods

When comparing some of the literature on the in situ determination of the horizontal stress state, the three methods of the earth pressure cell, self-boring pressuremeter and hydraulic fracturing are often mentioned as reference methods, yielding relatively repeatable values in different soil materials (Ku & Mayne, 2013). Typically, if investigations are conducted in the laboratory or new theoretical approaches are proposed, the values are compared to one or more of these reference methods (see for instance Hamouche et al., 1995; Massarsch, 1975; Tedd & Charles, 1981). Indeed, these methods all represent a more direct approach to the determination of K'_0 , compared to for instance the dilatometer which rely on empirical correlation methods (Lacasse & Lunne, 1989).

6.2.1 Soundings

The rotary pressure soundings and the CPTu sounding presented in Appendix A are quite similar in their representation of four key features of the Flotten site.

The first key feature is homogeneity. Since the rotary pressure soundings give comparable results over a larger area, the site may be assumed to be quite homogeneous in the horizontal direction. In the vertical direction, both the rotary pressure soundings and the CPTu show similar characteristics. The rotary pressure soundings demand steadily increasing pressure force down to between 7 and 8 m depth. From there and down to about 20 m depth the pressure force decreases steadily. The CPTu show a relatively smooth corrected tip resistance graph from 4 to 20 m. The side friction graph from the CPTu is relatively smooth, but is shifted between 7 and 8 m depth. Due to the steady changes in the rotary pressure soundings and the CPTu, it is assumed that the material is quite homogeneous in two layers in the vertical direction, with a transition between 7 and 8 m depth.

The second key feature of the Flotten site is the transition at 7 to 8 m depth. The decrease in the rotary pressure soundings from this depth suggests that the material below the transition is quick clay. At the more shallow depths the clay is presumably not quick. Similarly, a quite evident reduction in side friction is also witnessed at about the same depth in the CPTu results. On the other hand, no clear change in correct tip resistance is observable at these depths. The low side friction suggests that the clay is remoulded by

the cone tip, and that the clay is quick. The fall cone test results in Appendix F support the conclusion that the clay is quick below 7 to 8 m depth and not quick at shallower depths.

The third key feature is the less smooth graphs below about 20 m depth. The rotary pressure sounding graphs have spikes of high resistance, indicating that the material is no longer homogeneous clay. The increased resistance suggests layers of silt or sand. The CPTu shows similar results. At 20 m depth the measured pore pressure suddenly drops, most likely indicating a draining layer. The clear drops between 23 and 25 m depth indicate draining layers. The spikes at 23 m with increased corrected tip resistance and side friction simultaneously with a significant drop in pore pressure suggest a significantly draining layer, possibly a sand layer.

The fourth key feature is that above approximately 2 m depth there seems to be a dry crust. This is visible as spikes in the rotary pressure soundings. In the CPTu results, small spikes in the corrected tip resistance plot and higher side friction suggest approximately 2 m of dry crust.

The Quaternary geology discussed in section 6.1 suggested that there would be clay at Flotten, and possibly quick clay. This is in accordance with the results from the soundings.

6.2.2 Pore Pressure at Flotten

This section is dedicated to describing the assumed pore pressure distribution at Flotten and give a possible explanation of why the pore pressure is distributed in this way.

Figure B.1 shows measured pore pressure with depth. It may be seen that there is a scatter in the pore pressures measured with several earth pressure cells at 5 m and 10 m depth. As a consequence, it is not possible to draw an approximately straight line through all the data points, and hence the cells do not indicate an unambiguous linear increase in pore pressure with depth. Also, the earth pressure cells generally give higher values than the piezometers. One would expect the pore pressure distribution to be linearly increasing with depth if there are no abrupt changes in permeability between layers. The CPTu pore pressure measurements, as presented in Figure A.14, did not indicate any draining layers of importance between 5 and 15.75 m depth. Both the CPTu and the rotary pressure soundings suggest that there are two relatively homogeneous layers between 5 and 15.75 m depth. The spread and following non-linearity of the pore pressures from the earth pressure cells suggest that the measurements of pore pressure from the earth pressure cells are of limited quality. Possible reasons for wrong values of pore pressure obtained from the earth pressure cells will be discussed in section 6.2.3.2.

The Geotech PVT electric piezometers installed at Flotten are widely used for measuring pore pressure. Therefore, one would expect the results from the piezometers to be

of good quality. Figure B.1 shows that the piezometers at 5, 7, 10 and 15.75 m depth give values which almost lay on a straight line. This supports the assumption that there are no draining layers having a great impact on the pore pressure distribution between 5 and 15.75 m depth. Due to the credibility of the piezometers, the assumed pore pressure distribution in this thesis is based on the piezometer readings. The readings on 22 May corrected for air pressure are the ones used since all the piezometers were installed and stable at this time. The corrected readings are given in Table B.4. Between each of the points the pore pressure is approximated by linear lines. The pore pressure below 15.75 m is needed for the dilatometer data processing. Since there is no pore pressure data available below 15.75 m, it is assumed that the linear increase from 10 to 15.75 m continues at the same rate from 15.75 m to 20.6 m depth. Also, at shallower depths than 5 m there are no available pore pressure measurements. Therefore, a linear distribution is assumed between the piezometer reading at 5 m and an assumed ground water level 1.5 m below terrain. This ground water level is assumed based on measurements of the water level in open boreholes at 1.3 m below terrain, and the fact that the distribution is slightly below hydrostatic water pressure if the ground water level is 1.5 m below terrain. The assumed pore pressure is shown as the solid line in Figure B.1.

It is interesting to look at how stable the pore pressure measurements are with time. Figure B.3 in Appendix B indicates the development of pore pressure with time for the piezometers, not corrected for air pressure. Between 10 March and 12 May the pore pressure seems to be quite stable. However, the development between the measurements is unknown since the piezometers in question do not have a logging memory. Changes may have occurred, since the measurements are taken between one and four weeks apart. The measurements taken on 22 February indicate a drop of about 6 kPa compared to the previous and succeeding measurements, and the pore pressures show an increase of about 5 kPa from the measurement 12 May to the measurements 15 May and 22 May. The piezometers with memory show a variation of ± 1 kPa in the period between 17 May and 22 May. These measurements suggest that there are some slight changes in pore pressure at Flotten with time. The variations in pore pressure may be caused by changes in air pressure and the changes in ground water level due to the amount of rain, drying and snow melting.

An explanation of why the pore pressure is much lower than hydrostatic may be that there exists draining layers at greater depths. Such draining layers are indicated by both the CPTu and the rotary pressure soundings below 20 m depth, as more thoroughly discussed in section 6.2.1. If water is drained deeper down, this indicates that there is a downwards water flow. Figure B.2 shows that the assumed potential decreases with depth. Decreasing potential with depth causes a downward gradient, meaning that there is in

fact a downward water flow and that the pore pressure will not increase hydrostatically with depth.

In Figure 6.1 the elevation profile between the test site and the river Nidelva is given. The site is located at about 123 m altitude, while the river Nidelva is located at altitude 72 m. The horizontal distance from the test site to Nidelva is approximately 1 km. Looking at the elevation profile and keeping in mind that there exists draining layers below 20 m depth which might stretch over large areas, it is easy to believe that the layers may drain water from the test site to Nidelva. The potential is the same at the water surface of Nidelva as it is at the ground water surface at the test site. When the same potential exists at different altitudes which are connected through water, there will be a water flow towards the lower point. Due to the height difference between these surfaces and the assumption that there is continuous contact between them, there needs to be a water flow between the test site and Nidelva.

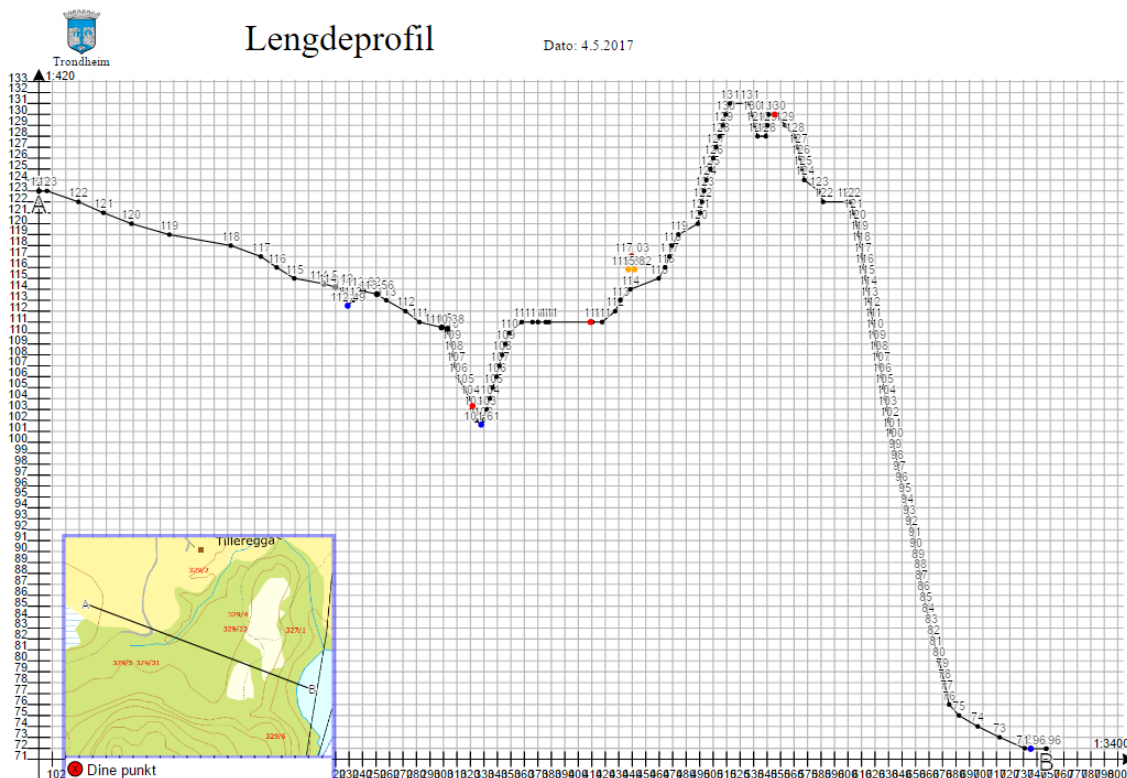


Figure 6.1: An elevation profile from the test site (left side) to the river Nidelva (right side). Figure from Trondheim Kommune Kart (trondheim.kommune.no/karttildeg/).

6.2.3 Earth Pressure Cells

A comparison of all values of K'_0 calculated from earth pressure cell measurements with depth is shown in Figure 5.2 along with the other methods used. The amount of variation between the individual measurements with the earth pressure cells is tremendous; making

a unique determination of K'_0 with depth very challenging. This section is devoted to discussing possible explanations to these results.

Two key issues have been the most important when working with the earth pressure cells. First, some of the cells have been permanently damaged by the installation. Therefore, attempting to find a repeatable and effective way to install the cells has been important. The second key issue is considering how much and in which way the installation affects the measured values. Both of these key issues will be addressed in this section.

In general, the graphs from the measurements of σ_h and u in Figure C.1 show the same trend when it comes to decreasing values after installation, and relatively stable values after some days. The time needed to stabilize the values at Flotten is shorter than what is given in some of the literature (see for instance Massarsch, 1975; Tedd & Charles, 1981; Ryley & Carder, 1995)

6.2.3.1 Stress Conditions

The goal of K'_0 investigations is to determine the in situ value of the horizontal effective stress. Measuring the in situ value is however challenging, since installation of the test equipment tends to alter the stress situation. In this section the best estimate of the in situ stress situation at Flotten and several hypotheses for how the stress situation alters during installation of earth pressure cells will be presented.

The in situ stress conditions with depth at Flotten are most likely quite similar throughout the test site. This assumption is mainly based on the soundings in Appendix A showing comparable results over a larger area. Also, the Quaternary geological history indicate that the site is most likely more or less old sea floor, which would suggest quite homogeneous in situ stress conditions. Finally, the site is quite flat, which leads to the conclusion that there are relatively small differences in in situ stress caused by elevation differences throughout the site. The exception from flat terrain is the approximately three meter deep recession next to the test site. This recession will give rise to rotation and change in the values of the in situ principal stresses in the proximity of the recession.

The change in in situ horizontal stress is most pronounced perpendicular to the longitudinal direction of the recession, and therefore the cells at 5 to 9 m depth were placed with the blade perpendicular to the recession in order to get the most correct measurement of the in situ horizontal stress representative for the test site. It was assumed that the deviation in stress from the representative in situ horizontal stress would be greater due to the recession, than the increased effective stresses caused by several cells installed next to each other.

During installation of cells at 8 and 9 m depth, a change in the obtained measurements

from the cell installed at 7 m depth was observed. These measurements will be described in more detail in section 6.2.3.6. Since the cell at 7 m was so influenced by boreholes perpendicular to the blade orientation, the cells at 10 m depth were installed with the blade parallel to the recession in an attempt to minimize the influence of nearby boreholes. It was assumed that the stress change from the representative in situ state for the test site due to the recession, was less than the change caused by boreholes perpendicular to the blade.

The stress situation in the ground during installation of an earth pressure cell is complex, and several different effects may affect the measurement in different ways. First of all, since the earth pressure cell is pushed into the ground, it is easy to believe that the cell displaces soil in a similar manner as a nail being hammered into a piece of wood. This would lead to increasing horizontal total stress and increasing pore pressure immediately after the installation. As time passes, the excess pore pressure will dissipate and cause a reduction of pore pressure and increase in horizontal effective stress. The horizontal effective stress after primary consolidation has finished will be larger than before the installation due to the displacement caused by the cell. This way of looking at the stress situation after installation of an earth pressure cell will be in line with the measurements of over-read made by the similar earth pressure cells, for instance reported by Tedd and Charles (1983), Carder and Symons (1989) and Ryley and Carder (1995). These articles do however not treat sensitive clays, and therefore one might argue that the reported over-read would possibly only affect the measurements in the upper 7 m of the soil at Flotten where the clay is not that sensitive.

When an earth pressure cell is installed in quick clay, it is likely that the clay around the blade is remoulded during installation. The effects of this are complex, but at least the surrounding clay does not behave in the same way as a piece of wood around a nail since the soil is not simply displaced some millimetres. Whether the earth pressure cells are expected to give a too high, correct or too low reading depends on what happens to the remoulded clay. If the clay is stuck between the earth pressure cell and the surrounding soil, it may transfer stress to the surrounding intact clay and possibly lead to an increase in horizontal stress. If however the remoulded clay is able to move away from the blade of the earth pressure cell and move along the drill rods when it is compressed, the measurement could be too low since there is not sufficient contact between the blade of the cell and the surrounding intact soil. Also, the stresses could be too low due to arching, which will be described next.

Kenney (1967) stated that installing equipment in sensitive clays will lead to remoulding of the clay next to the installed equipment. When the remoulded clay has consolidated, the horizontal effective stresses on the equipment will probably be lower than the in situ

horizontal effective stress due to the effect of arching (Kenney, 1967). The arching effect may be understood by considering old stone bridges carrying the load from the bridge by compressive forces in the arch. The load from the clay surrounding the cell may also be carried by arching when the clay tries to move towards the cell. The effect of arching will be a measured horizontal effective stress lower than in situ, and hence a too low value of K'_0 .

For the installations using ODEX-casings, a key question is whether soil moves up and into the casing, or if the cell with the metal guide rings pushes soil out of the casing. If soil moves up through the casing due to reduced overburden pressure, this would cause a reduction in the mean stress in the region around the earth pressure cell. The horizontal stress could be decreased due to this. The surrounding soil would tend to move towards the earth pressure cell, but may be partially carried by arching. The measured pressure would probably be too low in this case.

If the situation is however opposite, that soil trapped inside the casing during installation is pushed out of the casing due to the metal guide rings on the cell, it would lead to a completely different stress situation. One may suggest that the horizontal effective stress is permanently higher compared to the in situ horizontal effective stress, due to compaction of soil around the earth pressure cell when soil from inside the casing is pushed out. This would lead to an increased value of K'_0 . This possible compaction may also increase the stresses which tend to bend cells during installation.

The stress changes caused by the total sounding equipment are also complex and hard to predict. There are several possibilities for the extent to which the clay in the borehole is remoulded and to which degree the clay moves freely around the drill bit and rods. If much of the clay is compressed below the drill bit instead of passing the drill bit and up along the rods, it may cause the clay below to be compacted. This could possibly lead to an increased horizontal stress compared to the in situ state. On the other hand, clay could first be compressed below the drill bit and then be unloaded sufficiently when the total sounding equipment is retraced to the surface. This may lead to compression of the clay below the drill bit and hence cause movement of the surrounding soil outwards horizontally. When the clay is then unloaded, the soil would tend to move towards the center line of the borehole, and in this case arching effects could possibly result in measured horizontal stress lower than the in situ. This last situation would be similar to the unloading due to soil moving up inside the casing.

The stress condition after using an auger is also hard to predict. The auger may compact the masses below the pre-drilling permanently, resulting in higher effective horizontal stress than the in situ stress. Or the auger may remove the masses and thereby unload the soil in the same way as in the casing situation where soil moves up into the casing.

In this situation the calculated effective horizontal stress may be too low due to arching.

6.2.3.2 Pore Pressure from Earth Pressure Cells

The pore pressure situation around the earth pressure cell may not be as easy to predict as one would suppose. Ideally, the equilibrium state of the pore pressure should be equal to the pore pressure measured by the nearby piezometers, but the results do however deviate. Figure B.1 shows the pore pressures measured by both the piezometers and the earth pressure cells. For all but two cells, the measured pore pressure is higher from the earth pressure cells than the assumed pore pressure distribution from the piezometers. The two measurements which are lower are from two of the cells at 5 m depth, while the other three cells at the same depth show value higher than the piezometer installed nearby at the same depth.

There is a quite large scatter between the earth pressure cell pore pressure measurements. The earth pressure cells installed at the same depth should ideally give the same measured value if the readings are taken at the same time. For all the five cells at 5 m depth the measurements were taken within a short period of time on the same day. Still, the measurements deviate by 6 kPa. One possible explanation for this is that there is a communication between water in the boreholes and the cells. Different amount of water and varying degree of communication could explain why the measurements at the same depth at the same time are so scattered.

However, there seems to be no direct communication between the pore pressure sensors and the water in the boreholes. For the cells installed at 8, 9 and 10 m depth, the casings were filled with water. Only a limited amount of the water in the casings managed to drain away, so the water surface in the casing was close to the ground surface. If there had been a direct communication between the water column in the casings and the pore pressure sensors, the measurements should have been much higher. This indicates that there is no direct communication between the sensors on the cells and the water in the borehole, but there may be a partial communication leading to increased pore pressure measurements compared to the piezometers.

In Appendix B the pore pressure measurements from the damaged cells are included in the figures. This is because these measurements give reasonable values compared to the undamaged cells. Also, the zero measurements before and after installation, as given in Table 5.1, suggest that the pore pressure sensors were not permanently damaged even though the blade had been bent. The best example is probably the cells installed at 10 m depth, which give only 2 kPa difference between the measurements from the broken and the undamaged cell, even though these are taken a month apart.

6.2.3.3 Equipment Errors

At the beginning of the semester, the authors of this thesis had relatively high expectations for the earth pressure cell equipment based on the literature presented in section 2.4.1. Therefore, the issue of equipment errors was not treated thoroughly before it became evident that the spread in the measurements at Flotten was quite substantial. This section concerns possible equipment errors which could have affected the measurements. The two main sources of error in the total earth pressure measurements are probably elastic bending and permanent changes in zero readings due to bending deformation. It is likely that the error in manufacturing is not that important since the equipment is calibrated afterwards. The calibration could be erroneous, but the effect of this is probably negligible compared to the assumed two main sources of error. The errors due to transportation are hard to predict, but it is assumed herein that transportation should not be a major issue.

The first main source of error is elastic bending. It is evident from the photographs of permanently bent cells that the cells are subjected to bending moment in the ground during penetration, and this bending moment has given a permanent plastic deformation of the cells. In addition to the plastic deformation, the cells have been subjected to elastic bending with reversible deformations. In an attempt to quantify the effect of elastic bending on the measured total earth pressure, the authors of this thesis used the tip of a small screwdriver to apply lateral force on the tip of intact cells. The screwdriver was believed to only apply pressure to the outer frame of the earth pressure cell and not to the pressure pad itself. A close-up of the test setup is shown in Figure 6.2. The measurements of change in total earth pressure compared to air pressure due to pushing the screwdriver with one hand are given in Table 6.1. The change in zero measurements of the air pressure before and after the screwdriver was used, was negligible. Therefore, it is assumed that the bending was elastic.



Figure 6.2: Close-up of the test setup for quantifying the effect of elastic bending.

Table 6.1: Change in σ_h from air pressure measured when pushing a screwdriver on the tip of the two sides of the earth pressure cell blade.

Sensor id.	$\Delta\sigma_h$ side 1 [kPa]	$\Delta\sigma_h$ side 2 [kPa]
EE24698	-1.0	+5.5
EE24702	-0.7	+7.8
EE24708	-1.8	+5.4

Please note that the measured change in pressure deviated substantially between loading from one side of the cell and the other side. Thus, the effect of elastic bending is hard to predict. In the above test only the force from using one hand was applied to induce a bending moment, and it did not lead to noticeable plastic strains. Since the earth pressure cell is subjected to much larger bending moments when installed in soils, as is evident from the permanently bent cells, the misreading due to elastic bending of the cells in the ground remains an open question. The cells which have looked alright when retracted to the ground might have been exposed to elastic bending in the ground, potentially leading to quite large errors.

The second main source of error is permanent changes in the zero readings made in air at the surface, most likely due to permanent deformation of the cells due to bending. Table 5.1 shows that the cells that have the lowest zero readings after retracting the cells from the ground, are the broken cells. This is particularly pronounced for the cells with earth pressure sensor identities EE24692, EE24696 and EE24712. For the cell with earth pressure sensor identity EE24694 this is not equally evident, with a zero value after retracting the cell from the ground which is not that reduced compared to the zero reading

made before the cell with sensor identity EE24712 was installed on 11 April. The latter did not appear to be permanently bent before it was installed. Permanent deformation due to bending may lead to misalignment of the earth pressure membranes of the earth pressure cells. Such misalignment is clearly visible as a "bump" on only one side of the cell in Figure 6.3. This is the cell which has given the lowest zero reading after extraction from the ground.



Figure 6.3: Permanent misalignment of the earth pressure membranes due to bending.

Table 5.1 also shows that for the cells installed in borehole EPC004 and EPC005 at 5 m depth, the zero measurements of total earth pressure before and after installation change by approximately 8 to 9 kPa, even though the cells were seemingly unaffected by the installation and extraction. This change may not be explained by change in air pressure alone. One may suggest that the cells are slightly damaged due to bending, even though the cells appeared to be relatively unaffected by the installation. In general, the zero measurements are lower after installation than before.

A possible third main source of error is changes in temperature. On the calibration sheets (see Appendix C), a temperature coefficient is given for each sensor. This coefficient is quantified to be $< 0.5 \text{ \%}/^{\circ}\text{C}$ *v.E.* for all the sensors used. This means that the change in measured pressure for a change of one degree centigrade in temperature is less than 0.5 % of the full measuring range. Quantifying the possible change for the pore pressure sensor with serial number PWD24693, the maximum change in measured pressure due to temperature variations is $2.5 \text{ kPa}/^{\circ}\text{C}$ since the full measuring range is 0-5 bar. The corresponding value for the total earth pressure sensor with serial number EE24694 is $3.5 \text{ kPa}/^{\circ}\text{C}$ since the full measuring range is 0-7 bar. The calibration sheets showing these values are given in Appendix C.

The ground temperature has been registered by the piezometers to be approximately

3 to 5 °C. The calibration sheets are based on temperature 23 °C. This means that the maximum change in pore pressure measurements due to temperature change will be 45 kPa if ground temperature 5 °C is used for the calculations. The corresponding value for the earth pressure sensor is 63 kPa. The values for the other pore pressure and earth pressure sensors are of similar magnitude.

Because of the possibility of great deviations in the measurements due to temperature variations, the authors of this thesis have been in touch with Glötzl, the manufacturing company of the earth pressure cells. A Glötzl representative stated that the temperature coefficient given in the calibration sheets for the earth pressure cells are too high just to be on the safe side. Data sheets for the sensors Glötzl buy from other suppliers show that the actual temperature coefficient is $< 0.07 \text{ \%}/^{\circ}\text{C}$ *v.E.* for the sensor itself. Glötzl also stated that for practical purposes the temperature coefficient is $< 0.08 \text{ \%}/^{\circ}\text{C}$ *v.E.* for the cells. This corresponds to a worst case scenario of 11.2 kPa change in pressure for 20 °C change in temperature. The temperature change from the zero readings above ground to the ground temperature have never been greater than 20 °C for the tests in this thesis, and most of the times the change has been much less. This suggests that the influence of temperature on the measurements is not a major issue, even though the value of the temperature coefficient in the calibration sheets indicated otherwise.

The zero measurements of the pore pressure sensors given in Table 5.1 indicate that the pore pressure sensors probably give a reasonable value even when the earth pressure sensor of the same cell is broken. The deviations in zero measurements for the broken cells are much smaller for the pore pressure sensors compared to the earth pressure sensors. It is a general trend that the pore pressure zero measurements taken after extracting the cells from the ground are in general lower than the zero measurements before installation. This may be due to suction forces occurring when the cell is pulled out of the ground. The suction would decrease over time, as the pore pressure system have had time to equalize the pressure inside the cell to the surrounding pressure. Two observations which support this are given in Table 6.2. For both pore pressure sensors PWD24707 and PWD24693 the zero measurements have increased between measurements made shortly after extraction of the cells and measurements taken after the cells had been stored for some time in the NTNU basement.

Table 6.2: Zero readings taken in the field shortly after extraction of the cell and outside NTNU 30 May.

Sensor id.	Zero readings after	
	Field [kPa]	NTNU [kPa]
PWD24707	-3.7	2
PWD24693	-4.3	1.6

6.2.3.4 First Installations at 5 m

Since the installation procedure and the results from the earth pressure cells have varied so much with depth, each of the following section will discuss one cell installation depth.

All of the five cells installed at 5 m depth seem to be undamaged due to the installation based on visual inspection of the cells after retrieval to the ground surface. All of the five cells were installed at the same depth with the same orientation and the same spacing between the cells. All final readings were taken at about the same time on 27 February 2017. The last four cells were installed using the same total sounding equipment for pre-drilling, while the first hole (EPC001) was pre-drilled with an auger.

Still, there is a huge scatter in the results at 5 m depth, as may be seen in Figure 5.2, Figure B.1 and Table 5.1. This scatter is evident for both the measurements of pore pressure and total earth pressure, as well as the calculated K'_0 . There seems to be no obvious pattern in which cells have the highest pore pressure readings and total earth pressure readings.

The scatter may primarily be explained by two factors. First, the stress situation after installation is unknown, as described in section 6.2.3.1. The effect of the total sounding equipment during pre-drilling, as well as the installation of the cell itself into the soil, remain an open question. The different stress situations caused by the use of total sounding equipment, as described in section 6.2.3.1, will result in a value of effective horizontal stress deviating from in situ conditions. The effect of the auger suffer from the same uncertainty, as described in section 6.2.3.1. The value of effective horizontal stress found by pre-drilling with an auger lies within the scatter of the values obtained by pre-drilling with total sounding equipment. Hence, there is not sufficient data to give any concluding remarks regarding the differences between these two methods.

The second factor explaining the scatter is equipment errors, as addressed in section 6.2.3.3. Since elastic bending of the cells using one hand and a screwdriver resulted in deviations in measured horizontal total stress of 6.5 to 8.5 kPa, the effect of elastic bending of the cells in the ground might influence the measurements substantially. Also, by comparing zero readings taken before installing the cells to those taken after retracting

the cells, a reduction of about 8 to 9 kPa is evident for cells at 5 m in boreholes EPC004 and EPC005. Since this deviation is greater than what could be explained by change in air pressure, this might suggest that the cells were slightly bent during the installation, even though a visual inspection did not uncover this. Errors caused by temperature are probably neither able to explain the deviation. On the days of installation and extraction of the cells mentioned above, the air temperature deviated with less than 7 °C from the ground temperature at 5 m depth. This relatively small variation suggests that the error in the zero measurements due to temperature change is probably not that pronounced.

The earth pressure cells at 5 m depth show values of K'_0 both higher and lower than those found from the dilatometer with the correlation proposed by Lacasse and Lunne (1989) with $m = 0.44$ for highly plastic clay. However, all of the earth pressure cells at 5 m depth show values lower than the original correlation proposed by Marchetti (1980). The original correlation is known to give too high estimates for K'_0 in clays (Lacasse & Lunne, 1989).

6.2.3.5 Installation at 6 m

The installation at 6 m depth indicated that the earth pressure cells are too fragile to be pushed 1.30 m through undisturbed soil, even if the installation is performed in steps with frequent breaks to let excess pore pressure dissipate. 1.30 m is the distance down from the pre-drilling performed before the initial installation at 5 m in borehole EPC002. In the project thesis Lindgård and Ofstad (2016), a cell was bent when pushed almost 1 m into undisturbed soil without such breaks. The breaks made in the installation at Flotten were clearly not a sufficient measure to make the cell not get damaged during the pushing through undisturbed soil.

As discussed in section 6.2.3.3 the cells do not require much lateral force to be bent. The most likely cause of the bending of this particular cell is believed to be that more or less random differences in stress on the two sides of the cell blade has resulted in initial bending, causing a shift in the resultant of the force acting on the cell. The shifting of the resultant has intensified the bending moment acting on the cell. This effect has probably increased in magnitude as the cell was pushed 1.30 m through undisturbed soil, and the cell was permanently bent due to this treatment.

As it may be seen from Table 5.1, the total horizontal stress measured and the calculated value of K'_0 from the cell at 6 m depth are clearly too high. Due to this, the K'_0 value from this cell is not included in the collective plot in Figure 5.2. However, the measured pore pressure seems to be reasonable compared to the other measurements from the earth pressure cells. Therefore, the pore pressure value from the cell at 6 m depth is included along with the other pore pressure measurements in Appendix B.

6.2.3.6 Installation at 7 m

The installation of the cell at 7 m depth seemed to be conducted without any special issues. This is supported by the relatively small deviation in the zero measurements before and after installation.

The calculated value of K'_0 seems to be reasonable if one assumes that the dilatometer correlation proposed by Lacasse and Lunne (1989) with $m = 0.44$ for highly plastic clay applies at 7 m depth. It is however hard to determine if the measurements give a reasonable value just by coincidence. The limited understanding of the stress situation after pre-drilling with the total sounding equipment, as described in section 6.2.3.1, as well as the relatively large effect of bending discussed in section 6.2.3.3, gives rise to the conclusion that the reasonable K'_0 value at 7 m might just be a coincidence.

The cell at 7 m depth had reached equilibrium after its installation when the cells at 8 and 9 m were installed. Therefore, the effect of casings and cells being installed in the borehole approximately 2 m away from the cell at 7 m can be quantified. After installation of the cell at 8 m the measured total horizontal pressures increased by more than 20 kPa for the cell at 7 m depth. The measured pore pressure increased by approximately 10 kPa. The increase in measurements at 7 m depth were less pronounced when the cell at 9 m depth was installed, but the effect was still clearly noticeable. The increases in pressure due to nearby installations are clearly visible around 26000 and 45000 minutes in the σ_h versus time and u versus time plots in Figure C.1.

6.2.3.7 Installations at 8 m

During the first two attempts to install cells at 8 m depth, the cells showed sign of being bent. The sign was a decline in the total horizontal stress measurements during installation. On the contrary, for penetrations where the cells were not permanently damaged during the installation, an increase in the total horizontal stress measurements was observed. The problem seems to be that by the time the measurements showed a significant decrease, the cells were already permanently damaged. The declining measurements can therefore not be used as an indication of whether penetration should be stopped in order to not damage a cell.

The most likely explanation of why the two first cells were damaged before entering undisturbed soil, is that the cells somehow got stuck to the wall of the borehole and were bent during further penetration. Possibly the boreholes collapsed partially, making it even harder for the cells to continue in a straight line down the borehole. A partially collapsed borehole could have the same effect on the cell as on the cell pushed from 4.70 to 6 m depth. The theory of a collapsing borehole in the more sensitive clay below approximately

7 m depth is plausible, since installation at 5 m depth did not show the same problems. In the literature treated in section 2.4.1, the installations were not performed in quick clay. Possibly due to problems in quick clay, the problems were not anticipated from reviewed literature.

Due to the two damaged cells, a casing was installed before the next cell was penetrated into the ground. Based on observations after pre-drilling, it was evident that clay was sticking on to the last meter of the total sounding equipment. This suggest that the casing was filled with partially remoulded clay extending about one meter up from the bottom of the casing. When the cell had been pushed down inside the casing and to the final depth into undisturbed soil, the drill rods moved upwards some centimetres. This indicates that the cell with the solid metal guide rings had compressed some of the clay inside the casing and partially pushed it out of the casing. This caused a rise in pressure, which led to the drill rods being pushed upwards when the drill rig no longer held them down. This compression and subsequent unloading could possibly lead to either an increase or decrease in the measured value of K'_0 , as described in section 6.2.3.1.

The cell was pushed down to the desired final depth once more, and upon removal of the drill rig the rods moved 3 cm upwards. The hypotheses for the possible changes in K'_0 still apply. Looking at Figure 5.2, it is clear that the cell at 8 m depth gives a too low value of K'_0 compared to what one would expect from the dilatometer and correlation methods. The dilatometer, soundings and index testing give no indication that there should be completely different material properties at around 8 m depth compared to the surrounding clay. There is a transition from plastic clay to quick clay between 7 and 8 m depth, but no special layering at around 8 m depth. Since the measured horizontal effective stress is lower than what is expected, it may support the hypothesis that arching gives lower horizontal effective stress when some clay moves upwards into the casing. On the other hand, two cycles of loading the clay when attempting to install the cell at the final depth gives a complex and not easily predictable stress situation. Also, wrong measurements due to bending of the cell could be an issue, as described in section 6.2.3.3.

6.2.3.8 Installation at 9 m

Looking at Figure 5.2, the cell installed at 9 m depth gives a K'_0 value which is a bit on the low side compared to all the dilatometer correlations. It is also lower than the value found from the original Jaky's equation. This suggests that the value from the cell at 9 m depth is too low compared to the true in situ value. This might be due to complex changes in the stress situation due to installation with casing, as discussed in section 6.2.3.1, or due to bending of the equipment as discussed in section 6.2.3.3.

6.2.3.9 Installations at 10 m

The first cell installed at 10 m depth gives a reasonable value when compared to dilatometer, and the original and modified Jaky's equations. Due to the unknown effects of installation on the stress situation, as well as the problem with bending described in section 6.2.3.3, it is hard to predict if the reasonable calculated value of K'_0 is just coincidental. In addition to the stress situation discussed in section 6.2.3.1, the cells at 10 m depth were installed after pre-drilling with total sounding equipment with flushing. It is challenging to determine the extent of stress change caused by the flushing. The cells at 10 m had metal guide rings with reduced cross-sections as shown in Figure 3.4b. This probably helped the clay inside the casing pass the rings, and therefore the large pressure build-up observed during installation at 8 m was not seen at the installation to 10 m depth.

The second cell installed at 10 m depth was installed with the same installation procedure as the first. Still, the second cell was damaged when arriving at the final depth. There are two likely explanations of this. The first one is that the stress situation at installation in the ground is complex and seemingly a bit random. This means that more or less random variables could cause the second cell to be damaged, even though the first was not permanently damaged by similar treatment. The second explanation is that the cell had some permanent damage after the first installation at 10 m depth. This permanent damage was not noticed upon visual inspection before installation of the cell. The zero measurement of total earth pressure taken before the second installation at 10 m, is nearly as high as the zero reading taken after the cell at 6 m had been clearly damaged. This poses the question of whether the cell was already slightly bent before the second installation at 10 m depth. If the cell was a little bent before installation, this would increase the probability of the cell being permanently damaged during the installation.

Since the value of K'_0 from the second cell at 10 m depth is clearly not valid, it is not included in Figure 5.2.

6.2.3.10 Last Installation at 5 m

The last attempts to install an earth pressure cell at 5 m depth were unsuccessful. The problem seemed to be that more than half the casing was filled with partially remoulded clay. The rotation of a piece of wood inside the casing suggested that the clay inside the casing probably had quite low shear strength. Still, the clay had sufficient shear strength and viscosity to prevent the clay from passing the metal guide rings on the cell, or clods in the clay may have obstructed the stream of clay past the metal guide rings. Without the casing, the problem of lateral constraint causing the remoulded clay to not pass the metal rings would not have been an issue.

6.2.3.11 Installation at 5 m at Onsøy

At Onsøy one earth pressure cell has been installed at 5 m depth by NGI. The cell has not yet been extracted to the ground, but to the authors' knowledge this cell also gives an unreasonably high value of K'_0 . This cell is likely damaged, since unrealistically high K'_0 values seem to come from cells that have been permanently bent. The reason why this is interesting is that it suggests that the installation of cells is not only challenging at Flotten.

6.2.3.12 Possible Corrections

There are possible corrections of the earth pressure cell measurements, but none of them have been applied to the calculations in this thesis. Why the corrections have not been made will be discussed for the individual corrections.

First, one could correct the measurements for changes in air pressure. Measurements have shown that the cells are most likely able to capture changes in air pressure, as illustrated in Table 6.3 for the cell in borehole EPC003 at 5 m depth. The table shows that as the air pressure at the weather station at Voll in Trondheim changes for three subsequent days, the measured pore pressure and total horizontal earth pressure change in a similar way. The measurements are highest the first day, lowest the second and something in between the last day. The same trend is observed for the other four cells at 5 m depth at the same days. The measurements in this thesis are not corrected for air pressure, since changes in air pressure affect both the pore pressure and total horizontal earth pressure in a similar manner. Thus, the errors due to changes in air pressure will to some extent cancel each other when the effective horizontal stress is calculated as the difference between the total horizontal stress and the pore pressure.

Table 6.3: Change in air pressure, measured total horizontal stress and measured pore pressure for three subsequent days.

Date and time	Air pressure [kPa]	Measured σ_h [kPa]	Measured u [kPa]
2017-02-21 11:04	97.8	71.1	34.4
2017-02-22 10:08	95.5	69.0	31.4
2017-02-23 12:48	97.1	69.6	32.3

The second possible correction is accounting for the changes in pore pressure due to snow melting, rain, drying, drainage and other natural processes. This is not carried out in this thesis, since an increase in pore pressure will also be measured as an increase in total horizontal stress. Due to this, the calculated effective horizontal stress will be

less prone to errors than the individual measurements of total horizontal stress and pore pressure.

The third possible correction is accounting for the difference between the zero reading in air and the air pressure at the time of installation. The reason why this has not been done is that the zero readings before and after the installations deviate quite a bit, as may be seen in Table 5.1. Therefore, the zero measurements in general show a too large scatter to be reliable as basis for corrections of measurements.

The fourth possibility to correct the measurements, is to account for over-read due to displacement caused by installation. The value of the over-read has been quantified by Ryley and Carder (1995) to be $0.8 \cdot s_u$ for firm to stiff clays with s_u in the range of 40 to 150 kPa. The clay at Flotten is in the lower part of this range based on the triaxial results, see section 5.2.4. However, the over-read is quantified for clays which are not quick. The spread in the results of the earth pressure cells suggest that there may be a complex stress situation around the cells, including remoulded clay. Remoulded clay would probably lead to too low measured horizontal effective stresses. This will be more thoroughly discussed in section 6.2.3.1. Due to the uncertainties regarding the stress situation, and whether there is an over-read to account for, the measurements have not been corrected for over-read in this thesis.

6.2.4 Dilatometer

It is rather challenging to evaluate the dilatometer results based on measurements by the earth pressure cells, as the estimated values of K'_0 from the earth pressure cell measurements are so scattered. Also, there are several sources of error which could influence the earth pressure cell readings, as discussed in section 6.2.3. Instead, one may compare the dilatometer with K'_0 estimated from correlation methods as well. In the literature, Jaky's Equation 2.20 is often recognized as a quite good estimate of K'_0 in normally consolidated clays (P. W. Mayne & Kulhawy, 1982; Mesri & Hayat, 1993). As seen in Figure 5.2 this estimate is quite low compared to the dilatometer results. The different correlation methods will be discussed in section 6.4. In the literature, the dilatometer is in general expected to give a bit high K'_0 values (Roque et al., 1988). Therefore, it is logical that the dilatometer gives higher values of K'_0 than Jaky's Equation 2.20. Also, the clay at Flotten is overconsolidated according to the oedometer results, as will be discussed in section 6.3.2. This overconsolidation yields higher values of K'_0 compared to the normally consolidated state.

Four different lines indicate an estimated value of K'_0 with depth in Figure 5.2. A general trend when comparing these four lines in Figure 5.2 is the decrease in K'_0 with depth, between about 4 and 15 m. This complies well with the assumption that the

vertical effective stress increases more than the horizontal effective stress with depth for overconsolidated clays, leading to a reduced K'_0 with depth.

Originally, Marchetti (1980) proposed Equation 2.10 combined with a value of β_k equal to 1.5 for insensitive clays. This equation gives the highest estimate of K'_0 for the entire depth. Down to a depth of about 7 m, the Flotten clay appears to have a sensitivity well below 30 (see Figure F.1). However, based on both earth pressure cell measurements and correlation methods, Equation 2.10 seems to give a too high estimate of K'_0 .

On the other hand, using Equation 2.10 with β_k equal to 2, seems to give a better estimate of K'_0 , based on a comparison with the earth pressure cell measurements and the correlation methods. This was also found by Hamouche et al. (1995), comparing estimated values of K'_0 from Equation 2.10 to values achieved by the self-boring pressuremeter.

Furthermore, Lacasse and Lunne (1989) proposed Equation 2.11 after comparing estimates of K'_0 from both Equation 2.10 and different in situ equipment, stating that Equation 2.10 tended to overestimate K'_0 . This was found to be especially true for K_D between 1.5 and 4. Based on this suggestion and the fact that K_D from the Flotten measurements is found to be above 2 for the entire depth tested (see Figure D.1), this seems to support the assumption that the estimates of K'_0 from Equation 2.10 is higher than the in situ value of K'_0 .

In response to the high estimates of K'_0 by Equation 2.10, Lacasse and Lunne (1989) proposed $m = 0.44$ for highly plastic clays and $m = 0.64$ for low plastic clays. In Figure 5.2 it is interesting to note that for depths between 2 m and 7 m the line based on $m = 0.64$ gives approximately the same estimate of K'_0 as $\beta_k = 2.0$. Both of these are values proposed for low plastic clays. The clay between 2 and 7 m depth tends more towards highly plastic than low plastic. As $m = 0.64$ and $\beta_k = 2.0$ were suggested for low plastic clays, one would expect these lines to give a better estimate of K'_0 for the clay below 7 to 8 m depth, as the plasticity decreases substantially below this depth. As the depth increases, $\beta_k = 2.0$ seems to give the lowest estimate of the two.

Finally, Equation 2.11 with $m = 0.44$ gives the lowest estimate of K'_0 for the entire depth. This value of m was proposed for highly plastic clays, suggesting that this line should fit better above a depth of about 7 m compared to in the deeper more sensitive clay. The $m = 0.44$ line fits well with earth pressure cell measurements at both 5, 7, 9 and 10 m, although the spread in the earth pressure cell measurements makes a good comparison challenging, especially at 5 m depth. This estimate of K'_0 with $m = 0.44$ at 10 m depth also fits quite well with K'_0 estimated from both the original Jaky' Equation 2.20 as well as the modified Jaky' Equation 2.29, which takes a rather low OCR from Table 5.5 into account.

However, unlike for instance the rotary pressure soundings, the assumed transition

from plastic to more sensitive clay at around 7 to 8 m (as closer discussed in section 6.2.1) is not particularly evident in the plot of the key dilatometer parameters in Figure D.1. By careful scrutiny it is possible to observe that I_D decreases below 0.1 at about 7 m depth. As I_D is said to provide a rough estimate of soil type, this slight decrease may be taken as a weak indication of a change to a more sensitive material. According to Marchetti (1980), clay is defined between $I_D = 0.1$ and $I_D = 0.6$. $I_D = 0.1$ is the lower limit of the scale. Hence, the measurements taken below 7 m is in reality below the range of I_D and outside the clay range, suggesting that the interpretation of sensitive clays should possible not be conducted based on this parameter alone.

The parameter I_D may not be suited to describe the clay behaviour in sensitive clays. I_D is based on the difference between the measurements of the p_0 and p_1 pressure values, as well as the in situ pore pressure, see Equation 2.7. The amount of disturbance caused by the dilatometer blade insertion will depend on the sensitivity of the clay. One may hypothesize that when dilatometer measurements are taken in sensitive clays, the insertion of the blade is enough to at least partially liquefy the clay. If the soil is disturbed as a consequence of the dilatometer installation, one may suggest that both p_0 and p_1 are in reality measurements of partially remoulded clay. Therefore, the difference between p_0 and p_1 will not be the in situ difference, but rather a much lower difference which reflects the stiffness of the disturbed material. Therefore I_D may give a wrong view of the material properties. Please note that further details regarding these measurements are presented in Ozkul and L'Heureux (2017).

The dilatometer modulus E_D is also based on the difference between p_0 and p_1 . It seems to indicate approximately the same stiffness for the entire depth from 2.2 to 20.6 m. As described in the previous paragraph, this may be a wrong estimate of the in situ stiffness due to disturbance of the clay.

Another striking detail with the four lines based on K_D in Figure 5.2 is the sudden decrease around 15 m depth, which stays low for seven measurements in a row. This drop in values is not visible in either the I_D nor the E_D plot presented in Figure D.1. Also, none of the rotary pressure soundings or the CPTu suggest any change in material around 15 m depth. As the dilatometer estimates are utilized mainly for a comparison with other measurements between 5 and 10 m depth, no further evaluation of this decrease has been carried out.

Based on both Figure 5.2 and D.1, the initial dilatometer measurements taken in between 2 and 3 m depth show great variability. In fact, Lacasse and Lunne (1989) noted that dilatometer measurements in the dry crust quite often gave rather questionable results. At Flotten, sampling in depths of about 2 m indicated layers of sand and silt. A very layered deposit may to a great extent affect the dilatometer measurements. Hence,

the measurements between 2 and 3 m depth should be evaluated with great care.

In general, the dilatometer test seem to support the oedometer results at depths around 5 m, indicating that the Flotten clay is overconsolidated. Schnaid (2008) suggested that for an uncemented, normally consolidated clay, one would have $K_D = 2$. The right graph in Figure D.1 shows OCR calculated from Equation 2.12 with depth. Based on this equation, the overconsolidation seems to reach its peak value of $\text{OCR} \approx 6$ at around 4 m depth. This peak depth is supported by the oedometer tests performed by Konjit Paulos Gella, see Table 5.4. This high degree of overconsolidation fits with the idea that the ice shelf covering the test site has caused mechanical overconsolidation, as presented in section 2.2.7. The high overconsolidation found from the dilatometer does however not fit well with the oedometer tests performed at around 10 m depth, which indicate a normally consolidated deposit. Probably time effects are responsible for much of the high overconsolidation, as will be more closely discussed in section 6.3.2 and slightly in the next paragraph.

The fact that the value of OCR peaks at around 3 to 6 m depth fits quite well with Bjerrum (1967), stating that chemical changes resulting in an increased apparent preconsolidation is most evident in depths between 3 and 7 m. This zone is believed to be the most affected by precipitation of rainwater. Furthermore, based on findings by Tomás et al. (2007), the repeated process of drying and wetting of the dry crust may also to some extent explain the high values of OCR found in depths between 2 and 3 m.

It should however be noted that both the four different K'_0 correlations and the OCR correlation are purely based on the K_D -parameter, and consequently all the lines based on the K_D -parameter show the same development with depth. One could easily question whether the empirical constants in Equations 2.12 or any of the estimates of K'_0 are able to account for the rather complicated collection of factors affecting the stress history of a soil deposit, as closer discussed in section 2.2.1. Indeed, Lacasse and Lunne (1989) stated that the overconsolidation ratio as calculated with Equation 2.12 was in general not very clearly defined.

Moreover, one may not discuss the dilatometer without considering the heavily empirical background of the tool. On one side, the great amount of theoretical correlations makes the dilatometer able to determine almost any geotechnical parameter. In addition, the tool has proven quite robust and easy to operate. On the other hand, experimental testing at different sites throughout the last decades has shown that many of these correlations seem to apply mainly to different soil types (Lacasse & Lunne, 1989; Roque et al., 1988). The great variation associated with utilizing different correlations to estimate K'_0 is shown quite vividly in Figure D.1. At depths of 4 m, the lowest estimate (Equation 2.10) yields $K'_0 = 0.6$ whilst the highest estimate (Equation 2.11) yields $K'_0 = 1.4$.

Similar to what was found during pilot experiments at Tiller as part of the project thesis (Lindgård & Ofstad, 2016), the testing at Flotten seems to indicate that $\beta_k = 2$ proposed by Hamouche et al. (1995) in Equation 2.10 gives a better fit for sensitive clays than the original $\beta_k = 1.5$ proposed by Marchetti (1980). Additionally, Equation 2.11 with $m = 0.44$, which is used for highly plastic clays, seems to give the best fit to the measurements by the earth pressure cells. The earth pressure cells are however scattered and has quite a bit of uncertainty, as was discussed in section 6.2.3.

6.2.5 Field Vane

The values of K'_0 found from the field vane approach seem to be too low at 8.4 and 9.4 m depth, while the value at 10.4 m depth may be reasonable compared to the other methods as presented in Figure 5.2. The field vane approach generally gives low values compared to the other methods, but only the value of 0.53 at 10.4 m depth is near the values from the other methods.

When considering which parameters will affect the value of K'_0 calculated from Equation 2.14, the undrained shear strength s_{uv} and the minor principal effective stress at failure σ'_{3f} in the triaxial apparatus stand out as the parameters with the most possible impact. The in situ vertical stress is quite well defined through index testing and data from piezometers, and the deviations in σ'_{v0} may therefore be assumed to be relatively small. The values of remoulded shear strength s'_{uv} are so small that they hardly affect the calculated K'_0 . It may be noted that the s'_{uv} found from field vane tests, as given in Table E.1, are substantially higher than those from falling cone tests as presented in Figure F.1.

The s_{uv} values found from the field vane tests, see Table E.1, are all much lower than the values from fall cone tests at the same depths as given in Figure F.1 and the triaxial test from similar depths, as seen from graphs in Appendix I. When the undrained shear strength from field vane tests is compared to corresponding values of undrained shear strength from triaxial tests at similar depths, the field vane strengths are found to be less than half of the triaxial strengths. It is reasonable that the field vane strengths should be lower than the triaxial strengths since they are direct shear and compression tests, respectively. A compression test is likely to give substantially higher strength than a direct shear test (Chandler, 1988), but the observed spread in the results between field vane and triaxial tests may not be explained by this alone.

This leads to the explanation that the low undrained shear strengths from the field vane are possibly caused by disturbance during insertion of the field vane into the ground. If the field vane partially remoulds the clay during insertion, it means that the measured undrained shear strength s_{uv} is actually partially remoulded. This will lead to a too low measured s_{uv} . Since the material at the depths in question is quick clay, it is prone to

remoulding. The implication that a too low s_{uv} has on the calculated K'_0 is a too low value. Since the values from the field vane approach are in general low, the possible remoulding of the clay during insertion may partially explain the low values.

The other parameter which can heavily affect the calculations of K'_0 is the minor principal effective stress at failure σ'_{3f} in the triaxial apparatus. Since the material seems quite homogeneous between 8.4 and 10.4 m according to the soundings, one could expect that the values of σ'_{3f} should be quite similar. This is the reason why test CAUc-0934 from 9.34 m depth was used as input for the calculation at 8.4 m depth. There are no reasonable triaxial results closer to the calculation depth. However the values of σ'_{3f} vary a lot, as may be seen from Table E.1.

The variation in σ'_{3f} might be explained by the differences in consolidation, and also by sample disturbance. A sample from 10.56 m depth was used as input for the calculation at 10.4 m depth. This sample was stored in the refrigerator wrapped in plastic for two weeks before it was tested, and hence it was to some degree dried out. This sample disturbance might have influenced the determined σ'_{3f} . See section 6.3.4 for details.

All of the three tests were consolidated to K'_0 values between 0.70 and 0.79, but the difference in the vertical consolidation pressure is none the less quite substantial. The consolidation at 10.4 m is the most realistic when comparing it to the estimated in situ stress situation. Based on the density and pore pressure presented in this thesis, the vertical in situ stress at 10.4 m depth is 143 kPa, while the consolidation of the corresponding test was 152 kPa. The two other tests were consolidated to too low stresses, with the consolidation stresses deviating more from the in situ stresses.

If it is true that σ'_{3f} is totally dependent on the stress history and the consolidation stresses, as stated by Aas et al. (1986), the differences in consolidation between the tests is an important factor for explaining the deviations in σ'_{3f} . In that case, the K'_0 value found at 10.4 m depth is probably the one to rely the most on. Another implication is that the tests presented herein may illustrate the vulnerability of the field vane approach to wrong assumptions regarding triaxial consolidation. For the reliability of the 10.56 m sample, the sample disturbance should be considered an issue, changing the determined σ'_{3f} to an unknown degree. The data in this thesis is therefore too limited to draw any conclusions on the influence of the consolidation stresses on the calculated K'_0 .

It may be suggested that the low values of σ'_{3f} found from both the triaxial tests at 9.34 and 9.40 m depth are caused by the consolidation conditions. If this is true, the effect of choosing the wrong consolidation parameters may cause more change in the calculated value of K'_0 , than the extrapolation of using a triaxial test at 9.34 m depth as input for the calculation at 8.4 m depth.

Whichever way the values of K'_0 from the field vane approach compare to the other

methods presented in this thesis, the theoretical foundation for the method is still questionable. This flaw in the foundation of the method was addressed in section 2.4.8. The good results obtained by the method of field vane testing at Onsøy and Haga presented by Aas et al. (1986) should be treated with care since the validity of the theoretical foundation of the method appears to be outdated, as addressed in section 2.4.8.

6.2.6 In Situ Methods not Tested

Just a few of the in situ methods mentioned in Chapter 2 were tested as part of this thesis. The literature concerning these methods is included in the sections above, discussing each method. This section is dedicated to discussing the in situ methods not tested as part of this thesis.

Hydraulic fracturing is one of the three reference methods in the literature, along with earth pressure cells and the self-boring pressuremeter (Ku & Mayne, 2013). Hydraulic fracturing is often presented as a both straightforward and versatile approach to field measurements of the horizontal stress in clays. The measured water pressures may be taken as the horizontal total stresses without any further processing. Some of the equipment required is already part of any geotechnical field investigation and the method may in many cases be utilized without any need for pre-drilling. However, the method requires some time, as excess pore pressure generated during installation must be allowed to dissipate before the measurements are made. Additionally, even though several articles have found good repeatability of the method, some have pointed out that the results tend to deviate from other methods, when used in soil materials with high OCR (see for instance Hamouche et al., 1995; Lefebvre et al., 1991).

In much of the literature, the self-boring pressuremeter is regarded as a less intrusive method, causing smaller disturbance effects compared to the hydraulic fracturing and earth pressure cell (Hughes & Robertson, 1985; Ku & Mayne, 2013). Also, the measurements may be taken immediately after arriving at the desired depth, so no time for dissipation of excess pore pressure is required. Similar to the earth pressure cell, the amount of equipment needed is quite limited when using the self-boring pressuremeter. However, the self-boring pressuremeter stands out as the method requiring the most training and experience in order to gain reliable results (Hughes & Robertson, 1985; Lunne & L'Heureux, 2016). Also, the equipment in itself is rather expensive, and the usage beyond measuring of stresses in situ is limited.

Often presented as a completely non-intrusive method, shear wave velocity measurements may also be used for determining K'_0 (Ku & Mayne, 2013). However, there is a need for more research to evaluate the dependency on theoretical correlations, as well as to investigate the versatility and repeatability of the method in different types of soil.

The stepped blade seems to be too fragile to be of any real interest in field investigations in various soils. And since the assumptions on where the zero thickness should be taken are not good enough, the stepped blade should probably be regarded as less valuable than the reference methods mentioned earlier in this chapter (Lunne & L'Heureux, 2016).

The latest lateral stress seismic piezocone may be a promising method if one is to listen to the developers of the equipment. Nevertheless, a lot more testing is required before the method can be trusted. The older models of the lateral stress cone seem to be of limited value (Lunne & L'Heureux, 2016).

6.3 Laboratory Methods

6.3.1 Index Testing

The results of extensive index testing performed both by the authors of this thesis as well as by Gella is gathered in Appendix F. When evaluating these results, a couple of key points is especially interesting. First, the index testing may be utilized to indicate that quick clay is present at Flotten, and also give an idea of other material properties. Second, an estimate of the unit weight is of a great importance, as this is required in the calculations of the vertical effective stress.

6.3.1.1 Water Content

Based on Figure F.1 the water content seems to be quite stable with depth. There are two primary deviations from this. First, a total of three measurements between 2 and 3 m depth indicates a water content slightly below 30 %. In fact, the top part of the 54 mm sample retrieved from depth 2 - 2.8 m seemed to contain more sand than clay upon visual inspection, and therefore the determination of water content in these samples are of limited interest.

The second observation from the overview of water content with depth in Figure F.1, is the four measurements indicating a decreased water content from a depth of about 11.5 m. A small increase in corrected cone resistance is visible in the CPTu sounding (see Figure A.14). This could give reason to suspect a slightly more draining layer at this depth. However, as the distance between the location of this sounding and the sampling bore holes is several meters, the connection between the water content decrease and the CPTu sounding may just be considered to be more of a coincidence. None the less, based on the measurements of water content alone, there may be reasons to assume that the amount of silt or sand increased at a depth of about 11.5 m. On the other hand, there is

no evidence of a change in material behaviour when considering either the CAUc triaxial test results from a depth of 11.53 m (Figure I.2) or the CIUc test results from depth 11.42 m (Figure I.4). The failure lines of these two tests seems to fit quite well with the general trend in these collective plots. As the water content specimens will typically have very limited size, one may suggest that the layers of coarser material could be rather thin, and hence do not affect the material properties of the clay as shown when testing in triaxial shear.

6.3.1.2 Atterberg Limits

In addition to the water content, both the plastic limit w_P , the liquid limit w_L and the plasticity index I_P are indicated in Figure F.1. Two quite distinct changes seems to take place at about 7 m depth. First, the liquid limit decreases far below the water content of the clay. Second, the plasticity of the clay decreases quite substantially. Both a water content above the liquid limit as well as a reduced plasticity are typical features of quick clays (Bjerrum, 1954).

As presented in section 4.1, the liquid limit with depth in Figure F.1 is based on the fall cone method. A rough comparison of results found by both the Casagrande and the fall cone method indicates that the two methods show the same overall trend with depth. As ISO17892-12 recommends using the fall cone method for determining the liquid limit (ISO, 2004a), Figure F.1 contains values obtained by this method.

6.3.1.3 Falling Cone

The change in shear strength with depth indicate the same trend as the liquid limit with depth. A clear decrease in both intact and remoulded shear strength is evident at a depth of about 7 m. Simultaneously, the sensitivity of the clay increases substantially. In fact, all specimens from a depth below about 8.50 m gave a remoulded shear strength equal to or below 0.2 kPa. The Norwegian definition of a quick clay is clay with a remoulded shear strength below 0.5 kPa (Gylland et al., 2017). Hence, the fall cone test results seems to support the fact that a transition from plastic to sensitive clay takes place at about 7 to 8 m depth. For the sensitive clay below about 7 m, the scatter in the results increases a lot. This may be because more sensitive clay is more prone to sample disturbance (see for instance Karlsrud & Hernandez-Martinez, 2013; Gylland, Long, et al., 2013; Amundsen, Emdal, Sandven, & Thakur, 2015).

Previously, quick clay was indicated by sensitivity $S_t > 30$ (NGF, 1974). The solid line indicating this criterion in Figure F.1 seems to support a transition from plastic to quick clay at about 7 to 8 m depth.

6.3.1.4 Density

During laboratory investigations of the Flotten clay, the density has been determined with a total of three different methods, as given in Tables F.1 and F.2. First of all, the cylinder density represents a quite rough estimate of the average density of the entire sample cylinder. With one exception this measurement of density is consistently greater than the density determined from the small ring method. During cylinder density measurement, the determination of the length of the clay sample inside the sample tube is often challenging and may easily induce errors in the final estimate. In addition, errors may also have been induced during weighing of the unopened and empty cylinder.

The majority of the density measurements from the oedometer testing compare quite well with the measurements from the small ring method. Some deviations are found, most notably between the samples from 9.40 and 9.50 m depth. A key explanation for these minor variations may be that some of the oedometer samples were stored in a refrigerator for a longer period of time between opening of sample and consequent testing. As will be discussed for the triaxial samples in section 6.3.4, there is reason to believe that some water may have evaporated during storage. This would lead to a lower measured density. In fact, the specimen from 9.40 m depth, indicating the greatest density, was tested on the same day as the sample was opened. The specimen from 9.50 m was stored for about six days before testing was initiated, and hence gave a lower measured density.

The small ring method for determining the density of a smaller specimen of clay represents a more recognized test, and is standardized by the International Organization for Standardization in ISO 17892-2 (ISO, 2014b). As most of the small ring density measurements were conducted on the same day as the sample was opened, the effect of water evaporation is believed to have a rather negligible effect for these results. On the contrary, the length of storage varies between the oedometer test specimens, suggesting that variations in their water content may affect the final density calculation. In addition, slight deviations may have been introduced if the oedometer specimen was not sufficiently trimmed before weighing, since the volume when calculating density is defined to be the volume of a perfectly trimmed sample.

As all measurements of density are prone to different types of errors with varying consequences, an average unit weight of 17.5 kN/m^3 was utilized in all calculations of the overburden pressure.

Finally, the average particle density is an important input parameter to the sample quality evaluation of the oedometer tests. Based on extensive testing Gylland, Long, et al. (2013) determined an average particle density of 2.76 g/cm^3 for the clay at Tiller, located some kilometres away from the Flotten test site. This value is quite close to the particle density of 2.83 g/cm^3 found for the Flotten clay by Gella. A slight change in mineral

composition of the Flotten clay or smaller discrepancies in the testing procedures may explain these deviations. The effect is however considered quite negligible in the sample quality calculations.

6.3.2 Oedometer and Preconsolidation

Figure 5.1 shows the results from 15 oedometer tests interpreted by the Janbu method, as described in section 4.2, to find the preconsolidation stress. There are several interesting details with this plot. First of all, the test results are very scattered, especially for the tests performed on the deeper samples. The transition from plastic to quick clay occurring around 7 to 8 m depth is quite evident in the figure, as the preconsolidation seemingly decrease for the quick clay, while the amount of scatter increases. Several possible causes of these findings will be discussed below.

Whenever considering oedometer test results, sample quality is considered an important question. For the purpose of such an evaluation, the $\Delta e/e_0$ -criterion has been utilized. Unfortunately, as described in section 4.2, the wet and dry weight of the oedometer test specimens were only determined for about half of the tests conducted by the authors. Hence, the $\Delta e/e_0$ -criterion has only been calculated for these tests. However, only minor variations in dry weight were observed when comparing oedometer test specimens from approximately the same depth. Based on this observation, an average dry mass of specimens from about the same depth was used to obtain a preliminary sample quality evaluation for the remaining test specimens. Based on this rather rough estimate, all specimens where the dry weight was not determined directly is of either poor or very poor quality. Finally, in the detailed presentation of each oedometer in Appendix G, the measured axial strain at the assumed in situ stress level is presented. When the $\Delta e/e_0$ -criterion is unavailable, this may be used as a rough estimate of sample quality, at least for comparing different tests conducted on clay specimens from the same depth.

Some additional remarks should be made regarding the determination of the dry and wet mass of each oedometer test specimen. No water was used when extracting the sample from the oedometer equipment after the test. Hence, smaller parts of the sample may have been left on the filters, the ring or inside the oedometer cell. By drying a specimen with too little mass, a too high water content and too low dry mass may be calculated. Consequently, the $\Delta e/e_0$ -criterion will mistakenly indicate a better sample quality. The consequences of this is considered rather small for the shallow, plastic samples as only a negligible amount of clay was squeezed out of the oedometer ring during testing. On the other hand, as several of the deeper samples are believed to have partially liquefied during testing, more of the clay was stuck to either the filters or the top cap after the test. Also, a rather small amount of soil was squeezed out together with the water during

the test and floated to the top of the top filter. For the deeper specimens water should have been used to rinse out all clay from the test equipment. In addition, when testing sensitive soils, Sandbaekken, Berre, and Lacasse (1986) recommended using a wet filter paper below the top cap in order to avoid the squeezing of soil upwards in between the cap and oedometer ring. None the less, the possible deviations in dry weight is considered of less importance as most of the oedometer test results indicate samples of either poor or very poor quality.

Several factors may explain these sample quality evaluations. First, it is of great importance to remember that all tests have been conducted on specimens recovered by the use of a 54 mm piston sampler. In the literature, 54 mm samples are generally considered more disturbed and of less quality than for instance samples recovered by the Sherbrooke block sampler. This is particularly true when used in sensitive clays (see for instance Karlsrud & Hernandez-Martinez, 2013; Lunne et al., 1997). In fact, as seen in Figure F.1, the sensitivity of the Flotten clay increases dramatically below a depth of about 8 m. This compares rather well to the fact that based on the tables in section 5.2.2, the sample quality seems to decrease substantially for the samples from below a depth of about 9 m. The scatter in the interpreted preconsolidation stress increases for the tests on sensitive clay. Based on similar results at the nearby Tiller research site, Gylland, Long, et al. (2013) stated that extreme caution and minimal storage time was required when sampling sensitive clays with the 54 mm piston sampler.

A general challenge when considering all performed oedometer tests is the fact that a higher strain rate than the one recommended in NS8018 (NBR, 1993) was used. For the initial part of the tests, this may have led to a rather high pore pressure versus vertical stress ratio. After the build-up of some vertical stress, the use of a strain rate of 1 %/h was found to be approximately in accordance with the recommendations of keeping the ratio between 2 and 7 %, as presented in an article by Sandbaekken et al. (1986). It is assumed that the too high pore pressure ratio at low stresses in the beginning of the test probably has limited influence on the much higher preconsolidation pressure.

When testing more sensitive samples from depths of about 9 m, a steady increase in pore pressure was initially observed. This may be due to either inaccuracies during installation of the sample or beginning liquefaction of the clay. The increase was only observed for effective stresses well below p'_c .

Lunne et al. (1997) investigated the effect of sample disturbance on measured strength properties of Norwegian clays. When comparing the preconsolidation as interpreted by the Casagrande method, the authors of Lunne et al. (1997) found that in general 54 mm piston samples were prone to result in a slightly lower preconsolidation stress than what was found from block samples. The authors also pointed out that the interpreted value

of the preconsolidation is dependant on the rate of strain used. Findings by Lunne et al. (1997) indicated that a lower rate of strain typically resulted in a lower interpreted preconsolidation stress. The results presented in this thesis suggest that the scatter in the interpreted preconsolidation stresses at Flotten may not be explained by the differences in strain rate. Looking at the results from 9.40 and 9.50 m depth, there is a huge scatter in the interpreted preconsolidation stresses. The highest and lowest interpreted preconsolidation stresses at 9.40 m depth, respectively from tests CRS-0940-2 and CRS-0940-1, are both run at a rate of strain of 1 %/h. The interpreted preconsolidation stress at 9.50 m from test CRS-0950 lies in between the results from the other two tests. CRS-0950 was run at a rate of strain of 0.5 %/h. However, these results do not contradict the findings by Lunne et al. (1997) in any significant way due to the poor sample quality of the oedometer tests from Flotten.

On the other hand, Janbu, Tokheim, and Senneset (1981) presented CRS oedometer test results from 12 samples of Risvollan clay, performed with strain rates varying between 0.6 % and 6 %. No clear difference in deformation parameters were found when the authors of the proceedings compared the results. Based on this, Janbu et al. (1981) concluded that running CRS tests at very low speed was most likely unnecessary.

However, the sensitivity is a key difference between the Flotten and Risvollan clay. As already mentioned, the sensitivity of the Flotten clay seems to increase with depth, while this appears not to be as evident for the low sensitivity Risvollan clay. The possibility that a sensitive clay sample partially liquifies during oedometer testing is considered higher if the test is conducted with a higher rate of strain, as the vertical load on the sample is increased more rapidly. Hence, the rate of strain is believed to have a greater impact on the results of oedometer testing on sensitive clays.

Considering the Quaternary geology map in Figure 2.5 and the statements in Reite et al. (1999), one may say that the soil at Flotten is normally consolidated with respect to mechanical overconsolidation, if the ice shelf once covering the test site had sufficient buoyancy not to affect the site. If the ice shelf however affected the soil at the test site, it suggest a mechanically overconsolidated material. This is more thoroughly described in sections 2.2.7 and 6.1.

A high degree of overconsolidation is found for the shallow specimens tested, while the deeper oedometer tests suggest that the clay at the test site is close to normally consolidated. Thus the suggestion that the test site is basically old sea floor and that the ice shelf has not led to mechanical overconsolidation, seems to fit better with the preconsolidation stresses found for the deeper samples. Anyways, for a purely mechanically overconsolidated soil deposit, one would expect the preconsolidation stress to increase with depth, as the overburden load also increases with depth. This contradicts the general trend in

Figure 5.1, where the preconsolidation seems to decrease with depth. Indeed, the preconsolidation drops quite substantially between the plastic, shallow samples and the deeper, more quick samples.

As mechanical overconsolidation alone seems unable to explain these results, one may suggest that the apparent preconsolidation evident in the oedometer tests from Flotten may be the result of different types of time effects like chemical changes or secondary compression as discussed in section 2.2. Bjerrum (1967) named the exchange of cations as one of the most important factors when considering chemical bonding in Norwegian clays and found this effect to be the most pronounced between depths of about 3 to 7 m. This fits quite well with a key finding in Figure 5.1, namely a very high preconsolidation for the specimens from depths between 4 and 7 m. This may suggest that chemical bonding during several thousand years have resulted in an apparent preconsolidation for the Flotten clay deposit. The downward water flow at Flotten, as discussed in section 6.2.2, is likely to speed up the exchange of cations.

Drying, as closer presented in section 2.2.4, may also contribute to an increase in the overconsolidation stress. The effect of drying will be the greatest for the first few meters of clay, comparing quite well to the quite substantial overconsolidation interpreted from the shallowest samples of clay from Flotten. Furthermore, Mahar and O'Neill (1983) proposed that the drying process may result in highly variable suction forces in the material. Such variations may to some extent explain the scattered measurements of preconsolidation in the Flotten clay. One may assume that there have been drier periods during the last 10 000 years, resulting in a lower ground water table than the present. A lower ground table is likely to facilitate the effect of drying, where suction in the clay material leads to higher preconsolidation stresses than the current overburden loading.

In general, this is also supported by Gylland, Long, et al. (2013), discussing the overconsolidation at the nearby Tiller research site. Based on thorough field and laboratory investigations over more than three decades, the authors proposed that the relatively high overconsolidation of the rather homogeneous clay deposit may be due to time effects as discussed in section 2.2. Although the Tiller clay seems to be slightly less overconsolidated at shallow depths with a value of OCR of about 3 (Gylland, Long, et al., 2013), the OCR reduces with depth similarly to what is found for the Flotten clay (see Table 5.5 and Figure 5.1).

6.3.3 Work Criterion in Oedometer

The determination of p'_c with the work criterion method gave lower values than the Janbu interpretation. The differences were 50, 60 and 40 kPa, as may be seen from the p'_c values presented in Table 5.6. Based on the limited amount of data, one may assume that the

work criterion determination of p'_c is not as good as the authors of Becker et al. (1987) suggested.

That p'_c may be determined as the transition from small strain to large strain response, as presented by Becker et al. (1987), is in accordance with the Cam Clay model. Consequently the idea of a transition at p'_c is reasonable, and thus one would expect a change in the graphs around p'_c . However, the interpreted values of p'_c presented in Table 5.6 do not support the work criterion interpretation as good method compared to Janbu interpretation.

Figures H.1, H.2 and H.3 in Appendix H show that it is hard to determine the in situ stresses with the work criterion in oedometer. Therefore it is hard to use this method on vertically trimmed oedometer samples in order to find the in situ horizontal effective stress to use as input for K'_0 calculations. The point where the measurements start deviating from the initial linearly approximated line is not well-defined in the three graphs. Several reasonable linear curve fittings were attempted, with great variation in the interpreted in situ stress. The authors of Becker et al. (1987) suggest that change in stress condition and sample disturbance will cause a change in response around the in situ stress, and thereby may be determined from the cumulated work graph. As the limited amount of results in Appendix H indicated no well defined change in response, the authors of this thesis find no evidence to support this conclusion. It is hard to understand why sample disturbance would cause anything but poorer sample quality.

The sample quality of two of the oedometer tests is regarded as poor according to 5.6. The quantitative quality of the last test is unknown due to lack of data. Since the sample quality is poor, it may be argued that the results presented herein is of limited value when it comes to contradicting the work criterion method. However, the criticism of the in situ stress interpretation by the work criterion method is not only based on the tests presented herein. It is also based on a general idea that sample disturbance and changed stress conditions at sampling will not cause the material to "remember" the in situ stress. From normal oedometer testing it is only the preconsolidation stress which causes a change in the plotted curves. As the work criterion is only another way to present the same data material, the work criterion should only show a change in the curves around the preconsolidation stress.

One may argue that the amount of tests in Becker et al. (1987) is too limited, as all the tested material has a limited spread in OCR values. Due to the similarities between the tested materials, it is possible that the graphs of cumulated work per unit volume may be interpreted to find a reasonable in situ stress by coincidence. The limited amount of data with poor quality presented in this thesis is however not sufficient to conclude on this matter.

6.3.4 Triaxial Testing

As presented in Chapter 5, different values of attraction and friction angle were chosen above and below 8 m depth, as presented in Table 5.10. Several factors seem to support such a decision. The transition from plastic to more sensitive clay between 7 and 8 m depth has already been discussed in section 6.2.1. Since the material changes between 7 and 8 m depth, it is reasonable to assume that the materials may have different failure lines. A change in material properties is also considered likely when comparing the failure lines of all the triaxial tests from 3 to 12 m depth.

Based on laboratory investigations, Gylland, Long, et al. (2013) reported an approximate attraction of 11 kPa and a friction angle of $\phi = 29^\circ$ for Tiller clay. This compares quite well with the strength parameters found for the Flotten clay.

The plots in section 5.2.4 illustrate that in general the graphs show approximately the same failure line independently of the consolidation stresses. This supports the idea that results from tests consolidated to different stresses are comparable when ϕ and attraction shall be determined. It is however important to note that if the sample is consolidated to stresses higher than the in situ stresses, the structure of the material may alter, especially if the sample is close to normally consolidated.

Mainly the case has been the opposite for the triaxial tests presented in section 5.2.4, as Gella has assumed a hydrostatic pore pressure from 2 m depth. This gives too high pore pressures, as discussed in section 6.2.2. For the isotropic tests it may be an advantage that Gella has used too high pore pressures, since this has led to consolidation cell pressures being lower than the in situ horizontal stress. If she had used the correct in situ vertical stress for an isotropic consolidation, the cell pressure would have exceeded the in situ horizontal stress, and hence the structure of the material may have altered to an unknown degree.

It may be seen from the graphs in section 5.2.4 that the CAUc and CIUc tests between 3 and 8 m depth show peak strengths of approximately the same magnitude. This adds to the arguments for why triaxial tests consolidated to different stresses are comparable. However, the peak strengths of the deeper tests show larger scatter, and the peak strength increases with increasing consolidation stresses.

As previously discussed in Chapter 4, the estimates of the in situ stress state were altered between the different triaxial tests performed by the authors of this thesis. Test CAUc-0934 was consolidated based on too high pore pressures, while the other three tests were consolidated to vertical stresses being less than 10 kPa too high. If the assumed K'_0 for these tests is too high, it has led to the horizontal stress being more than 10 kPa too high. This may have altered the structure of the sample. However, the tests consolidated to slightly too high vertical stresses indicate the same failure line as the tests consolidated

to lower than in situ stresses.

The CIUc tests generally show that about one percent of strain is required before the shear stresses increase drastically. This corresponds to about 1 mm deformation. This phenomenon may be explained by lack of contact between the sample and the piston at the beginning of the test. The piston is responsible for the vertical deformation. If the drainage is closed and the test started before the piston is fully in contact with the sample, this would lead to water rather than the sample being compressed by the piston. Such a compression of water would lead to an increase in pore pressure without much increase in shear stress. Hence, the effective horizontal stress σ'_3 would decrease without much added shear stress. In the $\frac{1}{2}(\sigma'_1 - \sigma'_3)$ versus σ'_3 diagrams for the CIUc tests this seems to be happening, so it is fair to assume that the test was started without good contact between the sample and the piston. Probably this mainly affects the amount of strain needed to reach the peak strength.

Similar to results from oedometer testing, sample and test quality is of key importance when evaluating triaxial test results. This may to some extent be assessed by the volumetric strain during the consolidation phase. The amount of expelled water as well as the value of ε_{vol} at the end of consolidation is indicated for each triaxial test in Appendix I. In section 5.2.4 the tables show an overview of the ε_{vol} at the end of consolidation for the triaxial tests.

A general trend is that the amount of water expelled increases with depth, reaching its maximum values in the more sensitive clay below 7 - 8 m depth. Based on the sample quality evaluation criterion presented in Table 4.2 and an OCR above 3, chosen from Table 5.5, most of the samples tested by Gella from depths between 3 and 8 m seem to be of acceptable quality. Based on the same criterion, the samples from depths below 8 m are generally of disturbed quality. Similarly to what the $\Delta e/e_0$ -criterion indicated for the oedometer specimens, the amount of disturbance seems to increase with depth into the more sensitive clay. The causes of this disturbance with depth were addressed in section 6.3.2.

The strain at the point of the peak strength may also give an indication of the sample quality. For both the CAUc and the CIUc tests, more strain is required to reach the peak strength for the samples in the sensitive clay compared to the shallower less sensitive clay. This adds to the consideration that the deeper samples are more disturbed.

The time of storage varies quite substantially between the different specimens. For the two specimens from depths 10.36 m and 10.56 m, the water content is found to be about 10 percentage points lower than the average cylinder water content (see Figure F.1). One possible explanation to this is that these specimens were stored respectively three and two weeks in a refrigerator, wrapped in plastic. No extra measures were taken to ensure a

minimal loss of water content during storage. When samples with the wrong in situ water content are tested, this may lead to erroneous estimates of strength properties. However, Lessard and Mitchell (1985) found that the undisturbed shear strength and water content remained about the same independent of storage time, for a Canadian quick clay. It should be noted that the samples tested by Lessard and Mitchell (1985) were either stored in several layers of wax or in plastic containers. This suggests that the storage time in itself is probably less of a problem than the drying taking place during storage.

It should also be noted that evaporation of water from the specimens during storage might jeopardize the assumption of a fully saturated sample, used when calculating ΔV as the amount of water expelled from the sample during consolidation. When testing a partially dried sample, air will be compressed instead of water, and the assumption that the volumetric strains equal the amount of expelled water is no longer valid. Additionally, less water expulsion during the consolidation phase may lead to inaccurate estimates of sample quality through the ε_{vol} -criterion. This is because a dried sample where too little water is expelled will appear to have better quality than what it has in reality according to Table 4.2.

The samples tested by Gella were generally stored in plastic cans for a shorter time, compared to the specimens stored in plastic wrapping tested by the authors. Hence, the procedures used by Gella was more in accordance with the storage procedures used by Lessard and Mitchell (1985). As some water still is assumed to evaporate from the samples during storage, the short storage time should result in higher water content and more water being expelled during the subsequent consolidation. However, the opposite is evident when considering the individual test results in Appendix I. The amount of water expelled during consolidation is generally lower for the samples tested by Gella compared to the ones tested by the authors. There are several possible explanations for this. First, Gella's samples may have been consolidated to lower than in situ effective stresses, as a too high pore pressure was assumed. This is particularly important for the deeper samples, as the hydrostatic assumption would at a depth of 10 m give a pore pressure of 80 kPa, whilst measurements indicated a pore pressure of about 40 kPa. Consolidation to too low effective stresses will result in less water being expelled during the consolidation, compared to the water which would have been expelled if more correct in situ stresses had been assumed.

Next, the length of consolidation varies quite substantially between the tests conducted by Gella. The amount of water expelled from the samples depend on if the consolidation has been run for sufficiently long time. The time required will depend on the permeability of the sample. How the consolidation stresses were applied does also vary between the performed tests. For some of the shallow specimens tested, the in situ stresses of the

specimen were applied in one step and the consolidation phase was only run for about one hour. However, for most of the specimens tested, the in situ stresses were applied over a couple of steps and the consolidation phase was run for up to about 25 hours. The consequences of a too short consolidation phase will increase with the depth of the specimen tested, as the consolidation stresses typically increase with depth. Also, the material will be less permeable as the consolidation stresses increase, requiring more time to be sufficiently consolidated.

During Gella's initial triaxial testing, one of the scales used for measuring the expelled pore water repeatedly malfunctioned. Some of the tests were consequently conducted without a working scale, resulting in no pore water expulsion measured during the consolidation phase. For these tests, the graph indicating volumetric strain during consolidation is marked with "No value" and the sample quality is not evaluated. For some of the triaxial test, the scale stopped responding during the consolidation phase. This led to some period of time passing without any measurement of water expulsion from the sample, before the scale was reconnected. As the consolidation phase continued even though the scale did not register the expelled water, this is believed not to have affected the final results of the triaxial test.

6.3.5 Oedotriaxial

A value of K'_0 from oedotriaxial testing is calculated with Equation 2.17. The input is the inclination of the stress path in the $\frac{1}{2}(\sigma'_1 - \sigma'_3)$ versus σ'_3 plot. In general, the stress path follows the fitted line quite well, as shown in Figure J.1. The exception is mainly downward spikes, which will be more closely discussed below. The fitted straight line in the $\frac{1}{2}(\sigma'_1 - \sigma'_3)$ versus σ'_3 plot intersects the σ'_3 axis in the negative point of the attraction a , which is in accordance with Janbu and Senneset (1995).

Calculating K'_0 from Equation 2.17, namely $K'_0 = \frac{\sigma'_{30+a}}{\sigma'_{10+a}}$, will result in a higher estimate compared to $K'_0 = \frac{\sigma'_h}{\sigma'_v}$ for $K'_0 < 1$. For the clay at 9.2 m depth where the oedotriaxial sample is taken from, an attraction of $a = 12$ kPa has been chosen. By rearranging Equation 2.17 and inserting the assumed in situ overburden stress and attraction, $K'_0 = \frac{\sigma'_h}{\sigma'_v} = 0.58$ is calculated. This K'_0 value is the most comparable to the other values found in this thesis, since all values are calculated from $K'_0 = \frac{\sigma'_h}{\sigma'_v}$ at the assumed in situ stress.

The value found by $K'_0 = \frac{\sigma'_h}{\sigma'_v}$ from the oedotriaxial test is shown together with the other methods in Figure 5.2. The value is higher than those from the Jaky's Equation 2.20. Actually, the oedotriaxial test shows a K'_0 value close to the one found by the modified Jaky's Equation 2.29. Considering the clay at 9.2 m depth at Flotten to be slightly overconsolidated, is it reasonable that the modified Jaky's Equation 2.29 should be more comparable to the oedotriaxial test. When compared to the earth pressure cells,

the oedotriaxial test gives a quite high value of K'_0 . However, the uncertainties and scatter of the earth pressure cell results are great, as discussed in section 6.2.3. The oedotriaxial test gives a lower value than the dilatometer correlations meant for use in sensitive clays. One would expect a laboratory method to give a lower value of K'_0 than an in situ method, because the in situ methods can capture the effect of increased K'_0 due to secondary compression, as discussed in section 2.2.5. The oedotriaxial test seems to give a reasonable value of K'_0 compared to dilatometer and correlation methods. The basis of comparison is too scattered and uncertain to conclude any more precisely.

A challenge for running an oedotriaxial test with the triaxial apparatus and the procedure used in this thesis, is the need for manual adjustment of the cell pressure to keep the cross-sectional area constant. This requires frequent presence in the laboratory, as adjustments have to be made every 5 to 15 minutes. It was still necessary to use this specific triaxial apparatus and procedure since no automated oedotriaxial apparatus was available.

Whether an oedotriaxial test has been run under oedometer conditions may be evaluated by looking at the inclination of the test graph in the weight versus ε_{axial} diagram. The straight line in the weight versus ε_{axial} diagram in Figure J.1 in Appendix J has the inclination that the graph from the test needs to have, in order to be run under oedometer conditions. The inclination is as given in Equation 2.16. As may be seen, the graph from the test is in general parallel to the straight line, and one may assume the test to be run under oedometer conditions. The offset from the straight line in the weight versus ε_{axial} diagram is because the zero level for the weight of expelled water is not at weight equal to zero. This offset is for instance caused by evaporation from the measuring glass during over-night breaks. However, this offset is not a problem since the test is assumed to be run under oedometer conditions as long as the inclination of the graph is correct.

A basic assumption which needs to be true in order to use Equation 2.16 to give the ideal inclination of the test graph is that the sample is fully saturated at the beginning of the oedotriaxial test. The sample in the one completed oedotriaxial test was extruded from the sampling cylinder six days after sampling and then stored cold in plastic wrapping for one day before the test was started. Due to this and the fact that the sample is taken from many meters below the ground water table, it may be a reasonable assumption that the sample was close to fully saturated at the beginning of the test. If backpressure had been used before the test was started, one could have saturated the sample. Unfortunately, the triaxial equipment used did not allow for backpressure.

The downwards spikes in the $\frac{1}{2}(\sigma'_1 - \sigma'_3)$ versus σ'_3 and $\frac{1}{2}(\sigma'_1 - \sigma'_3)$ versus ε_{axial} diagrams may be explained by the breaks made during the test, as described in section 4.5. As may be seen from the $\frac{1}{2}(\sigma'_1 - \sigma'_3)$ versus σ'_3 diagram the test has been continued after

breaks at the same cell pressure that was before the break. The $\frac{1}{2}(\sigma'_1 - \sigma'_3)$ versus ε_{axial} diagram shows that some additional deformation is required in order to get to the same cell pressure level as before the break. The loops in the module versus σ'_1 diagram may also be explained by the breaks.

A central question is how the breaks during the nights and the weekend has affected the test. The fact that additional deformation was required in order to get to the same stress level as before the breaks, may be explained by two effects. The first effect is creep. Since the deformation is kept constant, the material has the possibility to creep under the given load. This would cause vertical stress reduction. The second effect is that there is no measurements controlling if additional water is expelled during the overnight breaks. One may think that some water has been expelled after the test was paused, and that this water was part of the water which evaporated from the water measuring glass during the night. If water is expelled under conditions of no change in deformation, this would cause the vertical stress to decrease.

The module M , as calculated from Equation 2.18, shown in the module versus σ'_1 diagram has reasonable values of between 2 and 4 MPa, which is approximately in the same range as the results from oedometer tests performed on Flotten clay at almost the same depth. However, while the oedometer tests in general show a decrease in M value from around 100 kPa vertical stress, the M curve from the oedotriaxial test increases a bit from 100 to 200 kPa vertical stress and is more or less constant from 200 to 300 kPa vertical stress. These limited results suggest that an ordinary oedometer test is more suited to determine M and p'_c than an oedotriaxial test. The decrease in M value found in the oedometer tests is necessary in order to be able to determine the value of p'_c .

6.4 Correlation Methods

Estimates of K'_0 from different correlation methods are presented in Table 5.12. A selection is also included in Figure 5.2. First, the simplest theoretical relationships as in the Jaky's Equation 2.20 give very reliable estimates of K'_{onc} (P. W. Mayne & Kulhawy, 1982; Mesri & Hayat, 1993). As presented in section 2.2.1, K'_0 appears to increase with the degree of overconsolidation. As the Flotten clay is believed to be overconsolidated to some extent, one may suggest that the original Jaky's equation, not taking the possible effect of overconsolidation into account, could represent a lower boundary estimate of K'_0 at Flotten.

The estimates in Table 5.12 seems to support the suggestion by Sivakumar et al. (2002), namely that Equations 2.20 to 2.24 all give quite similar values of K'_0 . This is also to be expected as these equations only represents minor adjustments of the original

Jaky's equation. It should be noted that all these estimates of K'_0 depend on the friction angle of the material in question. Hence, these estimates are in general quite vulnerable to discrepancies between the determined and in situ friction angle.

Next, Equation 2.25 and 2.26 represents an effort to relate the Atterberg limits and water content to K'_0 for Scandinavian clays. These equations were originally proposed by Larsson (1977), and later challenged by P. W. Mayne and Kulhawy (1982), finding no useful relationship between various index properties and K'_0 . Both equations give quite similar results for the Flotten clay, which is to be expected based on the link between w_L and I_P . These estimates are consistently lower than estimates by the earth pressure cells. This is particularly evident at 7.5 m depth, as the plastic and liquid limit changes quite substantially at about this depth.

Furthermore, estimating K'_0 by using 2.25 and 2.26 is vulnerable to variation in the Atterberg limits with depth. Testing of only smaller specimens for the determination of the Atterberg limits may not give a representative view of the soil properties in a layered deposit, where small lenses of sand or silt may affect the measurements. In fact, when considering Figure F.1, a clear drop in both plasticity and liquid limit is evident at a depth of about 7 m. There is no reason to believe that the value of K'_0 will change so rapidly over only a couple of meters. This abrupt drop may suggest that the equations proposed by Larsson (1977) are mainly suitable for rough estimates of K'_0 in relatively thick layers, if at all useful for estimating K'_0 based on the critique from P. W. Mayne and Kulhawy (1982).

Estimates by Equations 2.25 and 2.26 compare quite well to estimates by the original Jaky's equation. As the original Jaky's equation is assumed to be best suited for K'_{0nc} , this may indicate that Equations 2.25 and 2.26 lack the ability to address the possible overconsolidation of a soil deposit.

Of all the correlation methods, the modified Jaky's Equation 2.29 gives the highest estimates of K'_0 . At 5 m depth, the estimate by Equation 2.29 seems to be in the upper region of the estimates by the earth pressure cell measurements at the same depth. At both 5 m and 7.5 m depth, the estimates by Equation 2.29 compare quite well with dilatometer results interpreted both by Equation 2.10 with $\beta_k = 2.0$ and Equation 2.11 with $m = 0.64$. These dilatometer equations are however said to be best suited in sensitive low plasticity clays, which is not the case in the shallow layers at Flotten. At depth 10 m the estimate by Equation 2.29 is quite similar to the dilatometer estimate based on Equation 2.11 with $m = 0.44$, which should be suited for high plasticity clays. Between 5 m and 10 m, the estimate by Equation 2.29 changes from about $K'_0 = 1$ to $K'_0 = 0.6$. This clearly demonstrates that estimates from Equation 2.29 depend heavily on the estimated value of OCR.

As closer presented in section 2.6, Equation 2.29 originates from Equation 2.27 proposed by Schmidt (1966). Later P. W. Mayne and Kulhawy (1982) suggested that $\alpha = 1 - \sin\phi'$. By comparing in situ measurements of K'_0 to K'_0 values calculated with Equation 2.29, Hamouche et al. (1995) found that for overconsolidated Canadian clays, α varied between 0.79 and 1.15. One key point from the article by Hamouche et al. (1995) is the fact that α seems to increase with increased sensitivity. At Flotten, the sensitivity seems to increase from depths of about 7 m. In fact, with an increased value of α , the estimate of K'_0 from Equation 2.29 will agree better with K'_0 estimated from Equation 2.10 with $\beta = 2.0$ for sensitive clays and Equation 2.11 with $m = 0.64$ for low plastic clays.

It should however be noted that in the work by Hamouche et al. (1995), OCR was estimated using field vane results. Slight inaccuracies in the estimate of OCR may easily impose errors in the later calibration of the α -value. This suggests that extensive information of high quality regarding soil properties is required in order to give a good estimate of the α parameter. Hamouche et al. (1995) also pointed out that the value of α may vary to a great extent between different sites.

In general, this touches a key problem when trying to estimate K'_0 for an overconsolidated soil deposit. The OCR parameter is based on an estimated preconsolidation stress, typically interpreted from oedometer test results. Based on such testing, it is often difficult to distinguish between mechanical overconsolidation, referred to as true overconsolidation by Aas et al. (1986), and other forms of overconsolidation. As closer presented in section 2.2.1, during unloading of a soil deposit, the horizontal stress tends to reduce less than the vertical. This suggests that K'_0 can increase substantially as a consequence of increased OCR due to mechanical overconsolidation. On the other hand, research by several authors (see for instance Jamiolkowski et al., 1985; Kavazanjian Jr & Mitchell, 1984; Mesri & Castro, 1987) suggests that K'_0 is fairly constant with time when the soil is not affected by mechanical overconsolidation. Time effects may however lead to an increase in the apparent overconsolidation (see for instance Jamiolkowski et al., 1985; Mesri & Castro, 1987; Fioravante et al., 1998), and thereby a great increase in the OC calculated from p'_c found from oedometer tests. As the type of overconsolidation will vary to a great extent between different sites tested, Equation 2.29 may not be able to give a precise estimate of K'_0 since mechanical OCR affects K'_0 to a much greater degree than apparent overconsolidation. Based on this, Hamouche et al. (1995) suggested that the C_α/C_c -concept may be more suited for estimating K'_0 in overconsolidated soils.

Finally, Equation 2.31 is included in Table 5.12. The estimated values of K'_0 based on this method is however considered of limited value, as only generalized values suggested by Sivakumar et al. (2009) were used. These generalized values may or may not give a good

representation of the Flotten clay. The generalized values are used since the necessary laboratory tests including both loading and unloading have not been performed. The estimates by 2.31 in Table 5.12 seem to end up in between the estimates by the Jaky's Equation 2.20 and the modified Jaky's Equation 2.29. This is reasonable, since the Equation seems to share certain similarities with Equation 2.29, as both K'_{onc} and OCR are included.

Chapter 7

Summary and Further Work

7.1 Summary and Conclusions

Any laboratory test or computational modelling procedure in geotechnical engineering relies on accurate determination of soil parameters and the in situ stress state. The vertical effective stress state is well defined by the overburden pressure, while determination of the horizontal effective stress has proved more challenging. Despite several investigations, the factors influencing the coefficient of earth pressure at rest, K'_0 remain unresolved. Also, in situ and laboratory measurements tend to alter the stress situation, and thus the measured horizontal stress is not the true in situ stress. This thesis has looked into field and laboratory methods to determine the coefficient at earth pressure at rest, as well as the geological evolution of K'_0 .

Based on literature presented in Chapter 2, one of the key findings on the geological evolution of K'_0 is that the stress history of the deposit is crucial. Also, time effects can explain the change in apparent preconsolidation and K'_0 with time.

Many different approaches to determine K'_0 in situ have been presented in Chapter 2. The repeatability, reliability and ease of use varies a lot. Some methods have a great need for empirical factors to relate in situ data to K'_0 . These factors may have limited value between different sites and soil properties. In much literature, the three direct measurement methods of earth pressure cells, hydraulic fracturing and self-boring pressuremeter stand out as reference methods.

Some laboratory methods discussed in the literature have been presented in Chapter 2. The split-ring oedometer and the oedotriaxial procedure seem to give the most reliable results.

Several correlation methods have been presented in Chapter 2. Jaky's equation $K'_{0nc} = 1 - \sin\phi'$ is repeatedly validated by both laboratory and in situ studies. There is more uncertainty and spread in the calculations of K'_{0oc} , and the complexity of the correlation

methods for overconsolidated soils is varying. The results presented in Chapter 5.3 support that the spread in calculations of K'_{0nc} is small compared to K'_{0oc} . Also, the dependency on correct OCR input is addressed in section 6.4.

The general site classification presented in section 6.2.1 is based on soundings, index testing and Quaternary geology information. At Flotten there is a 2 m dry crust overlaying a quite homogeneous plastic clay layer extending to 7 m depth. A transition zone lies between the plastic clay and the quick clay starting at 8 m depth. Below approximately 20 m depth coarser materials act as draining layers. This is the cause of the under-hydrostatic pore pressure with depth discussed in section 6.2.2.

Earth pressure cells have been installed to the desired final depth 11 times, to measure horizontal total stress and pore pressure. The resulting K'_0 values are presented along with the other methods in Figure 5.2. Installations at 5 m gave huge scatter in the calculated values of K'_0 . Consequently, several different installation procedures have been tested and evaluated. Some have proven more successful than other. In general the results are scattered. The influence of the installation procedure on the in situ stress conditions is discussed in section 6.2.3. The possibility to produce a protective cover has been evaluated. It has not been made due to the expected amount of disturbance during installation and time consuming production.

The dilatometer test performed at Flotten gives quite reasonable, albeit slightly high estimates of K'_0 compared to both earth pressure cells and correlation methods, as seen in Figure 5.2. This is to be expected based on similar findings in the literature, closer discussed in section 2.4.2. However, when used in highly sensitive clays, the validity of the dilatometer parameters and the amount of disturbance remain open questions.

The field vane approach combining field vane results with a triaxial compression test gave low estimates of K'_0 compared to the other methods in Figure 5.2 at 8.4 and 9.4 m depth. The most reasonable field vane value of K'_0 is at 10.4 m depth, where consolidation of the corresponding triaxial test was closest to in situ conditions. The sample used as input at 10.4 m was probably more disturbed than the samples used as input at 8.4 and 9.4 m depth. The limited amount of data suggest that the chosen parameters for the triaxial test is determining for the calculated K'_0 , but it is not possible to conclude on this matter based on the limited data available and the amount of sample disturbance. Also, the input undrained shear strengths found from the field vane are probably too low compared to in situ, as discussed in section 6.2.5. The theoretical foundation of the field vane approach has some weaknesses addressed in section 2.4.8.

A total of 17 oedometer tests performed on Flotten clay have given quite scattered results, probably linked to disturbance of the 54 mm samples. The general trend in the preconsolidation interpretation presented in Figure 5.1 is a quite overconsolidated deposit

at shallow depth, with a decreasing overconsolidation with depth. As the geological history of the site (see sections 2.2.7 and 6.1) is not able to explain the observed overconsolidation, the high preconsolidation pressure is believed to be the effect of various time effects, as discussed in section 2.2.1.

The theoretical background for determining in situ stresses from the work criterion has some weaknesses, as discussed in section 6.3.3. An unambiguous determination appears to be difficult in practice. Also, the determination of p'_c using the work criterion seems to be less good than presented in Becker et al. (1987).

Based on a total of 19 triaxial tests performed both by the authors of this thesis and Konjit Paulos Gella, estimates of key strength parameters for the Flotten clay have been determined. The triaxial testing supports the idea of a transition from plastic to quick clay at a depth of about 7 to 8 m.

The manual oedotriaxial test compares rather well to estimates based on both in situ and correlation methods to determine K'_0 in Figure 5.2. However, to ensure a drained test the utilized procedure requires the test to run for a substantial amount of time.

Based on the above summary it may be concluded that all but two of the objectives for this thesis are wholly fulfilled. Objective 3, namely to install and evaluate earth pressure cell tests at Flotten, has to some extent been accomplished. Cells have been installed to the desired final depth 11 times, and the results have been evaluated. However, due to severe difficulties during installation of the cells, the authors have not managed to develop a method that ensures reasonable and repeatable measurements. In accordance with objective 6, a number of oedometer tests have been performed and interpreted with respect to p'_c . The sample quality is however generally low and the interpreted values of p'_c are too scattered to conclude on a single estimate of the preconsolidation pressure with depth.

7.2 Recommendations for Further Work

There are several in situ and laboratory efforts which may be part of the further work at Flotten. Numerical simulations may also be of interest.

The first issue is to find a way to install the earth pressure cells which gives reasonable and repeatable results. Glötzl has offered to produce a frame supporting the earth pressure cell blade against lateral deformation. Based on the results presented herein, buying cells with such a frame could be valuable to avoid bending. Due to limitations in time and uncertainties regarding the effect of welding in the NTNU workshop close to the earth pressure sensor system, this has not been pursued within this thesis.

Some installation methods not attempted as part of this thesis may be worth closer

examination. First, pre-drilling and remove masses from a bore hole with an auger featuring a diameter larger than 85 mm, and not use ODEX casings. Tedd and Charles (1981) obtained reasonable results with a 150 mm auger. However, the testing was not performed in quick clay. The influence of the larger auger on the stress situation is hard to predict. Second, one may install casings without pre-drilling. The masses inside the casings may be removed with a piston sampler. Third, a tool able to remove remoulded masses from inside casings installed by the use of pre-drilling could be utilized.

In order to reduce contact between water in the boreholes and the earth pressure cells, the boreholes could be backfilled with low-permeability bentonite after the cells are installed.

Performing tests with the Camkometer self-boring pressuremeter would be valuable, since it is mentioned among the reference methods in the literature.

Hydraulic fracturing is another reference methods, and the necessary equipment is under development at NGI. When the equipment is ready, it should be tested at Flotten.

Performing more dilatometer tests to evaluate the repeatability of the method is useful. If the method produces repeatable results, they should be compared to the values of K'_0 obtained from the reference methods. The correlations proposed by Marchetti (1980) and Lacasse and Lunne (1989) may then be revised for quick clay if necessary.

Shear wave measurement may be carried out to check how this non-intrusive method compares to other methods in quick clay.

Triaxial and oedotriaxial tests should be performed with the use of back pressure to ensure completely saturated samples. The procedure for the oedotriaxial test should be automated to reduce time consumption and allow for continuous testing.

In order to gain more trustworthy values of the preconsolidation pressure with depth, high quality block samples or mini-block samples should be used. Triaxial samples should also be taken from the block samples to get more reliable strength parameters.

In addition, the site characterization through index testing should be continued to greater depths, preferably based on high quality samples.

Running split-ring tests on Flotten clay would be interesting in order to see how the results compare to the other methods.

When better quality laboratory data is available, the calculations using the correlation methods presented herein should be repeated and evaluated.

The laboratory tests needed as input for the C_α/C_c -concept and the correlation method by Sivakumar et al. (2009) could be performed, and the results compared to the other methods.

It is interesting to use PLAXIS or other numerical tools to investigate the influence of different installation procedures of earth pressure cells and other field equipment.

Bibliography

- Aas, G., Lacasse, S., Lunne, T., & Hoeg, K. (1986). Use of in situ tests for foundation design on clay. *Norwegian Geotechnical Institute Publication 166*, 1–15.
- Amundsen, H., Emdal, A., Sandven, R., & Thakur, V. (2015). On engineering characterisation of a low plastic sensitive soft clay. *GeoQuebec 2015*.
- Andersen, K. H., Rawlings, C. G., Lunne, T. A., & By, T. H. (1994). Estimation of hydraulic fracture pressure in clay. *Canadian Geotechnical Journal*, 31(6), 817–828.
- Anderson, W. F. & Pyrah, I. C. (1991). Pressuremeter testing in a clay calibration chamber. In *Proceedings of the First International Symposium on Calibration Chamber Testing/ISOCC1, Potsdam, New York* (pp. 55–66).
- Andresen, A. & Kolstad, P. (1979). The NGI 54-mm Samplers for Undisturbed Sampling of Clays and Representative Sampling of Coarser Materials. In *Proceedings of the International Symposium of Soil Sampling, State of the Art on Current Practice of Soil Sampling* (pp. 13–21).
- Becker, D., Crooks, J., Been, K., & Jefferies, M. (1987). Work as a criterion for determining in situ and yield stresses in clays. *Canadian Geotechnical Journal*, 24(4), 549–564.
- Berre, T. (1981). Triaxial Testing at the Norwegian Geotechnical Institute. *Norwegian Geotechnical Institute Publication 134*.
- Bjerrum, L. & Anderson, K. (1972). In-situ measurement of lateral pressures in clay. *Norwegian Geotechnical Institute Publication 91*.
- Bjerrum, L. (1954). Geotechnical properties of Norwegian marine clays. *Géotechnique*, 4(2), 49–69.
- Bjerrum, L. (1967). Engineering geology of Norwegian normally-consolidated marine clays as related to settlements of buildings. *Géotechnique*, 17(2), 83–118.
- Blight, G. (1968). A note on field vane testing of silty soils. *Canadian Geotechnical Journal*, 5(3), 142–149.
- Bolton, M. (1991). Geotechnical stress analysis for bridge abutment design.
- Brooker, E. W. & Ireland, H. O. (1965). Earth Pressures at Rest Related to Stress History. *Canadian Geotechnical Journal*, 2(1), 1–15. doi:10.1139/t65-001

- Campanella, R. & Robertson, P. (1991). Use and interpretation of a research dilatometer. *Canadian Geotechnical Journal*, 28(1), 113–126.
- Campanella, R. & Stewart, W. (1992). Seismic cone analysis using digital signal processing for dynamic site characterization. *Canadian Geotechnical Journal*, 29(3), 477–486.
- Campbell, C. S. (2003). A problem related to the stability of force chains. *Granular Matter*, 5(3), 129–134.
- Carder, D. & Symons, I. (1989). Long-term performance of an embedded cantilever retaining wall in stiff clay. *Géotechnique*, 39(1), 55–75.
- Chandler, R. J. (1988). The in-situ measurement of the undrained shear strength of clays using the field vane. In *Vane Shear Strength Testing in Soils: Field and Laboratory studies*. ASTM International.
- de Jong, G. J. & Verruijt, A. (1965). Primary and secondary consolidation of a spherical clay sample. In *Proceedings of the 6th International Conference on Soil Mechanics and Foundations Engineering* (Vol. 1, pp. 254–258).
- Diaz-Rodriguez, J., Leroueil, S., & Aleman, J. (1992). Yielding of Mexico City clay and other natural clays. *Journal of Geotechnical Engineering*, 118(7), 981–995.
- Fahey, M. & Randolph, M. F. (1984). Effect of disturbance on parameters derived from self-boring pressuremeter tests in sand. *Géotechnique*, 34(1), 81–97.
- Fioravante, V., Jamilokowski, M., Lo Presti, D., Manfredini, G., & Pedroni, S. (1998). Assessment of the coefficient of the earth pressure at rest from shear wave velocity measurements. *Géotechnique*, 48(5), 657–666.
- Fischer, K., Andersen, K. H., & Moum, J. (1978). Properties of an artificially cemented clay. *Canadian Geotechnical Journal*, 15(3), 322–331.
- Ghionna, V., Jamiolkowski, M., & Lancellotta, R. (1982). Characteristics of saturated clays as obtained from SBP tests. In *Symposium on the Pressuremeter and its Marine Applications* (Vol. 37, pp. 165–185).
- Grimstad, G., Andresen, L., & Jostad, H. P. (2012). NGI-ADP: Anisotropic shear strength model for clay. *International Journal for Numerical and Analytical Methods in Geomechanics*, 36(4), 483–497.
- Gylland, A. S., Jostad, H. P., Nordal, S., & Emdal, A. (2013). Micro-level investigation of the in situ shear vane failure geometry in sensitive clay. *Géotechnique*, 63(14), 1264.
- Gylland, A. S., Long, M., Emdal, A., & Sandven, R. (2013). Characterisation and engineering properties of Tiller clay. *Engineering Geology*, 164, 86–100.
- Gylland, A. S., Sandven, R., Montafia, A., Pfaffhuber, A. A., Kåsin, K., & Long, M. (2017). CPTU classification diagrams for identification of sensitive clays. In *Landslides in Sensitive Clays* (pp. 57–66). Springer.

- Haimson, B. (1978). The hydrofracturing stress measuring method and recent field results. *International Journal of Rock Mechanics and Mining Science*, 15(4), 167–178.
- Hamouche, K., Leroueil, S., Roy, M., & Lutenecker, A. (1995). In situ evaluation of K_0 in eastern Canada clays. *Canadian Geotechnical Journal*, 32(4), 677–688.
- Handy, R. L., Mings, C., Retz, D., & Eichner, D. (1990). Field Experience with the Back-pressured K_0 Stepped Blade. *Transportation Research Record*, (1278).
- Hanzawa, H. & Kishida, T. (1981). Fundamental considerations on undrained strength characteristics of alluvial marine clays. *Soils and Foundations*, 21(1), 39–50.
- Holtz, R., Jamiolkowski, M., & Lancellotta, R. (1986). Lessons from oedometer tests on high quality samples. *Journal of Geotechnical Engineering*, 112(8), 768–776.
- Hughes, J. & Robertson, P. K. (1985). Full-displacement pressuremeter testing in sand. *Canadian Geotechnical Journal*, 22(3), 298–307.
- ISO. (2004a). *Geotechnical investigation and testing - laboratory testing of soil Part 12: Determination of Atterberg limits*. Switzerland: International Organization for Standardization.
- ISO. (2004b). *Geotechnical investigation and testing - laboratory testing of soil Part 9: Consolidated triaxial compression tests on water-saturated soil*. Switzerland: International Organization for Standardization.
- ISO. (2012). *Geotechnical investigation and testing. Field testing. Part 1: Electrical cone and piezocone penetration test*. Switzerland: International Organization for Standardization.
- ISO. (2014a). *Geotechnical investigation and testing - laboratory testing of soil Part 1: Determination of water content*. Switzerland: International Organization for Standardization.
- ISO. (2014b). *Geotechnical investigation and testing - laboratory testing of soil Part 2: Determination of bulk density*. Switzerland: International Organization for Standardization.
- ISO. (2015). *Geotechnical investigation and testing - laboratory testing of soil Part 3: Determination of particle density*. Switzerland: International Organization for Standardization.
- Jaky, J. (1944). The coefficient of earth pressure at rest. *Journal of the Society of Hungarian Architects and Engineers*, 78(22), 355–358.
- Jaky, J. (1948). Pressure in silos. In *Proceedings of the 2nd International Conference on Soil Mechanics and Foundations Engineering* (Vol. 1, pp. 103–107).
- Jamiolkowski, M., Ladd, C., Germaine, J., & Lancellotta, R. (1985). New development in field and laboratory testing of soils. In *Proceedings of the 11th International*

- Conference on Soil Mechanics and Foundations Engineering* (Vol. 1, pp. 57–153). A.A. Balkema.
- Janbu, N. (1991). Stress-strain-time behaviour of porous media. A case record based review. In *Proceedings of the 10th European Conference on Soil Mechanics and Foundation Engineering* (Vol. 1, pp. 129–132). A.A. Balkema.
- Janbu, N. & Senneset, K. (1995). Soil parameters determined by triaxial testing. In *Proceedings of the 11th European Conference on Soil Mechanics and Foundation Engineering* (Vol. 3, pp. 101–106).
- Janbu, N., Tokheim, O., & Senneset, K. (1981). Consolidation tests with continuous loading. In *Proceedings of the 10th International Conference on Soil Mechanics and Foundations Engineering* (Vol. 1, pp. 645–654).
- Janbu, N. (1970). *Grunnlag i geoteknikk (in Norwegian)*. Tapir Forlag.
- Karlsrud, K. & Hernandez-Martinez, F. G. (2013). Strength and deformation properties of Norwegian clays from laboratory tests on high-quality block samples. *Canadian Geotechnical Journal*, 50(12), 1273–1293.
- Kavazanjian Jr, E. & Mitchell, J. K. (1984). Time dependence of lateral earth pressure. *Journal of Geotechnical Engineering*, 110(4), 530–533.
- Kavazanjian Jr, E. & Mitchell, J. K. (1985). Closure to “Time Dependence of Lateral Earth Pressure” by Edward Kavazanjian, Jr., and James K. Mitchell (April, 1984). *Journal of Geotechnical Engineering*, 111(10), 1246–1248.
- Kenney, T. (1967). Field measurements of in-situ stresses in quick clays. In *Proceedings of Oslo Geotechnical Conference, Oslo, Norway* (Vol. 1, pp. 49–56).
- Kimura, T. & Saitoh, K. (1983). The influence of strain rate on pore pressures in consolidated undrained triaxial tests on cohesive soils. *Soils and Foundations*, 23(1), 80–90.
- Ku, T. & Mayne, P. W. (2013). Evaluating the In Situ Lateral Stress Coefficient (K_0) of Soils via Paired Shear Wave Velocity Modes. *Journal of Geotechnical and Geoenvironmental Engineering*, 139(5), 775–787.
- Ku, T. & Mayne, P. W. (2015). In Situ Lateral Stress Coefficient (K_0) from Shear Wave Velocity Measurements in Soils. *Journal of Geotechnical and Geoenvironmental Engineering*, 141(12), 06015009.
- Kulhawy, F. H. & Mayne, P. W. (1990). *Manual on estimating soil properties for foundation design*. Electric Power Research Inst., Palo Alto, CA (USA); Cornell Univ., Ithaca, NY (USA). Geotechnical Engineering Group.
- Lacasse, S. & Lunne, T. (1989). Calibration of dilatometer correlations. *Norwegian Geotechnical Institute Publication 177*, 1–10.

- Larsson, R. (1977). Basic behaviour of Scandinavian soft clays. *Swedish Geotechnical Institute Publication 4*.
- Law, K. T. & Eden, W. (1980). Influence of cutting shoe size in self-boring pressuremeter tests in sensitive clays. *Canadian Geotechnical Journal*, 17(2), 165–173.
- Lefebvre, G., Bozozuk, M., Philibert, A., & Horny, P. (1991). Evaluating K_0 in Champlain clays with hydraulic fracture tests. *Canadian Geotechnical Journal*, 28(3), 365–377. doi:10.1139/t91-047
- Lessard, G. & Mitchell, J. K. (1985). The causes and effects of aging in quick clays. *Canadian Geotechnical Journal*, 22(3), 335–346.
- Lindgård, A. & Ofstad, C. S. (2016). An evaluation of methods to determine K'_0 in clays - Literature study and pilot experiments conducted at Tiller in connection with NGTS. *Project work, Geotechnical Engineering NTNU*.
- Lunne, T., Lacasse, S., & Rad, N. (1992). SPT, CPT, pressuremeter testing and recent developments in in-situ testing-Part 1: All tests except SPT. In *Proceedings of the 12th International Conference on Soil Mechanics and Foundations Engineering* (Vol. 4, pp. 2339–2403). A.A. Balkema.
- Lunne, T., Berre, T., & Strandvik, S. (1997). Sample disturbance effects in soft low plastic Norwegian clay. In *Symposium on Recent Developments in Soil and Pavement Mechanics*.
- Lunne, T., Lacasse, S., Rad, N., & Decourt, L. (1990). SPT, CPT, pressuremeter testing and recent developments on in situ testing. *Norwegian Geotechnical Institute Publication 179*.
- Lunne, T. & L'Heureux, J.-S. (2016). SP8 – Geotekniske dimensjoneringsparametere (GEODIP): Evaluation of K_0 in soft lightly OC Clays from in situ tests. *Norwegian Geotechnical Institute Report*, (20150030-05).
- Lutenegger, A. J. (1990). Determination of in situ lateral stresses in a dense glacial till. *Transportation Research Record*, (1278).
- Lutenegger, A. J. & Timian, D. A. (1986). In Situ Tests with K_0 Stepped Blade. In *Use of In Situ Tests in Geotechnical Engineering* (pp. 730–751). ASCE.
- Mahar, L. J. & O'Neill, M. W. (1983). Geotechnical characterization of desiccated clay. *Journal of Geotechnical Engineering*, 109(1), 56–71.
- Marchetti, S., Monaco, P., Totani, G., & Calabrese, M. (2006). The flat dilatometer test (DMT) in soil investigations - A report by the ISSMGE committee TC16. In *2nd International Conference on the Flat Dilatometer* (pp. 7–48). Reprint official version approved by the ISSMGE Technical Committee TC16 (May 2001).
- Marchetti, S. (1980). In situ tests by flat dilatometer. *Journal of Geotechnical and Geoenvironmental Engineering*, 106(3), 299–321.

- Marchetti, S. (2015). Some 2015 updates to the TC16 DMT Report 2001. In *The 3rd International Conference on the Flat Dilatometer DMT-15, Rome* (pp. 43–68).
- Marchetti, S., Monaco, P., Totani, G., & Marchetti, D. (2008). In situ tests by seismic dilatometer (SDMT). *From Research to Practice in Geotechnical Engineering*, 180, 292–311.
- Massarsch, K. R. (1975). New Method for Measurement of Lateral Earth Pressure in Cohesive Soils. *Canadian Geotechnical Journal*, 12(1), 142–146. doi:10.1139/t75-013
- Massarsch, K. R. (1978). New aspects of soil fracturing in clay. *Journal of Geotechnical and Geoenvironmental Engineering*, 104(8), 1109–1123.
- Mayne, P. W. & Kulhawy, F. (1982). K_0 -OCR Relationships in Soil. *Journal of the Soil Mechanics and Foundations Division*, 108(6), 851–872.
- Mayne, P. & Martin, G. (1998). Commentary on Marchetti Flat Dilatometer Correlations in Soils. *Geotechnical Testing Journal*, 21(3).
- Mesri, G. & Castro, A. (1987). C_α/C_c concept and K_0 during secondary compression. *Journal of Geotechnical Engineering*, 113(3), 230–247.
- Mesri, G. & Choi, Y. (1984). Discussion, Time effects on the stress–strain behavior of natural soft clays, by J. Graham, JHA Crooks and AL Bell. *Géotechnique*, 34, 439–442.
- Mesri, G. & Hayat, T. (1993). The coefficient of earth pressure at rest. *Canadian Geotechnical Journal*, 30(4), 647–666.
- Mesri, G. & Godlewski, P. M. (1977). Time-and stress-compressibility interrelationship. *Journal of Geotechnical and Geoenvironmental Engineering*, 103(ASCE 12910).
- Muthuswamy, M., Peters, J., & Tordesillas, A. (2006). Uncovering the secrets to relieving stress: discrete element analysis of force chains in particulate media. *ANZIAM Journal*, 47, 355–372.
- NBR. (1993). *Geoteknisk prøving Laboriemetoder Bestemmelse av endimensjonale konsolideringsegenskaper ved ødometerprøving Metode med kontinuerlig belastning (in Norwegian)*. Norway: Standard Norge Standard Online.
- NGF. (1974). *Retningslinjer for presentasjon av geotekniske undersøkelser (In Norwegian)*. Norwegian Geotechnical Society.
- NGF. (1989a). *Måling av grunnvannstand og poretrykk (in Norwegian)*. Norwegian Geotechnical Society.
- NGF. (1989b). *Veiledning for utførelse av dreietrykksondering (in Norwegian)*. Norwegian Geotechnical Society.
- Oda, M., Takemura, T., & Takahashi, M. (2004). Microstructure in shear band observed by microfocus X-ray computed tomography. *Géotechnique*, 54(8), 539–542.

- Ozkul, Z. H. & L'Heureux, J.-S. (2017). Norwegian GeoTest Sites (NGTS) Factual Report - Tiller Flotten Research Site. *Norwegian Geotechnical Institute Report*, (20160154-19).
- Panah, A. K. & Yanagisawa, E. (1989). Laboratory Studies on Hydraulic Fracturing Criteria in Soil. *Soils and Foundations*, 29(4), 14–22. doi:10.3208/sandf1972.29.4_14
- Peters, J., Muthuswamy, M., Wibowo, J., & Tordesillas, A. (2005). Characterization of force chains in granular material. *Physical review E*, 72(4), 041307.
- Peters, J. F. & Berney IV, E. S. (2009). Percolation threshold of sand-clay binary mixtures. *Journal of Geotechnical and Geoenvironmental Engineering*, 136(2), 310–318.
- Radjai, F., Wolf, D. E., Jean, M., & Moreau, J.-J. (1998). Bimodal character of stress transmission in granular packings. *Physical Review Letters*, 80(1), 61.
- Reite, A. J., Sveian, H., & Erichsen, E. (1999). *Trondheim fra istid til nåtid: landskapshistorie og løsmasser (in Norwegian)*. Norges Geologiske Undersøkelse.
- Roque, R., Janbu, N., & Senneset, K. (1988). Basic interpretation procedures of flat dilatometer tests. In *Proceedings of 1st International Symposium on Penetration Testing, Orlando, Florida* (Vol. 1).
- Roy, M. & Leblanc, A. (1988). Factors affecting the measurements and interpretation of the vane strength in soft sensitive clays. In *Vane Shear Strength Testing in Soils: Field and Laboratory Studies*. ASTM International.
- Ryley, M. & Carder, D. (1995). The performance of push-in spade cells installed in stiff clay. *Géotechnique*, 45(3), 533–539.
- Sandbækken, G., Berre, T., & Lacasse, S. (1986). Oedometer testing at the Norwegian Geotechnical Institute. In *Consolidation of soils: Testing and Evaluation*. ASTM International.
- Schmertmann, J. H. (1983). A simple question about consolidation. *Journal of Geotechnical Engineering*, 109(1), 119–122.
- Schmertmann, J. H. (1991). The mechanical aging of soils. *Journal of Geotechnical Engineering*, 117(9), 1288–1330.
- Schmidt, B. (1966). Earth pressures at rest related to stress history. *Canadian Geotechnical Journal*, 3(4), 239–242.
- Schnaid, F. (2008). In situ testing in geomechanics - the main tests.
- Schofield, A. & Wroth, P. (1968). *Critical state soil mechanics*. McGraw-Hill London.
- Senneset, K. (1989). A new oedometer with splitted ring for the measurement of lateral stress. In *Proceedings of the 12th International Conference on Soil Mechanics and Foundations Engineering* (Vol. 1, pp. 115–118). A.A. Balkema.

- Senneset, K. & Janbu, N. (1994). Lateral stress and preconsolidation pressure measured by laboratory tests. In *Proceedings of the 13th International Conference on Soil Mechanics and Foundations Engineering* (Vol. 1, pp. 309–312). A.A. Balkema.
- Shin, H. & Santamarina, J. C. (2009). Mineral dissolution and the evolution of k_0 . *Journal of Geotechnical and Geoenvironmental Engineering*, 135(8), 1141–1147.
- Simpson, B. (1992). Retaining Structures: Displacement and Design. *Géotechnique*, 42(4), 541–576.
- Sivakumar, V., Doran, I., Graham, J., & Navaneethan, T. (2002). Relation between K_0 overconsolidation ratio: a theoretical approach. *Géotechnique*, 52(3), 225–230.
- Sivakumar, V., Navaneethan, T., Hughes, D., & Gallagher, G. (2009). An assessment of the earth pressure coefficient in overconsolidated clays. *Géotechnique*, 59(10), 825–838.
- Sully, J. & Campanella, R. (1991). Effect of lateral stress on CPT penetration pore pressures. *Journal of Geotechnical Engineering*, 117(7), 1082–1088.
- Sully, J. & Campanella, R. (1995). Evaluation of in situ anisotropy from crosshole and downhole shear wave velocity measurements. *Géotechnique*, 45(2), 267–238.
- SVV. (1997). *Håndbok 014 Laboratorieundersøkelser (In Norwegian)*. Statens Vegvesen.
- Tavenas, F., Blanchette, G., Leroueil, S., Roy, M., & Rochelle, P. L. (1975). Difficulties in the In Situ Determination of K_0 in Soft Sensitive Clays. In *In Situ Measurement of Soil Properties* (p. 450). ASCE.
- Tedd, P. & Charles, J. A. (1981). In situ measurement of horizontal stress in overconsolidated clay using push-in spade-shaped pressure cells. *Géotechnique*, 31(4), 554–558. doi:doi:10.1680/geot.1981.31.4.554
- Tedd, P. & Charles, J. A. (1982). Discussion: In situ measurement of horizontal stress in overconsolidated clay using push-in spade-shaped pressure cells. *Géotechnique*, 32(3), 285–286. doi:doi:10.1680/geot.1982.32.3.285
- Tedd, P. & Charles, J. (1983). Evaluation of push-in pressure cell results in stiff clay. In *Proceedings of the International Symposium on Soil and Rock Investigation by in-situ Testing* (Vol. 2, pp. 579–584).
- Tomás, R., Domenech, C., Mira, A., Cuenca, A., & Delgado, J. (2007). Preconsolidation stress in the Vega Baja and Media areas of the River Segura (SE Spain): Causes and relationship with piezometric level changes. *Engineering Geology*, 91(2), 135–151.
- Tordesillas, A., Zhang, J., & Behringer, R. (2009). Buckling force chains in dense granular assemblies: physical and numerical experiments. *Geomechanics and Geoengineering: An International Journal*, 4(1), 3–16.
- Vaslestad, J. (1989). K_0 -måling: Hensikt og metoder (in Norwegian). *Norwegian Public Roads Administration Internal Report*, (1410).

- Wan, C. F. & Fell, R. (2004). Investigation of rate of erosion of soils in embankment dams. *Journal of Geotechnical and Geoenvironmental Engineering*, 130(4), 373–380.
- Watabe, Y., Tanaka, M., Tanaka, H., & Tsuchida, T. (2003). K_0 -consolidation in a triaxial cell and evaluation of in-situ K_0 for marine clays with various characteristics. *Soils and Foundations*, 43(1), 1–20. doi:10.3208/sandf.43.1

Appendix A

Soundings

This appendix contains a table presenting coordinates of bore holes used for soundings, earth pressure cells and piezometers at Flotten. Next, a map indicating the location of the test site in relation to Trondheim city centre is presented in Figure A.1. Next, an overview map showing a larger area of the Flotten test is presented in Figure A.2. This map indicates the relative location of the initial rotary pressure soundings and the CPTu conducted by operators from NTNU on the 24 to 27 January 2017, as well as the location of the first sample cylinder borehole.

A detailed map indicating the relative distance between the bore holes used for testing the earth pressure cells is presented in Figure A.3. The figure also indicates the location of the piezometers as well as the sampling bore holes, where both samples for the authors of this master's thesis as well as Gella were retrieved. Please note that as the coordinates of the bore hole VANE001 were not registered, an approximate location is shown in Figure A.3.

Finally, the results of these soundings are presented in the subsequent figures. All 10 rotary pressure soundings are included to give the best possible indication of the soil conditions at Flotten. Novapoint GeoSuite Toolbox and Autodesk AutoCAD were used to draw and present the soundings. As GeoSuite is not available in English, the sounding illustrations are equipped with text in Norwegian.

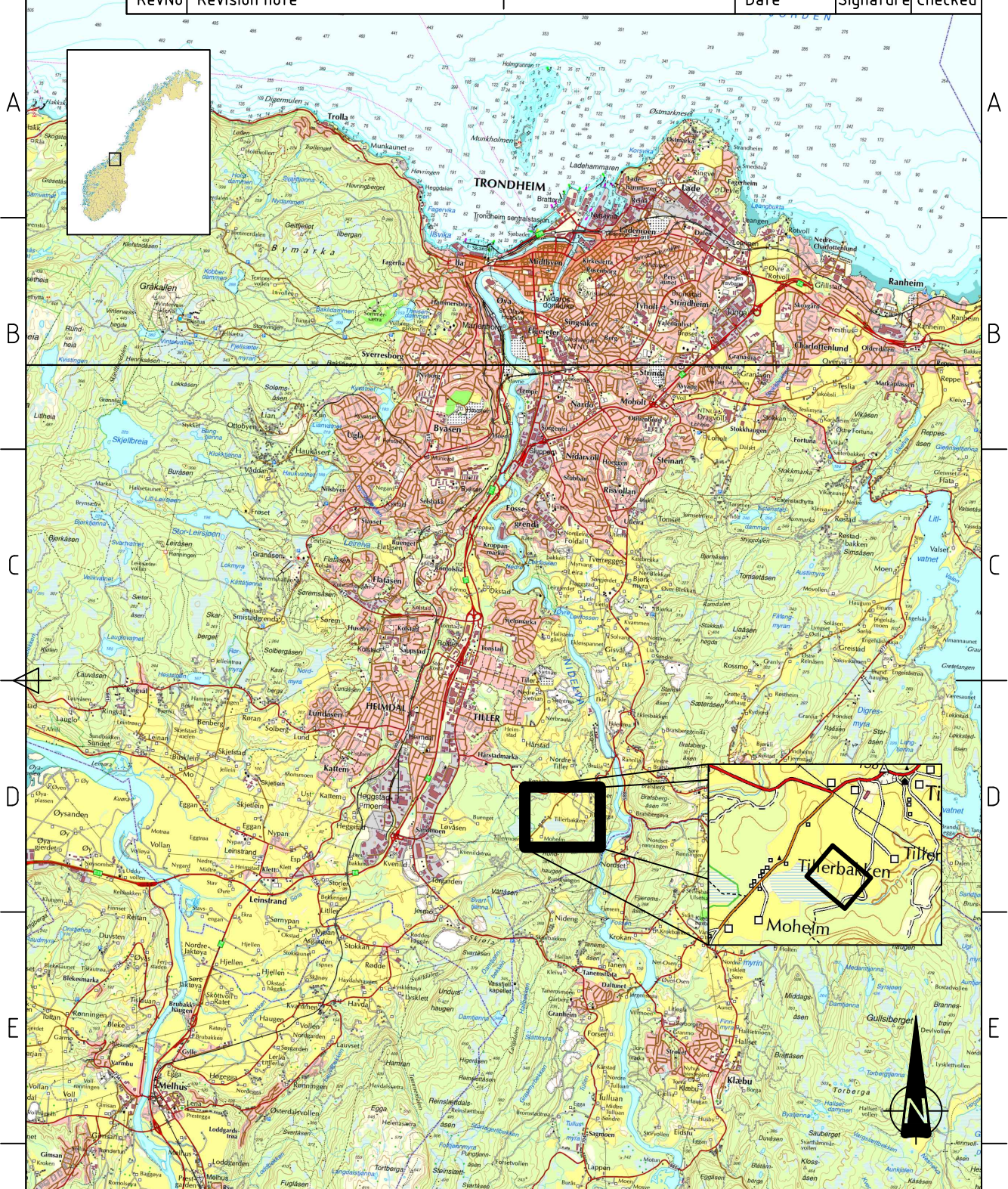
It is assumed that the rotary pressure soundings were performed in accordance with guidelines given in NGF Melding 7 NGF, 1989b and that the CPTu was conducted in accordance with ISO 22476-1 ISO, 2012.

Table A.1: Coordinates of bore holes at Flotten.

Bore hole	Coordinates			Test
	N	E	A	
54MM_1	7023918.94	571105.58	122.63	54 mm sample
54MM_K0	7023917.84	571086.12	123.59	54 mm sample
54MM_KPG	7023912.39	571095.49	123.37	54 mm sample
CPTU1	7023916.62	571103.18	122.76	CPTu
EPC001	7023914.02	571093.74	123.57	Earth pressure cell
EPC002	7023914.74	571092.38	123.69	Earth pressure cell
EPC004	7023916.75	571089.72	123.71	Earth pressure cell
EPC003	7023915.93	571090.94	123.71	Earth pressure cell
EPC005	7023917.61	571088.35	123.71	Earth pressure cell
EPC006	7023913.81	571097.26	123.03	Earth pressure cell
PZ_4363	7023898.12	571294.30	113.54	Piezometer
PZ_4362	7023897.52	571294.23	113.54	Piezometer
PZ_6081	7023915.37	571094.59	123.43	Piezometer
PZ_6082	7023915.99	571093.67	123.50	Piezometer
PZ_11360	7023912.43	571098.56	122.93	Piezometer
PZ_11361	7023914.50	571095.62	123.12	Piezometer
SDMT001	7023916.60	571092.42	123.44	Dilatometer
VANE001*	-	-	-	Field Vane

*The coordinates of VANE001 were not registered.

1	2	3	4
RevNo	Revision note	Date	Signature
			Checked



Itemref	Quantity	Title/Name, designation, material, dimension etc			Article No./Reference	
Designed by CSO	Checked by AnL	Approved by - date AnL - 14.02.2017	File name Map.dwg	Date 14.02.2017	Scale 1:118 000 (B5)	
Flotten Map provided by Kartverket			Test site location Figure A.1			
			Edition 1	Sheet 1/1		

RevNo	Revision note	Date	Signature	Checked
-------	---------------	------	-----------	---------

⊙ 54 mm sample
 ▽ CPTu
 ● Rotary pressure sounding

DRT6 ● $\frac{123.63}{33.40}$

DRT8 ● $\frac{121.99}{90.14}$ 31.85

DRT5 ● $\frac{124.86}{33.25}$

DRT7 ● $\frac{123.92}{33.37}$

DRT4 ● $\frac{123.53}{33.33}$

DRT9 ● $\frac{122.76}{33.45}$

DRT10 ● $\frac{122.63}{29.40}$

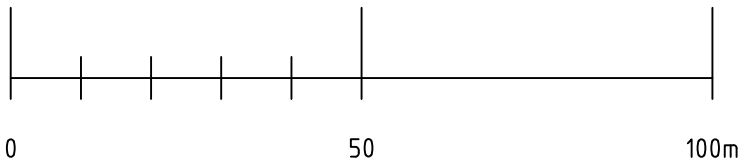
DRT3 ● $\frac{123.88}{33.32}$

DRT2 ● $\frac{123.60}{33.30}$



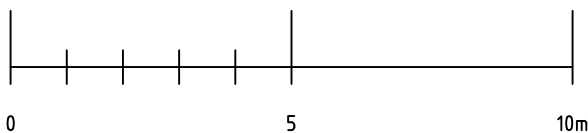
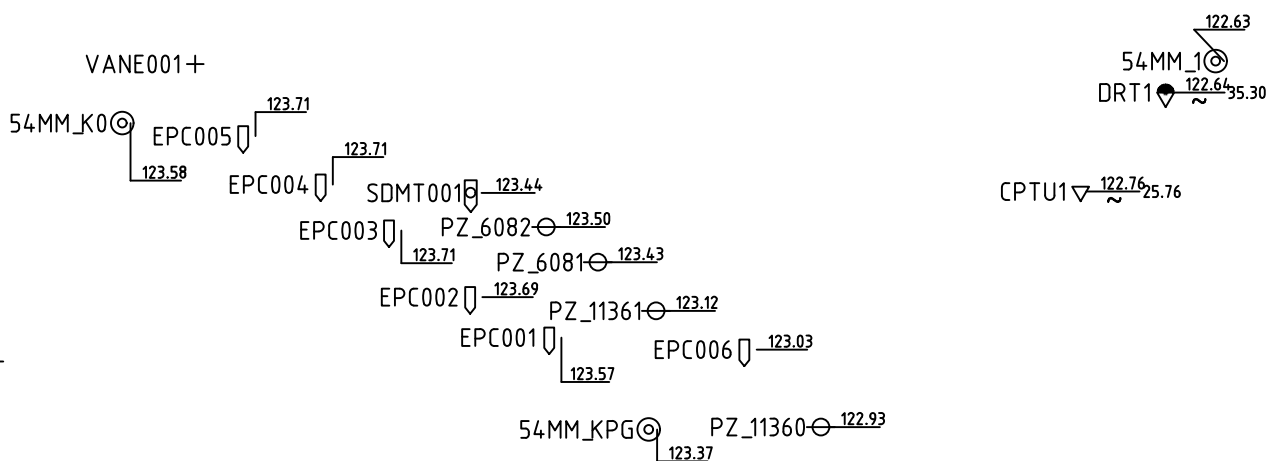
See detailed map of boreholes in Figure A.3.

54MM_1 ● $\frac{122.63}{35.30}$
 DRT1 ● $\frac{122.64}{25.76}$
 CPTU1 ▽ $\frac{122.76}{25.76}$



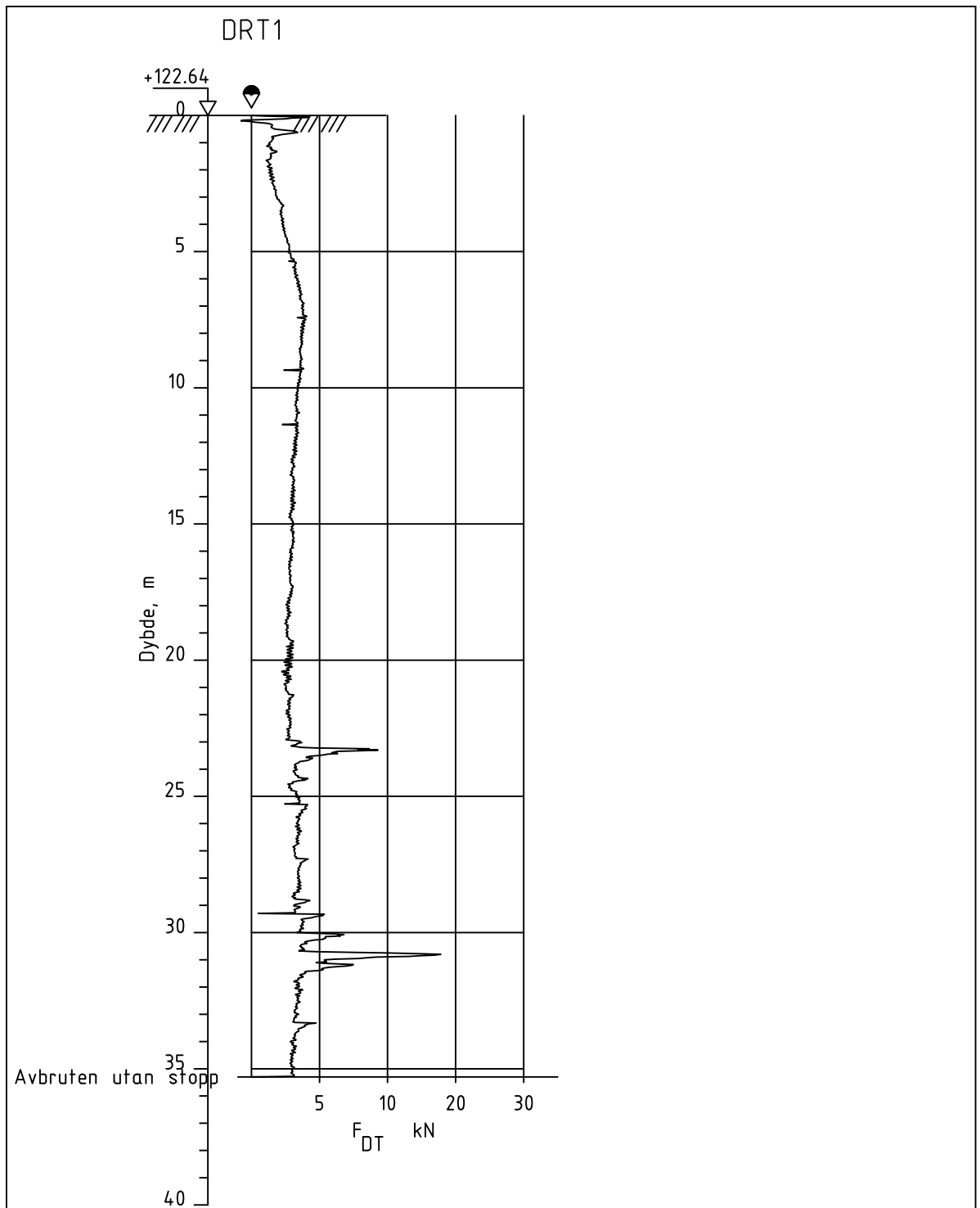
Itemref	Quantity	Title/Name, designation, material, dimension etc			Article No./Reference	
Designed by CSO	Checked by AnL	Approved by - date AnL - 31.05.2017	File name Boreplan2.dwg	Date 31.05.2017	Scale 1:1200 in B5	
Flotten			Overview map of boreholes			
			Figure A.2		Edition 1	Sheet 1/1

RevNo	Revision note	Date	Signature	Checked
-------	---------------	------	-----------	---------



⊙	54 mm sample
▽	CPTu
∩	Earth pressure cell
+	Field vane
⊖	Piezometer
⦿	Rotary pressure sounding
⊞	Seismic dilatometer

Itemref	Quantity	Title/Name, designation, material, dimension etc			Article No./Reference	
Designed by CSO	Checked by AnL	Approved by - date AnL - 31.05.2017	File name Boreplan1.dwg	Date 31.05.2017	Scale 1:150 in B5	
Flotten			Detailed map of boreholes			
			Figure A.3	Edition 1	Sheet 1/1	



Flotten - Trondheim

Rapport nr.

Figur nr.

A.4

Dreietrykksondering

M = 1 : 200

Dato boret: 24.01.2017

Borhull DRT1

Posisjon: X 7023918.39 Y 571104.69

Tegner

CSO

Dato:

300117

Kontrollert

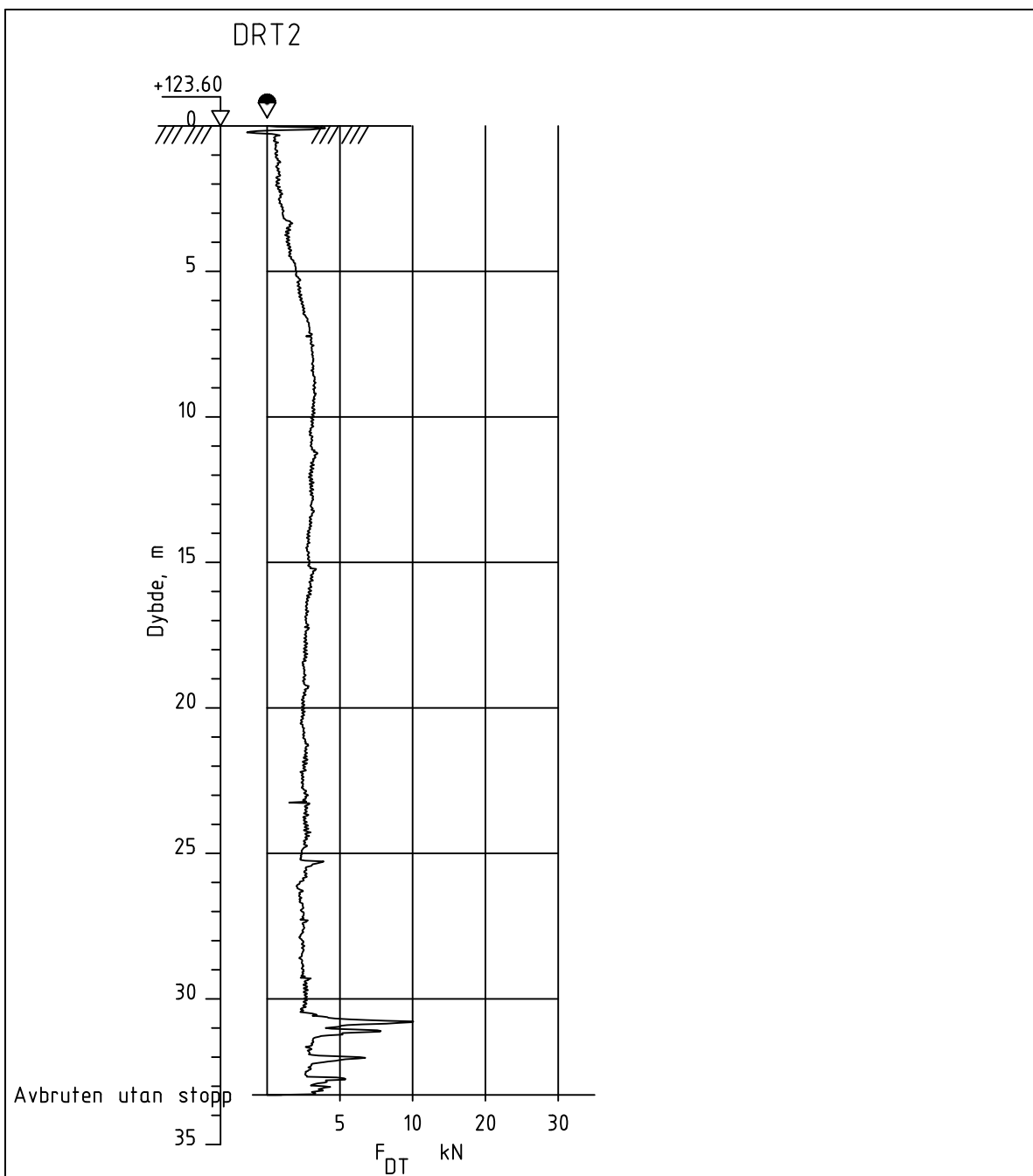
AnL

Godkjent

AnL



NTNU



Flotten - Trondheim

Rapport nr.

Figur nr.

A.5

Dreietrykksondering

M = 1 : 200

Dato boret: 24.01.2017

Borhull DRT2

Posisjon: X 7023945.04 Y 571061.99

Tegner

CSO

Dato:

300117

Kontrollert

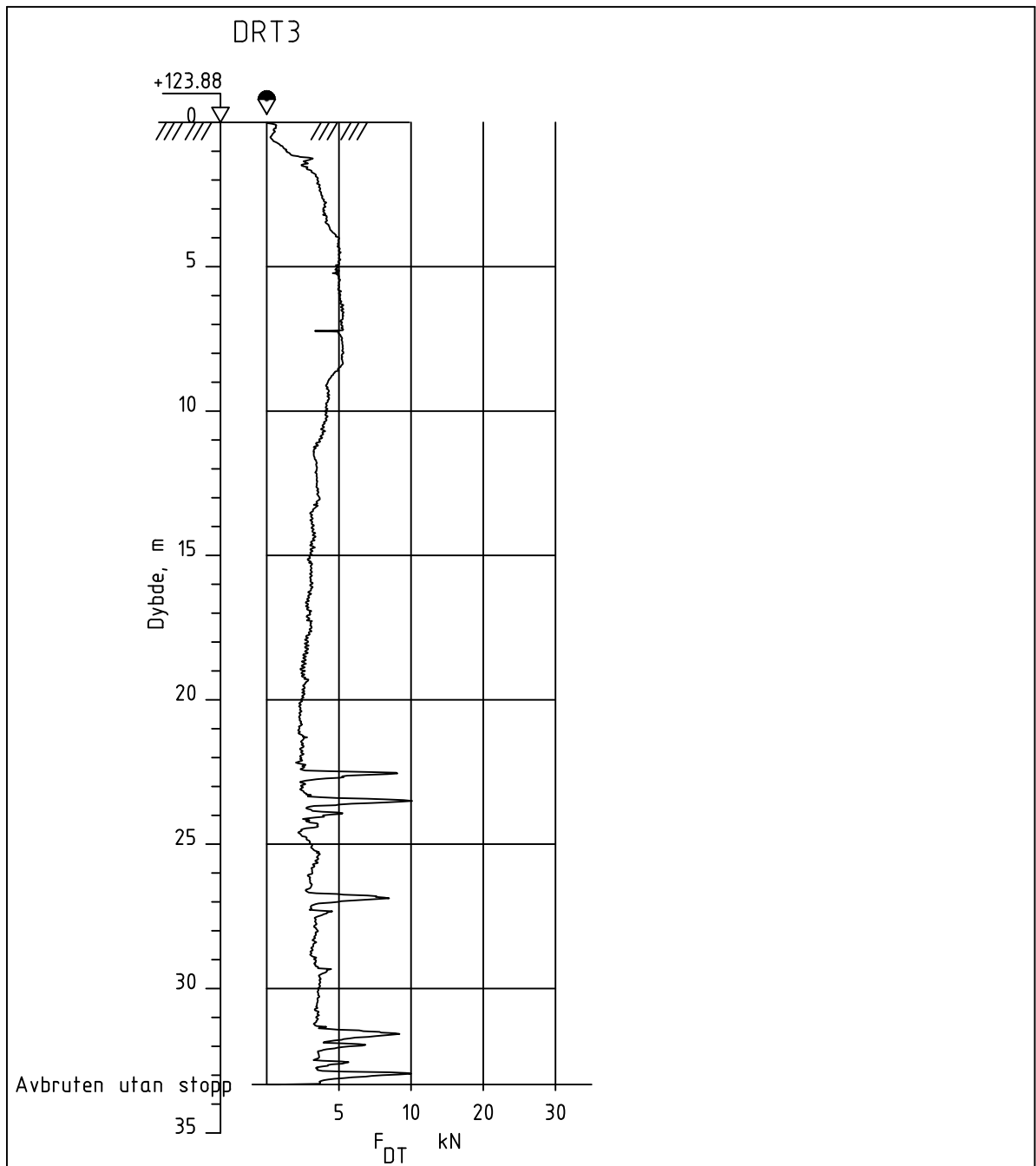
AnL

Godkjent

AnL



NTNU



Flotten - Trondheim

Rapport nr.

Figur nr.

A.6

Dreietrykksondering

M = 1 : 200

Dato boret: 24.01.2017

Borhull DRT3

Posisjon: X 7023972.86 Y 571020.53

Tegner

CSO

Dato:

300117

Kontrollert

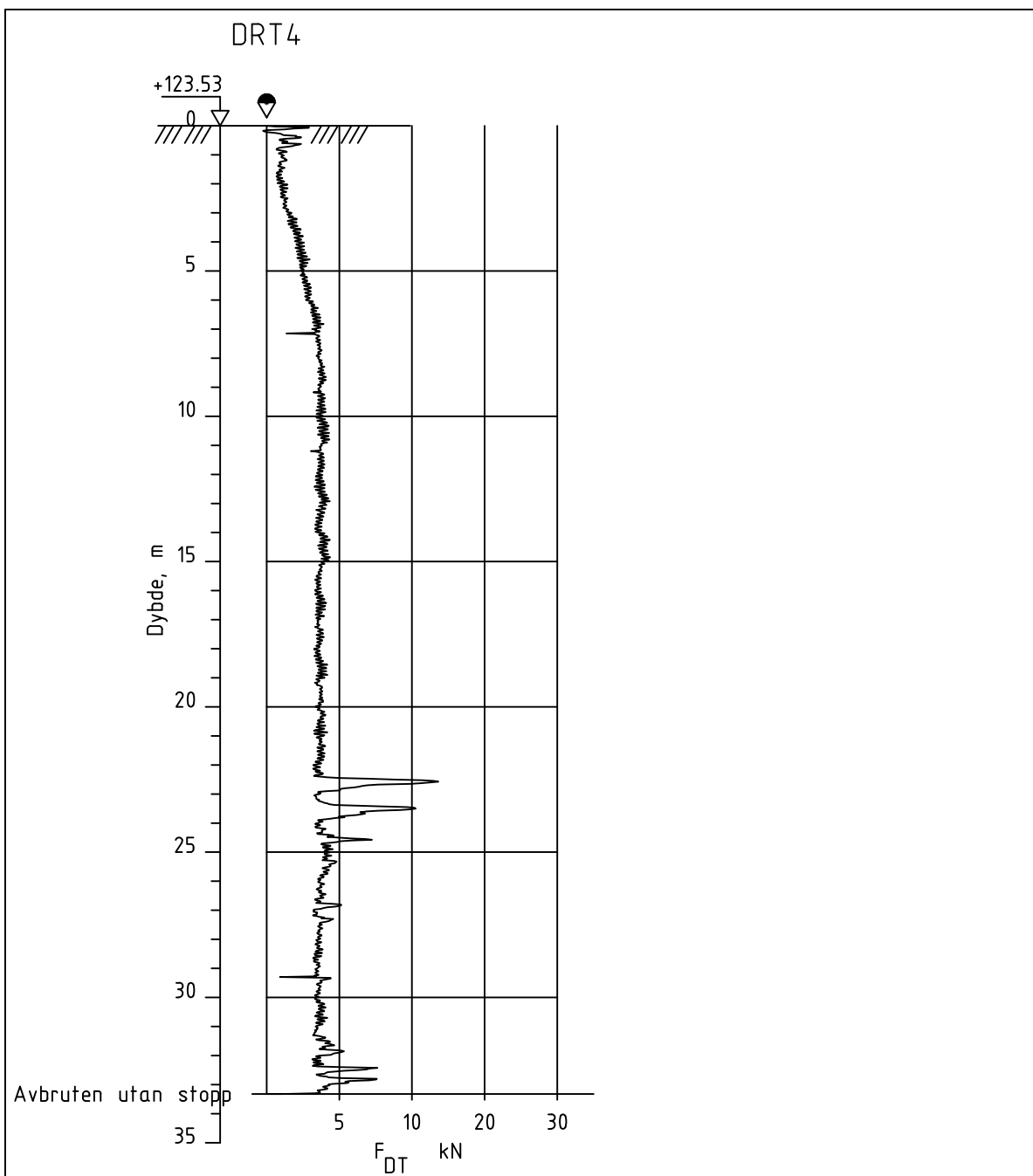
AnL

Godkjent

AnL



NTNU



Flotten - Trondheim

Rapport nr.

Figur nr.

A.7

Dreietrykksondering

M = 1 : 200

Dato boret: 24.01.2017

Borhull DRT4

Posisjon: X 7023997.97 Y 570983.80

Tegner

CSO

Dato:

300117

Kontrollert

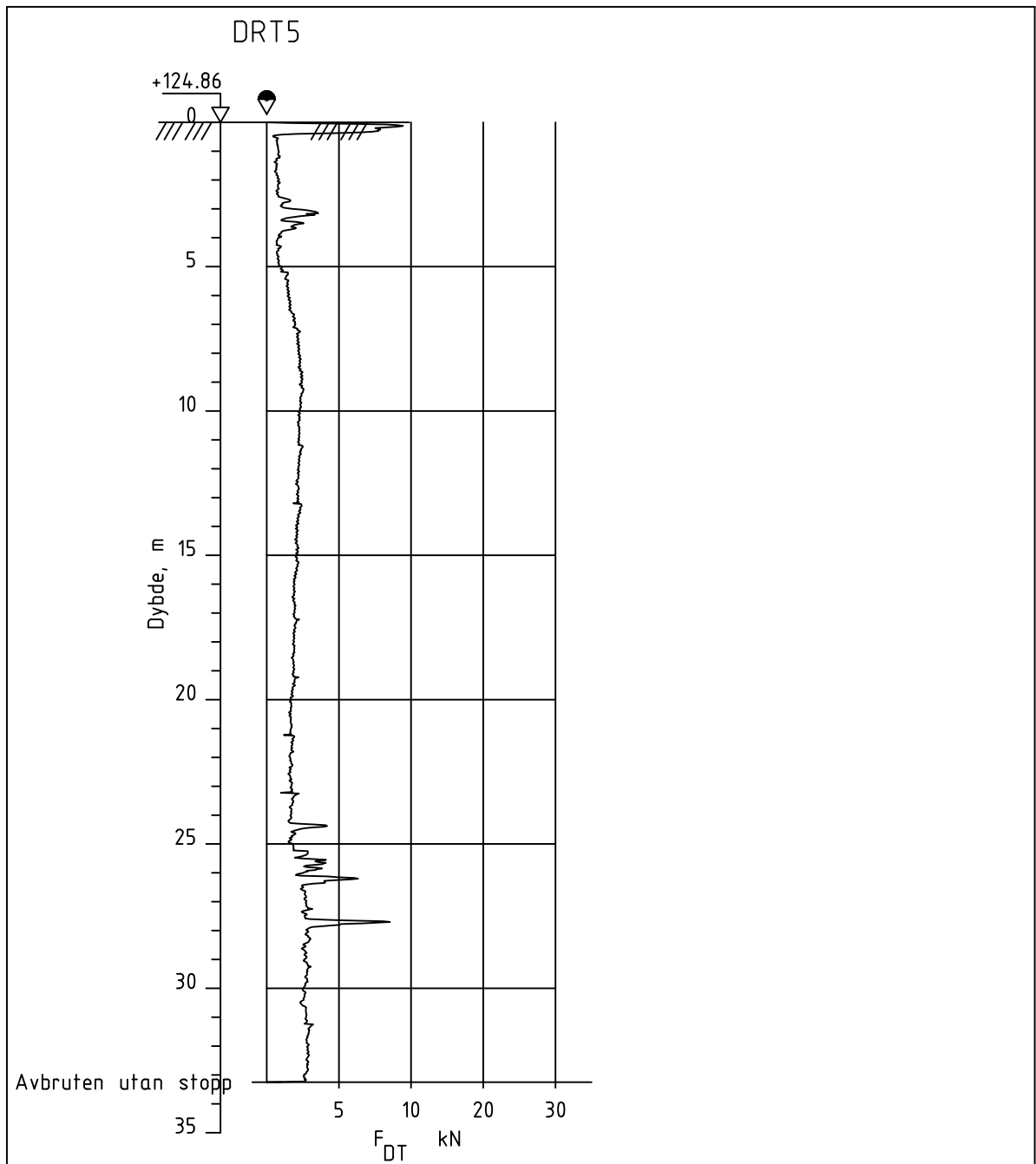
AnL

Godkjent

AnL



NTNU



Flotten - Trondheim

Rapport nr.

Figur nr.

A.8

Dreietrykksondering

M = 1 : 200

Dato boret: 24.01.2017

Borhull DRT5

Posisjon: X 7024028.34 Y 570936.32

Tegner

CSO

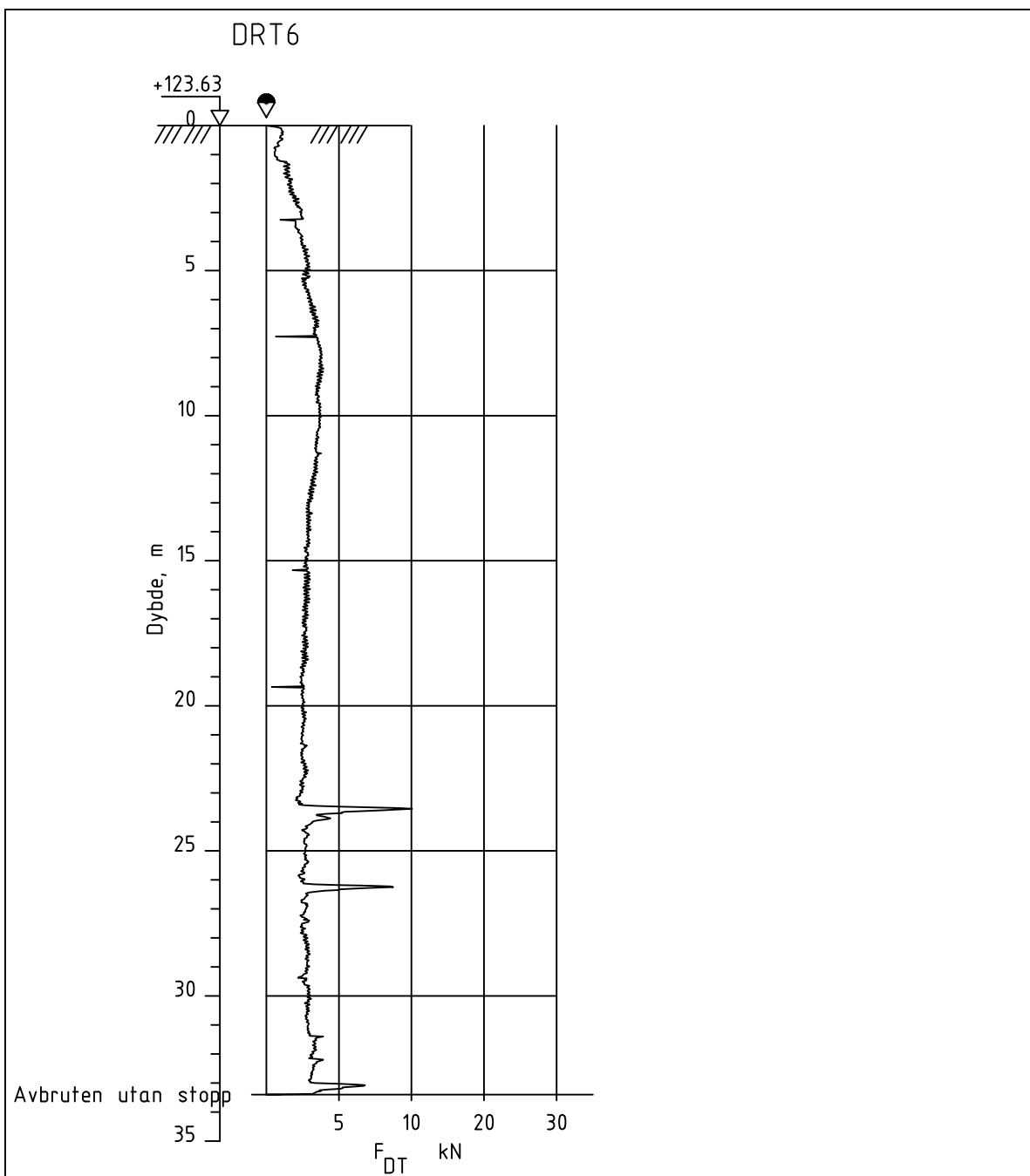
Kontrollert

AnL

Godkjent

AnL





Flotten - Trondheim

Rapport nr.

Figur nr.

A.9

Dreietrykksondering

M = 1 : 200

Dato boret: 25.01.2017

Borhull DRT6

Posisjon: X 7024074.59 Y 570954.27

Tegner

CSO

Dato:

300117

Kontrollert

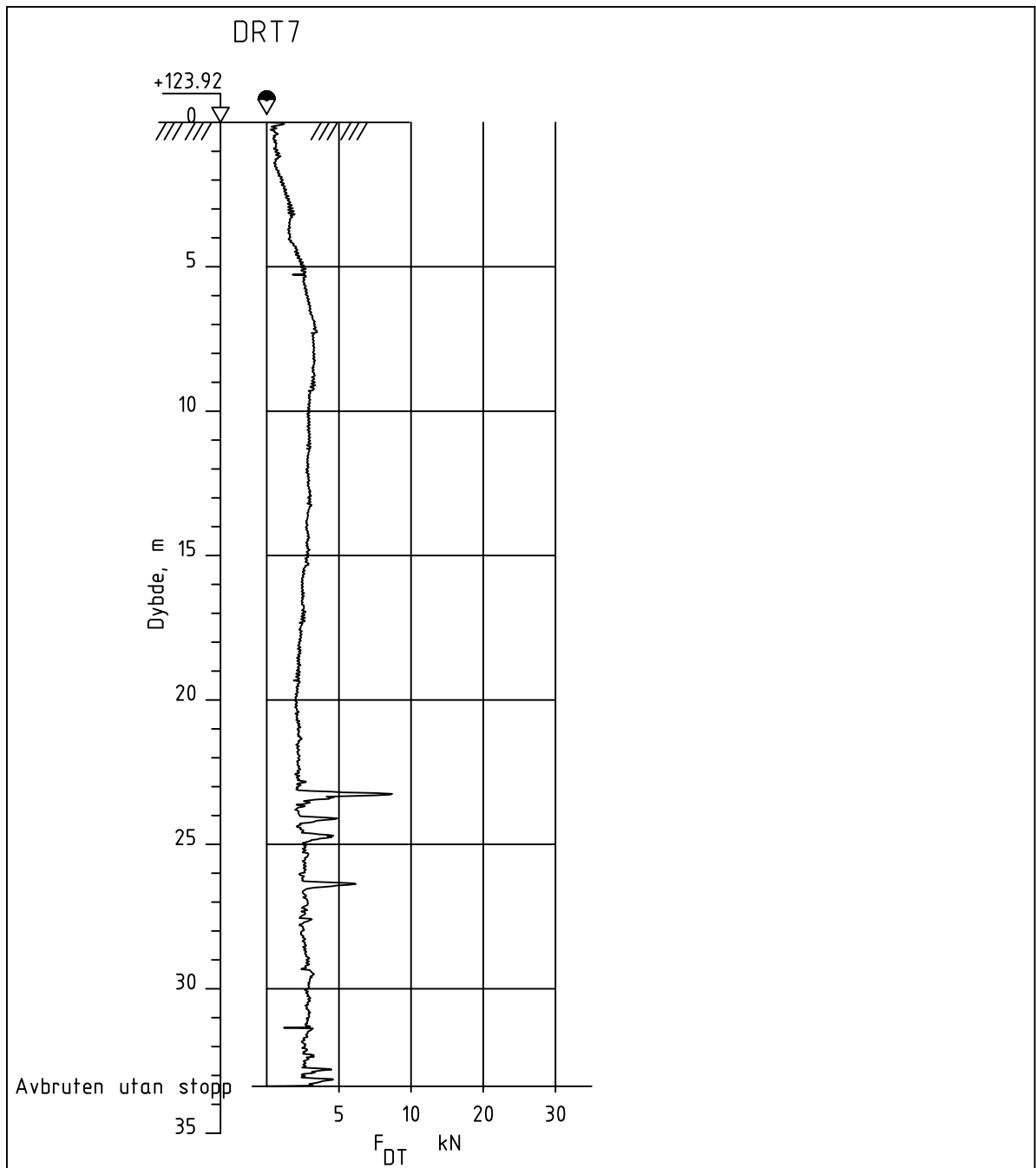
AnL

Godkjent

AnL



NTNU



Flotten - Trondheim

Rapport nr.

Figur nr.

A.10

Dreietrykksondering

M = 1 : 200

Dato boret: 25.01.2017

Borhull DRT7

Posisjon: X 7024028.63 Y 570967.26

Tegner

CSO

Dato:

300117

Kontrollert

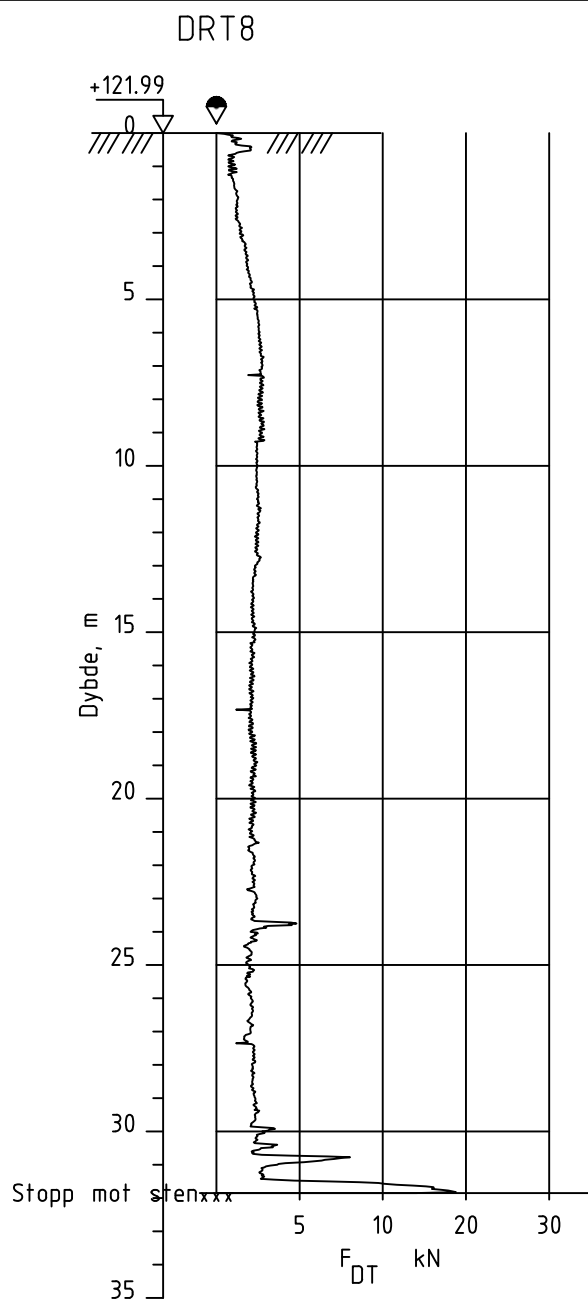
AnL

Godkjent

AnL



NTNU



Flotten - Trondheim

Rapport nr.

Figur nr.

A.11

Dreietrykksondering

Tegner

CSO

Dato:

300117

M = 1 : 200

Dato boret: 25.01.2017

Borhull DRT8

Kontrollert

AnL

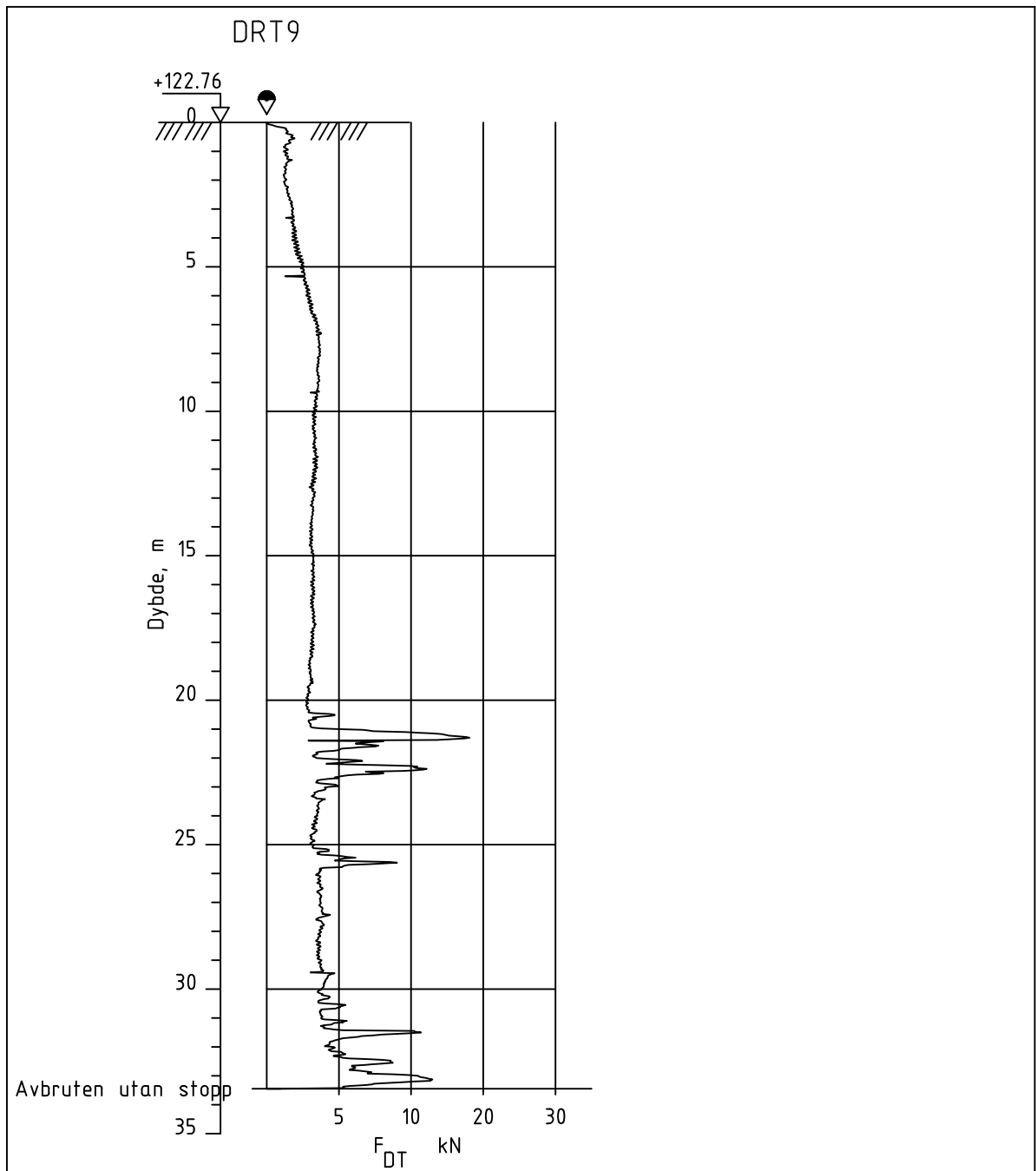
Godkjent

AnL

Posisjon: X 7024070.95 Y 571022.81



NTNU



Flotten - Trondheim

Rapport nr.

Figur nr.

A.12

Dreietrykksondering

M = 1 : 200

Dato boret: 25.01.2017

Borhull DRT9

Posisjon: X 7023997.93 Y 571046.09

Tegner

CSO

Dato:

300117

Kontrollert

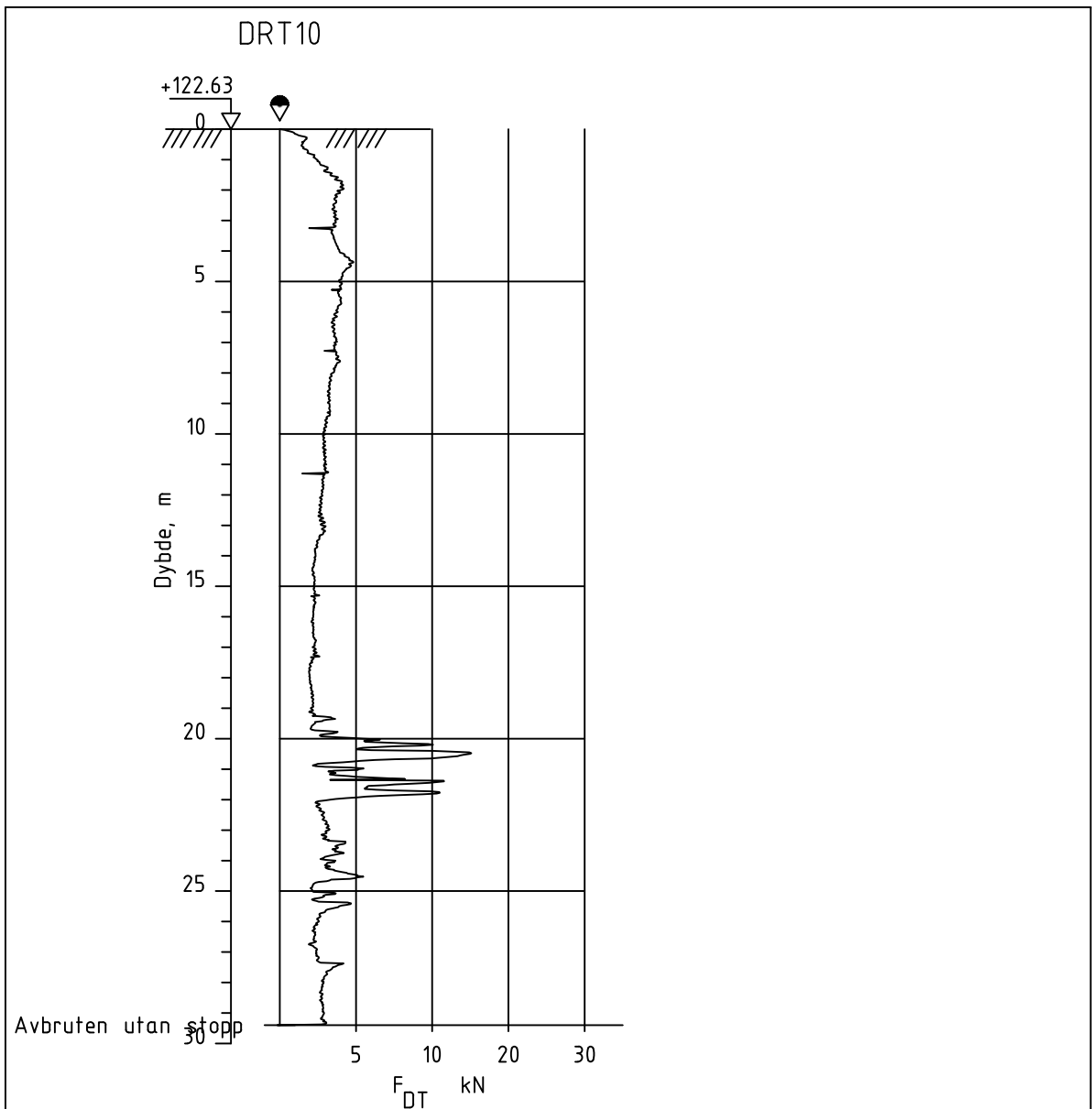
AnL

Godkjent

AnL



NTNU



Flotten - Trondheim

Rapport nr.

Figur nr.

A.13

Dreietrykksondering

M = 1 : 200

Dato boret: 25.01.2017

Borhull DRT10

Posisjon: X 7023990.38 Y 571100.01

Tegner

CSO

Dato:

300117

Kontrollert

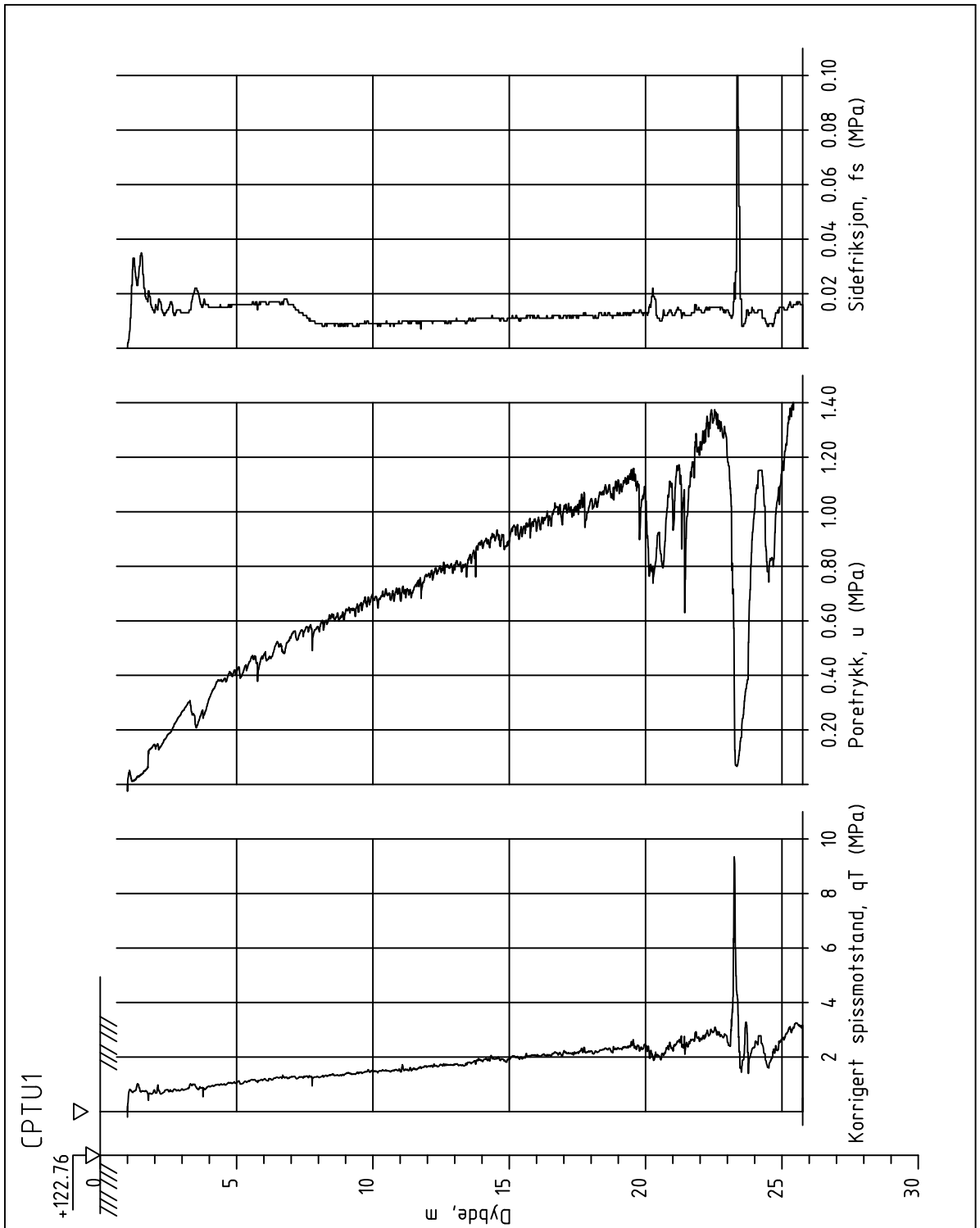
AnL


Godkjent

AnL



NTNU



Trondheim - Flotten		Rapport nr.	Figur nr. A.14
CPT-sondering M = 1 : 200 Dato boret: 27.01.17 Borhull CPTU1		Tegner CSO	Dato: 300117
Posisjon: X 7023916.62 Y 571103.18		Kontrollert AnL	 NTNU
Sonde nr.: 4784		Godkjent AnL	

Appendix B

Pore Pressure Measurements

This appendix contains the results of pore pressure measurements conducted by the use of six Geotech PVT piezometers with and without an automatic data logging system installed at Flotten. Table B.1 gives an overview of the altitudes at surface as well as depths of the installed piezometers. Coordinates of all the piezometers are given in Appendix A. Please note that the two piezometers with serial numbers 4362 and 4363 are installed about 100 m east of the test site, whilst the remaining four are installed in close proximity to the earth pressure cells. Please see the map of boreholes presented in Appendix A.

Table B.1: Overview of Geotech PVT piezometers at Flotten.

Serial Number	Altitude [m]	Depth [m]
4362	113.54	10
4363	113.54	25
11360	122.93	5
11361	123.12	7
6081	123.43	10
6082	123.50	15.75

On the following pages, Table B.2 shows the dates and individual pore pressure measurements, while Table B.3 gives the dates of final pore pressure measurements from earth pressure cells. An assumed pore pressure distribution with depth at Flotten, corrected for air pressure, is presented in Figure B.1. The final pore pressure measurements taken on 22 May, which were used when establishing this assumed distribution, are presented in Table B.4. Next, a plot indicating the potential with depth, corrected for air pressure is given in Figure B.2. Finally, Figure B.3 presents piezometer measurements with time.

Please note that the piezometers with serial numbers 4362, 4663, 6081 and 6082 were not equipped with a logging memory. These individual measurements are summarized in Table B.2. Consequently, separate measurements were taken several times during the spring of 2017. The piezometers with serial number 11360 and 11361 were equipped with a logging memory and were installed on 15 May 2017. Based on readings taken on the 22 May, any excess pore pressure due to the installation was assumed to have dissipated by 17 May. Hence, the lines for these piezometers show measurements registered for every hour between 17 May and 22 May.

Table B.2: Individual pore pressure measurements taken at Flotten during the spring 2017. Measurements have not been corrected for air pressure.

Date	Piezometer sensor number			
	4362	4363	6081	6082
2017-02-15	35.6	65.4	38.1	51.4
2017-02-22	30.0	60.3	32.1	45.7
2017-03-10	33.7	64.1	37.0	50.9
2017-03-27	33.4	63.8	37.2	51.3
2017-03-31	32.7	63.4	36.5	50.8
2017-04-24	32.6	63.7	36.6	50.6
2017-04-26	32.9	63.9	36.9	51.0
2017-05-12	-	-	37.5	51.3
2017-05-15	-	-	40.9	54.8
2017-05-22	35.3	66.7	41.0	54.5

Table B.3: Dates of final pore pressure measurements from earth pressure cells.

Depth [m]	Borehole	Date
5.0	EPC001	2017-02-27
5.0	EPC002	2017-02-27
5.0	EPC003	2017-02-27
5.0	EPC004	2017-02-27
5.0	EPC005	2017-02-27
6.0	EPC002	2017-05-15
7.0	EPC003	2017-04-04
8.0	EPC004	2017-03-29
9.0	EPC004	2017-04-04
10.0	EPC004	2017-05-11
10.0	EPC003	2017-05-12

Table B.4: Final pore pressure measurements from piezometers used for establishing the assumed pore pressure distribution. Measurements have been corrected for air pressure.

Serial Number	Depth [m]	Pore pressure [kPa]
11360	5	31.0
11361	7	37.0
6081	10	40.6
6082	15.75	54.0

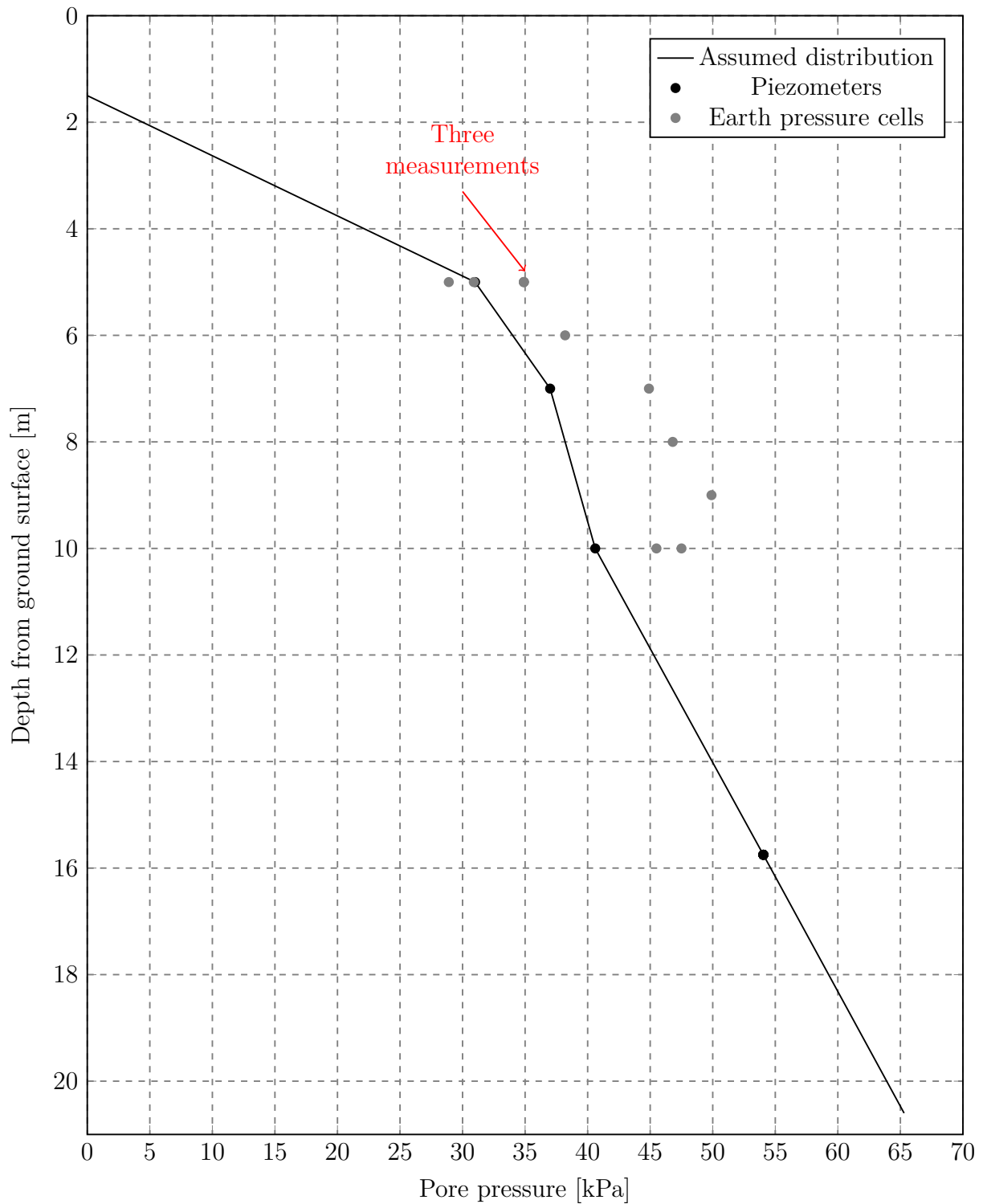


Figure B.1: Overview of pore pressure measurements taken at Flotten. The black line indicates the assumed pore pressure distribution used for calculating the pore pressure at different depths. Measurements have been corrected for air pressure.

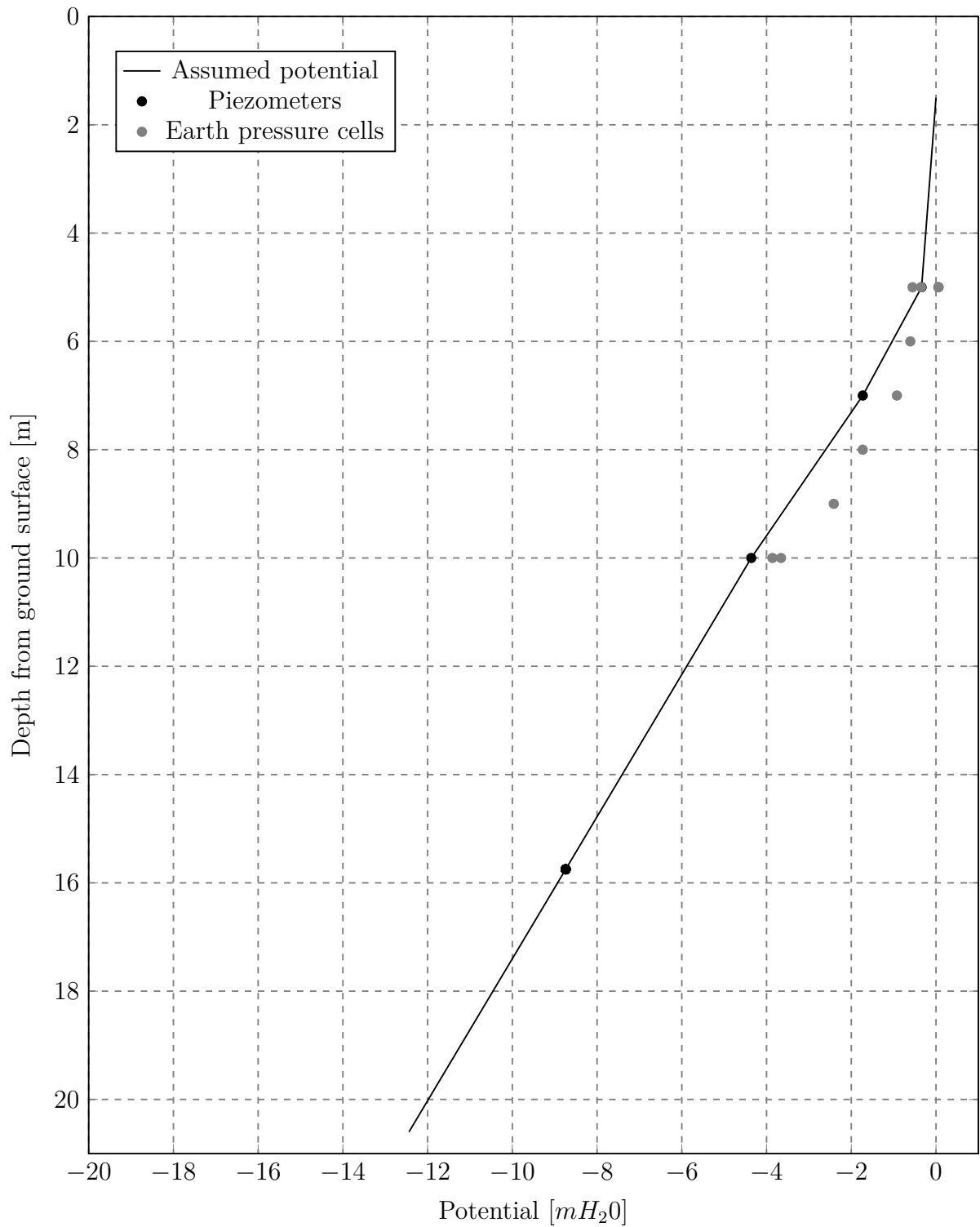


Figure B.2: Overview of potential with depth. Zero assumed at depth 1.5 m. The black line indicates the potential based on the assumed pore pressure distribution. Measurements have been corrected for air pressure.

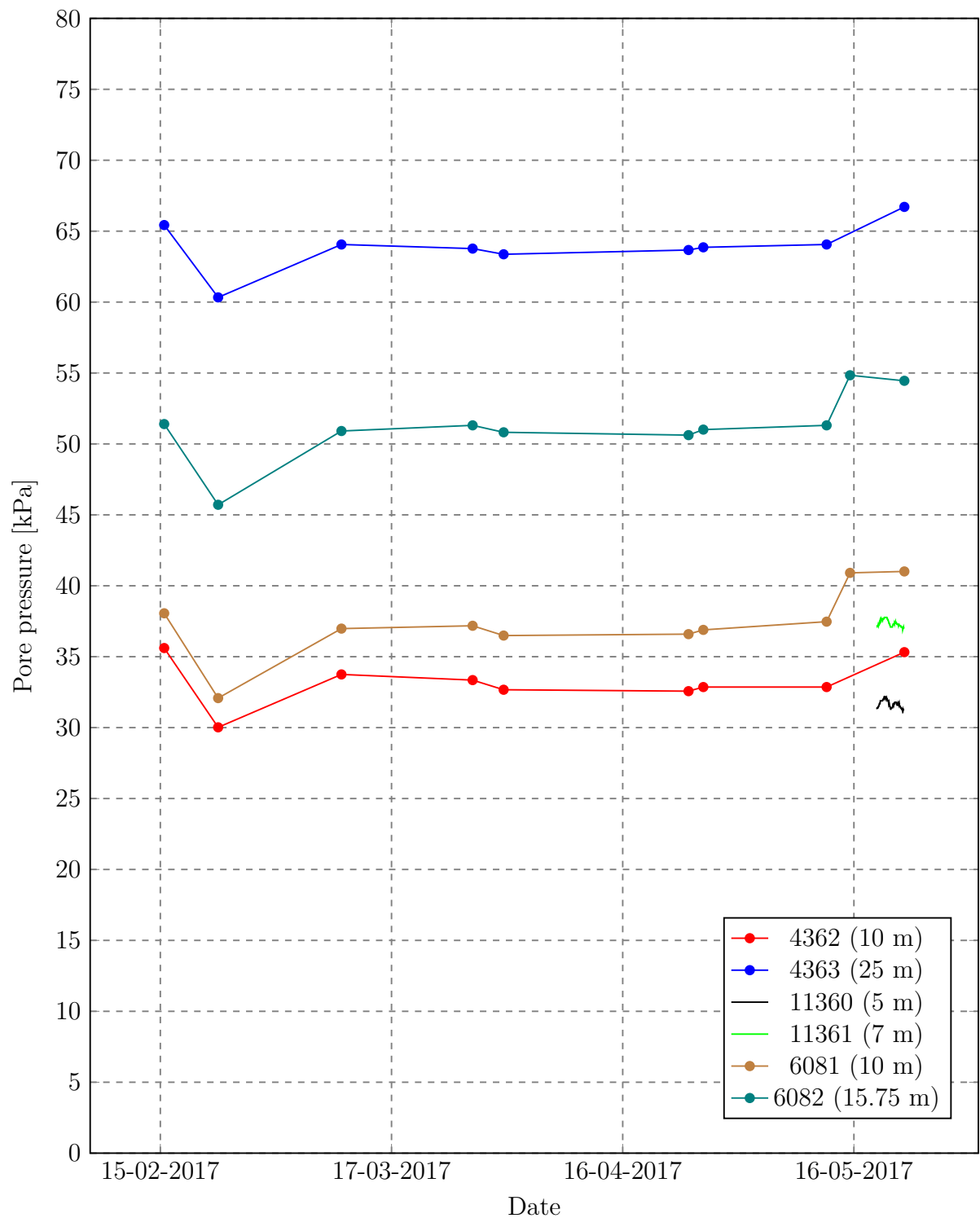


Figure B.3: Pore pressure measurements with time at Flotten. Measurements have not been corrected for air pressure.

Appendix C

Earth Pressure Cells

In this appendix there is first a description of how the raw data from the earth pressure cells was processed. Second comes a collective plot of all the earth pressure cell data against time in Figure C.1. Then there is an example of raw data from one cell put into a calculation sheet in Microsoft Excel. Next, an example of one set of calibration sheets used for each earth pressure cell is presented. Values from the calibration sheets are used as input for the pressure calculation in Excel. The calibration sheets for the rest of the cells are included in the zip-file handed in along with this thesis. In addition, a data sheet for the Glötzl earth pressure cells is included along with the instruction manual for the cells.

The raw data was processed in accordance with the instruction manual. The two main equations for converting the readings into pressures are given below.

$$\sigma_h = 100 \frac{EE_{measured} - pV}{EE_{sens}} \quad (C.1)$$

where σ_h is total earth pressure relative to atmospheric pressure in kPa, $EE_{measured}$ is the measured value in mA, pV is a calibration sheet factor taking into account pre-excitation due to welding of the blade and EE_{sens} is the mean sensitivity given in the calibration sheets.

$$u = 100 \frac{PWD_{measured} - PWD_0}{PWD_{sens}} \quad (C.2)$$

where u is the pore pressure relative to atmospheric pressure in kPa, $PWD_{measured}$ is the measured value in mA, PWD_0 is the current at atmospheric pressure given in the calibration sheets and PWD_{sens} is the mean sensitivity given in the calibration sheets.

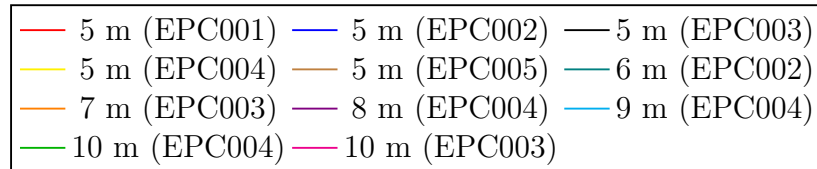
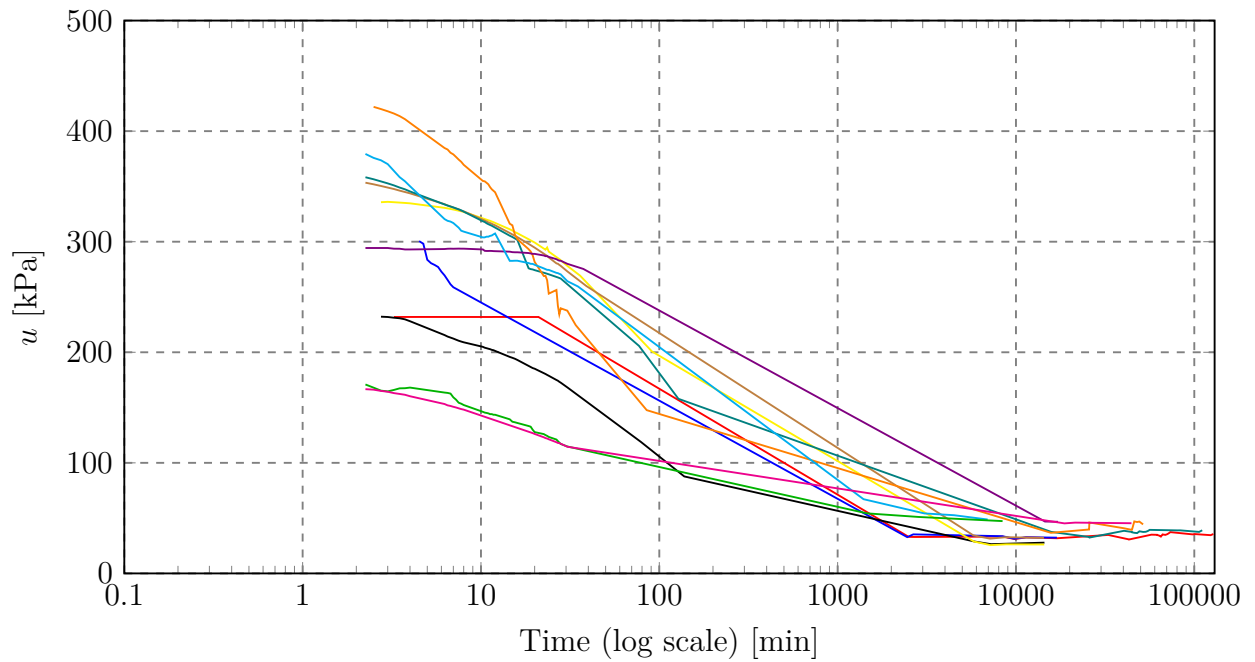
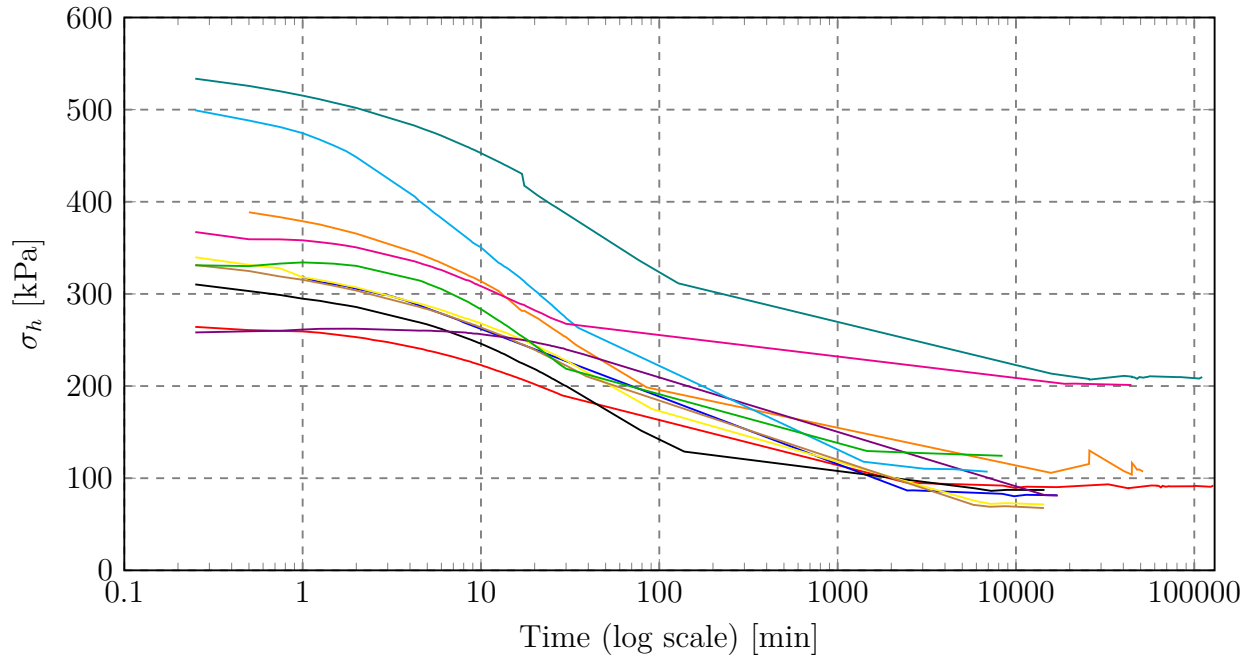


Figure C.1: Total horizontal stress and pore pressure from the earth pressure cells plotted versus logarithmic time. Stresses are relative to 100 kPa.

Site and bore hole	Flotten EPC005
Time of installation	17.02.2017 10:51:00
Depth middle of cell	5.00
Predrilling depth	4.70

Earth pressure sensor serial no.	EE24692
Mean sensitivity [mA/bar]	2.28571
Current at 0 bar [mA]	4
pV [mA]	8.6

Pore pressure sensor serial no.	PWD24691
Mean sensitivity [mA/bar]	3.2
Current at 0 bar [mA]	4

Steady pore pressure reading [kPa]	32
Steady total earth pressure reading [kPa]	68
Calculated horizontal effective stress [kPa]	36

Earth pressure

Date and time (before)	17.02.2017 10:36:00
Zero reading at surface (before) [mA]	8.505
Zero reading at surface (before) [kPa]	-4.2

Date and time (after)	27.02.2017 10:17
Zero reading at surface (after) [mA]	8.313
Zero reading at surface (after) [kPa]	-12.6

Pore pressure

Date and time (before)	17.02.2017 10:37:00
Zero reading at surface (before) [mA]	4.096
Zero reading at surface (before) [kPa]	3

Date and time (after)	27.02.2017 10:16
Zero reading at surface (after) [mA]	3.926
Zero reading at surface (after) [kPa]	-2.3

Earth pressure

Time	Time after installation	Reading [mA]	Calculated pressure [bar]	Calculated pressure [kPa]
17.02.2017 10:51:00	0.00	16.804	3.58925673	358.925673
17.02.2017 10:51:15	0.25	16.173	3.313193712	331.3193712
17.02.2017 10:51:30	0.50	16.025	3.248443591	324.8443591
17.02.2017 10:51:45	0.75	15.888	3.188505978	318.8505978
17.02.2017 10:52:00	1.00	15.807	3.153068412	315.3068412
17.02.2017 10:52:15	1.25	15.727	3.118068346	311.8068346
17.02.2017 10:52:30	1.50	15.658	3.08788079	308.788079
17.02.2017 10:52:45	1.75	15.596	3.060755739	306.0755739
17.02.2017 10:53:00	2.00	15.54	3.036255693	303.6255693
17.02.2017 10:53:15	2.25			
17.02.2017 10:53:30	2.50			
17.02.2017 10:53:45	2.75			
17.02.2017 10:54:00	3.00			
17.02.2017 10:54:15	3.25			
17.02.2017 10:54:30	3.50			
17.02.2017 10:54:45	3.75			
17.02.2017 10:55:00	4.00			
17.02.2017 10:55:15	4.25	15.164	2.871755385	287.1755385
17.02.2017 10:55:30	4.50	15.137	2.859942862	285.9942862
17.02.2017 10:55:45	4.75	15.104	2.845505335	284.5505335
17.02.2017 10:56:00	5.00	15.08	2.835005316	283.5005316
17.02.2017 10:56:15	5.25	15.051	2.822317792	282.2317792
17.02.2017 10:56:30	5.50	15.02	2.808755266	280.8755266
17.02.2017 10:56:45	5.75	14.995	2.797817746	279.7817746
17.02.2017 10:57:00	6.00	14.973	2.788192728	278.8192728
17.02.2017 10:57:15	6.25			
17.02.2017 10:57:30	6.50			
17.02.2017 10:57:45	6.75			
17.02.2017 10:58:00	7.00			
17.02.2017 10:58:15	7.25			
17.02.2017 10:58:30	7.50			
17.02.2017 10:58:45	7.75			
17.02.2017 10:59:00	8.00			
17.02.2017 10:59:15	8.25	14.758	2.694130051	269.4130051
17.02.2017 10:59:30	8.50	14.739	2.685817536	268.5817536
17.02.2017 10:59:45	8.75	14.721	2.677942521	267.7942521
17.02.2017 11:00:00	9.00	14.698	2.667880002	266.7880002
17.02.2017 11:00:15	9.25	14.686	2.662629992	266.2629992
17.02.2017 11:00:30	9.50	14.661	2.651692472	265.1692472
17.02.2017 11:00:45	9.75	14.645	2.644692459	264.4692459
17.02.2017 11:01:00	10.00	14.623	2.635067441	263.5067441
17.02.2017 11:01:15	10.25			
17.02.2017 11:01:30	10.50			
17.02.2017 11:01:45	10.75			
17.02.2017 11:02:00	11.00			
17.02.2017 11:02:15	11.25			
17.02.2017 11:02:30	11.50			
17.02.2017 11:02:45	11.75			
17.02.2017 11:03:00	12.00			
17.02.2017 11:03:30	12.50	14.458	2.562879805	256.2879805

17.02.2017 11:04:00	13.00	14.432	2.551504784	255.1504784
17.02.2017 11:04:30	13.50	14.408	2.541004764	254.1004764
17.02.2017 11:05:00	14.00	14.376	2.527004738	252.7004738
17.02.2017 11:05:30	14.50			
17.02.2017 11:06:00	15.00			
17.02.2017 11:06:30	15.50			
17.02.2017 11:07:00	16.00			
17.02.2017 11:07:30	16.50	14.229	2.462692118	246.2692118
17.02.2017 11:08:00	17.00	14.208	2.4535046	245.35046
17.02.2017 11:08:30	17.50	14.19	2.445629586	244.5629586
17.02.2017 11:09:00	18.00	14.163	2.433817063	243.3817063
17.02.2017 11:09:30	18.50			
17.02.2017 11:10:00	19.00			
17.02.2017 11:10:30	19.50			
17.02.2017 11:11:00	20.00			
17.02.2017 11:11:30	20.50	14.048	2.383504469	238.3504469
17.02.2017 11:12:00	21.00	14.019	2.370816945	237.0816945
17.02.2017 11:12:30	21.50	14.005	2.364691934	236.4691934
17.02.2017 11:13:00	22.00	13.977	2.352441911	235.2441911
17.02.2017 11:13:30	22.50			
17.02.2017 11:14:00	23.00			
17.02.2017 11:14:30	23.50			
17.02.2017 11:15:00	24.00			
17.02.2017 11:15:30	24.50	13.876	2.308254328	230.8254328
17.02.2017 11:16:00	25.00	13.861	2.301691816	230.1691816
17.02.2017 11:16:30	25.50	13.838	2.291629297	229.1629297
17.02.2017 11:17:00	26.00	13.823	2.285066785	228.5066785
17.02.2017 11:17:30	26.50			
17.02.2017 11:18:00	27.00			
17.02.2017 11:18:30	27.50			
17.02.2017 11:19:00	28.00			
17.02.2017 11:19:30	28.50	13.728	2.243504207	224.3504207
17.02.2017 11:20:00	29.00	13.713	2.236941694	223.6941694
17.02.2017 11:20:30	29.50	13.693	2.228191678	222.8191678
17.02.2017 11:21:00	30.00	13.681	2.222941668	222.2941668
17.02.2017 11:21:30	30.50			
17.02.2017 11:30:00	39.00	13.413	2.105691448	210.5691448
21.02.2017 11:04:00	5773.00	10.224	0.710501332	71.05013322
22.02.2017 10:08:00	7157.00	10.177	0.689938794	68.99387936
23.02.2017 12:48:00	8757.00	10.191	0.696063805	69.60638051
27.02.2017 10:02:00	14351.00	10.145	0.675938767	67.59387674

Pore pressure

Time	Time after installation	Reading [mA]	Calculated pressure [bar]	Calculated pressure [kPa]
17.02.2017 10:51:00	0.00			
17.02.2017 10:51:15	0.25			
17.02.2017 10:51:30	0.50			
17.02.2017 10:51:45	0.75			
17.02.2017 10:52:00	1.00			
17.02.2017 10:52:15	1.25			
17.02.2017 10:52:30	1.50			
17.02.2017 10:52:45	1.75			
17.02.2017 10:53:00	2.00			
17.02.2017 10:53:15	2.25	15.308	3.53375	353.375
17.02.2017 10:53:30	2.50	15.261	3.5190625	351.90625
17.02.2017 10:53:45	2.75	15.213	3.5040625	350.40625
17.02.2017 10:54:00	3.00	15.167	3.4896875	348.96875
17.02.2017 10:54:15	3.25	15.125	3.4765625	347.65625
17.02.2017 10:54:30	3.50	15.078	3.461875	346.1875
17.02.2017 10:54:45	3.75	15.038	3.449375	344.9375
17.02.2017 10:55:00	4.00	15	3.4375	343.75
17.02.2017 10:55:15	4.25			
17.02.2017 10:55:30	4.50			
17.02.2017 10:55:45	4.75			
17.02.2017 10:56:00	5.00			
17.02.2017 10:56:15	5.25			
17.02.2017 10:56:30	5.50			
17.02.2017 10:56:45	5.75			
17.02.2017 10:57:00	6.00			
17.02.2017 10:57:15	6.25	14.686	3.339375	333.9375
17.02.2017 10:57:30	6.50	14.648	3.3275	332.75
17.02.2017 10:57:45	6.75	14.62	3.31875	331.875
17.02.2017 10:58:00	7.00	14.588	3.30875	330.875
17.02.2017 10:58:15	7.25	14.559	3.2996875	329.96875
17.02.2017 10:58:30	7.50	14.535	3.2921875	329.21875
17.02.2017 10:58:45	7.75	14.492	3.27875	327.875
17.02.2017 10:59:00	8.00	14.48	3.275	327.5
17.02.2017 10:59:15	8.25			
17.02.2017 10:59:30	8.50			
17.02.2017 10:59:45	8.75			
17.02.2017 11:00:00	9.00			
17.02.2017 11:00:15	9.25			
17.02.2017 11:00:30	9.50			
17.02.2017 11:00:45	9.75			
17.02.2017 11:01:00	10.00			
17.02.2017 11:01:15	10.25			
17.02.2017 11:01:30	10.50	14.213	3.1915625	319.15625
17.02.2017 11:01:45	10.75	14.188	3.18375	318.375
17.02.2017 11:02:00	11.00	14.159	3.1746875	317.46875
17.02.2017 11:02:15	11.25	14.141	3.1690625	316.90625
17.02.2017 11:02:30	11.50	14.119	3.1621875	316.21875
17.02.2017 11:02:45	11.75	14.095	3.1546875	315.46875
17.02.2017 11:03:00	12.00	14.075	3.1484375	314.84375
17.02.2017 11:03:30	12.50			

17.02.2017 11:04:00	13.00			
17.02.2017 11:04:30	13.50			
17.02.2017 11:05:00	14.00			
17.02.2017 11:05:30	14.50	13.852	3.07875	307.875
17.02.2017 11:06:00	15.00	13.809	3.0653125	306.53125
17.02.2017 11:06:30	15.50	13.771	3.0534375	305.34375
17.02.2017 11:07:00	16.00	13.732	3.04125	304.125
17.02.2017 11:07:30	16.50			
17.02.2017 11:08:00	17.00			
17.02.2017 11:08:30	17.50			
17.02.2017 11:09:00	18.00			
17.02.2017 11:09:30	18.50	13.537	2.9803125	298.03125
17.02.2017 11:10:00	19.00	13.501	2.9690625	296.90625
17.02.2017 11:10:30	19.50	13.464	2.9575	295.75
17.02.2017 11:11:00	20.00	13.429	2.9465625	294.65625
17.02.2017 11:11:30	20.50			
17.02.2017 11:12:00	21.00			
17.02.2017 11:12:30	21.50			
17.02.2017 11:13:00	22.00			
17.02.2017 11:13:30	22.50	13.254	2.891875	289.1875
17.02.2017 11:14:00	23.00	13.221	2.8815625	288.15625
17.02.2017 11:14:30	23.50	13.189	2.8715625	287.15625
17.02.2017 11:15:00	24.00	13.145	2.8578125	285.78125
17.02.2017 11:15:30	24.50			
17.02.2017 11:16:00	25.00			
17.02.2017 11:16:30	25.50			
17.02.2017 11:17:00	26.00			
17.02.2017 11:17:30	26.50	12.973	2.8040625	280.40625
17.02.2017 11:18:00	27.00	12.961	2.8003125	280.03125
17.02.2017 11:18:30	27.50	12.929	2.7903125	279.03125
17.02.2017 11:19:00	28.00	12.901	2.7815625	278.15625
17.02.2017 11:19:30	28.50			
17.02.2017 11:20:00	29.00			
17.02.2017 11:20:30	29.50			
17.02.2017 11:21:00	30.00			
17.02.2017 11:21:30	30.50	12.741	2.7315625	273.15625
17.02.2017 11:29:30	38.50	12.317	2.5990625	259.90625
21.02.2017 11:05:00	5774.00	5.1	0.34375	34.375
22.02.2017 10:09:00	7158.00	5.006	0.314375	31.4375
23.02.2017 12:48:00	8757.00	5.048	0.3275	32.75
27.02.2017 10:02:00	14351.00	5.028	0.32125	32.125

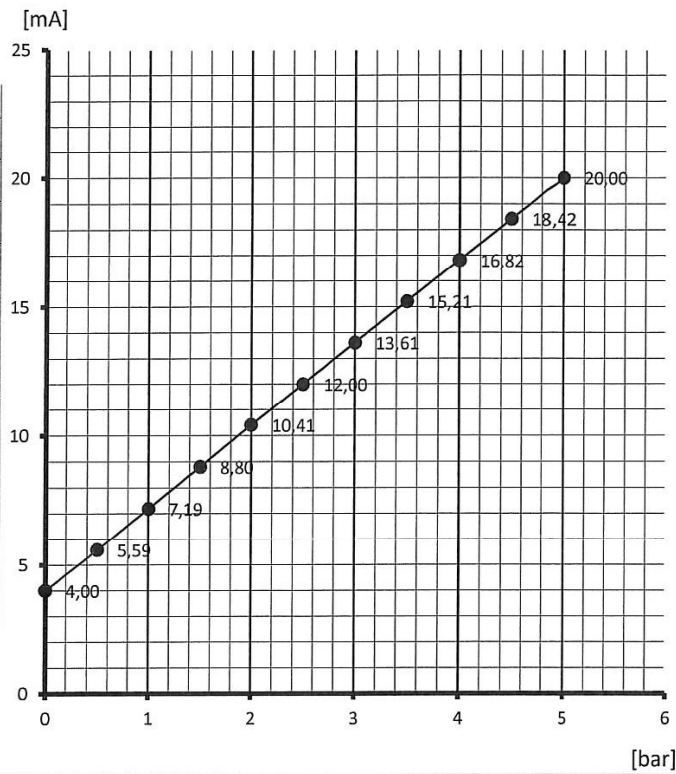
Calibration Data Sheet Advanced Solutions **GLÖTZL**

EPE/P AI 7/14 K5

Name of measuring point: **PWD**

Order No.: 26537/3	Cell / Transducer for: Einpressgeber Porenwasserdruck			Responsible: Stab
Serial No.: 16 24693	Client / Project: Norwegian Geotechnical Institute			Date: 27.09.2016
Surrounding parameter: 23°C / 1000 mbar	Measuring range: 0-5 bar	Transducer: PA-8-10 / 30	Cable / Length [m]: PE 2(4)x0,5 / 20	Tested: <i>[Signature]</i>
Linearity: < ± 0,5 %v.E.	Testing equipment: DPI 610 / FMG 2 K-T		Temperature coefficient: <0,5 % / °C v.E.	Temperature range: +5 ... +60 °C
Supply: 15 - 30 A	Output signal: 4 - 20 mA	Load:	Mean sensitivity: 3,2 mA/bar	Overload security: 20%
Remarks:	Initialization time of the sensor is 6 seconds. Please take over the measuring value only after init. has been finished.			

Calibration:		Measured value in
Basis in	[bar]	[mA]
	0,00	4,00
	0,50	5,59
	1,00	7,19
	1,50	8,80
	2,00	10,41
	2,50	12,00
	3,00	13,61
	3,50	15,21
	4,00	16,82
	4,50	18,42
	5,00	20,00
Calibration factor:		3,2 mA/bar
Calibration factor:		



Parameters of measuring equipment:				
Offset:	Factor:	Zero:	A-time:	pV-value:

Grouping plan:								
Temp.- MV	Resistivity	Pin con-figuration	Connection line		Main cable	Terminator	Measuring device	
			Color	Number			Connection	Channel
		Supply +	red					
		Supply -	blue					
		Screen	transp.					

Calibration Data Sheet

Advanced Solutions

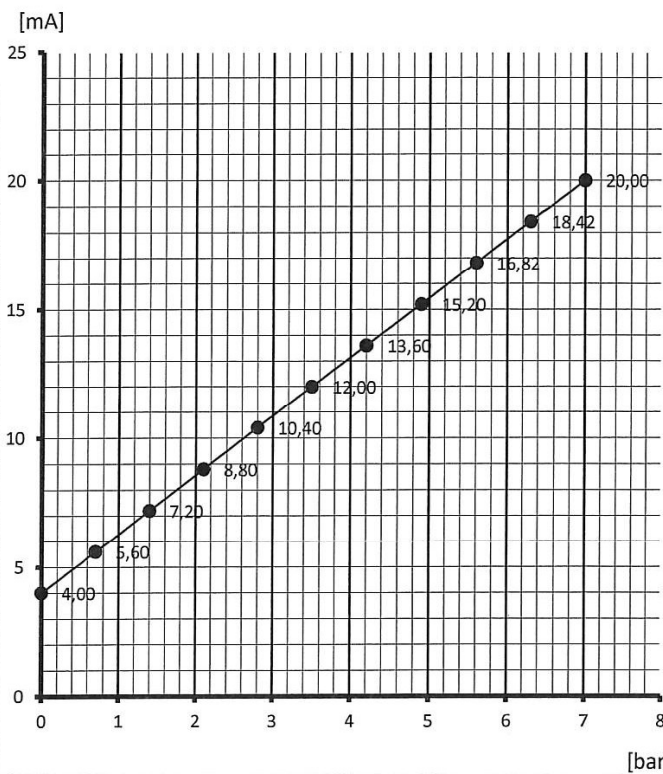
EPE/P AI 7/14 K5

Name of measuring point: **EE**

Order No.: 26537/3	Cell / Transducer for: Einpressgeber Erddruck			Responsible: Stab
Serial No.: 16 24694	Client / Project: Norwegian Geotechnical Institute			Date: 28.09.2016
Surrounding parameter: 23°C / 1000 mbar	Measuring range: 0-7 bar	Transducer: PA-8-10 / 98	Cable / Length [m]: PE 2(4)x0,5 / 20	Tested:
Linearity: < ± 0,5 %v.E.	Testing equipment: DPI 610 / FMG 2 K-T		Temperature coefficient: <0,5 % / °C v.E.	Temperature range: +5 ... +60 °C
Supply: 15 - 30 A	Output signal: 4 - 20 mA	Load:	Mean sensitivity: 2,28571 mA/bar	Overload security: 20%
Remarks: Initialization time of the sensor is 6 seconds. Please take over the measuring value only after init. has been finished.				

Calibration:

Basis in [bar]	Measured value in [mA]
0,00	4,00
0,70	5,60
1,40	7,20
2,10	8,80
2,80	10,40
3,50	12,00
4,20	13,60
4,90	15,20
5,60	16,82
6,30	18,42
7,00	20,00
Calibration factor: 2,28571 mA/bar	
Calibration factor:	



Parameters of measuring equipment:

Offset:	Factor:	Zero:	A-time:	pV-value:	mA 8,79
---------	---------	-------	---------	-----------	------------

Grouping plan:

Temp.- MV	Resistivity	Pin con-figuration	Connection line		Main cable Grouping	Terminator	Measuring device	
			Color	Number			Connection	Channel
		Supply +	red					
		Supply -	blue					
		Screen	transp.					

GLÖTZL Baumeßtechnik

PRESS-IN PRESSURE CELL for EARTH PRESSURE, combined with POREWATER PRESSURE

Type EPE, EPE/P

Art. No.: 68.60/68.70

With the earth pressure cell to press in, also in combination with a water or porewater pressure cell for effective stress, it is possible to carry out subsequent measurements at or in constructions or in possibly undisturbed underground. The robust model enables an application of pressing powers of up to 2 tons. The cells are available in two pressure pad dimensions, material stainless steel and with load ranges of up to 50 bars. When loading the pressure pad, the arising hydraulic pressure is transferred to the diaphragm

of the electric transducer, and converted into a stress proportional to the loading.

Some application fields:

- Subsequent installation in or at constructions
- Investigation and control of landfills
- Installation behind supporting walls, e.g. port installations
- Earth pressure and porewater pressure in dams
- Pressing into soft, binding soils for control of consolidation at backfills

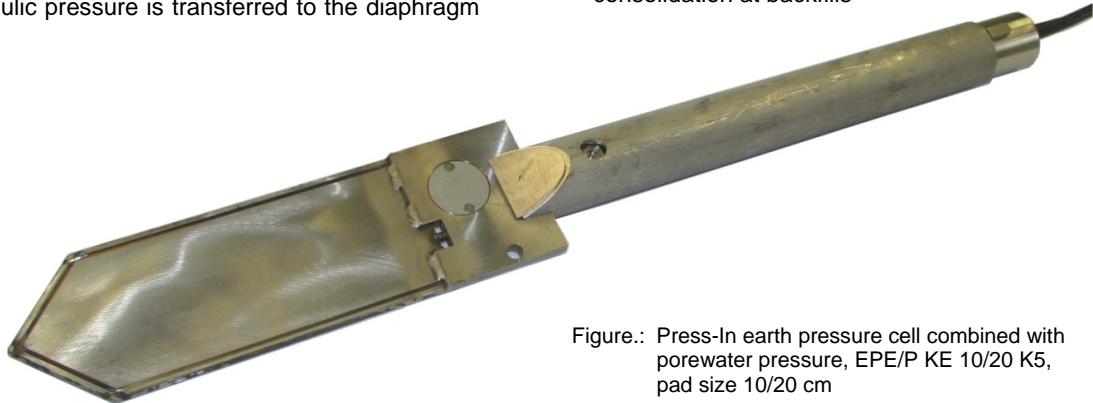


Figure.: Press-In earth pressure cell combined with porewater pressure, EPE/P KE 10/20 K5, pad size 10/20 cm

Models:

EPE Press-In Earth pressure cell

EPE/P Press-In Earth pressure cell combined with porewater pressure

Types:

KE Pressure sensor piezoelectric, 4-conductor system

Technical data:

Supply	constant current 1 mA	Operating temperature range	+5 up to +80 °C
Supply optional	4 mA or 10V _{DC}	Storage temperature range (dry)	-40 up to +100 °C
Output signal	0 – 250 mV	Long-term drift temperature dependent	(at 0 °C up to 50 °C), typ. 0.25 mV
Overload protection (1–50 bars)	50% f.s.	Resonance	> 30 KHz
Linearity incl. hysteresis	< 0.5% f.s.	Meas. frequency	1 KHz
Linearity incl. hysteresis optional	< 0.1% f.s.		
Thermal zero drift	0.025 mV/K		

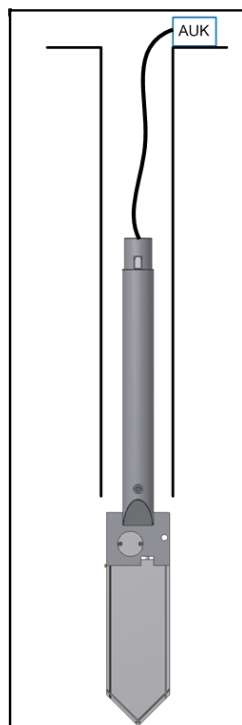
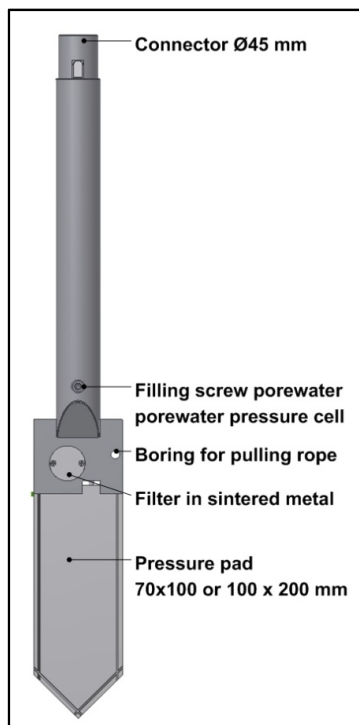
KO Pressure sensor piezoelectric as above, but with installed amplifier and optional temperature sensor

Technical data:

Supply	15 up to 30 V
Output signal	4 – 20 mA, 2-conductor system
Overload protection	1 – 50 bars, 50% f.s.
Linearity incl. hysteresis	< 0.5% f.s. (optional 0.1% f.s.)
Temperature coefficient	< 0.01%/ °C f.s.
Burden	(U _s -9V) : 20 mA
Operating temperature range	-15 up to +70 °C
Storage temperature range	-15 up to +125 °C
Initialization time after switch-on	6 seconds

Optional with temperature sensor AD 590, output signal 1µA/K

VW Vibrating wire sensor, operating frequency from 2000 cps up to 3300 cps
Thermistor type BR55, T₂₅ = 3000 Ohm



Installation in borings

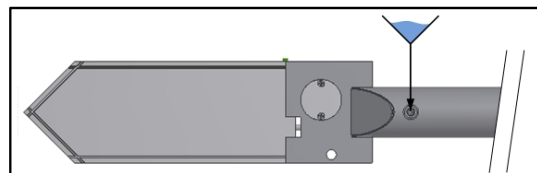
Normally, a boring is done till approx. 0.5 m before the installation point of the cell. From this position, the cell is injected into the surrounding material by means of rods. In soft soils, also an injection is possible without rough-boring.

Injection procedure is done with rods. For this, a thread G 1 ½" or optionally a connection pivot with diameter 45 mm is fitted at the cell.

After installation, the borehole is backfilled and sealed according to the respective requirements.

Filling of pressure filter of porewater cell

Remove filling screw, screw in water bottle and press the water in. After pressing-in procedure, close again the filling connection with the screw.



Pressure pad size:

70 x 140 mm, 100 x 200 mm, other sizes available on request
720 mm 780 mm total length

Filling:

K Pressure pad with oil filling for the material surrounding the cell, E-modulus ≤ 10.000 bars

Measuring ranges:

1 bars = 100 kPa

Pressure sensor piezoelectric (KE/KO): 0 – 2, 0 – 5, 0 – 10, 0 – 50 bars

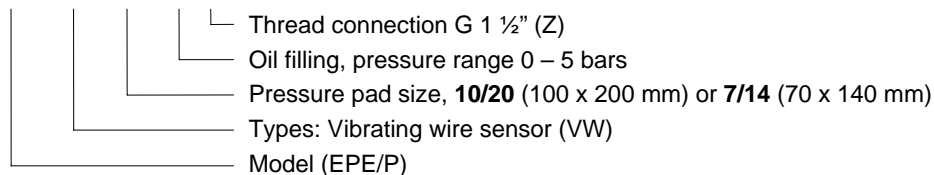
Vibrating wire sensor (VW): 1.7, 3.5, 7, 10, 20, 50 bars

Connection

R = rods connection G 1 ½" Z = thread connection Ø 45 mm

Type key (example for ordering):

EPE/P VW 10/20 K5 Z



Registration:

- Battery-operated readout units
- Manually operated change-over manifolds
- Intermediate amplifier for remote control
- Automatic measuring and recording devices with data carrier resp. memory

Subject to technical alterations

GLÖTZL Gesellschaft für Baumeßtechnik mbH · Forlenweg 11 · 76287 Rheinstetten · Germany
☎ +49 (0)721 51 66 - 0 · 📠 +49 (0)721 51 66 - 30 · 🌐 <http://www.gloetzl.com> · ✉ info@gloetzl.com

Instruction manual: Glötzl pressure cells for horizontal earth pressure

The pressure cells contains two sensors; pore water pressure and earth pressure as shown in the image below. The instrument is inserted vertically using bore rods so that the large sides of the pressure pad are aligned with the gravity vector. Measuring the porewater pressure at the same time allows for compensation of the water pressure and calculating only the horizontal earth pressure.

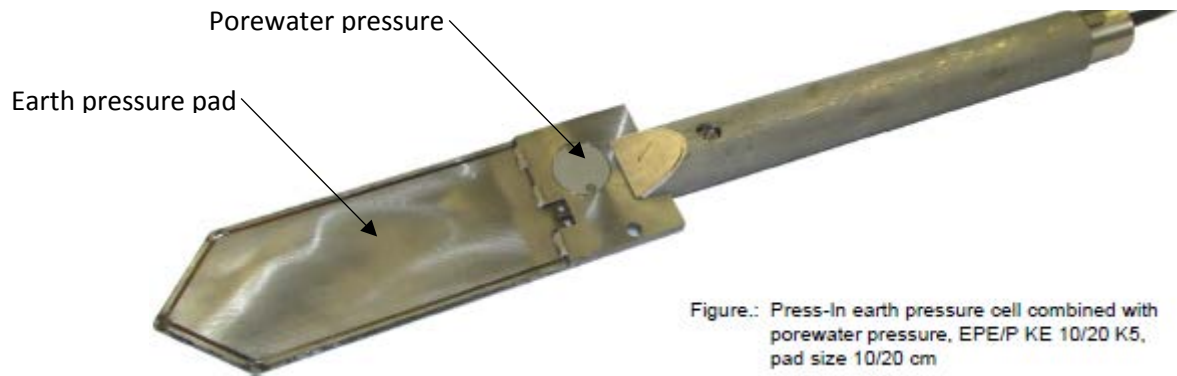
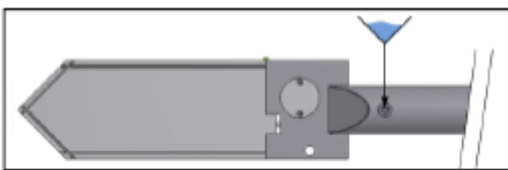


Figure.: Press-In earth pressure cell combined with porewater pressure, EPE/P KE 10/20 K5, pad size 10/20 cm

Consult the calibration sheets to find a pressure cell with the correct measurement range (e.g. 0-2 bar, 0-5 bar or 0-10 bar). The calibration sheets contains parameters necessary for converting raw data to engineering values, so print a copy to bring with you. The serial number of each sensor can be found on a sticker on the pressure pad, or on a sticker near the end of the cables.

Preparations before usage

Make sure that the space behind the porewater pressure filter is filled with water. Remove the filling screw (see image below) and fill as described in the data sheet and water filling instructions. Tap water may contain oily or calcium components that can block the filter. Use either water provided by Glötzl or Milli-Q water from the NGI chemistry lab. If the sensor is to be used in below zero temperatures, pure glycol may be added to the water to avoid freezing. The pressure cells are delivered from Glötzl with a pivot shaft connection without threads. The NGI workshop has added a 5/4" threaded bore rod connection. The data cables have to pass through the bore rods all the way to the surface.



Measurements

Data read out is done with a handheld measurement device (HMG), see operation manual. The earth pressure and pore water pressure is read from different data cables, locate the sticker with serial number near the end of the cable to identify the sensor. Use the grey wire clamps to connect the HMG to the sensor you want to read. Connect the red wire with the red wire from the sensor, and the blue wire with the blue wire from the sensor. The other wires (green, white) can stay disconnected.

After connecting the HMG, one push on the button will start the data read out from channel 1. Channel 2 is for temperature read out, and is not in use on the pressure cells. Normal operation is that the HMG will power down after a few minutes. If you want to avoid this, a long push on the button will enter 'always on' mode.



The raw value range of both earth and pore water pressure sensors is 4-20mA, with a corresponding pressure value in bar, see the calibration sheet for the particular sensor.

Insertion

The sensors should not be exposed to pressures exceeding 150% of full range. For insertion into hard soils or at great depths, this could be an issue. Make sure to read the pressure during insertion and use a sensor with adequate range.

Raw data conversion example

Consult the calibration sheet. The **pore water cell** with serial no. 1624703 has a calibration factor of 3.2 mA/bar. Air pressure at the time of insertion is 1024.3 hpa = 1.0243 bar. The sensor measurement in air is 4.02 mA = $(4.02-4.0)\text{mA}/3.2\text{mA}/\text{bar} = 0.0625$ bar. Sensor measurement after insertion is 15.6mA = $(15.6-4)\text{mA}/3.2\text{mA}/\text{bar} = 3.625$ bar. 1.0 bar is 10.2 meter water level. If desired, this can then be compensated for air pressure changes if the air pressure is measured simultaneously with another sensor.

The earth pressure cells have a pre-excitation from the welding of the sensor plates. This is quantified by the pV value in the calibration sheet. For the **earth pressure cell** with serial no. 1624702, we have pV = 8.72mA. The calibration factor is 2.28571mA/bar. The zero-point of this cell is $(8.72-3.98)\text{mA}/2.28571\text{mA} \approx 2.074\text{bar}$, which means that the zero point of the measuring value is 2.074bar.

Appendix D

Dilatometer

This appendix contains selected data material from the dilatometer test performed at Flotten test site on 14 February 2017. The location and coordinates of the bore hole used for the dilatometer test is found in Appendix A.

Figure D.1 presents the key parameters I_D , K_D as well as E_D with depth. An estimate of OCR with depth, based on Equation 2.12 is also included. Please note that further details regarding this test is found in Ozkul and L'Heureux (2017).

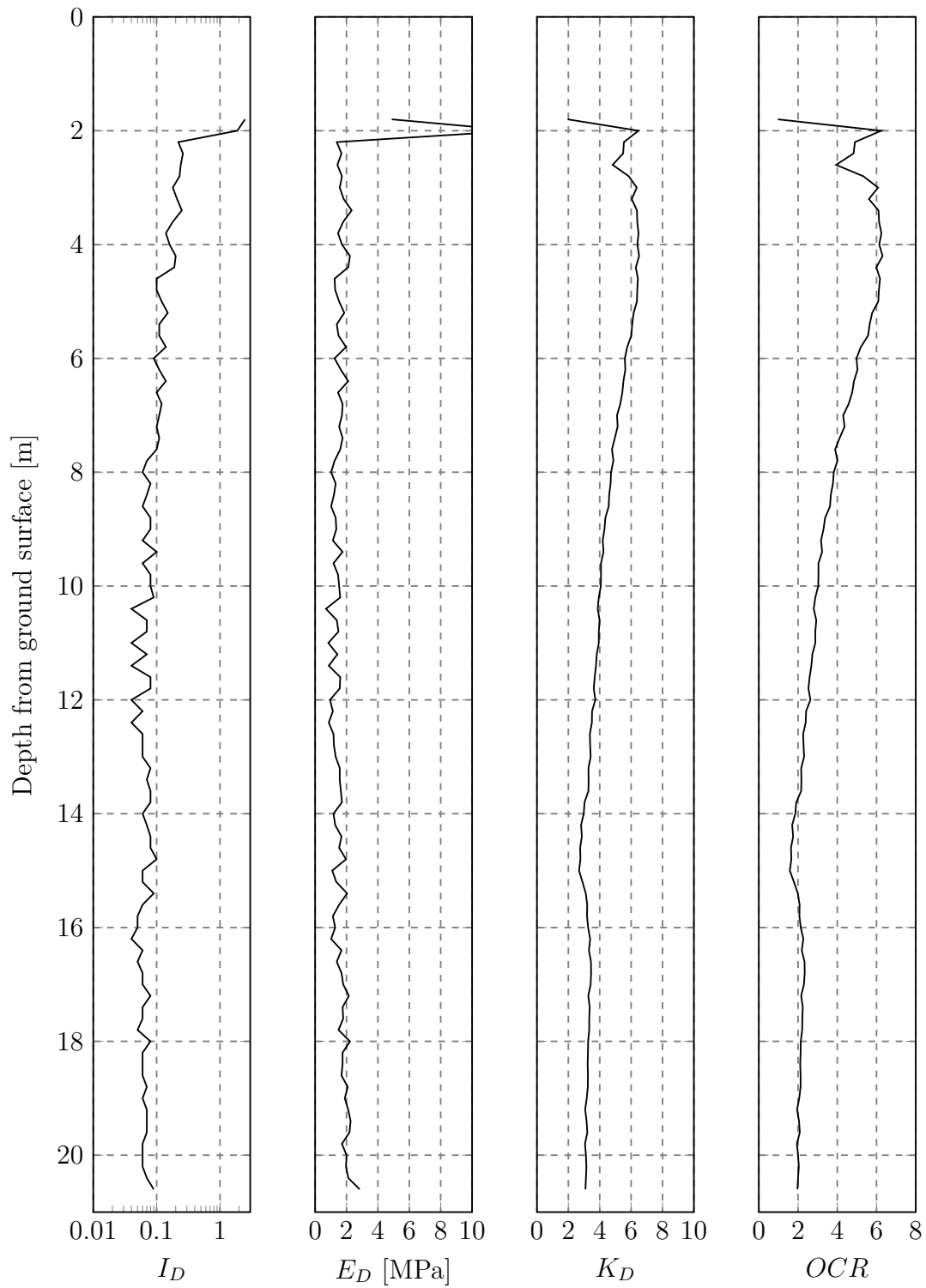


Figure D.1: Presentation of key parameters from dilatometer test at Flotten.

Appendix E

Field Vane

This appendix begins with Table E.1 which is a tabular view of the calculation method in section 2.4.8. Table E.2 shows which triaxial tests have been used as input for the calculations in Table E.1. Note the triaxial test used as input at 8.4 m. This deviation was addressed in section 6.2.5. Figure E.1 shows the results from the field vane tests performed at Flotten. The relative location of the bore hole used for the field vane testing is presented in Appendix A.

The values of σ'_{v0} in Table E.1 are the best estimates of the overburden pressure, as presented in sections 5.2.1.4 and 6.2.2.

Table E.1: Table for calculation of K'_0 .

Depth [m]	s_{uv} [kPa]	s'_{uv} [kPa]	σ'_{v0} [kPa]	σ'_{3f} [kPa]	K'_0 (Equation 2.14) [-]
8.4	12	1.5	108	31	0.38
9.4	14	1.1	125	32	0.36
10.4	15	0.8	140	60	0.53

Table E.2: Triaxial tests used as input for field vane calculations of K'_0 . The order is the same as in Table E.1.

Depth [m]	Test id.	Consolidation σ'_{v0} [kPa]	Consolidation K'_0 [-]	Figure number
9.34	CAUc-0934	93	0.74	I.10
9.40	KPG-CAUc-0940	92	0.7	I.11
10.56	CAUc-1056	152	0.79	I.15

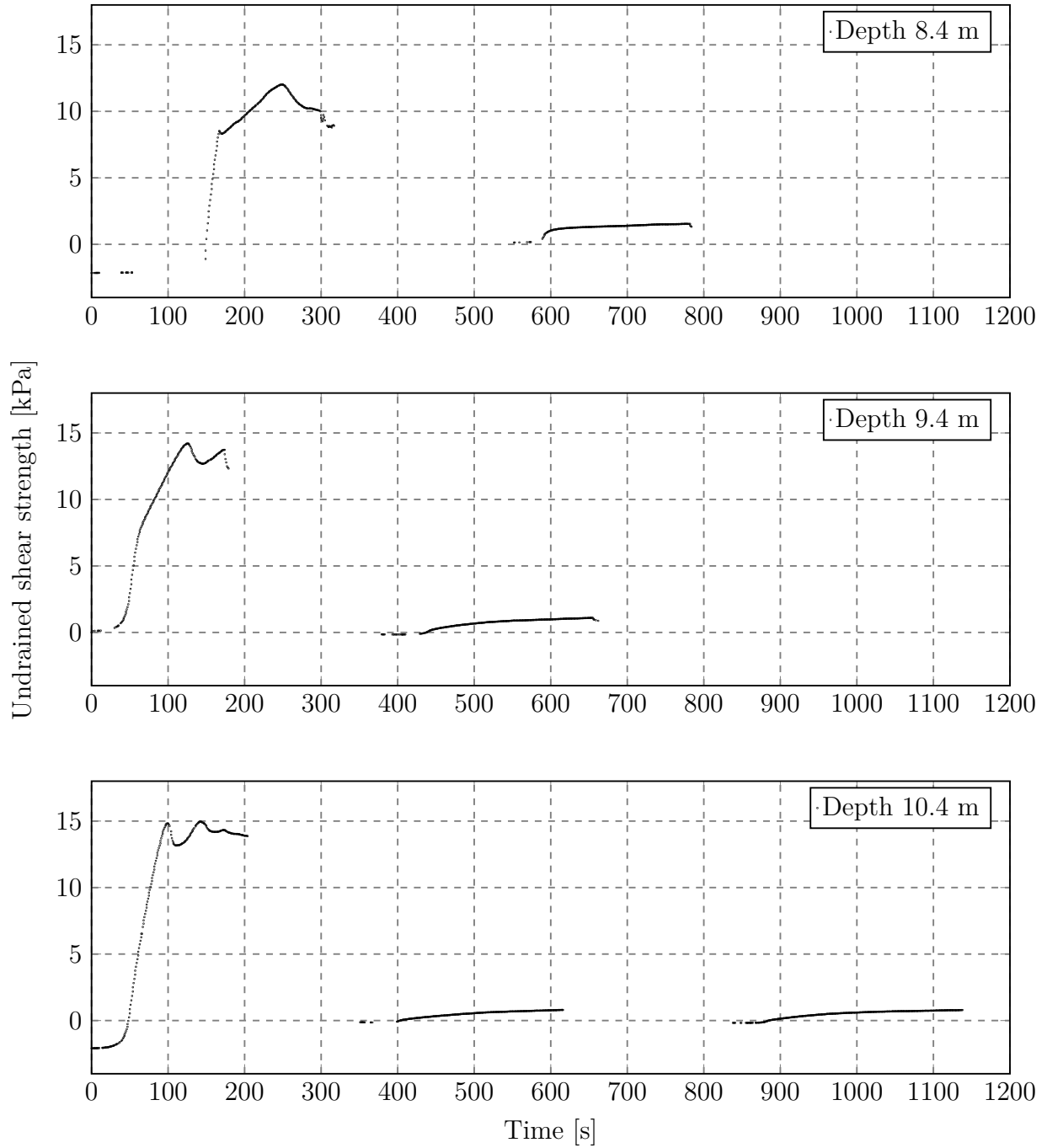


Figure E.1: Undrained shear strength with time from field vane measurements.

Appendix F

Index Properties

This appendix contains the results of index testing performed in the Geotechnical laboratories at NTNU during the spring semester of 2017. 54 mm samples from depths between 2 and 11 m have been tested. The majority of index data has been determined from samples retrieved from borehole 54MM_KPG, see borehole location in Appendix A. Please note that as mentioned in the acknowledgments, the testing has been conducted by both the authors as well as fellow master student Konjit Paulos Gella.

An overview of key index parameters is presented in Figure F.1. The first plot from the left shows the Atterberg limits and the in situ water content. The lower whisker indicates the plastic limit, w_P , whilst the upper whisker indicates the liquid limit, w_L . Next, the second plot indicates the unit weight, as determined by the use of a small ring. The third plot indicates both the intact and remoulded undrained shear strength determined through the falling cone test. The final plot illustrates the sensitivity, S_t calculated based on the falling cone measurements. A vertical line indicates $S_t = 30$.

Table F.1 gives the density and unit weight determined from cylinder and small ring. Table F.2 shows the same for oedometer samples. Last, Table F.3 shows the particle density and particle unit weight.

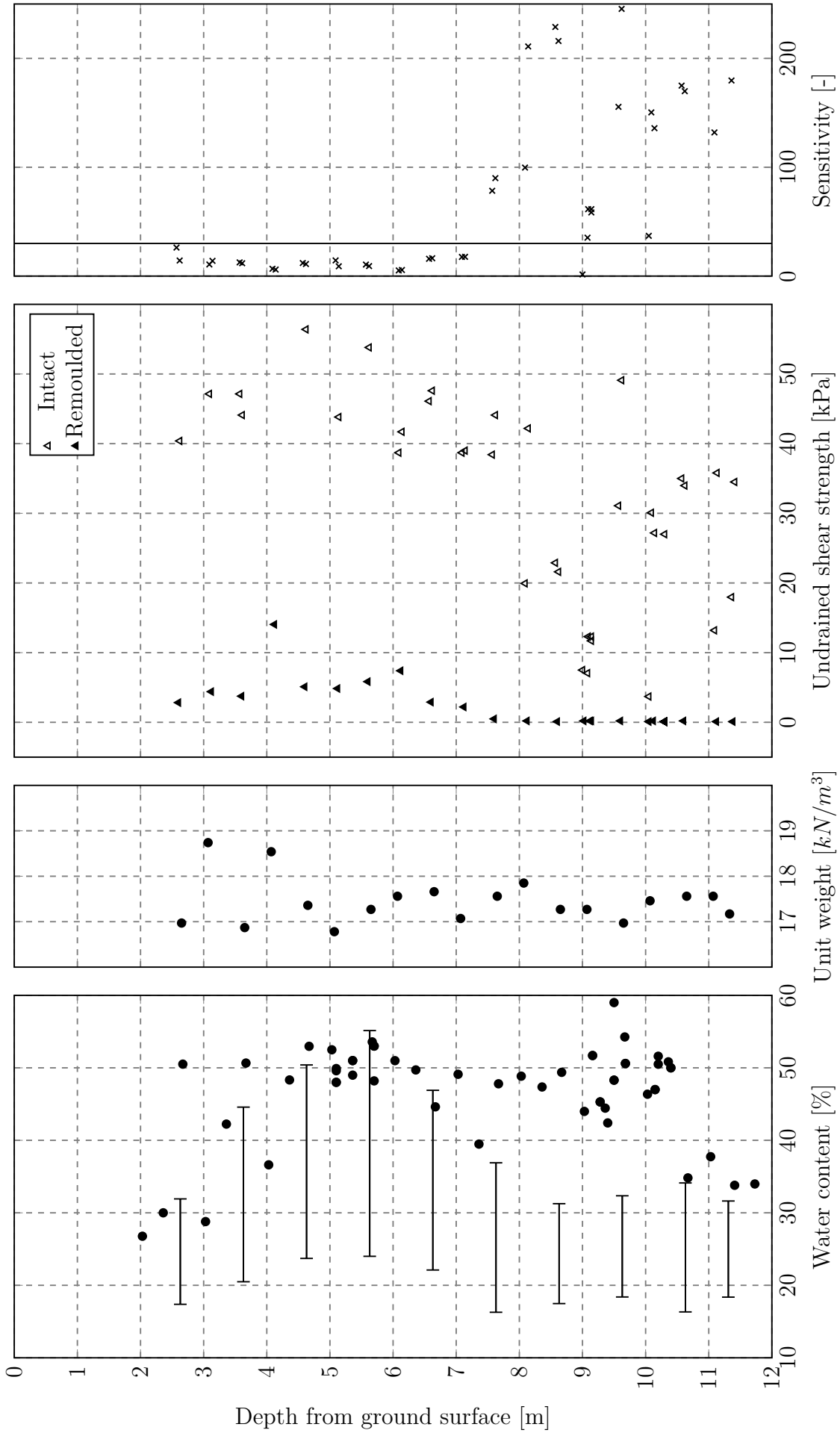


Figure F.1: Overview of key index parameters for the Flotten clay. Unit weight based on small ring measurements.

Table F.1: Results of cylinder and small ring density measurements with depth. $g = 9.81 \text{ m/s}^2$ is assumed.

Cylinder depth [m]	Cylinder		Small ring			
	Density [g/cm^3]	Unit weight [kN/m^3]	Density [g/cm^3]	Unit weight [kN/m^3]	Bottom	
					Density [g/cm^3]	Unit weight [kN/m^3]
2-2.8	1.96	19.2	-	-	1.73	17.0
3-3.8	1.92	18.8	1.91	18.7	1.72	16.9
4-4.8	1.86	18.2	1.89	18.5	1.77	17.4
5-5.8	1.81	17.8	1.71	16.8	1.76	17.3
6-6.8	1.81	17.8	1.79	17.6	1.80	17.7
7-7.8	1.85	18.2	1.74	17.1	1.79	17.6
8-8.8	1.83	18.0	1.82	17.9	1.76	17.3
9-9.8	1.83	18.0	1.76	17.3	1.73	17.0
10-10.8	1.86	18.2	1.78	17.5	1.79	17.6
11-11.8	1.88	18.4	1.79	17.6	1.75	17.2

Table F.2: Results of oedometer ring density measurements with depth. $g = 9.81 \text{ m/s}^2$ is assumed.

Depth [m]	Density [g/cm^3]	Unit weight [kN/m^3]
5.10	1.76	17.2
5.10	1.75	17.2
5.50	1.76	17.3
5.50	1.76	17.2
5.70	1.76	17.3
5.70	1.77	17.3
9.40	1.86	18.2
9.50	1.73	17.0
10.20	1.80	17.6
10.20	1.79	17.5
10.40	1.77	17.4

Table F.3: Results of particle density measurements with depth.

Cylinder depth [m]	Density			
	Top		Bottom	
	Density [g/cm ³]	Unit weight [kN/m ³]	Density [g/cm ³]	Unit weight [kN/m ³]
2-2.8	1.75	17.6	2.85	28.0
3-3.8	2.78	27.3	2.82	27.7
4-4.8	2.84	27.9	2.85	28.0
5-5.8	2.82	27.7	2.82	27.2
6-6.8	2.85	28.0	2.86	28.1
7-7.8	2.83	27.8	2.83	27.8
8-8.8	2.84	27.9	2.85	28.0
9-9.8	2.83	27.8	2.85	28.0
10-10.8	2.85	28.0	2.86	28.1
11-11.8	2.84	27.9	2.84	27.9

Appendix G

Oedometer Testing

This appendix contains the test results from a total of 17 oedometer tests. Please note that as mentioned in the acknowledgment, the testing has been conducted by both the authors as well as fellow master student Konjit Paulos Gella. One test by NTNU engineer Espen Andersen is also included. The operator of each test will be stated explicitly in the consequent plots. In addition, a detailed description of the data processing conducted on the data material from each test is presented.

Specimens tested by the authors, from depths between five and six meters, originates from the borehole 54MM_1, whilst the remaining specimens tested by the authors originates from the borehole 54MM_K0. All specimens tested by Gella were sampled from the borehole 54MM_KPG. The specimen tested by Andersen was retrieved from 54MM_1. See also the map of boreholes in Figure A.3.

The oedometer test equipment will log key information like deformation, vertical stress and pore pressure at the base of the oedometer with a given time interval. For all testing presented, data was registered every 5th second. Further processing of the resulting oedometer text file was conducted in Microsoft Excel. The same spreadsheet with formulas for calculating key parameters was used for every test. A selection of the most important formulas is given below. As a CRS test procedure with a logging interval of five seconds results in a very large amount of data points, a running average procedure containing 200 data points was used to smooth out the scatter in between individual data points. Next, every 20th data point is included in the resulting plots due to the initially very large amount of data points. This is believed to have no visible effect on the resulting plots.

First of all, the strain was calculated using Equation G.1

$$\varepsilon_a = \frac{\delta}{h_0} \quad (\text{G.1})$$

where δ is the deformation and $h_0 = 20$ mm is the original specimen height.

An approximate average effective stress σ'_v over the sample was calculated using Equa-

tion G.2

$$\sigma'_v = \sigma_v - \frac{2}{3}u_b \quad (\text{G.2})$$

where σ is the vertical stress and u_b is the base pore pressure. Both measured by the oedometer equipment.

For the ensuing plots, the modulus M , defined in Equation G.3 was calculated based on the difference between two consecutive data points using Equation G.4.

$$M = \frac{d\sigma'_v}{d\varepsilon} \quad (\text{G.3})$$

$$M = \frac{\sigma_{vi} - \sigma_{vi-1}}{\varepsilon_i - \varepsilon_{i-1}} \quad (\text{G.4})$$

Finally, the coefficient of consolidation, c_v was calculated using Equation G.5 and G.6.

$$\frac{d\sigma'}{dt} = \sigma_{vi} - \sigma_{vi-1} \quad (\text{G.5})$$

$$c_v = \frac{d\sigma' [h_0(1 - \varepsilon)]^2}{dt \quad 2u_b} \quad (\text{G.6})$$

As the main goal with the oedometer testing was the determination of the preconsolidation and hence the OCR at Flotten, no further evaluation of drainage properties through the coefficient of consolidation, c_v , or settlements properties through the modulus number, M , has been conducted. These parameters are however included for completeness.

On each plot, the depth as well as sampling, opening and testing dates are given. The strain rate of the test is also presented. For most of the tests conducted by the authors, assumptions and measurements used to calculate an initial evaluation of sample quality through the $\Delta e/e_0$ -relationship are also presented. Please note that for these tests, the presented value of γ is calculated from the weight of the oedometer specimen before testing. They may therefore deviate from the average value of $\gamma = 17.5 \text{ kN/m}^3$ used in calculating the overburden pressure.

For the tests by Gella, the oedometer specimens were not weighed before or after the tests. Consequently, the information presented regarding water content and density was taken from adjacent index test data, performed as close to the oedometer samples as possible. See also Appendix F for information about the index data. As described in section 4.2 the $\Delta e/e_0$ -relationship has not been evaluated for the tests by Gella.

Please note that the test CRS-0940-1 was terminated prematurely at about 360 kPa, due to a required test equipment relocation. Also note that the short-lasting peak indicated in the plots for the CRS-0950 oedometer test was most likely caused by a test

equipment malfunction.

For the rest of this appendix, collective plots comparing all oedometer tests are presented first. Test results with specimens from depth between 4 to 8 m are presented in Figure G.1 and test results from depth 9 to 11 m are presented in Figure G.2. In the subsequent Figures G.3 to G.19, a more detailed presentation of each oedometer test is given.

**Collection plot
Flotten, Trondheim
54 mm sample**

Depth	4.5 m - 7.5 m	γ	-	p'_c	-
Sampling date	25.01.17 - 23.03.17	u	-	OCR	-
Opening of sample	02.02.17 - 03.04.17	σ'_{v0}	-		
Testing date	02.02.17 - 20.04.17	w	-		
Strain rate	1 % /hr	ε_{a0}	-		
Operator	CSO & KPG	$\Delta e/e_0$	-		

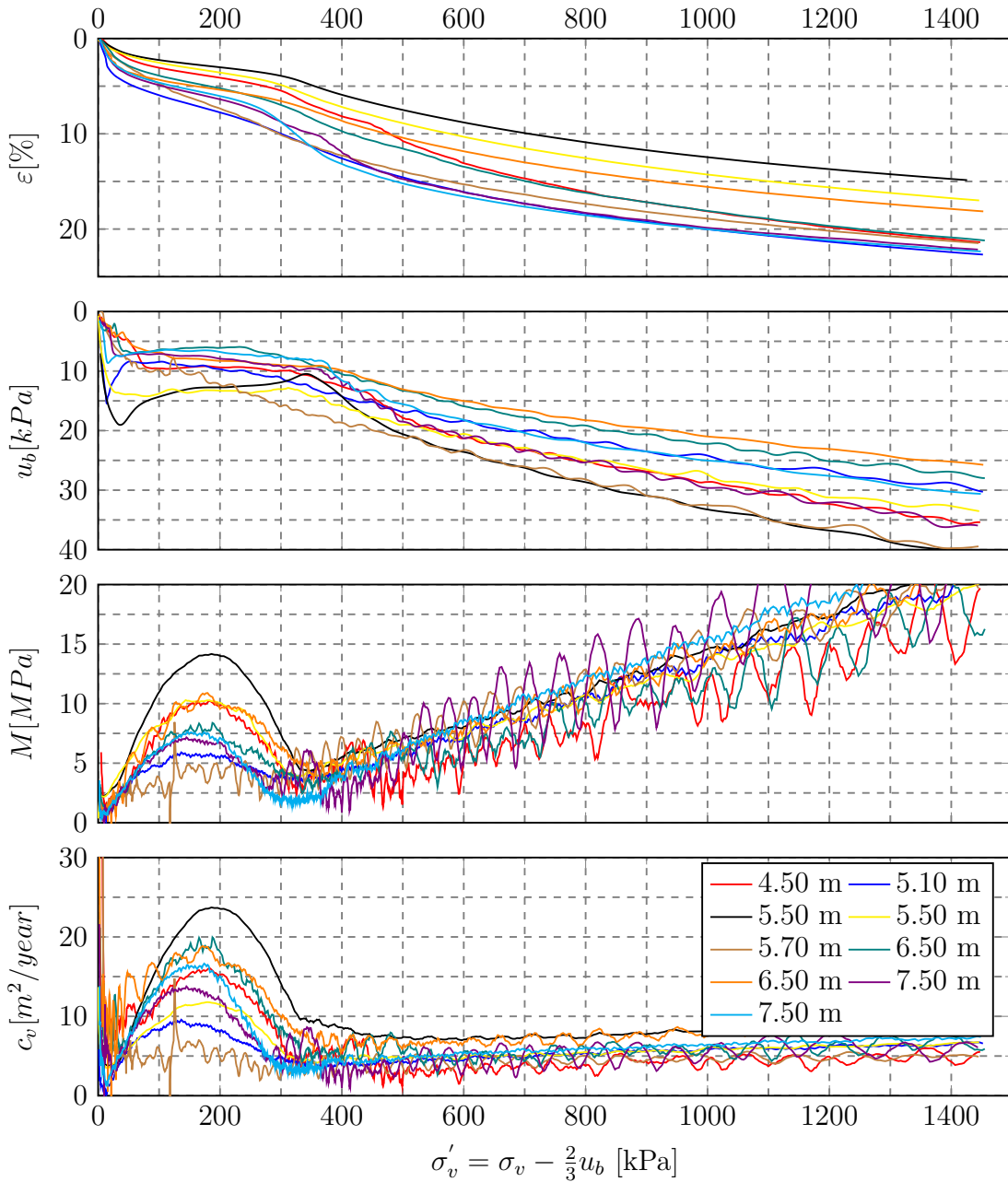


Figure G.1: Presentation of CRS-results from depths 4 to 8 m.

Collection plot
Flotten, Trondheim
54 mm sample

Depth	9.4 m - 10.6 m	γ	-	p'_c	-
Sampling date	25.01.17 - 23.02.17	u	-	OCR	-
Opening of sample	30.01.17 - 13.03.17	σ'_{v0}	-		
Testing date	30.01.17 - 29.03.17	w	-		
Strain rate	1 % - 0.5 % /hr	ε_{a0}	-		
Operator	CSO & EA	$\Delta e/e_0$	-		

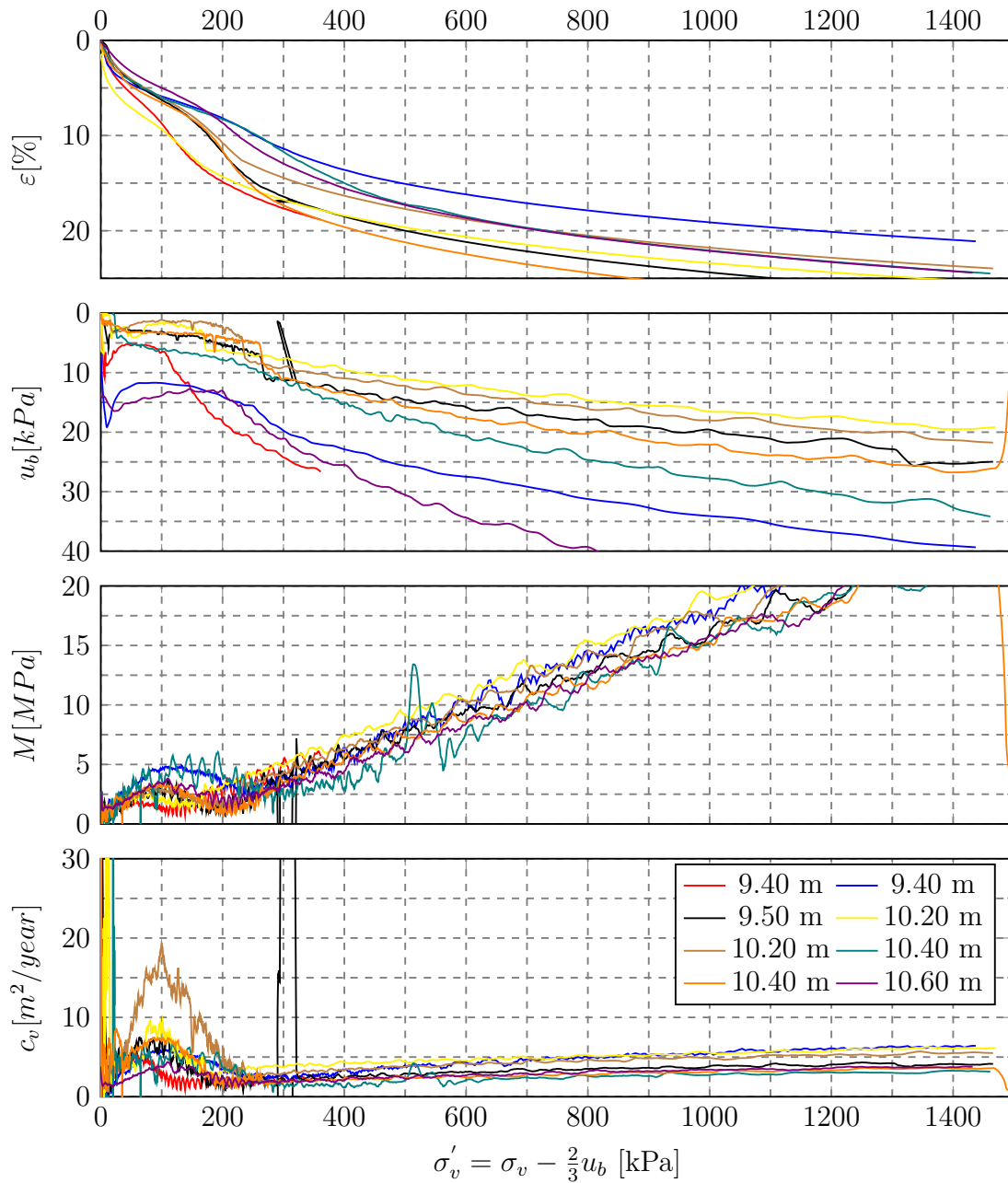


Figure G.2: Presentation of CRS-results from depths 9 to 11 m.

KPG-CRS-0450
Flotten, Trondheim
54 mm sample

Depth	4.5 m	γ	-	p'_c	320 kPa
Sampling date	23.02.17	u	27 kPa	OCR	6.2
Opening of sample	06.03.17	σ'_{v0}	52 kPa		
Testing date	31.03.17	w	-		
Strain rate	1%/hr	ε_{a0}	2.2 %		
Operator	KPG	$\Delta e/e_0$	-		

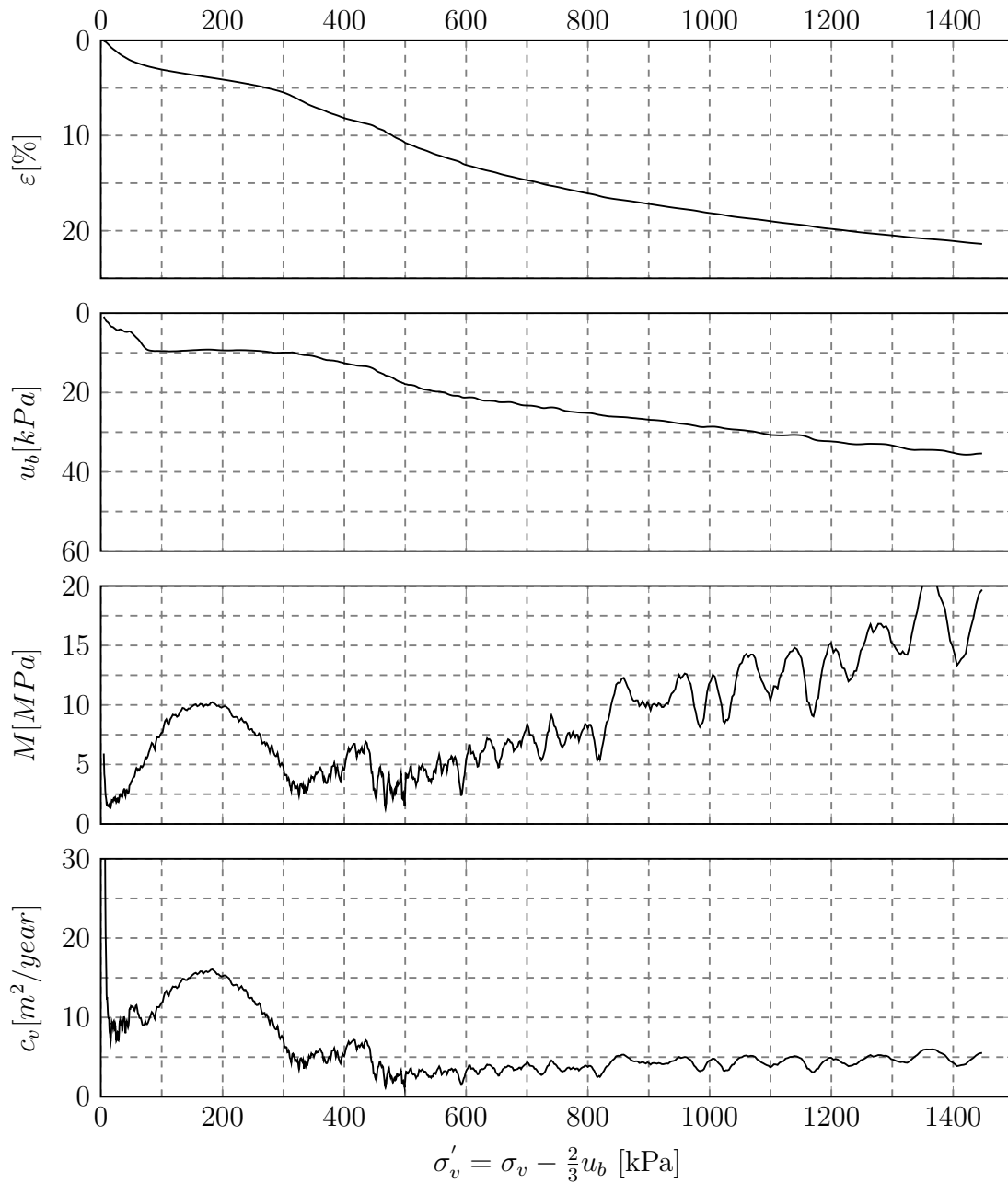


Figure G.3: Presentation of CRS-results from depth 4.5 m.

CRS-0510
Flotten, Trondheim
54 mm sample

Depth	5.1 m	γ	17.2 kN/m ³	p'_c	280 kPa
Sampling date	25.01.17	u	31 kPa	OCR	4.8
Opening of sample	02.02.17	σ'_{v0}	58 kPa		
Testing date	03.02.17	w	50 %		
Strain rate	1 % /hr	ε_{a0}	5.0 %		
Operator	CSO	$\Delta\varepsilon/e_0$	0.09		

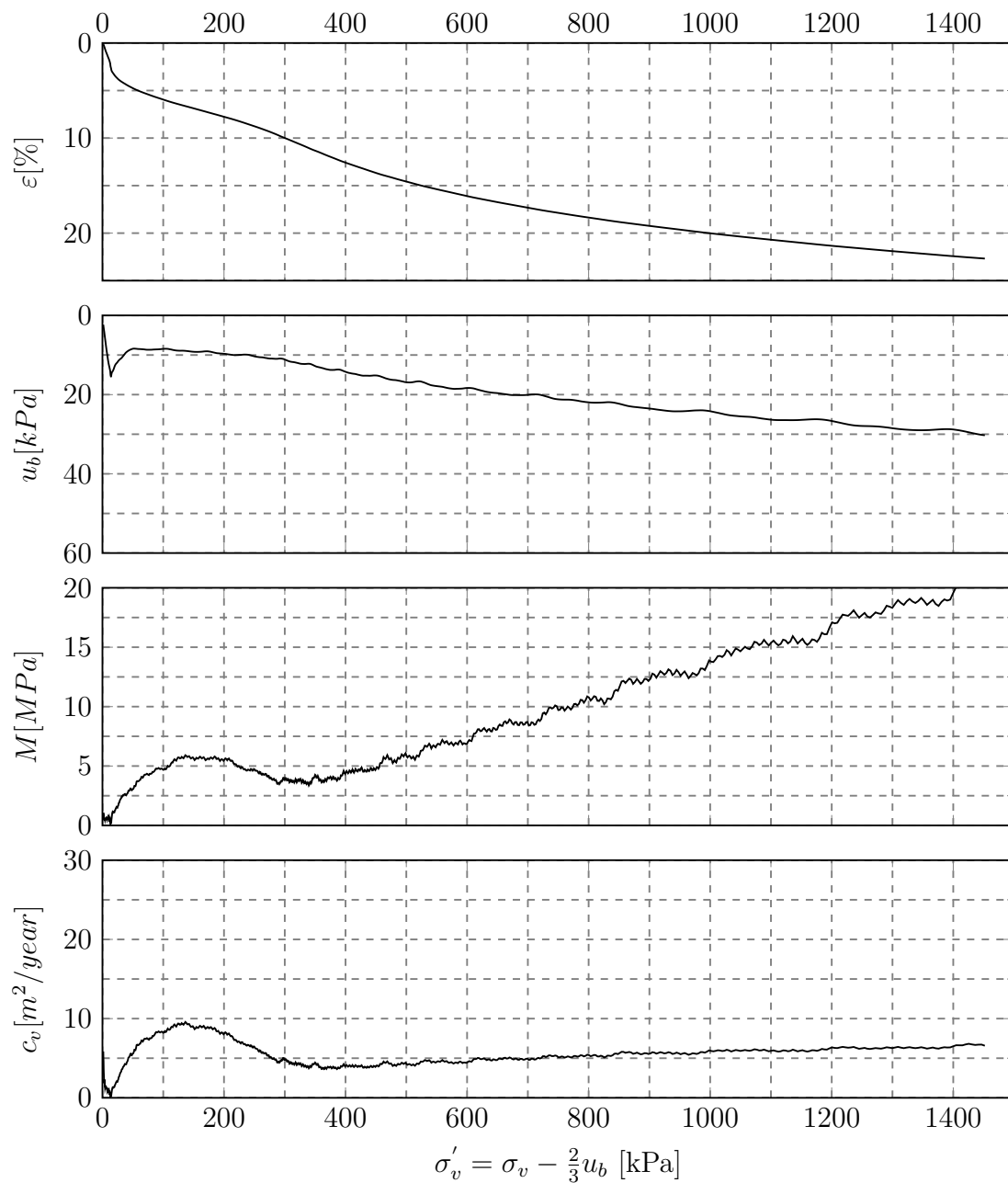


Figure G.4: Presentation of CRS-results from depth 5.1 m.

KPG-CRS-0550-1
Flotten, Trondheim
54 mm sample

Depth	5.5 m	γ	-	p'_c	330 kPa
Sampling date	23.02.17	u	33 kPa	OCR	5.2
Opening of sample	16.03.17	σ'_{v0}	64 kPa		
Testing date	17.03.17	w	-		
Strain rate	1.5%/hr	ε_{a0}	1.9 %		
Operator	KPG	$\Delta e/e_0$	-		

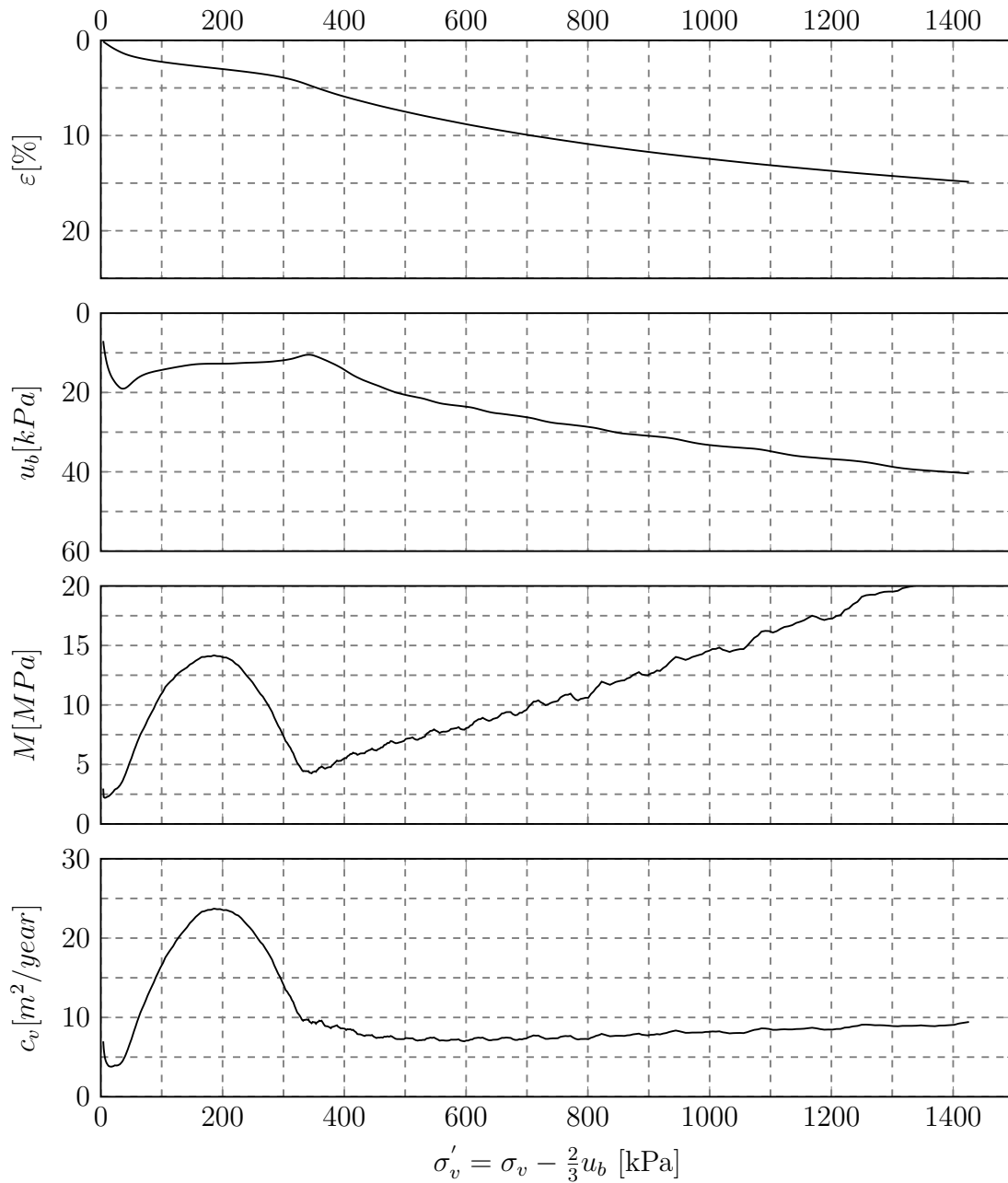


Figure G.5: Presentation of CRS-results from depth 5.5 m.

KPG-CRS-0550-2
Flotten, Trondheim
54 mm sample

Depth	5.5 m	γ	-	p'_c	300 kPa
Sampling date	23.02.17	u	33 kPa	OCR	4.7
Opening of sample	16.03.17	σ'_{v0}	64 kPa		
Testing date	07.04.17	w	-		
Strain rate	1%/hr	ε_{a0}	2.1 %		
Operator	KPG	$\Delta e/e_0$	-		

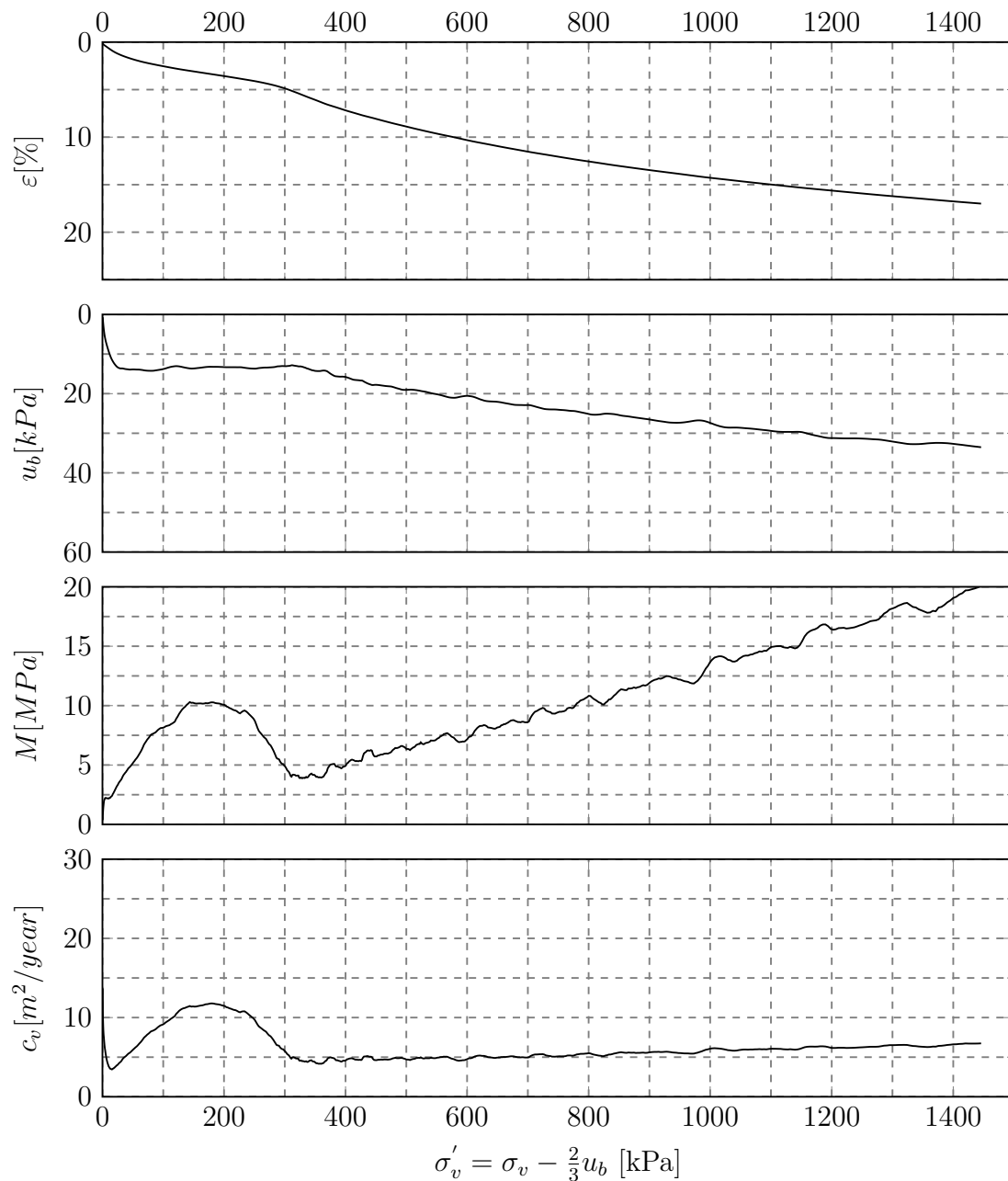


Figure G.6: Presentation of CRS-results from depth 5.5 m.

CRS-0570
Flotten, Trondheim
54 mm sample

Depth	5.7 m	γ	17.3 kN/m ³	p'_c	260 kPa
Sampling date	25.01.17	u	33 kPa	OCR	3.9
Opening of sample	02.02.17	σ'_{v0}	67 kPa		
Testing date	02.02.17	w	48 %		
Strain rate	1 % /hr	ε_{a0}	3.6 %		
Operator	CSO	$\Delta\varepsilon/e_0$	0.06		

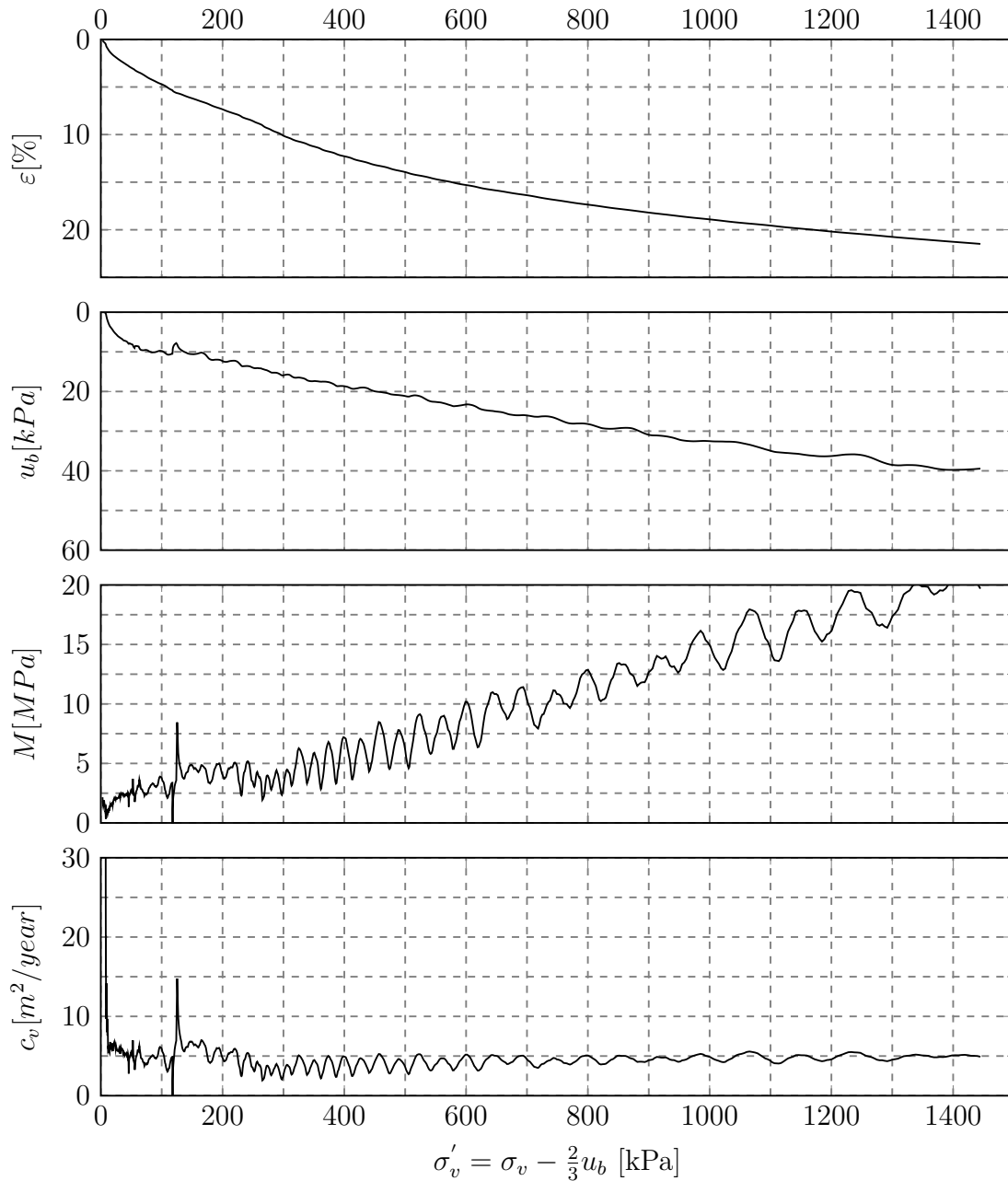


Figure G.7: Presentation of CRS-results from depth 5.7 m.

KPG-CRS-0650-1
Flotten, Trondheim
54 mm sample

Depth	6.5 m	γ	-	p'_c	330 kPa
Sampling date	23.03.17	u	36 kPa	OCR	4.2
Opening of sample	27.03.17	σ'_{v0}	78 kPa		
Testing date	28.03.17	w	-		
Strain rate	1%/hr	ε_{a0}	3.5 %		
Operator	KPG	$\Delta e/e_0$	-		

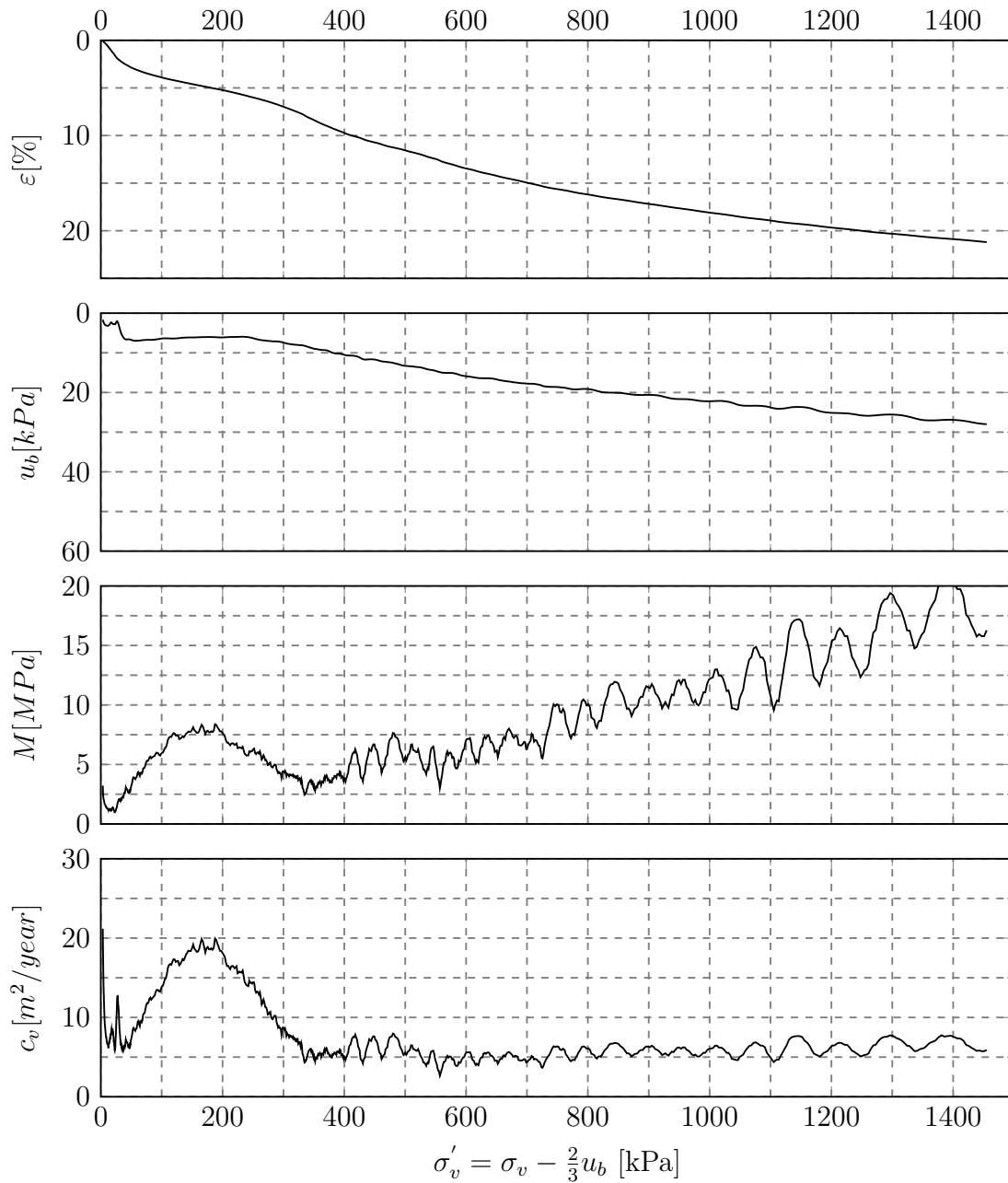


Figure G.8: Presentation of CRS-results from depth 6.5 m.

KPG-CRS-0650-2
Flotten, Trondheim
54 mm sample

Depth	6.5 m	γ	-	p'_c	340 kPa
Sampling date	23.03.17	u	36 kPa	OCR	4.4
Opening of sample	27.03.17	σ'_{v0}	78 kPa		
Testing date	19.04.17	w	-		
Strain rate	1%/hr	ε_{a0}	4.1 %		
Operator	KPG	$\Delta e/e_0$	-		

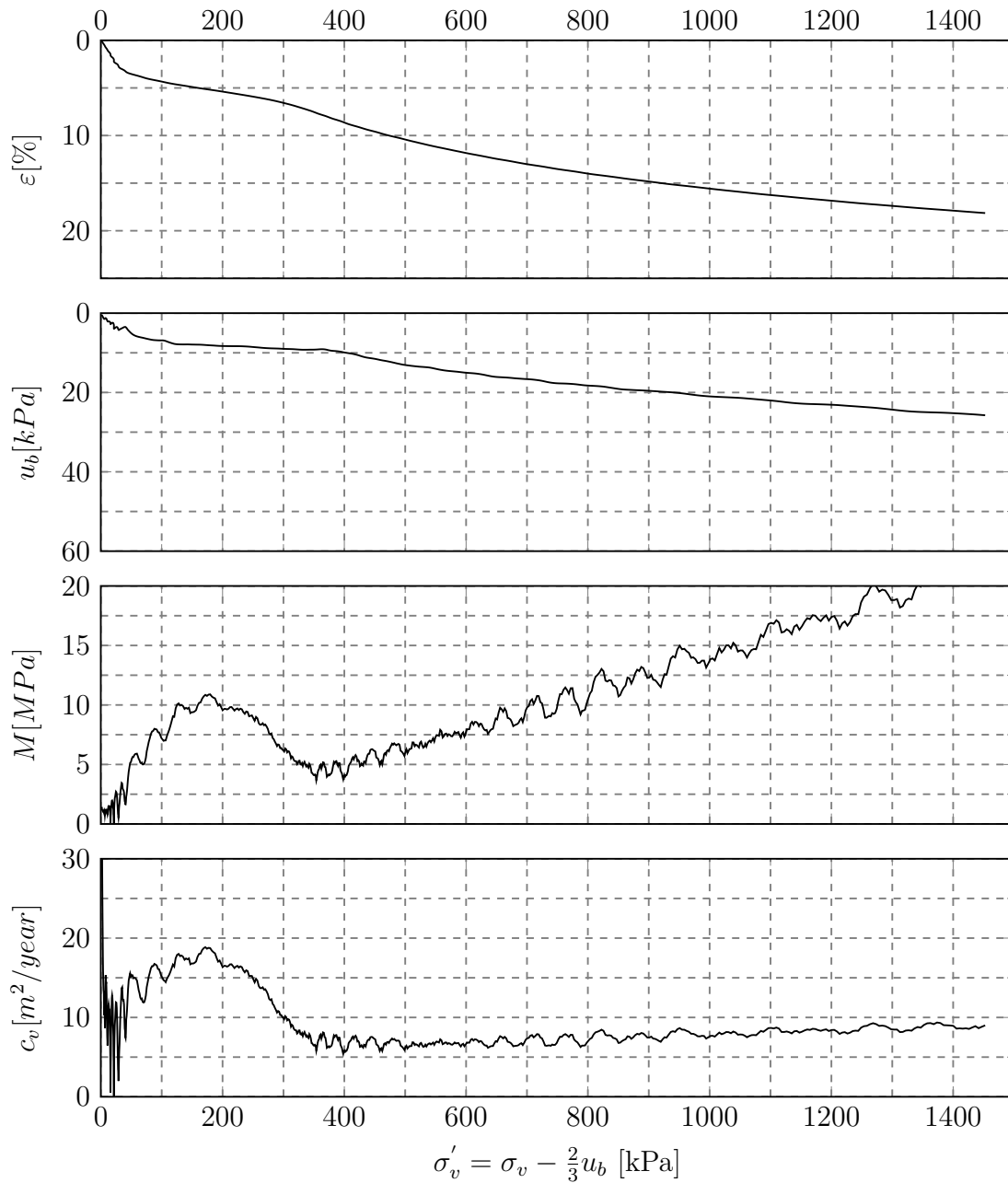


Figure G.9: Presentation of CRS-results from depth 6.5 m.

KPG-CRS-0750-1
Flotten, Trondheim
54 mm sample

Depth	7.5 m	γ	-	p'_c	290 kPa
Sampling date	23.03.17	u	38 kPa	OCR	3.1
Opening of sample	03.04.17	σ'_{v0}	94 kPa		
Testing date	04.04.17	w	-		
Strain rate	1%/hr	ε_{a0}	4.8 %		
Operator	KPG	$\Delta e/e_0$	-		

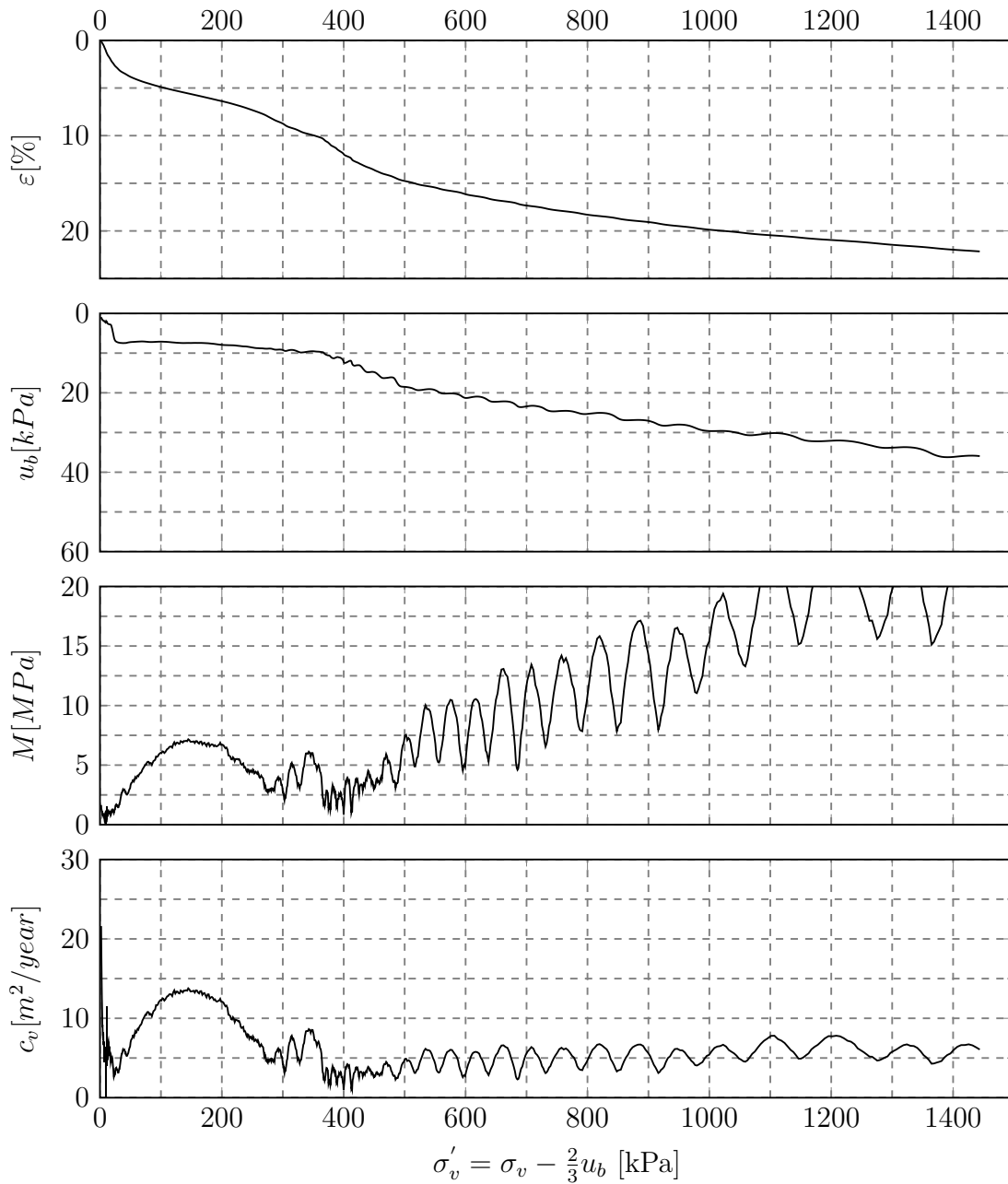


Figure G.10: Presentation of CRS-results from depth 7.5 m.

KPG-CRS-0750-2
Flotten, Trondheim
54 mm sample

Depth	7.5 m	γ	-	p'_c	280 kPa
Sampling date	23.03.17	u	38 kPa	OCR	3.2
Opening of sample	03.04.17	σ'_{v0}	94 kPa		
Testing date	20.04.17	w	-		
Strain rate	1%/hr	ε_{a0}	4.5 %		
Operator	KPG	$\Delta e/e_0$	-		

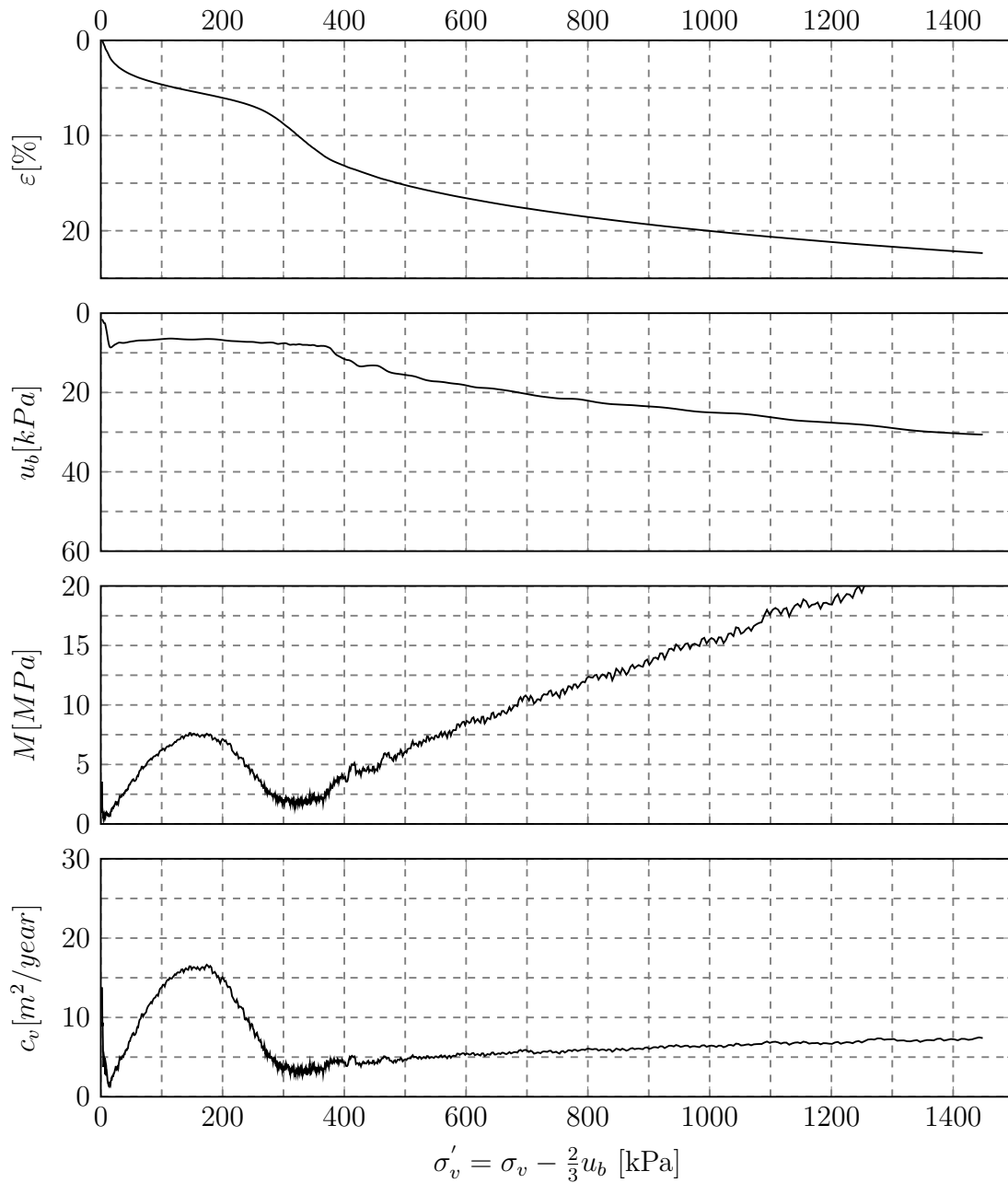


Figure G.11: Presentation of CRS-results from depth 7.5 m.

CRS-0940-1
Flotten, Trondheim
54 mm sample

Depth	9.4 m	γ	18.2 kN/m ³	p'_c	120 kPa
Sampling date	23.02.17	u	40 kPa	OCR	0.96
Opening of sample	01.03.17	σ'_{v0}	125 kPa		
Testing date	01.03.17	w	42 %		
Strain rate	1 % /hr	ε_{a0}	11 %		
Operator	CSO	$\Delta\varepsilon/e_0$	0.19		

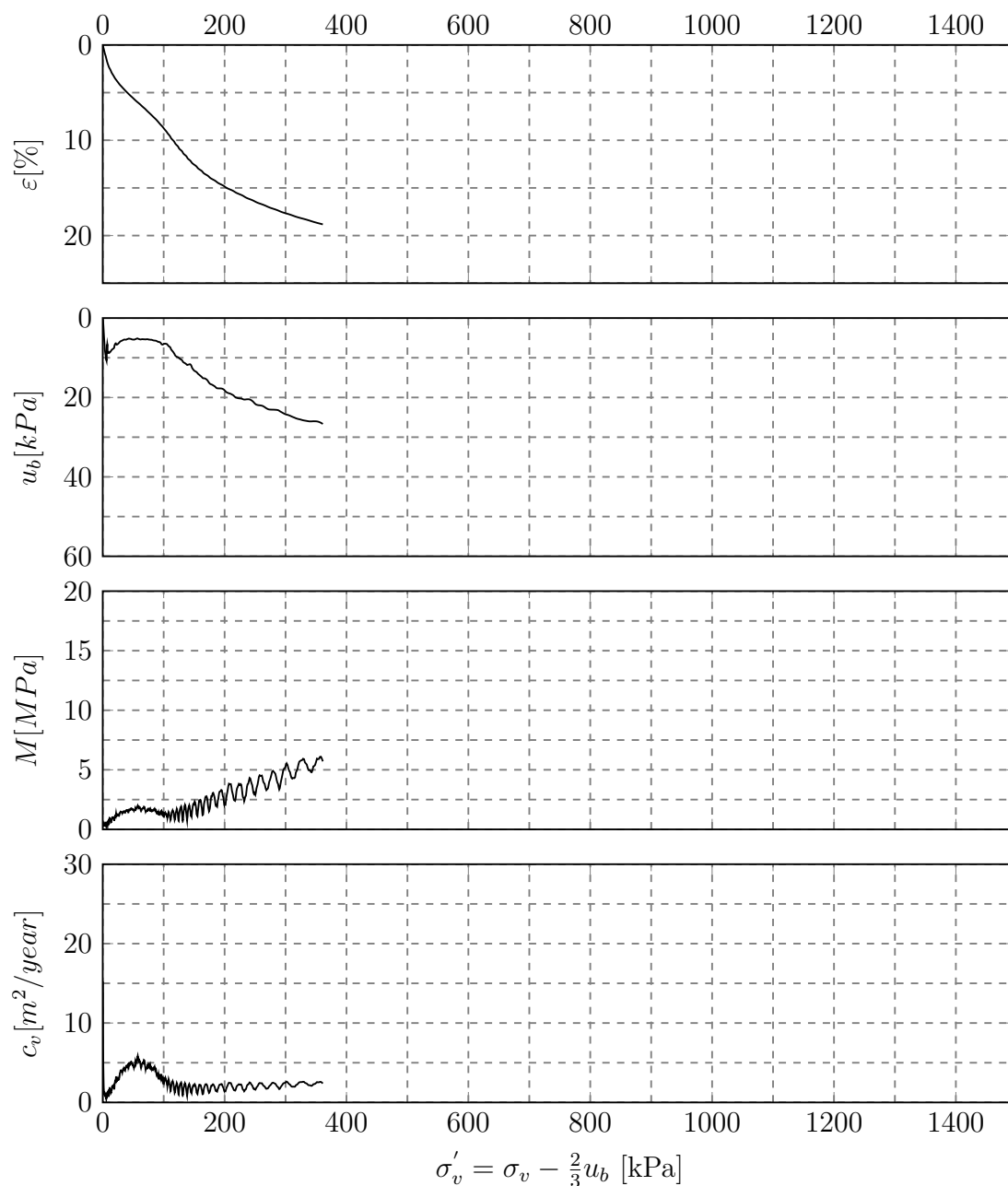


Figure G.12: Presentation of CRS-results from depth 9.4 m. The test was terminated prematurely due to a required test equipment relocation.

CRS-0940-2
Flotten, Trondheim
54 mm sample

Depth	9.4 m	γ	-	p'_c	230 kPa
Sampling date	23.02.17	u	40 kPa	OCR	1.8
Opening of sample	01.03.17	σ'_{v0}	125 kPa		
Testing date	02.03.17	w	-		
Strain rate	1 % /hr	ε_{a0}	6.4 %		
Operator	CSO	$\Delta e/e_0$	-		

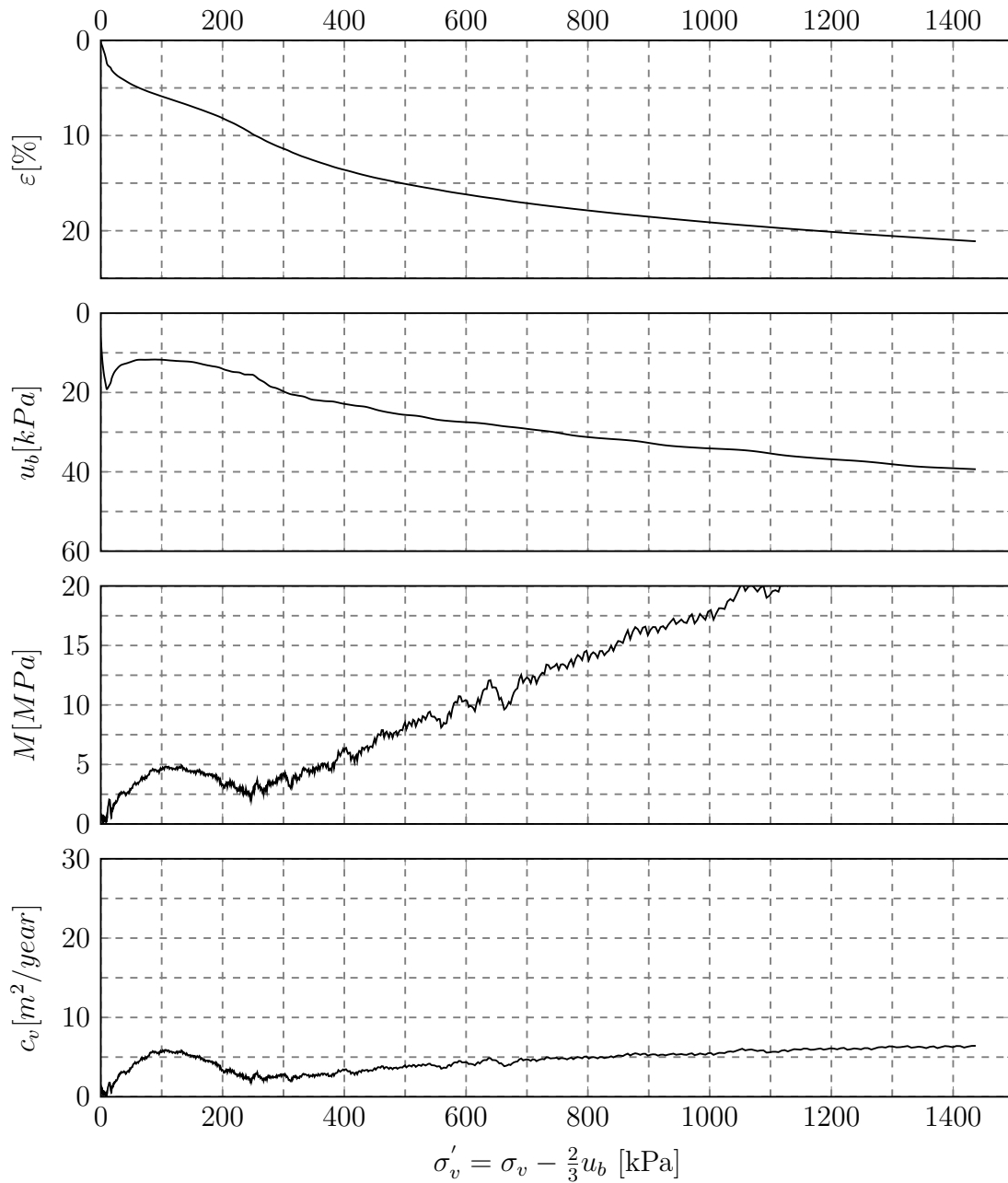


Figure G.13: Presentation of CRS-results from depth 9.4 m.

CRS-0950
Flotten, Trondheim
54 mm sample

Depth	9.5 m	γ	17.0 kN/m ³	p'_c	170 kPa
Sampling date	23.02.17	u	40 kPa	OCR	1.4
Opening of sample	01.03.17	σ'_{v0}	126 kPa		
Testing date	06.03.17	w	59 %		
Strain rate	0.5 % /hr	ε_{a0}	7.2 %		
Operator	CSO	$\Delta e / \varepsilon_0$	0.12		

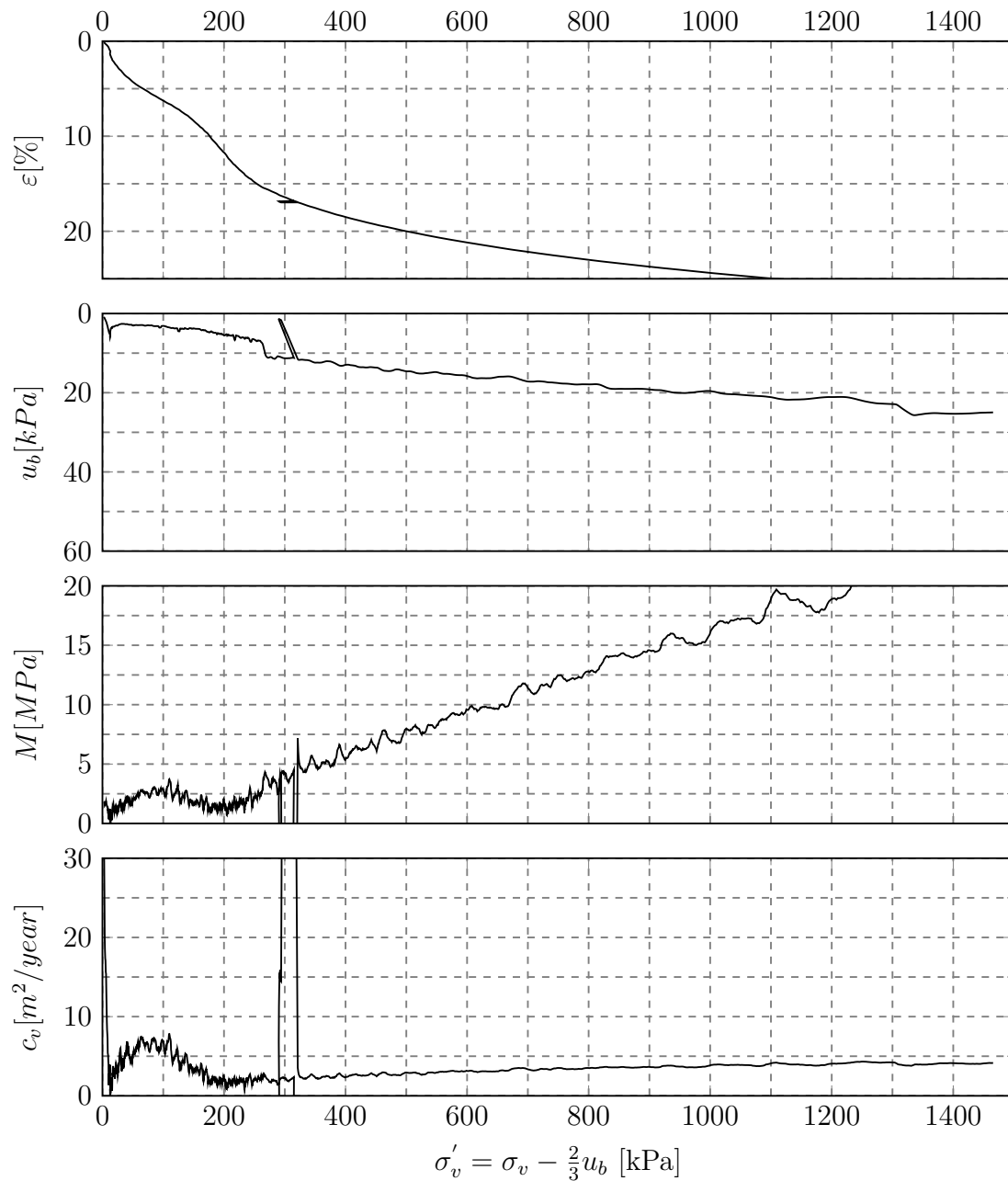


Figure G.14: Presentation of CRS-results from depth 9.5 m. The sudden peak values are most likely caused by a test equipment malfunction.

CRS-1020-1
Flotten, Trondheim
54 mm sample

Depth	10.2 m	γ	17.6 kN/m ³	p'_c	140
Sampling date	23.02.17	u	41 kPa	OCR	1.0
Opening of sample	13.03.17	σ'_{v0}	137 kPa		
Testing date	13.03.17	w	52 %		
Strain rate	0.5%/hr	ε_{a0}	11 %		
Operator	CSO	$\Delta e/e_0$	0.20		

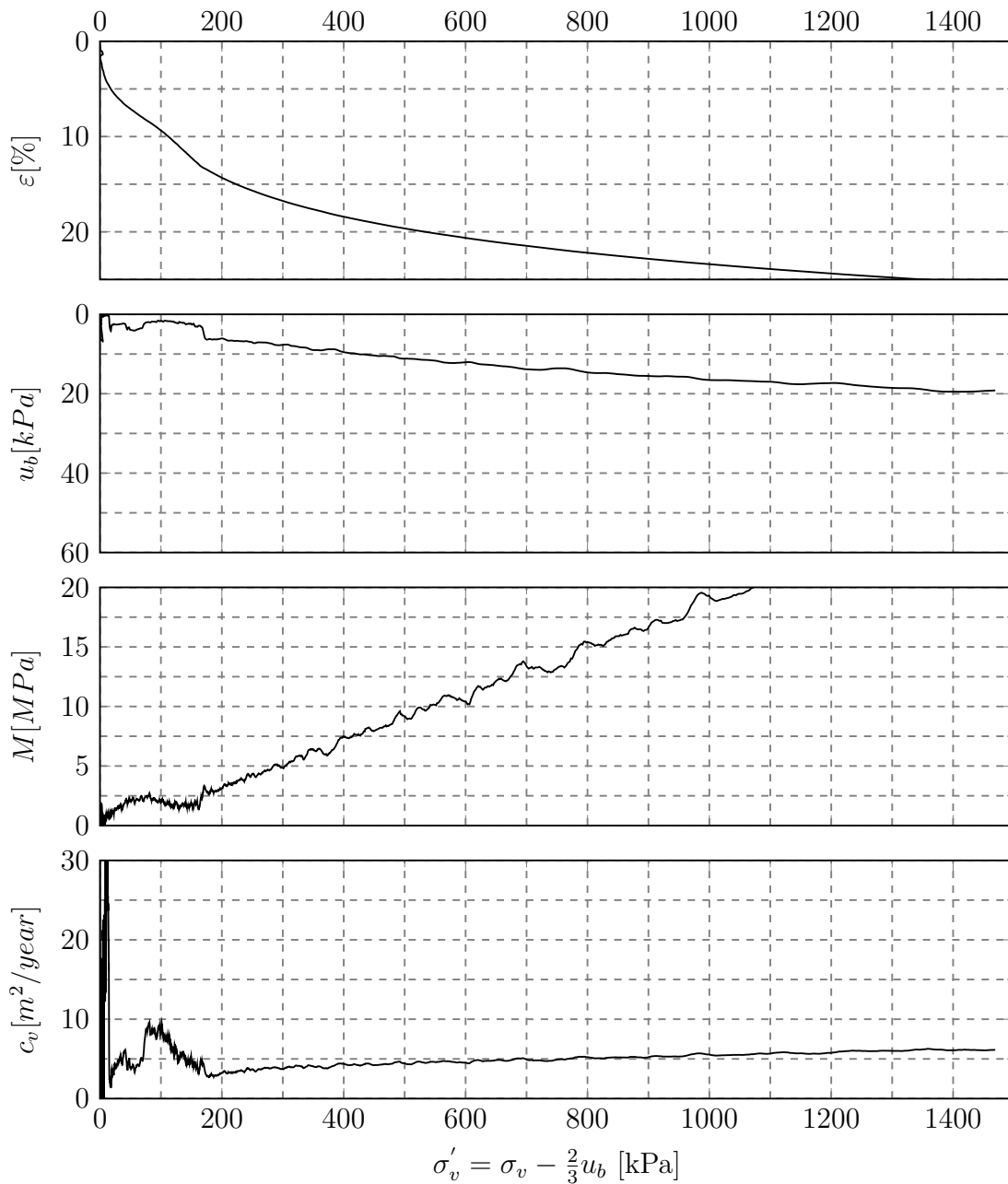


Figure G.15: Presentation of CRS-results from depth 10.2 m.

CRS-1020-2
Flotten, Trondheim
54 mm sample

Depth	10.2 m	γ	17.5 kN/m ³	p'_c	180 kPa
Sampling date	23.02.17	u	41 kPa	OCR	1.3
Opening of sample	13.03.17	σ'_{v0}	137 kPa		
Testing date	16.03.17	w	51 %		
Strain rate	0.5%/hr	ε_{a0}	7.4 %		
Operator	CSO	$\Delta e/e_0$	0.13		

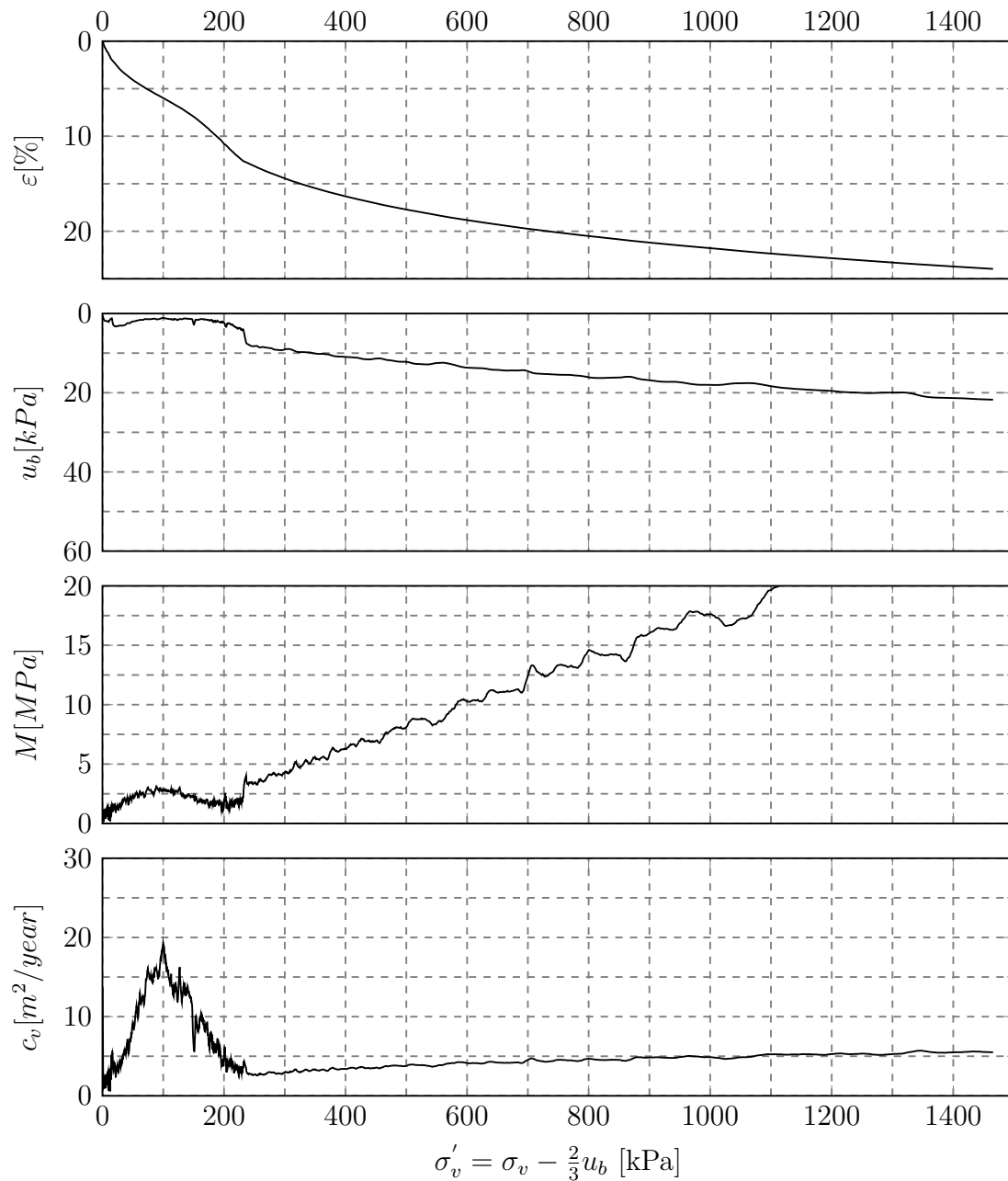


Figure G.16: Presentation of CRS-results from depth 10.2 m.

CRS-1040-1
Flotten, Trondheim
54 mm sample

Depth	10.4 m	γ	-	p'_c	230 kPa
Sampling date	23.02.17	u	42 kPa	OCR	1.6
Opening of sample	13.03.17	σ'_{v0}	141 kPa		
Testing date	20.03.17	w	51 %		
Strain rate	0.5%/hr	ε_{a0}	7.0 %		
Operator	CSO	$\Delta e/e_0$	-		

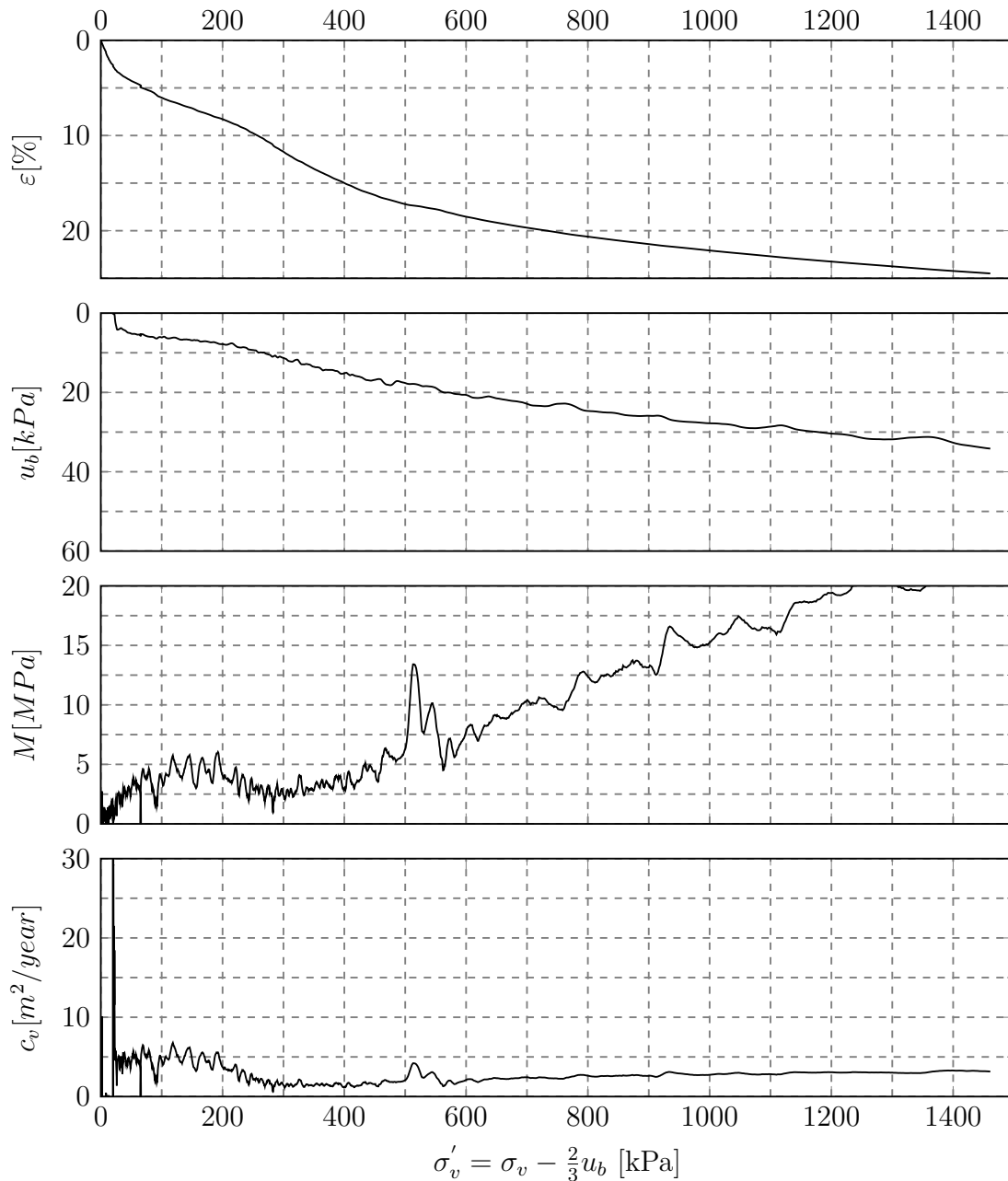


Figure G.17: Presentation of CRS-results from depth 10.4 m.

CRS-1040-2
Flotten, Trondheim
54 mm sample

Depth	10.4 m	γ	-	p'_c	190 kPa
Sampling date	23.02.17	u	42 kPa	OCR	1.5
Opening of sample	13.03.17	σ'_{v0}	141 kPa		
Testing date	29.03.17	w	50 %		
Strain rate	0.5%/hr	ε_{a0}	7.9 %		
Operator	CSO	$\Delta e/e_0$	-		

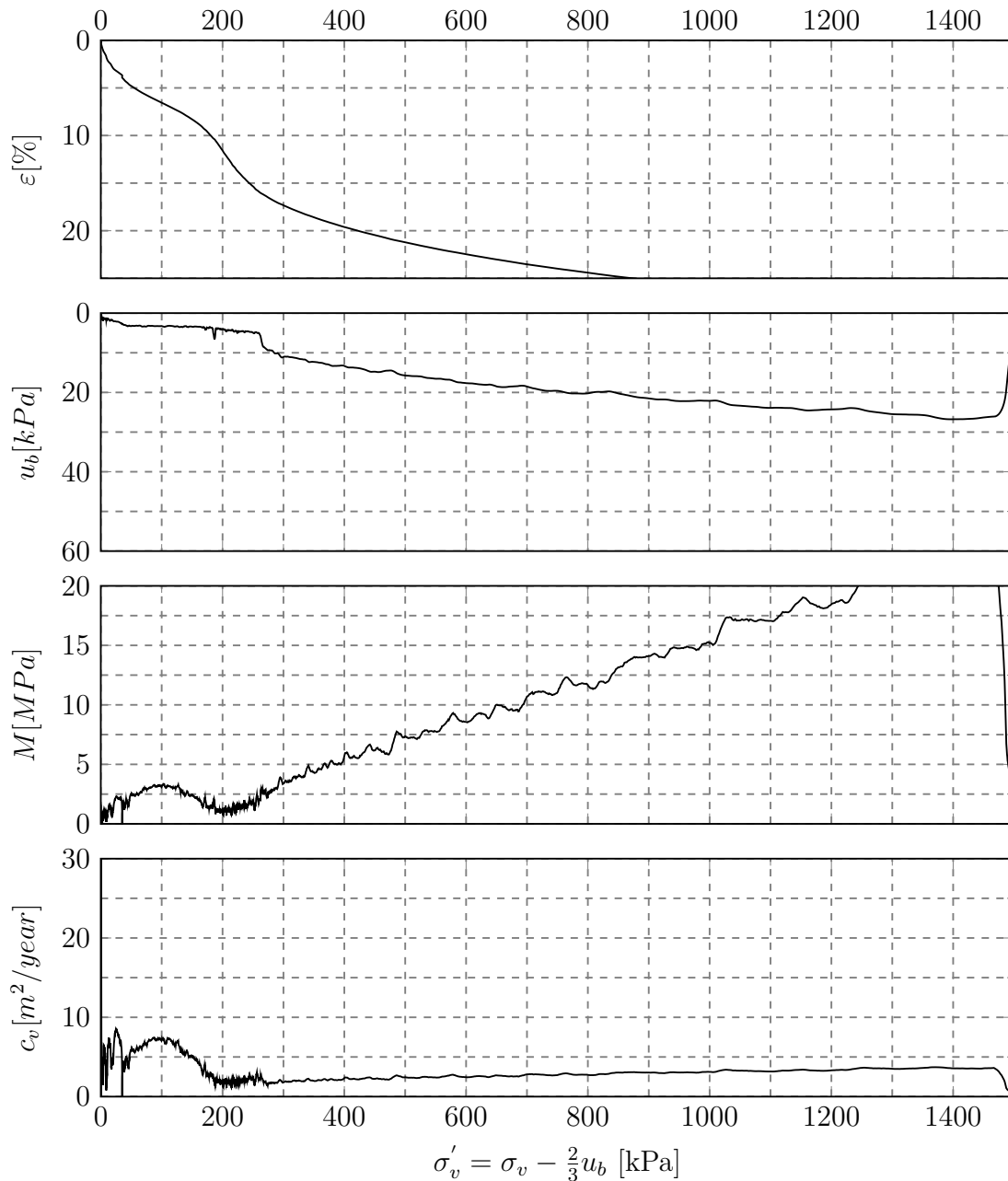


Figure G.18: Presentation of CRS-results from depth 10.4 m.

EA-CRS-1060
Flotten, Trondheim
54 mm sample

Depth	10.6 m	γ	-	p'_c	200 kPa
Sampling date	25.01.17	u	42 kPa	OCR	1.4
Opening of sample	30.01.17	σ'_{v0}	144 kPa		
Testing date	30.01.17	w	-		
Strain rate	1 % /hr	ε_{a0}	6.4		
Operator	EA	$\Delta e/e_0$	-		

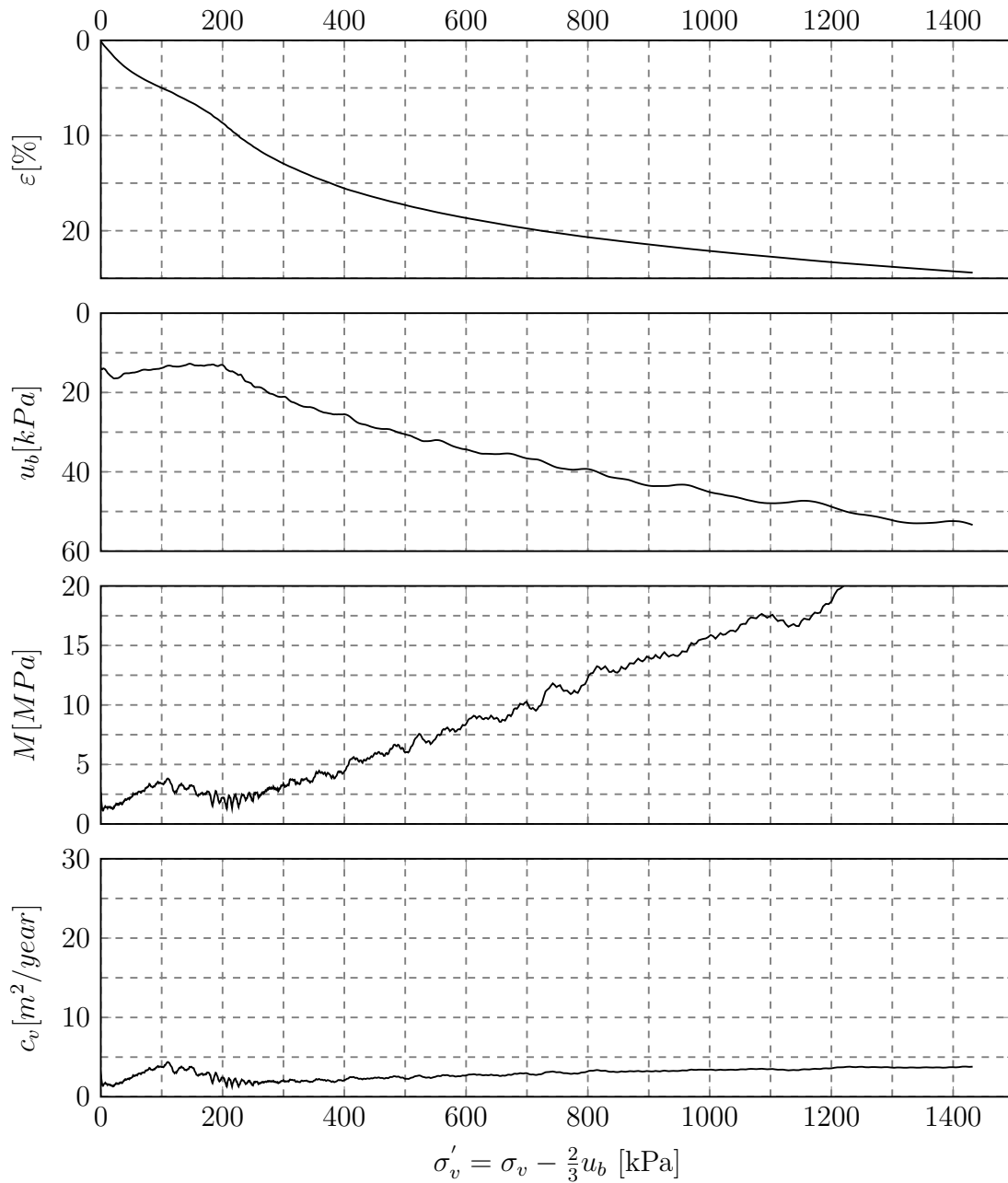


Figure G.19: Presentation of CRS-results from depth 10.60 m.

Appendix H

Work Criterion in Oedometer

This appendix contains the work criterion interpretations of three oedometer tests presented in Figure H.1, H.2 and H.3. The interpretation is in accordance with the procedure described in section 2.5.1. Please note that a short-lasting peak which was most likely caused by equipment malfunction has been removed from the graph in Figure H.3. This figure is based on the CRS-0950 oedometer test, and the peak is hence visible in the detailed results of this oedometer test in Figure G.14.

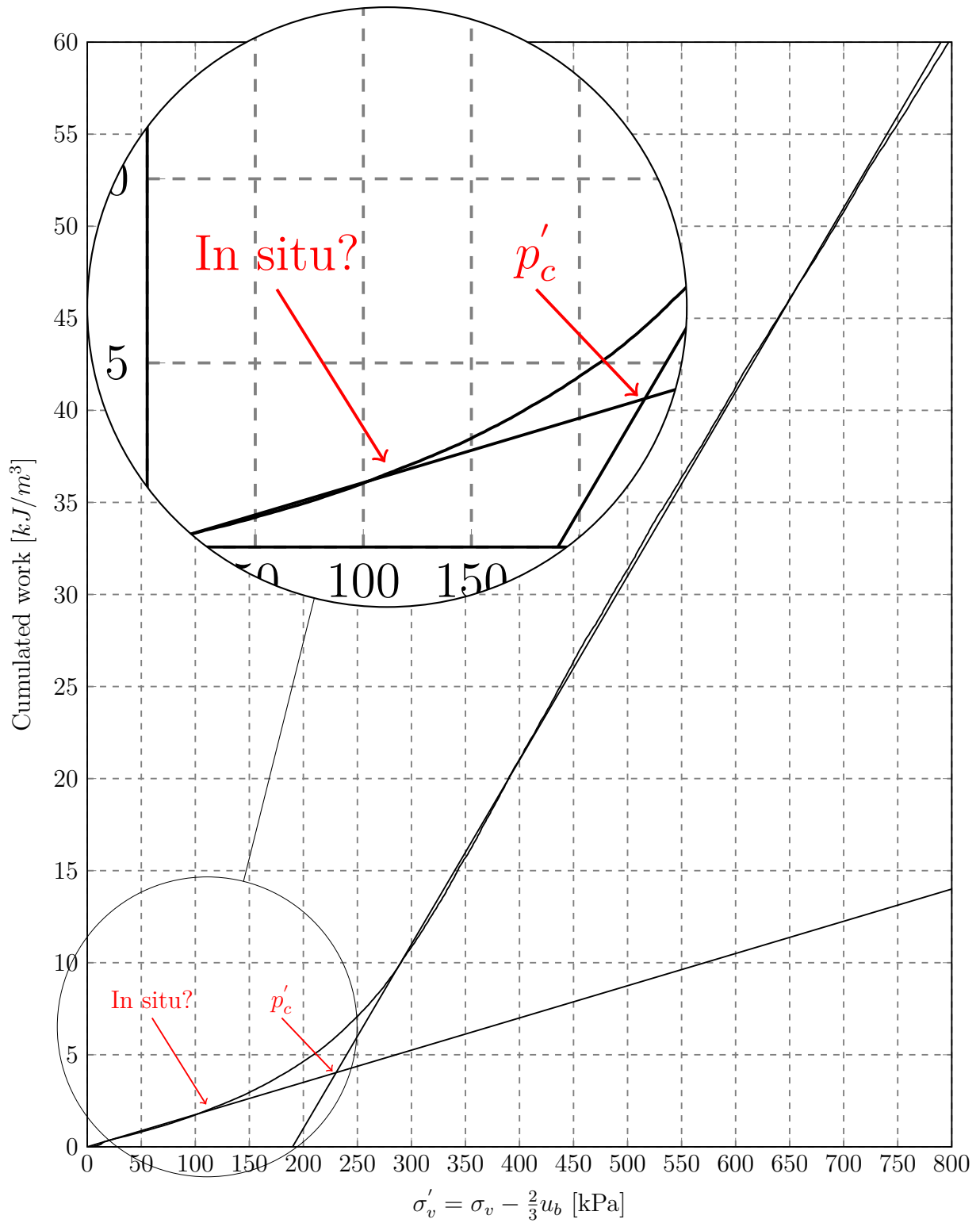


Figure H.1: Work criterion calculation based on oedometer test CRS0510 from depth 5.10 m.

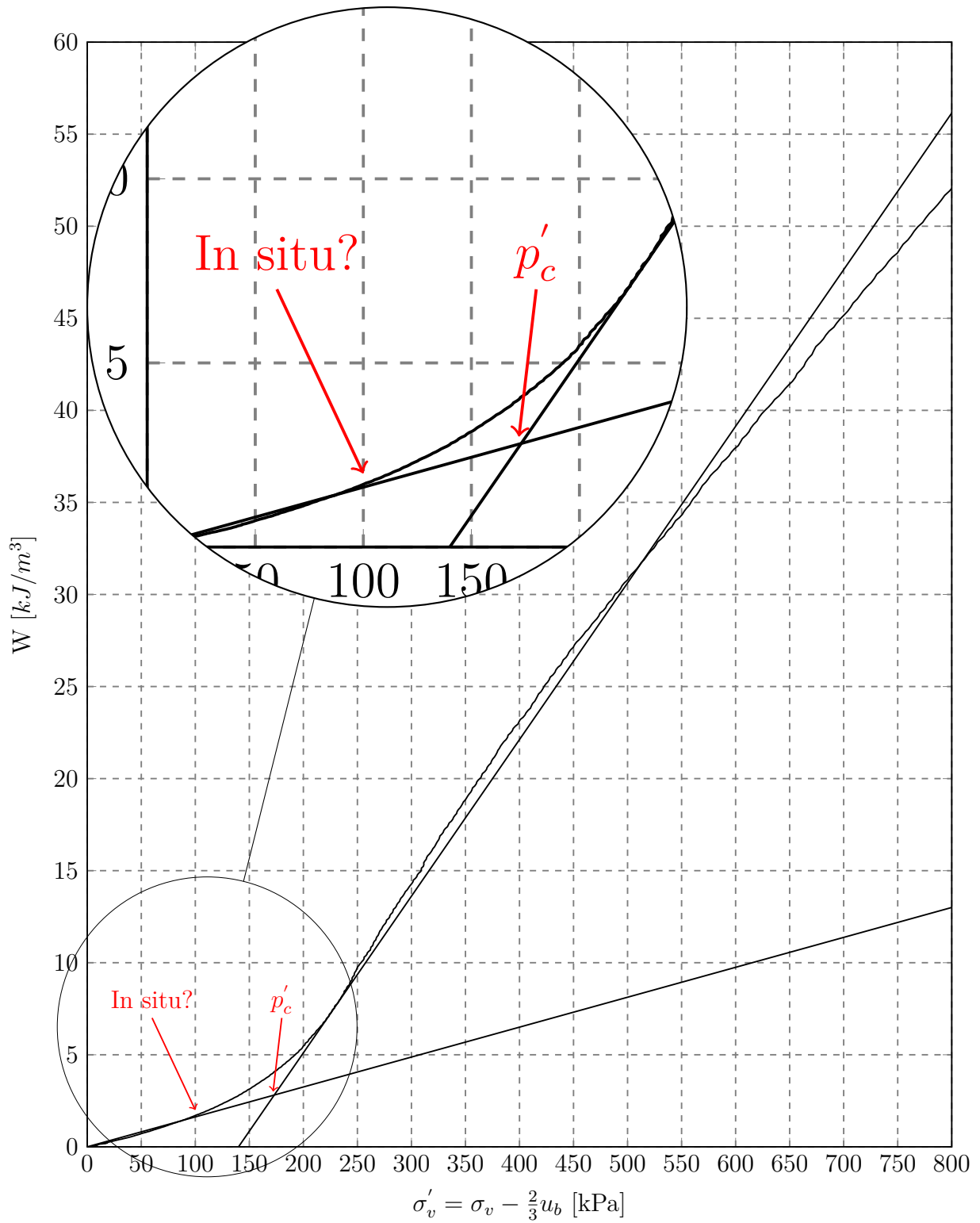


Figure H.2: Work criterion calculation based on oedometer test CRS0940-2 from depth 9.40 m.

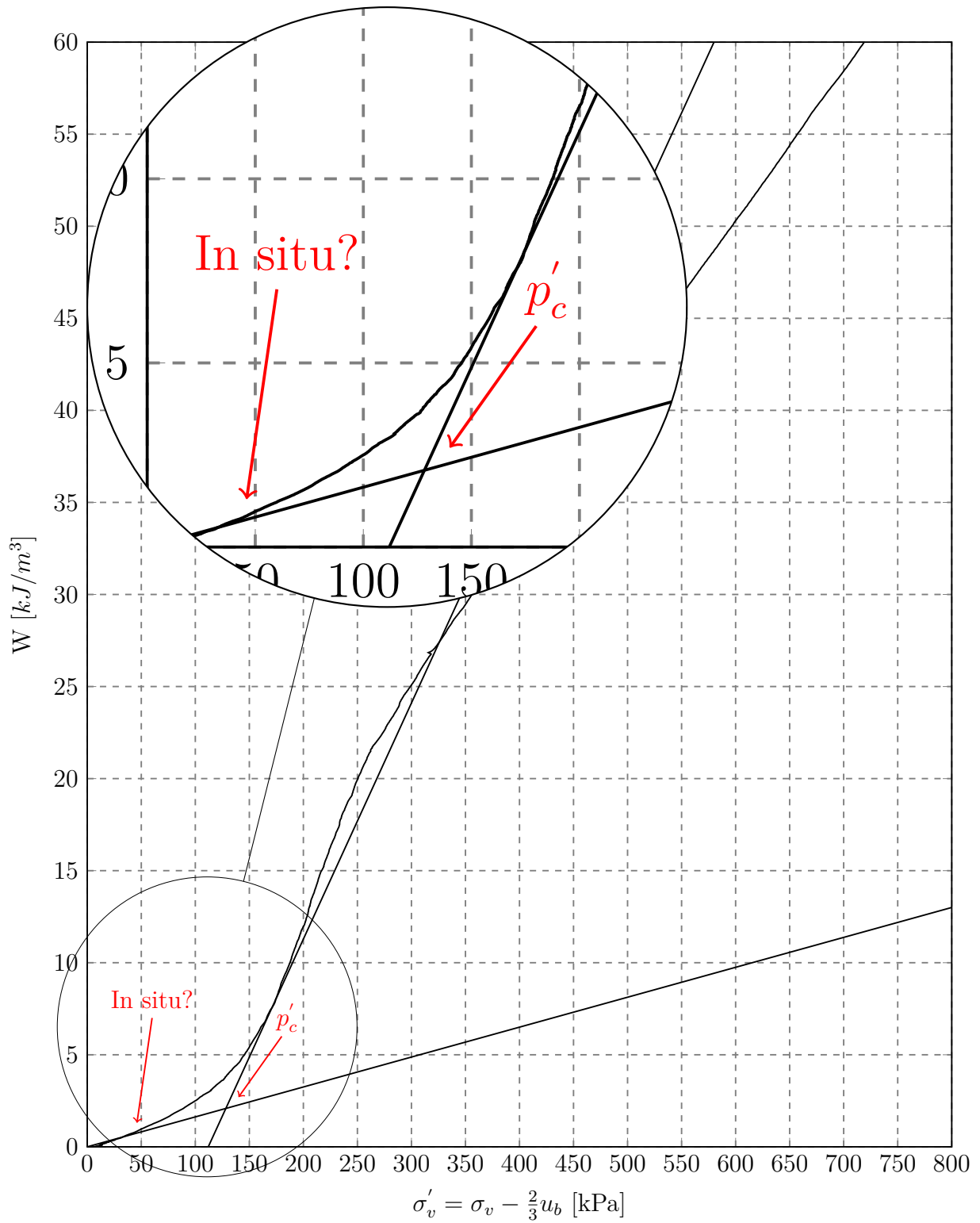


Figure H.3: Work criterion calculation based on oedometer test CRS0950 from depth 9.50 m.

Appendix I

Triaxial Testing

All specimens tested by the authors were sampled from borehole 54MM_K0. All specimens tested by Gella were sampled from the borehole 54MM_KPG, with the exception of the specimen used in KPG-CIUc-0540, which was sampled from the borehole 54MM_1. The map of boreholes is given in Figure A.3.

Similar to the oedometer test equipment, the triaxial test equipment will log key information like deformation, force of the piston, cell and pore pressure as well as amount of expelled water with a given time interval. For all testing presented, data was registered every 10th second. Further processing of the resulting triaxial raw data file was conducted in Microsoft Excel. The same spreadsheet with formulas for calculating desired parameters was used for every test. The formulas presented below were utilized on every logging in the raw data file.

σ'_3 was calculated as the cell pressure minus the pore pressure. The axial strain was calculated as shown in Equation I.1.

$$\varepsilon_a = \frac{\delta}{h_0} \quad (\text{I.1})$$

where δ is the deformation in mm and $h_0 = 100$ mm is the initial height of the test specimen.

The area of the test specimen may change slightly during the consolidation phase. Equation I.2 is applied to give a more accurate area in the subsequent stress calculations.

$$A_a = A_0 \left(1 - \frac{\Delta V}{V_0}\right) / \left(1 - \frac{\Delta V}{3V_0}\right) \quad (\text{I.2})$$

where A_a is the adjusted area after the consolidation phase, A_0 is the original area, ΔV is the amount of expelled pore water during consolidation and $V_0 = 229 \text{ cm}^3$ is the original volume of the triaxial test specimen.

In the shear phase, the cross sectional area is adjusted for increasing shear strains,

using Equation I.3.

$$A_s = \frac{A_a}{1 - \varepsilon} \quad (\text{I.3})$$

where A_s is the adjusted area used during the shear phase, A_a is the adjusted area after the consolidation phase and ε is the current shear strain.

σ'_1 was calculated as in equation I.4, and the values of σ'_1 and σ'_3 were then utilized to calculate other stress parameters used when presenting the triaxial test results in the subsequent figures.

$$\sigma'_1 = \sigma_{cell} + 10 \cdot \frac{F}{A_s} - u \quad (\text{I.4})$$

where σ_{cell} is the cell pressure, F is the piston force, A_s is the corrected area of the test specimen and u is the measured pore pressure.

$$p = \frac{1}{3}(\sigma'_1 + \sigma'_2 + \sigma'_3) = \frac{1}{3}(\sigma'_1 + 2\sigma'_3) \quad (\text{I.5})$$

where the last equation may be used as all triaxial tests in this thesis were performed as active tests where $\sigma'_2 = \sigma'_3$.

$$q = (\sigma'_1 - \sigma'_3) \quad (\text{I.6})$$

$$\tau = \frac{1}{2}(\sigma'_1 - \sigma'_3) \quad (\text{I.7})$$

The shear strength of a material may be expressed by the Mohr-Coulomb failure criterion given in Equation I.8 Janbu and Senneset, 1995.

$$\tau = (\sigma' + a)\tan\phi \quad (\text{I.8})$$

By considering the stress path from a triaxial test plotted in a NTNU plot, one may use S to denote the inclination of an arbitrary line between $-a$ on the σ'_3 axis and a point on the stress path Janbu and Senneset, 1995, as presented in Equation I.9.

$$\sin\rho = \frac{S}{1 + S} \quad (\text{I.9})$$

Finally, by rewriting Equation I.9, the mobilization may be calculated by Equation I.10.

$$f = \frac{\tan\rho}{\tan\phi} = \frac{S}{\sqrt{1+2S}} \quad (\text{I.10})$$

where f is the mobilization of the material, ρ is the mobilized friction angle and ϕ is the ultimate friction angle of the material. In this appendix, graphs showing the mobilization against axial strain are included for all the triaxial tests. They give an indication of how well the chosen friction angle and attraction fit with the individual triaxial tests.

All triaxial tests run by the authors of this master's thesis were run at a strain rate of 0.75 mm/h. With a logging interval of 10 seconds, the tests resulted in a quite large amount of data. Similar to the oedometer tests, the raw data material for all triaxial tests conducted by the authors have hence been smoothed through a running average procedure containing 200 data points, before every 20th data point is included in the resulting plots. As all tests by Gella have been performed using a rate of strain higher than 0.75 mm/h, the amount of data is more limited and no smoothing has been applied. For the test KPG-CIUc-0826, every 20th data point registered during consolidation was used, as the consolidation was run for a very long period of time for this particular test.

Key information regarding the tests is given in the table above the group of plots indicating the results of each test. First, the depth; sampling, opening and testing dates as well as the water content of the test specimen are presented. The water content presented for each test was determined based on adjacent clay when trimming the triaxial specimen. Next, key consolidation properties like assumed overburden pressure, pore pressure and the chosen value of K'_0 is indicated. Finally, an initial evaluation of sample quality through the change in ε_{vol} during consolidation is introduced. This is further discussed in section 6.3.4.

For the tests by Gella, the same assumptions were made as for her oedometer tests with respect to water content and density from adjacent index test data. Please see Appendix G. $K'_0 = 0.7$ was assumed for all anisotropic triaxial tests performed by Gella.

First, collective NTNU and stress-strain plots of all tests are presented. Based on Table 5.10, CAUc tests from depth 3 to 8 m are presented in Figure I.1 and CAUc tests from depth 8 to 12 m are presented in Figure I.2. Next, CIUc tests from depth 3 to 8 m are presented in Figure I.3 and CIUc tests from depth 8 to 12 m are presented in Figure I.4. Finally, detailed plots of each test are presented in Figures I.5 to I.23. These plots are presented in order of increasing specimen depth, with the anisotropically consolidated (CAUc) tests first, and subsequently the isotropically consolidated (CIUc) tests.

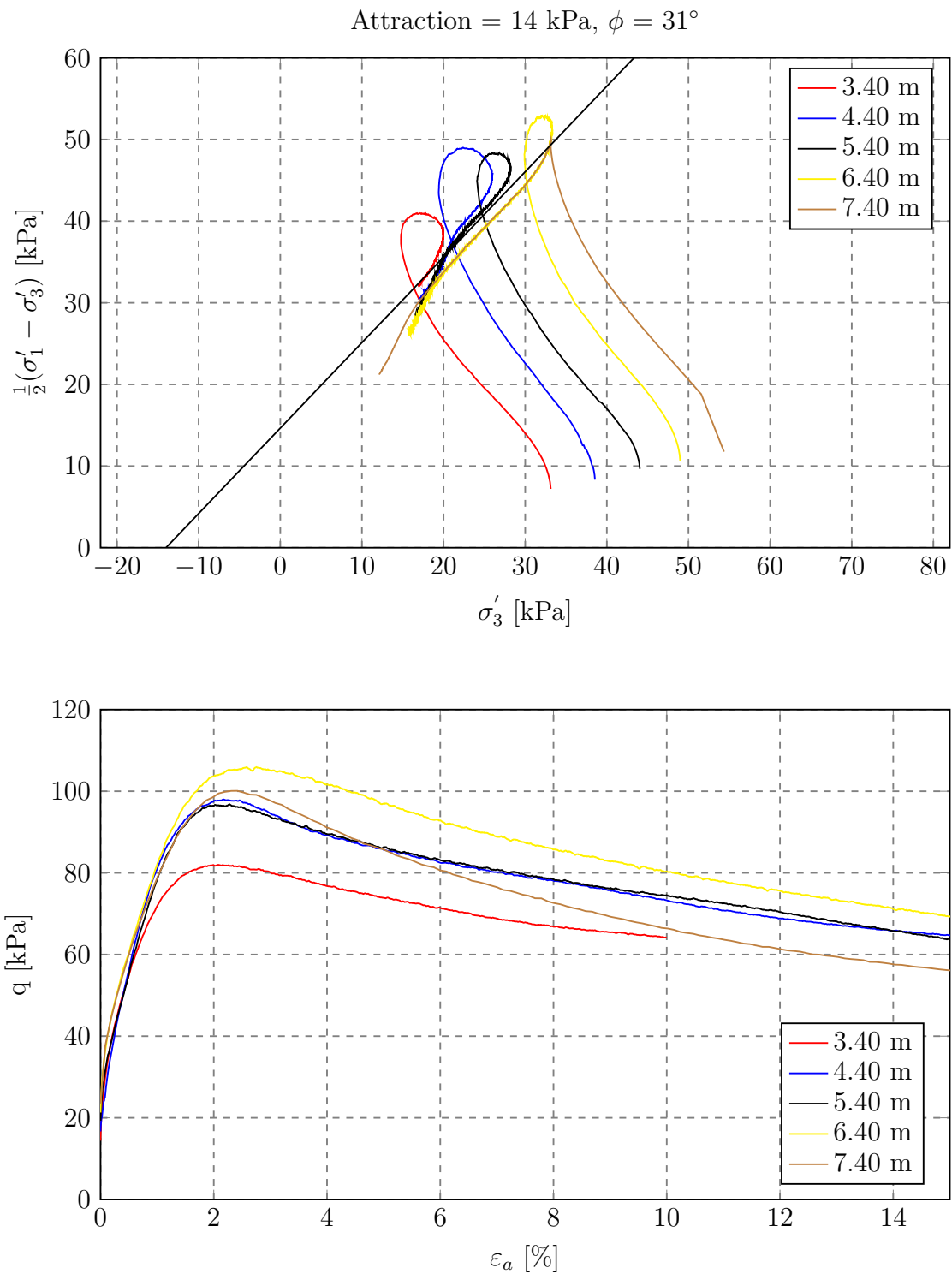


Figure I.1: Presentation of all CAUc triaxial test results from depths 3 to 8 m.

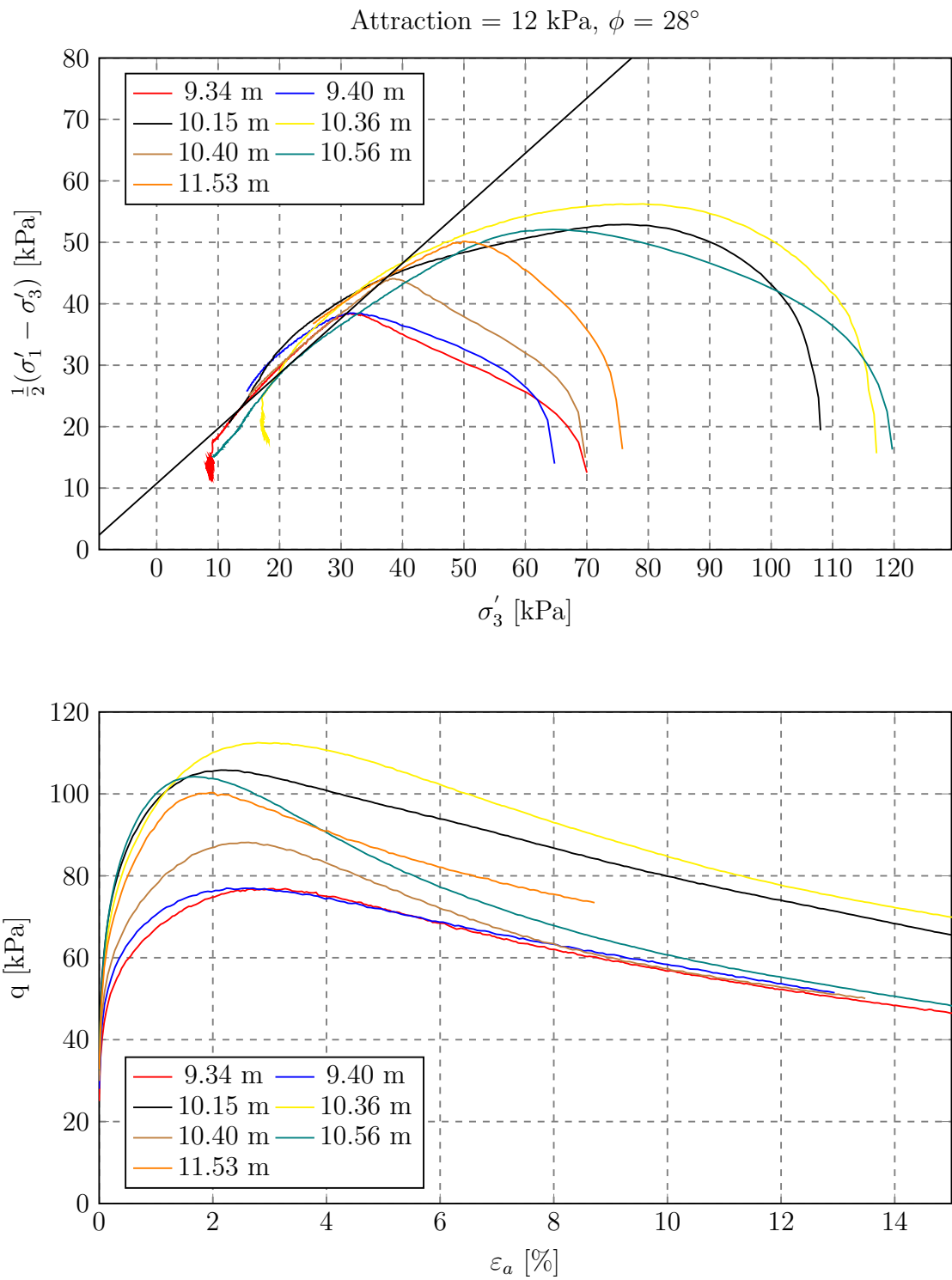


Figure I.2: Presentation of all CAUc triaxial test results from depths 8 to 12 m.

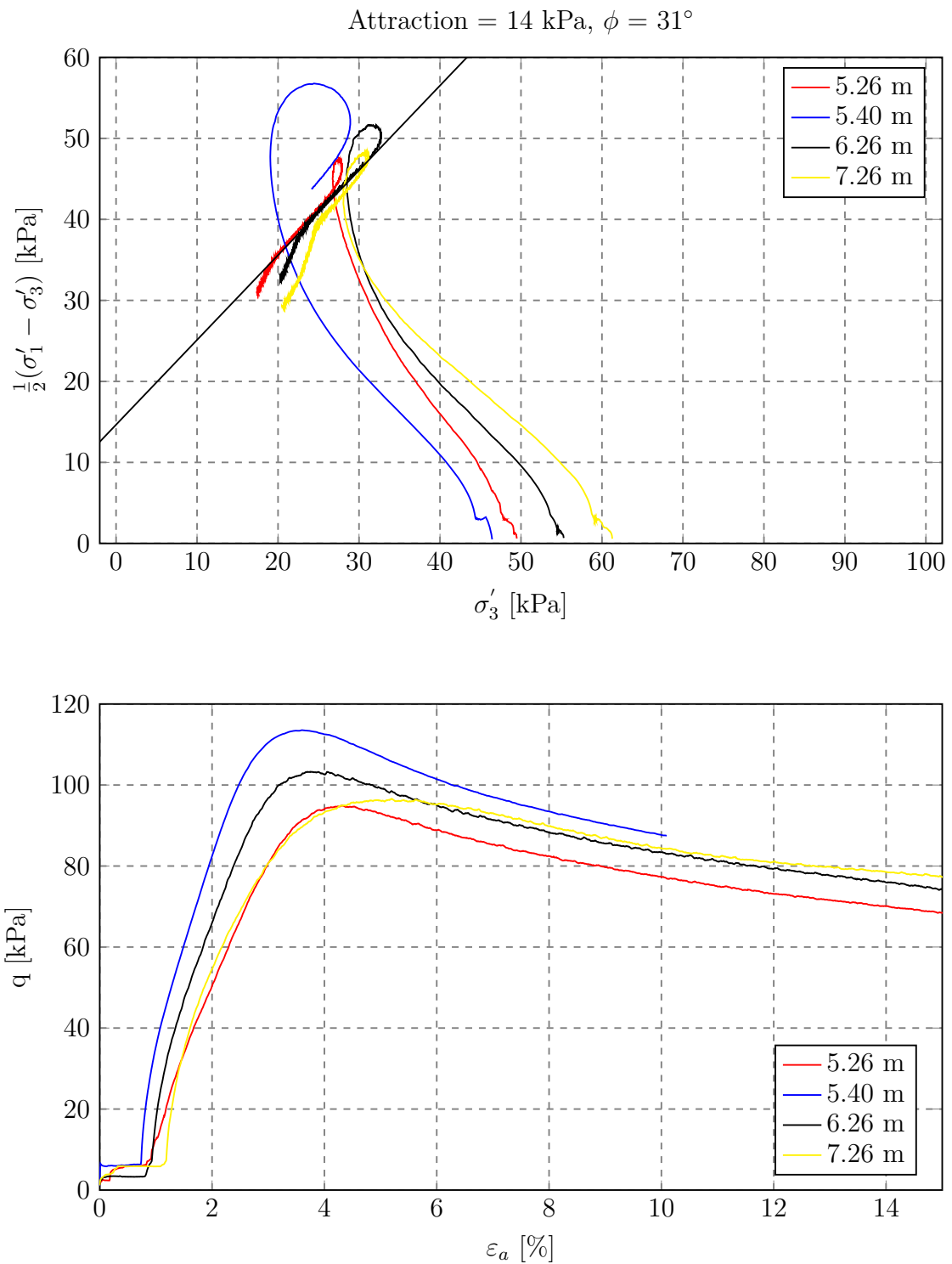


Figure I.3: Presentation of all CIUC triaxial test results from depths 3 to 8 m.

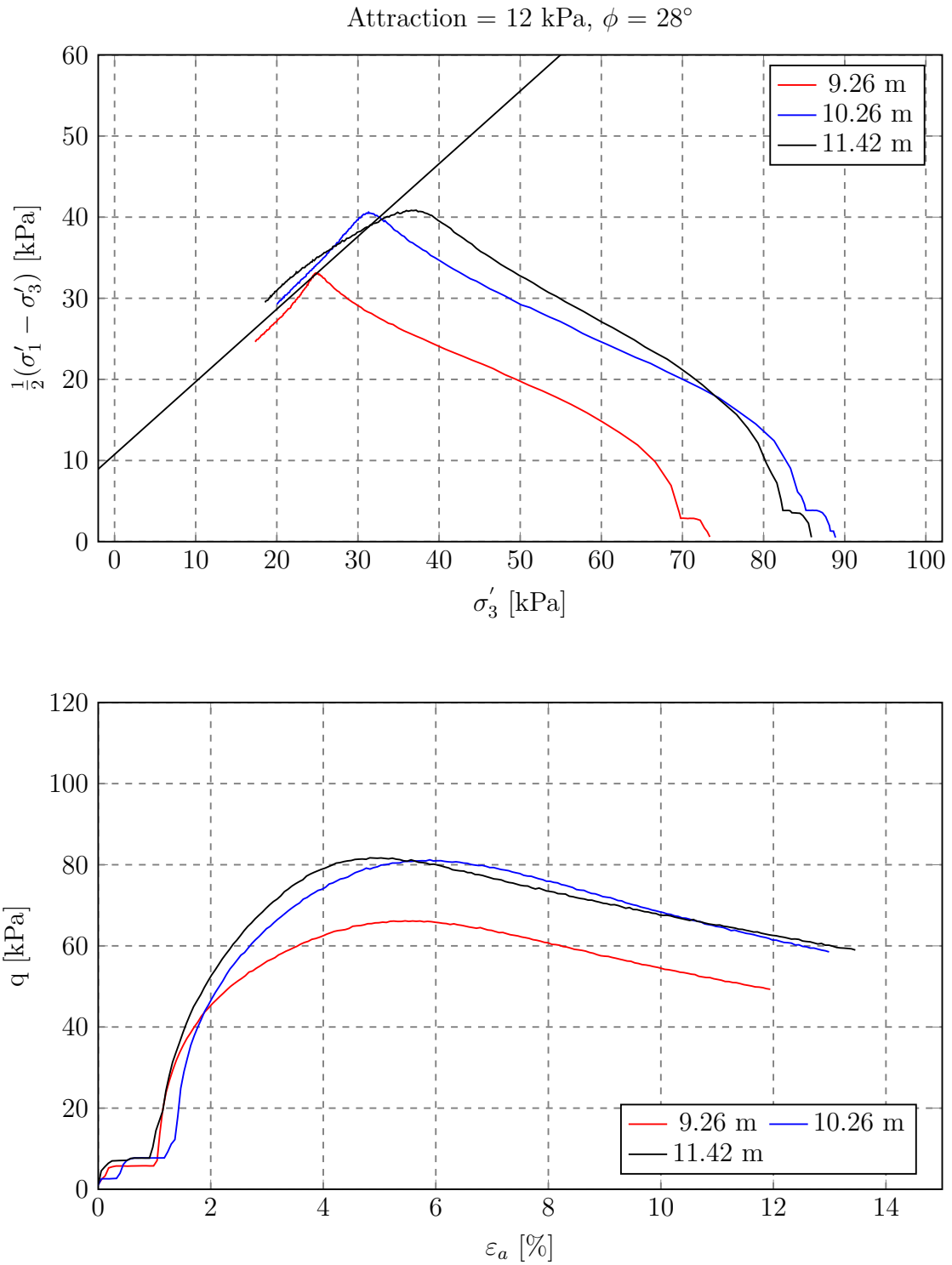


Figure I.4: Presentation of all CIUC triaxial test results from depths 8 to 12 m.

KPG-CAUc-0340
Flotten, Trondheim
54 mm sample

Depth	3.4 m
Sampling date	17.02.17
Opening date	27.02.17
Testing date	07.03.17
Vertical strain rate	3 %/hr
σ'_{v0}	47.2 kPa
w	42.2 %
γ	17.8 kN/m ³
K'_0	0.7
u	14 kPa
ΔV	-
ε_v	-
Operator	KPG

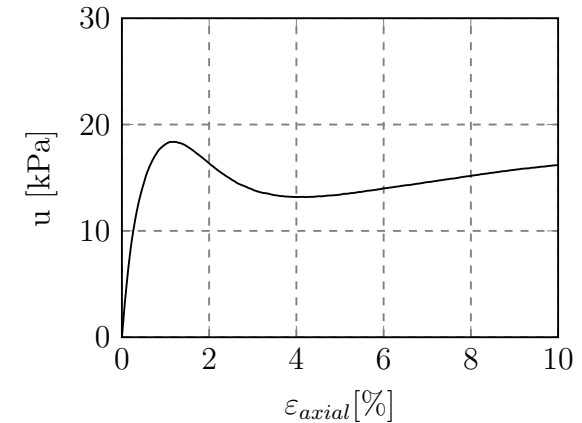
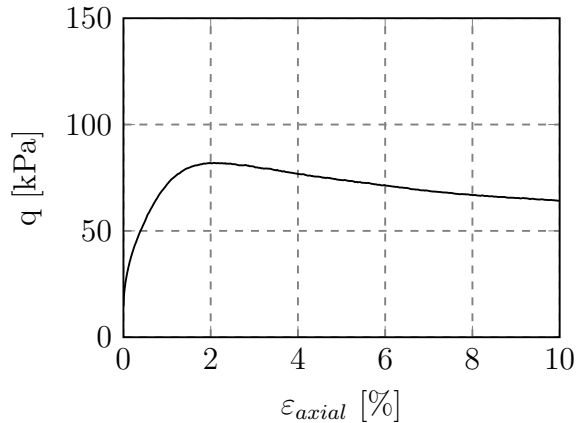
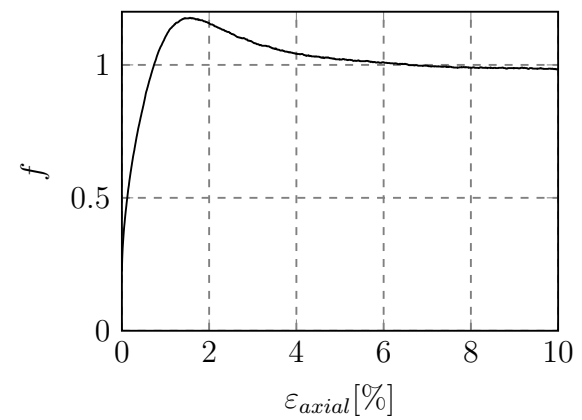
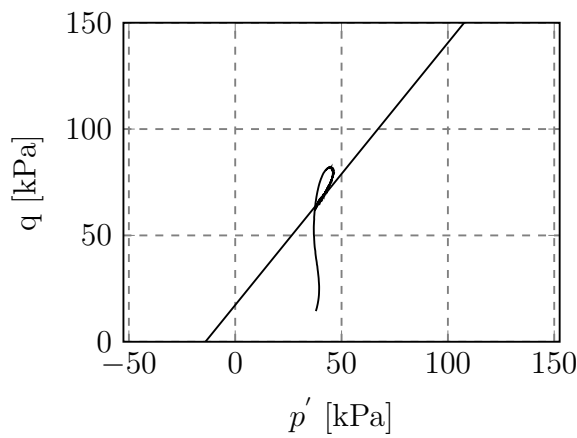
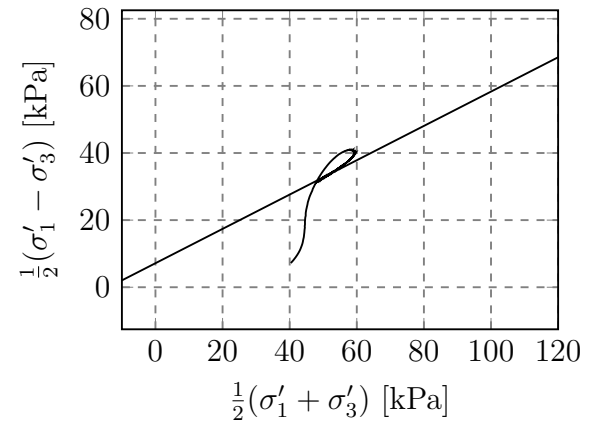
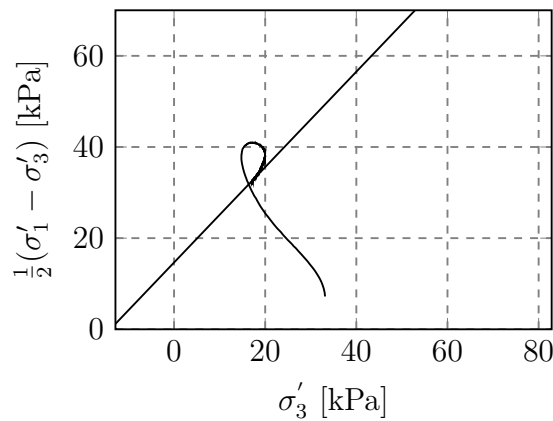
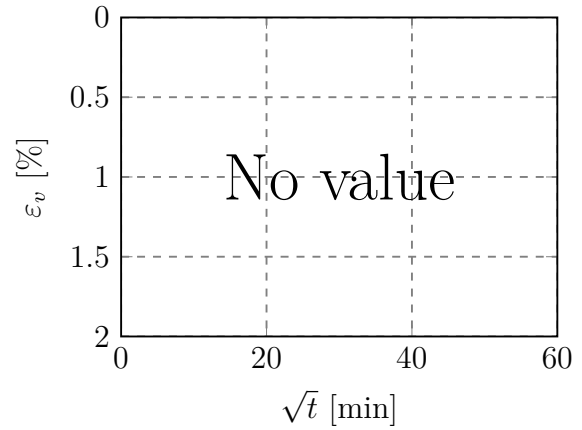


Figure I.5: Presentation of CAUc-results from depth 3.40 m. ΔV was not registered due to a malfunctioning scale.

KPG-CAUc-0440
Flotten, Tiller
54 mm sample

Depth	4.40 m
Sampling date	23.03.17
Opening date	06.03.17
Testing date	10.03.17
Vertical strain rate	3 %/hr
σ'_{v0}	55.3 kPa
w	48.3 %
γ	18.0 kN/m ³
K'_0	0.7
u	24 kPa
ΔV	2.49 cm ³
ε_v	1.1 %
Operator	KPG

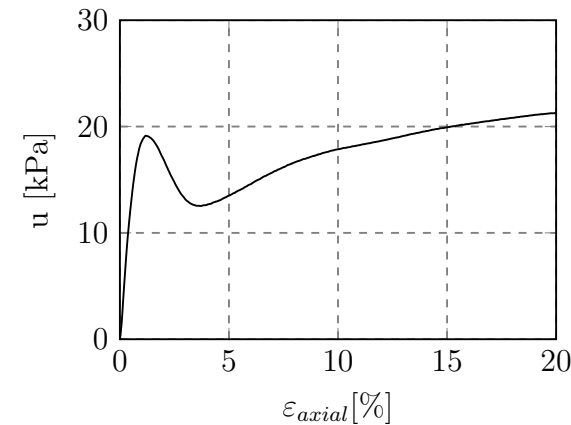
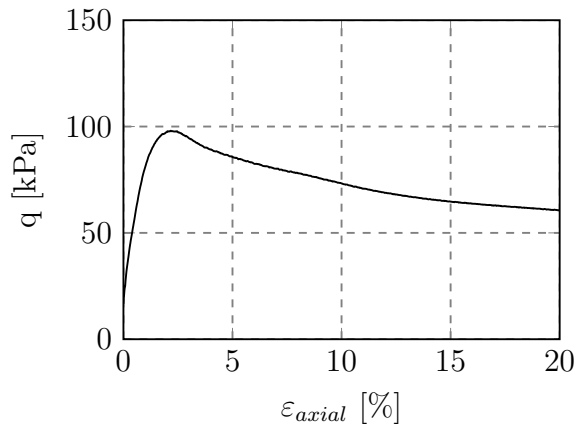
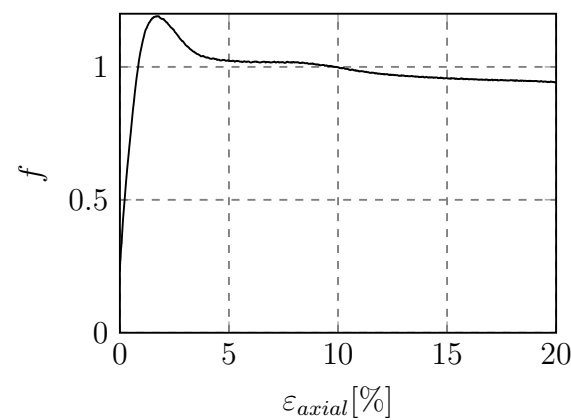
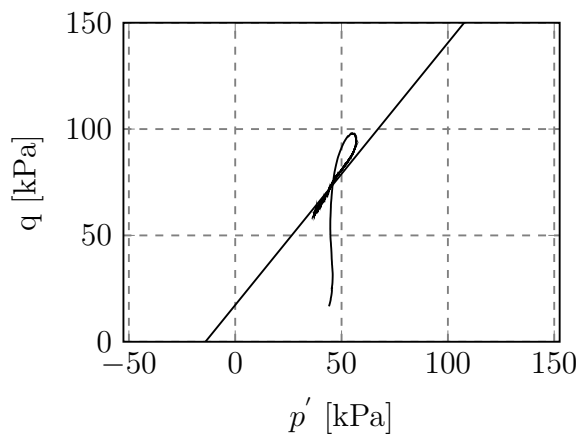
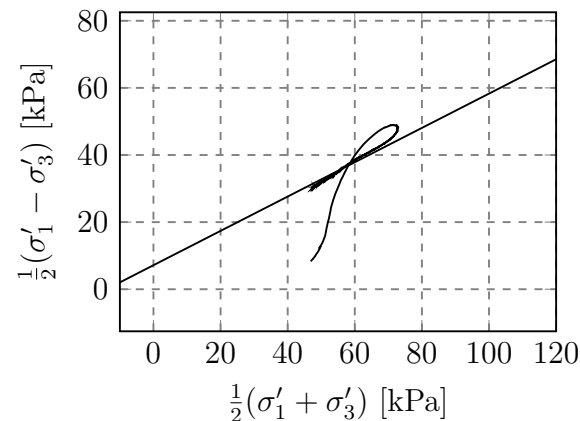
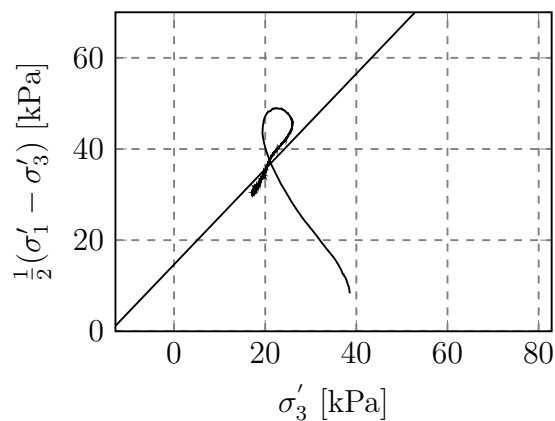
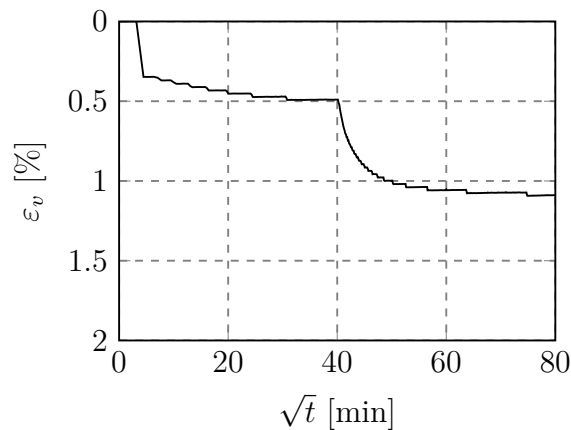


Figure I.6: Presentation of CAUc-results from depth 4.40 m.

KPG-CAUc-0540
Flotten, Trondheim
54 mm sample

Depth	5.40 m
Sampling date	23.02.17
Opening date	16.03.17
Testing date	21.03.17
Vertical strain rate	2 %/hr
σ'_{v0}	63.1 kPa
w	49.0 %
γ	17.0 kN/m ³
K'_0	0.7
u	34 kPa
ΔV	3.05 cm ³
ε_v	1.3 %
Operator	KPG

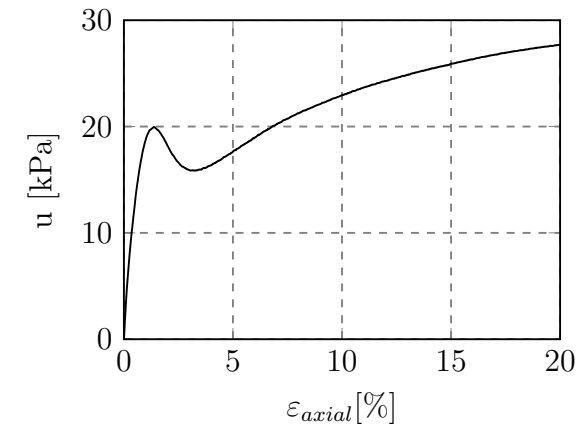
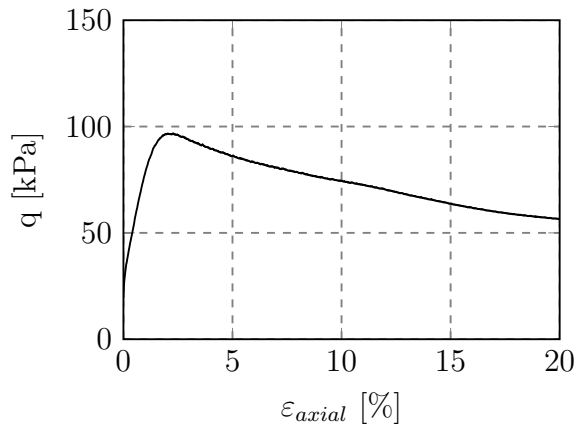
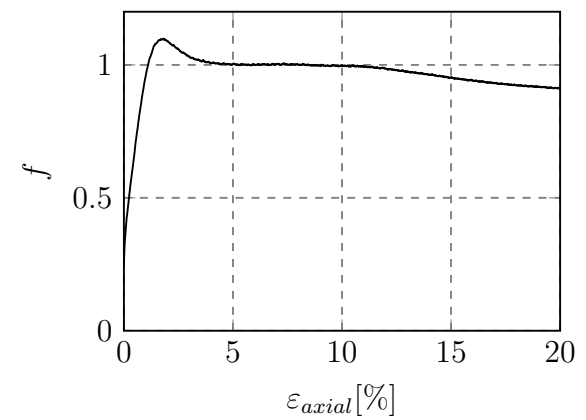
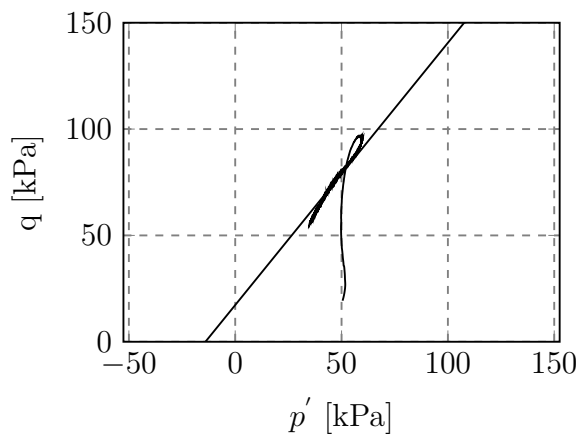
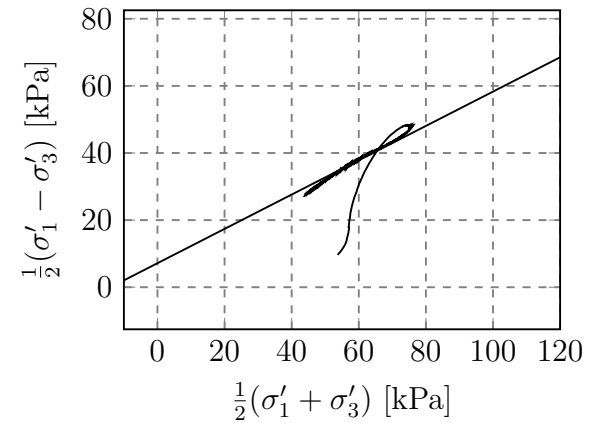
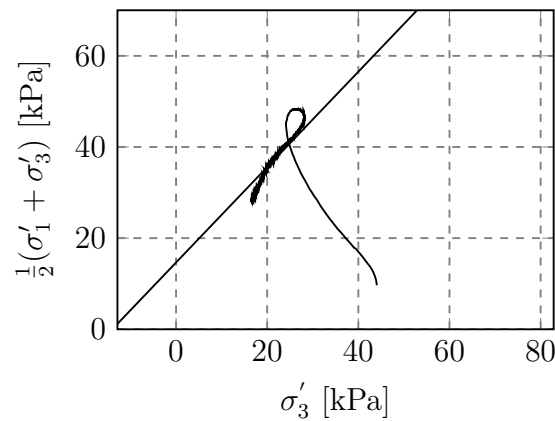
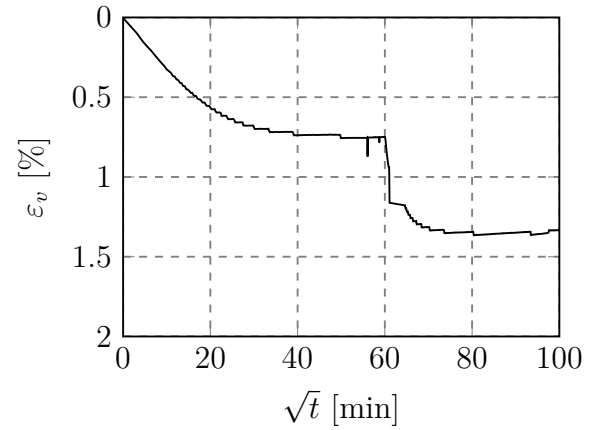


Figure I.7: Presentation of CAUc-results from depth 5.40 m.

KPG-CAUc-0640
Flotten, Trondheim
54 mm sample

Depth	6.40 m
Sampling date	23.03.17
Opening date	27.03.17
Testing date	29.03.17
Vertical strain rate	2 %/hr
σ'_{v0}	70.0 kPa
w	49.7 %
γ	17.6 kN/m ³
K'_0	0.7
u	44 kPa
ΔV	3.50 cm ³
ε_v	1.5 %
Operator	KPG

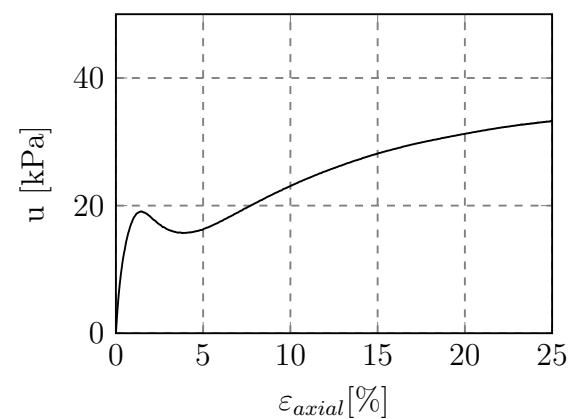
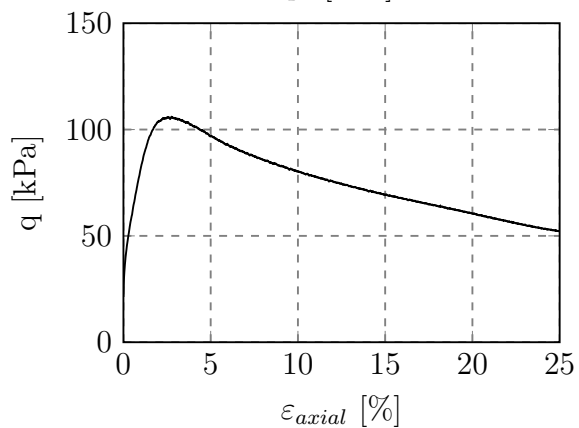
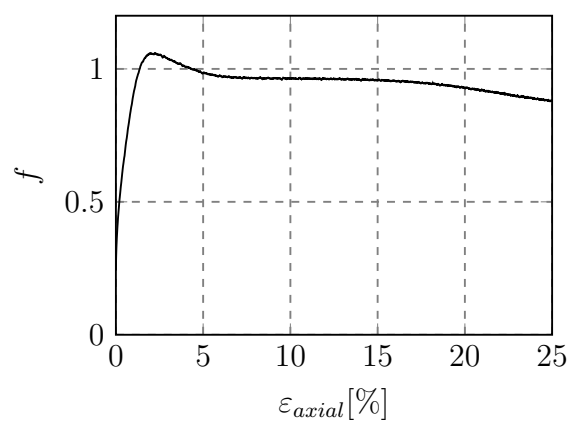
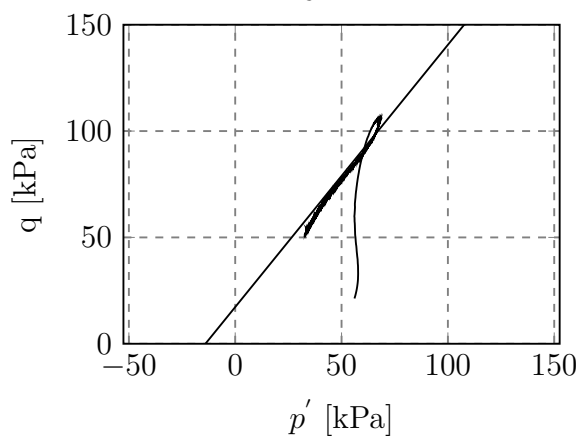
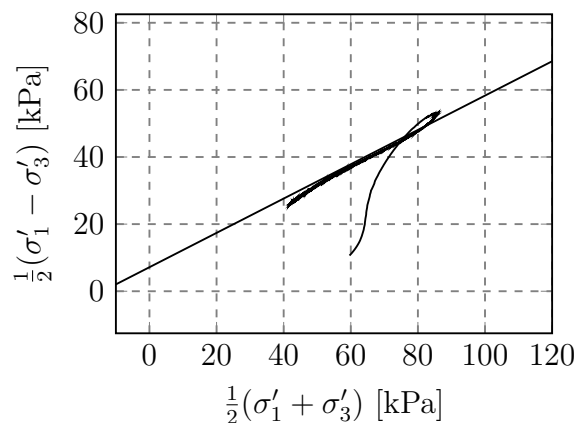
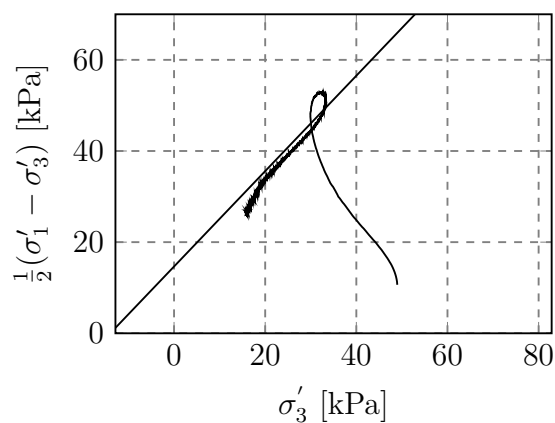
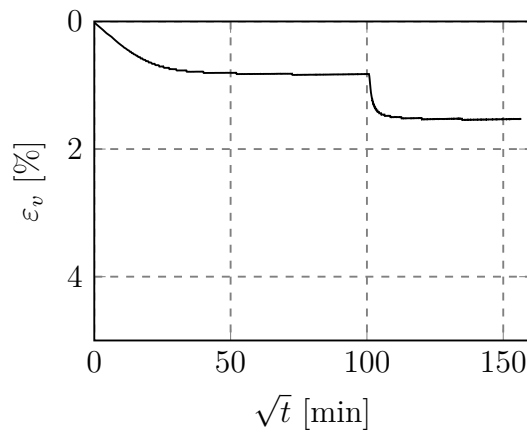


Figure I.8: Presentation of CAUc-results from depth 6.40 m.

KPG-CAUc-0740
Flotten, Trondheim
54 mm sample

Depth	7.40 m
Sampling date	23.03.17
Opening date	03.04.17
Testing date	05.04.17
Vertical strain rate	2 %/hr
σ'_{v0}	77.7 kPa
w	39.5 %
γ	17.3 kN/m ³
K'_0	0.7
u	54 kPa
ΔV	4.55 cm ³
ε_v	2.0 %
Operator	KPG

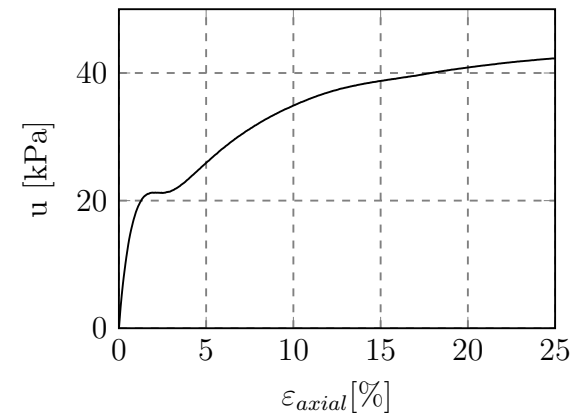
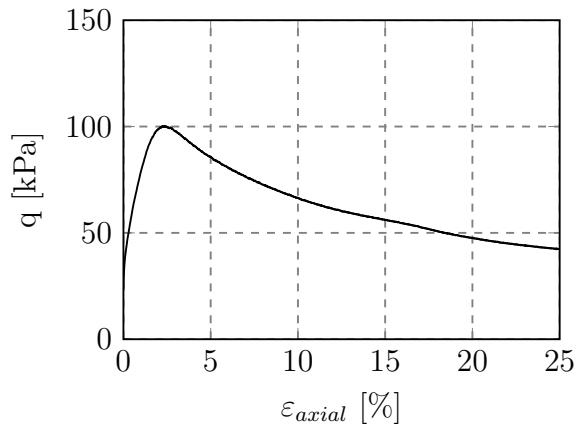
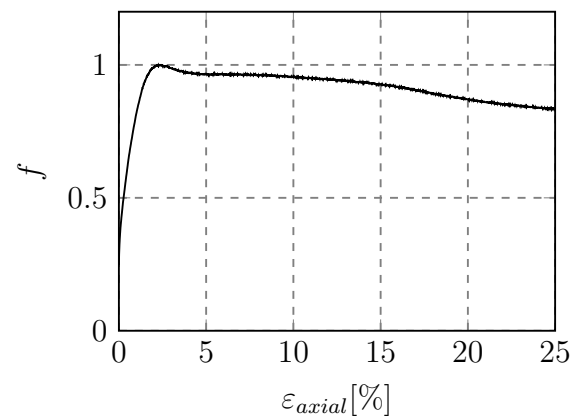
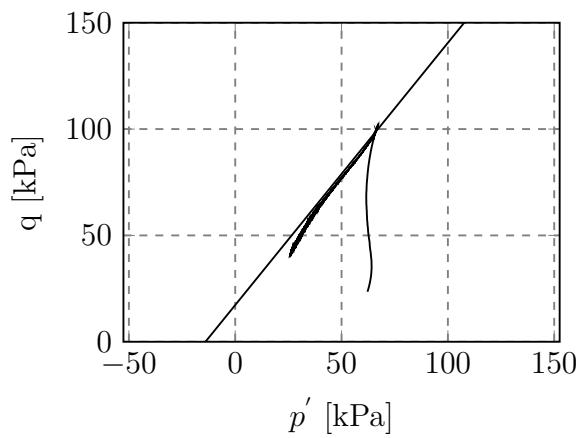
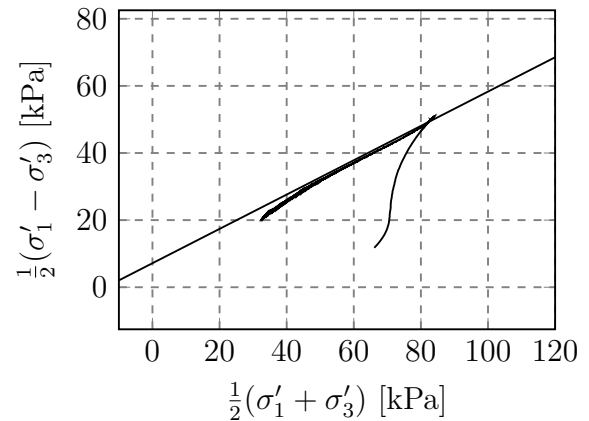
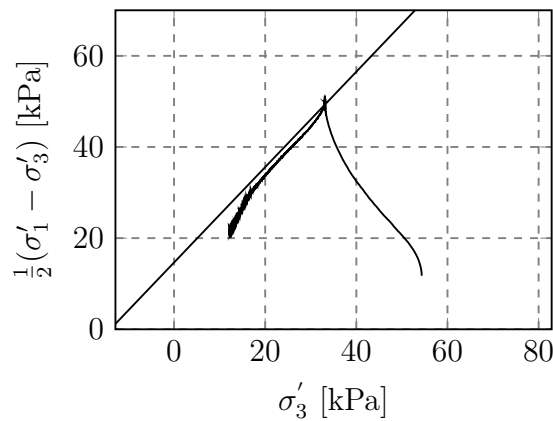
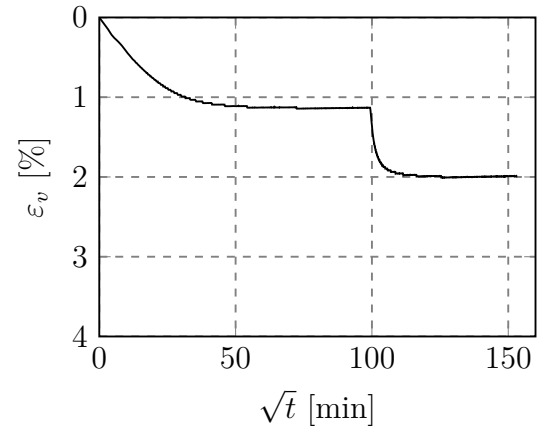


Figure I.9: Presentation of CAUc-results from depth 7.40 m.

CAUc-0934
Flotten, Trondheim
54 mm sample

Depth	9.34 m
Sampling date	23.02.17
Opening date	01.03.17
Testing date	10.03.17
Vertical strain rate	0.75 %/hr
σ_{v0}	93 kPa
w	48 %
γ (0-2 m)	17 kN/m ³
γ (2-9.34 m)	18 kN/m ³
K'_0	0.74
u	73.4 kPa
ΔV	-
ε_v	-
Operator	AnL & CSO

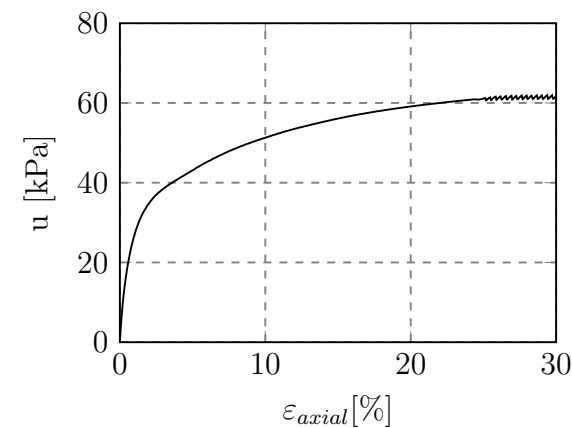
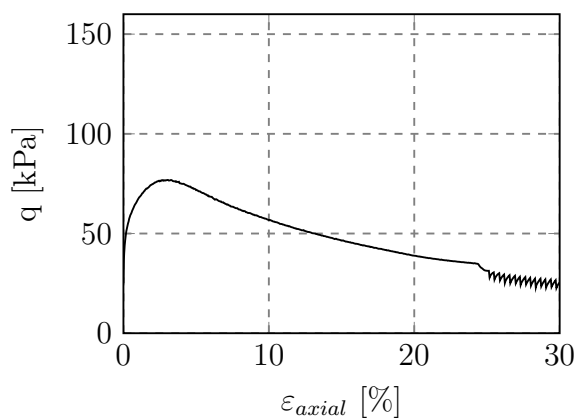
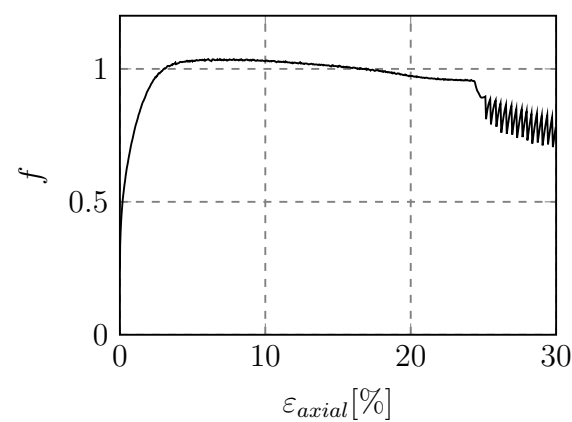
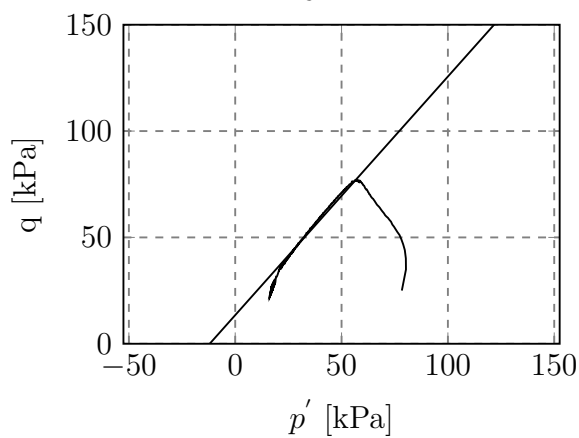
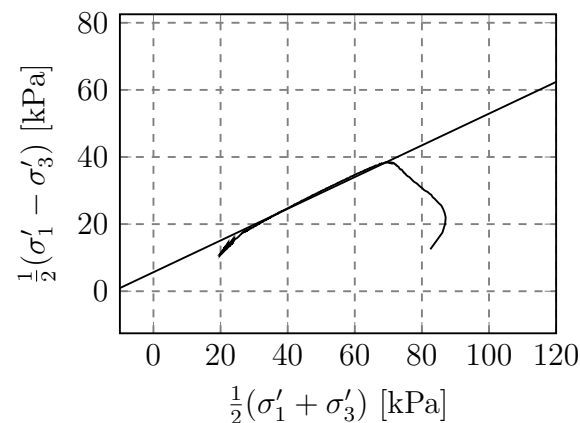
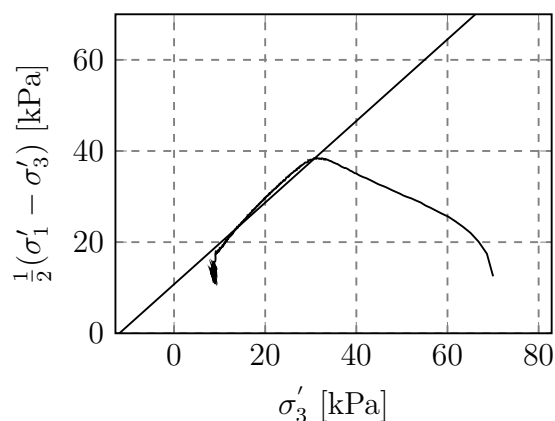
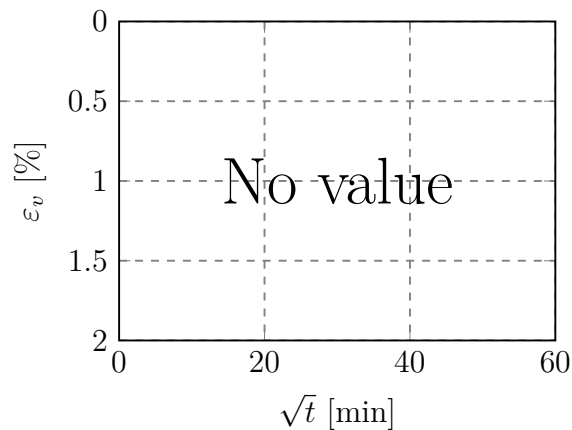


Figure I.10: Presentation of CAUc-results from depth 9.34 m. ΔV was not registered due to a malfunctioning scale.

KPG-CAUc-0940
Flotten, Trondheim
54 mm sample

Depth	9.40 m
Sampling date	07.04.17
Opening date	18.04.17
Testing date	21.04.17
Vertical strain rate	1.2 %/hr
σ'_{v0}	92.4 kPa
w	44.4 %
γ	17.1 kN/m ³
K'_0	0.7
u	74 kPa
ΔV	10.56 cm ³
ε_v	4.6 %
Operator	KPG

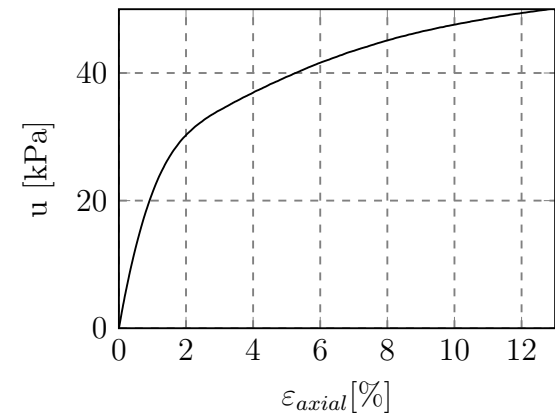
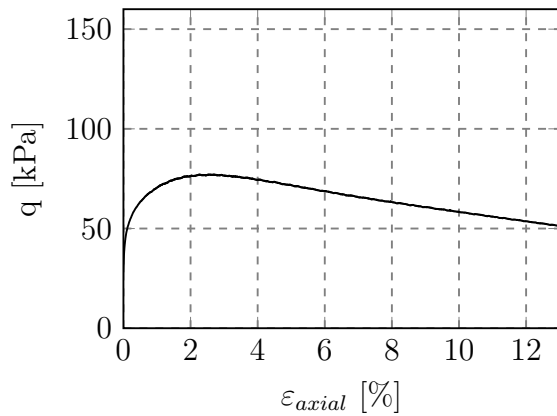
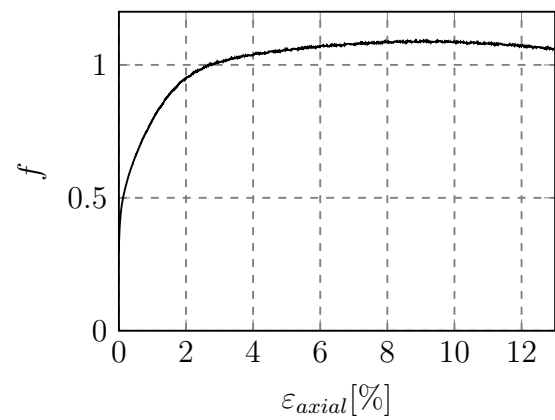
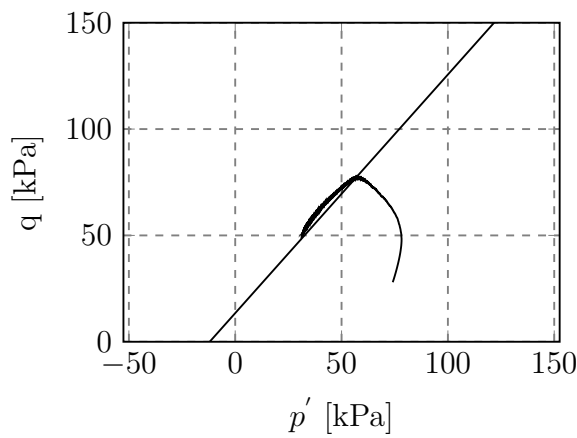
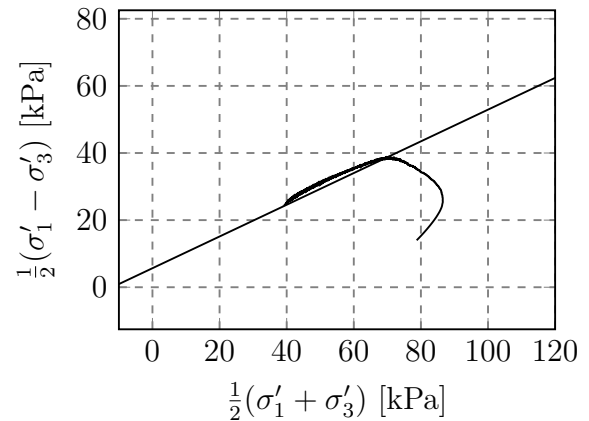
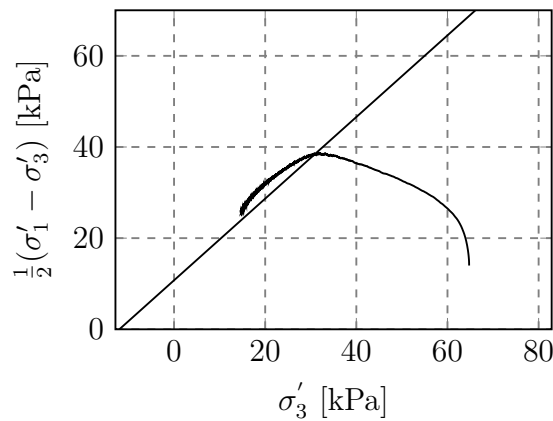
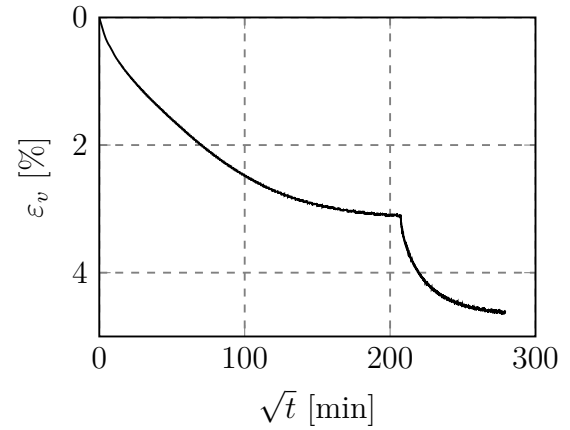


Figure I.11: Presentation of CAUc-results from depth 9.40 m.

CAUc-1015
Flotten, Trondheim
54 mm sample

Depth	10.15 m
Sampling date	23.02.17
Opening date	13.03.17
Testing date	13.03.17
Vertical strain rate	0.75 %/hr
σ'_{v0}	146 kPa
w	47 %
γ	18 kN/m ³
K'_0	0.74
u	34.7 kPa
ΔV	18.02 cm ³
ε_v	7.9 %
Operator	AnL & CSO

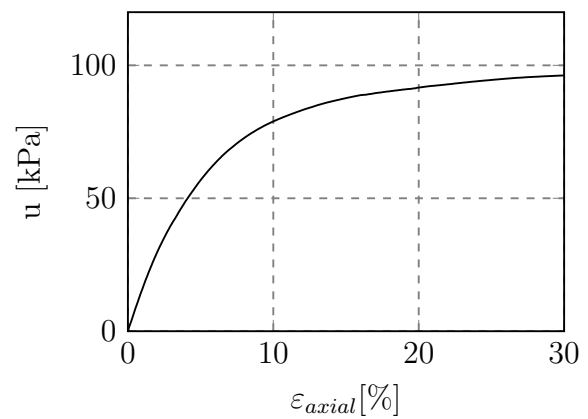
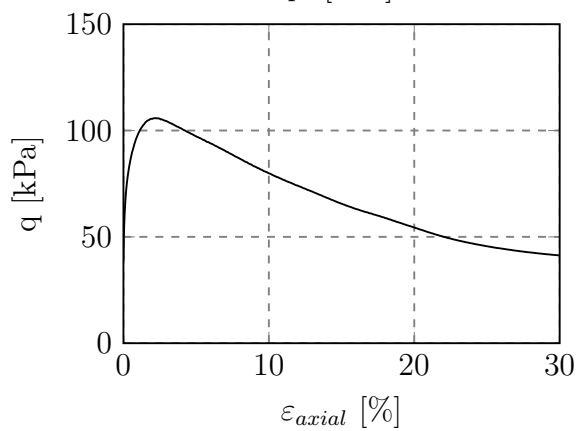
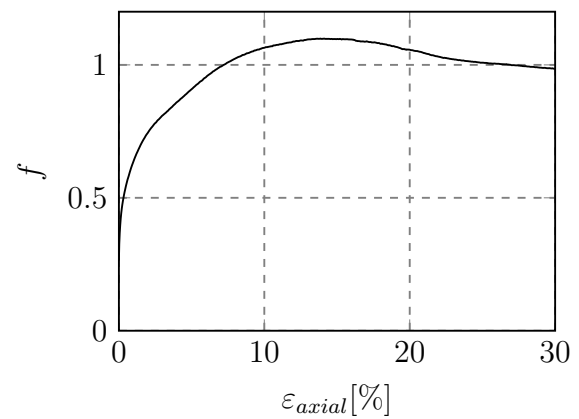
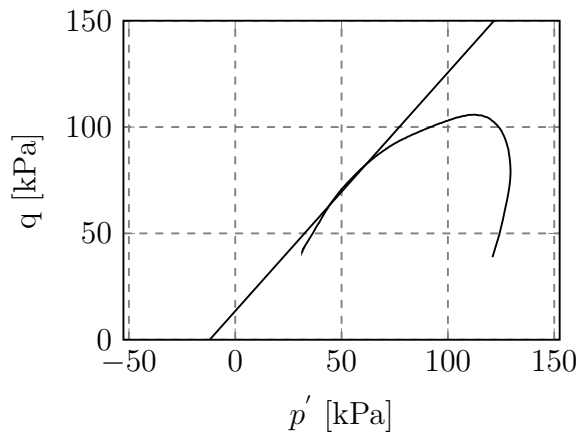
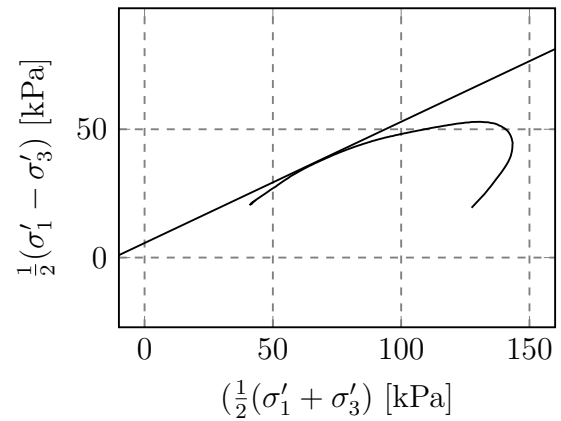
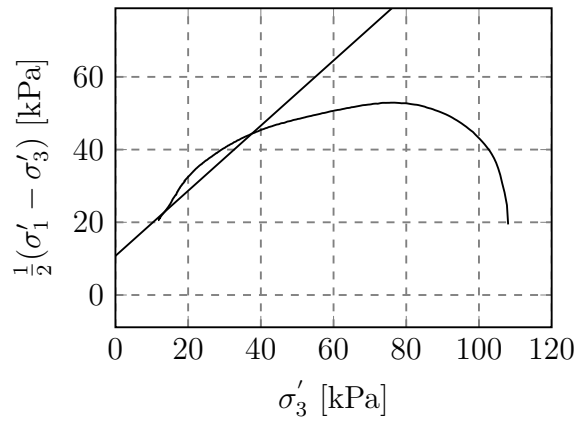
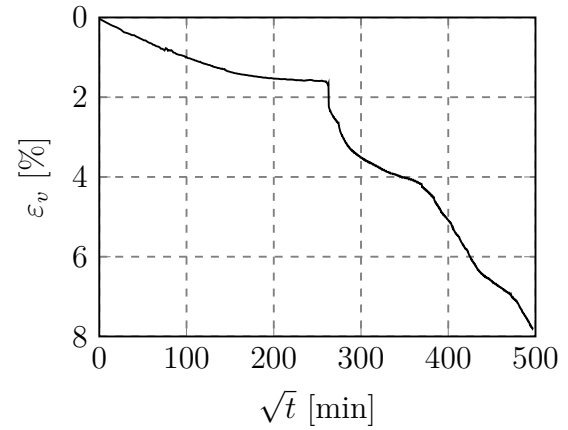


Figure I.12: Presentation of CAUc-results from depth 10.15 m.

CAUc-1036
Flotten, Trondheim
54 mm sample

Depth	10.36 m
Sampling date	23.02.17
Opening date	13.03.17
Testing date	03.04.17
Vertical strain rate	0.75 %/hr
σ'_{v0}	148 kPa
w	38 %
γ	18 kN/m ³
K'_0	0.79
u	38.1 kPa
ΔV	18.52 cm ³
ε_v	8.1 %
Operator	AnL & CSO

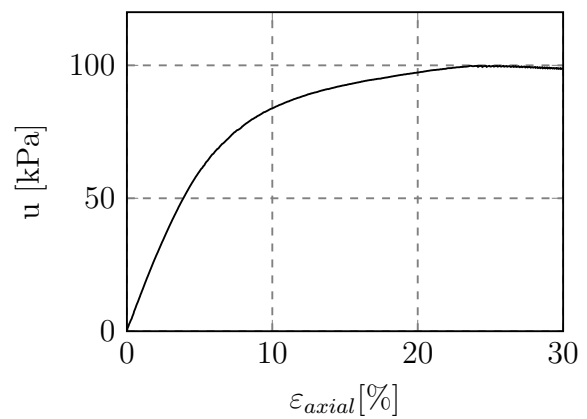
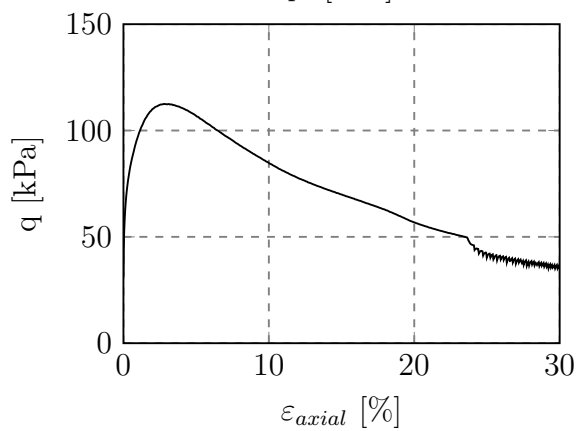
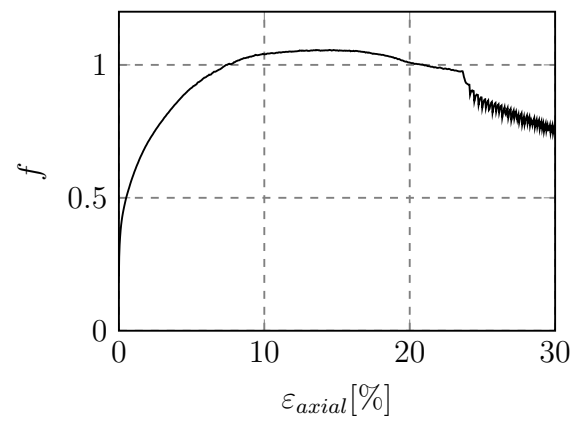
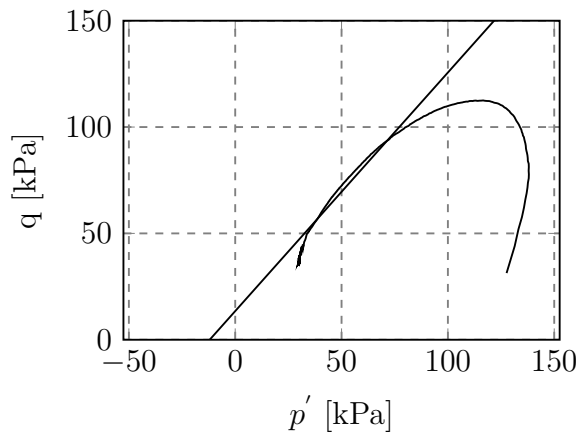
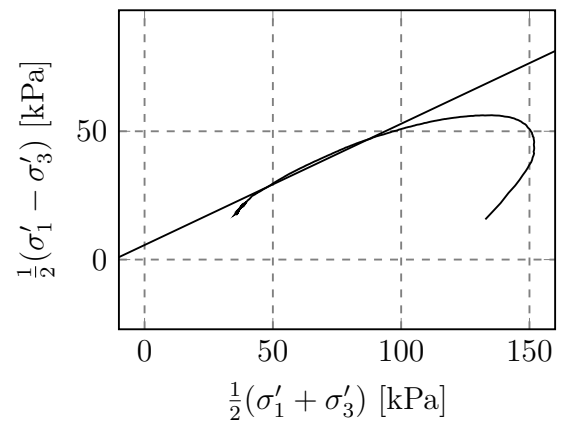
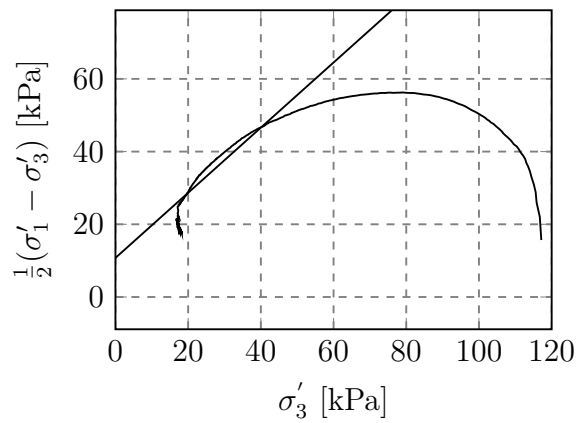
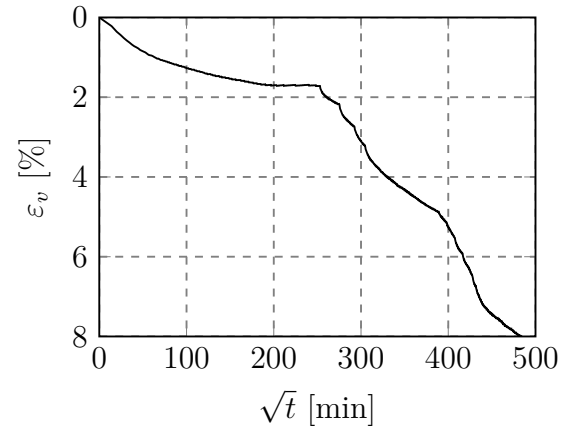


Figure I.13: Presentation of CAUc-results from depth 10.36 m.

KPG-CAU_c-1040
Flotten, Trondheim
54 mm sample

Depth	10.40 m
Sampling date	26.04.17
Opening date	27.04.17
Testing date	29.04.17
Vertical strain rate	1.2 %/hr
σ'_{v0}	99.6 kPa
w	50.8 %
γ	17.5 kN/m ³
K'_0	0.7
u	84 kPa
ΔV	8.44 cm ³
ϵ_v	3.7 %
Operator	KPG

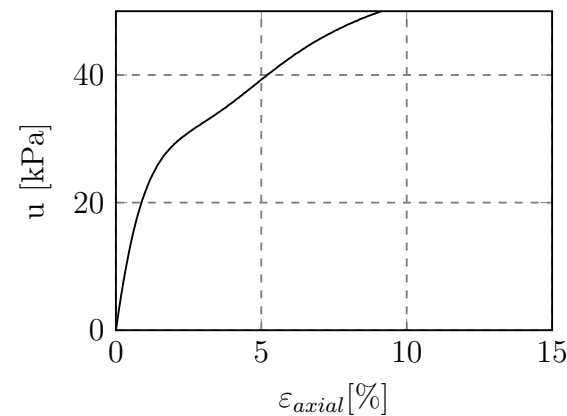
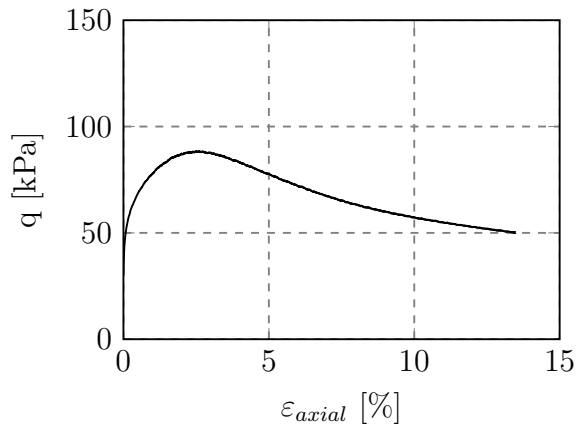
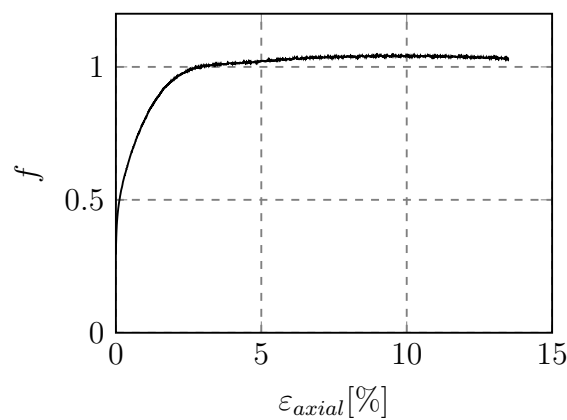
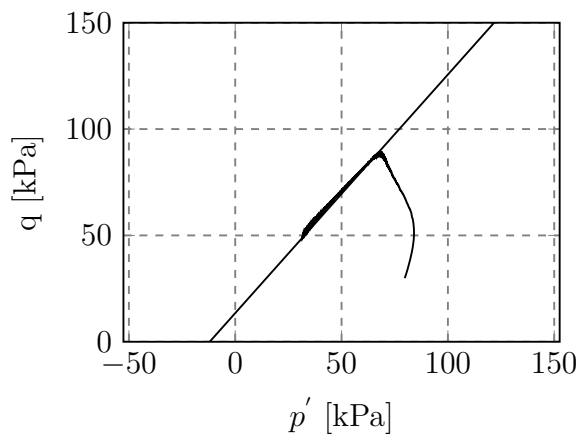
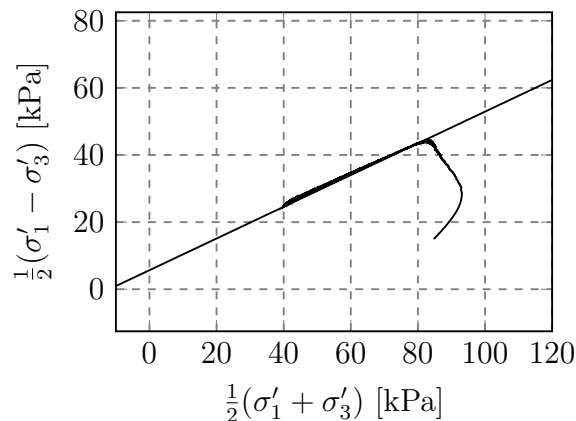
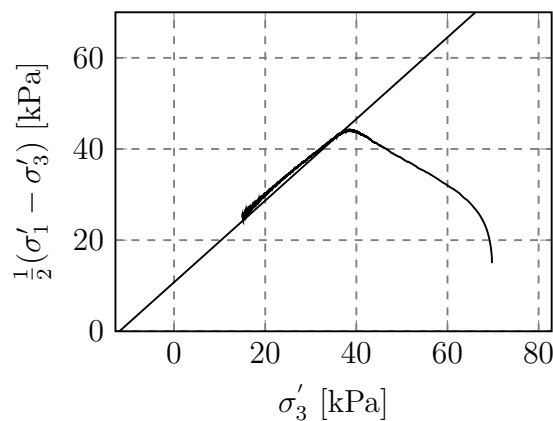
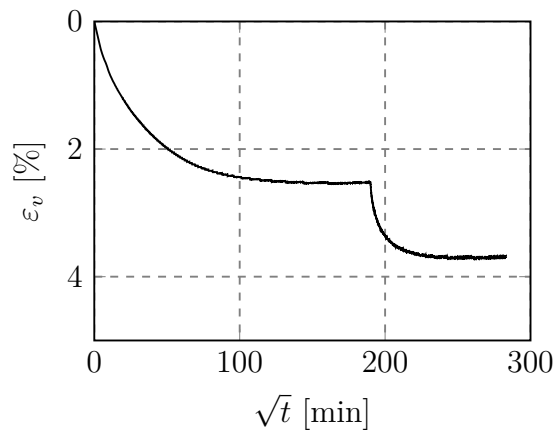


Figure I.14: Presentation of CAU_c-results from depth 10.40 m.

CAUc-1056
Flotten, Trondheim
54 mm sample

Depth	10.56 m
Sampling date	23.02.17
Opening date	13.03.17
Testing date	27.03.17
Vertical strain rate	0.75 %/hr
σ'_{v0}	152 kPa
w	39 %
γ	18 kN/m ³
K'_0	0.79
u	38.1 kPa
ΔV	15 cm ³
ε_v	6.6 %
Operator	AnL & CSO

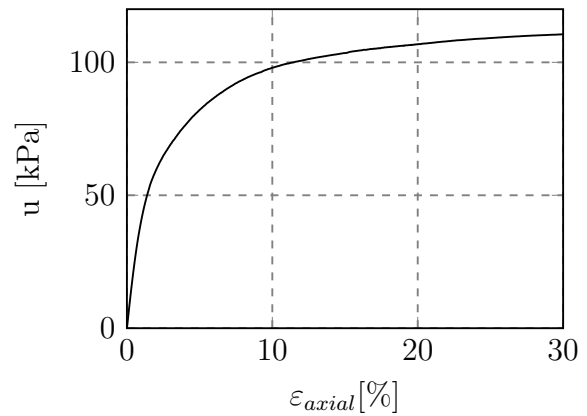
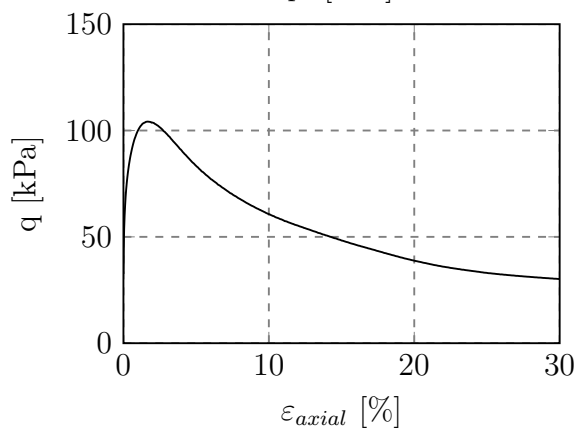
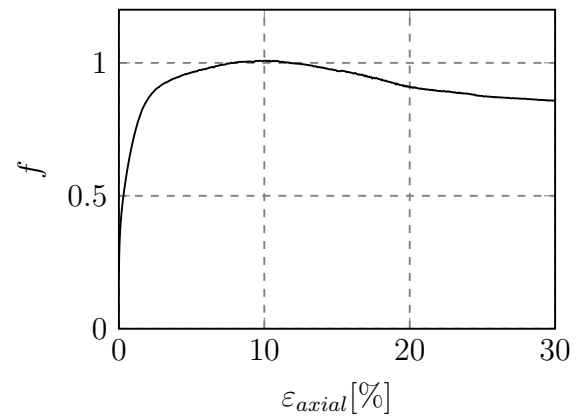
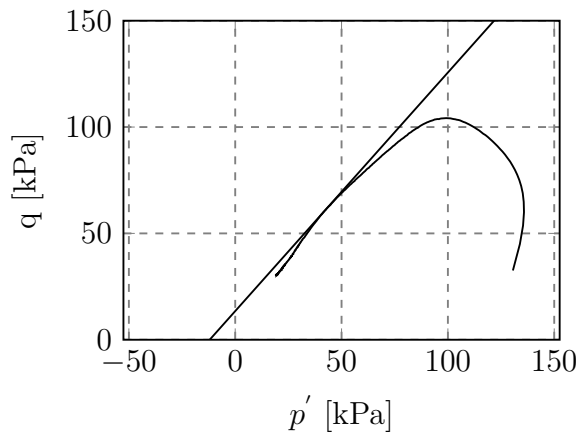
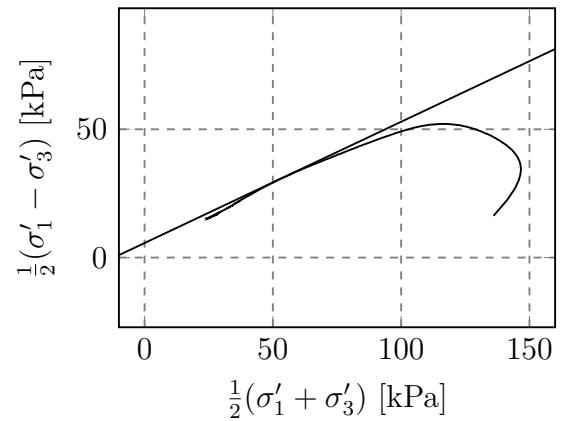
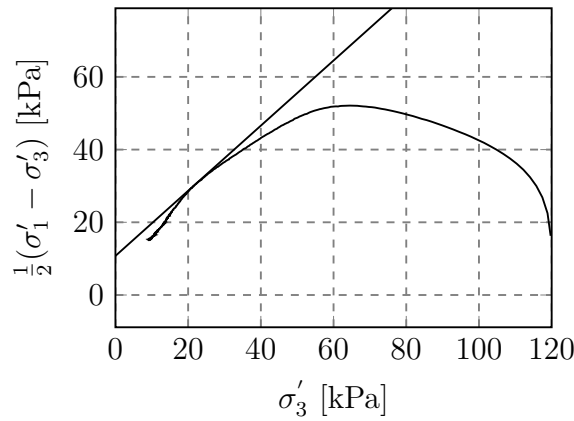
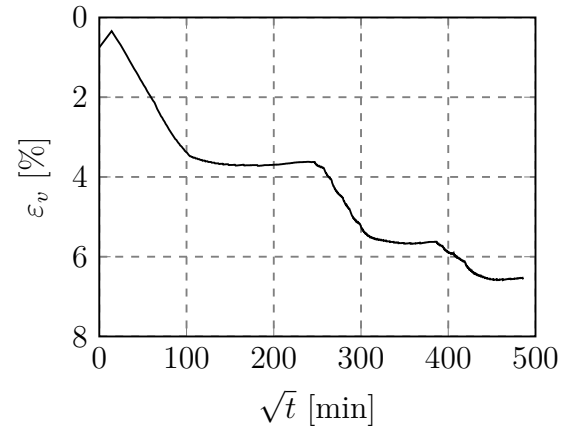


Figure I.15: Presentation of CAUc-results from depth 10.56 m.

KPG-CAUc-1153
Flotten, Trondheim
54 mm sample

Depth	11.53 m
Sampling date	26.04.17
Opening date	01.05.17
Testing date	03.05.17
Vertical strain rate	1.2 %/hr
σ'_{v0}	108.1 kPa
w	33.8 %
γ	17.2 kN/m ³
K'_0	0.7
u	95.3 kPa
ΔV	8.86 cm ³
ϵ_v	3.9 %
Operator	KPG

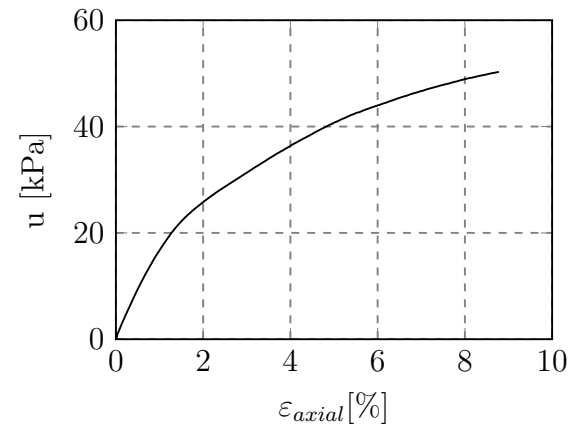
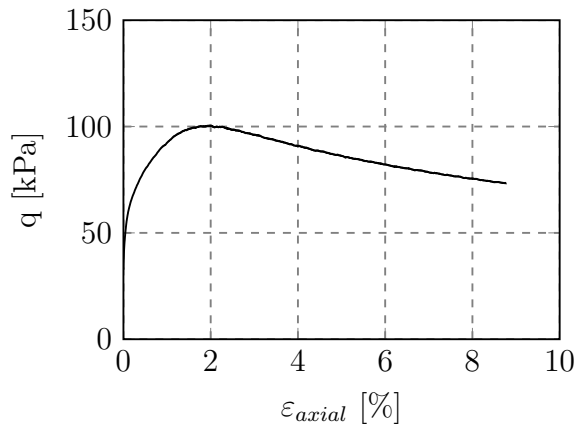
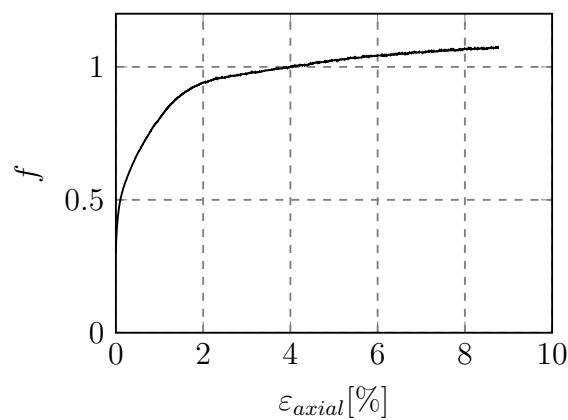
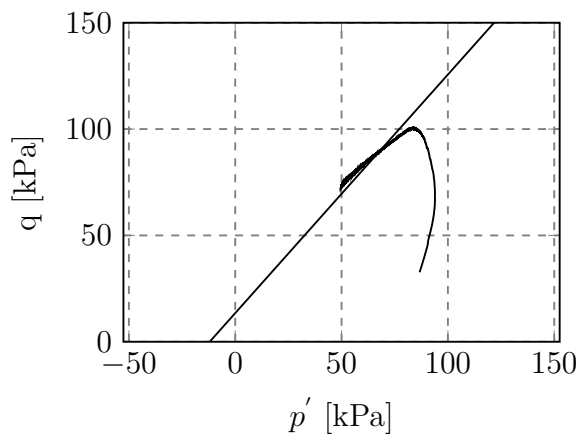
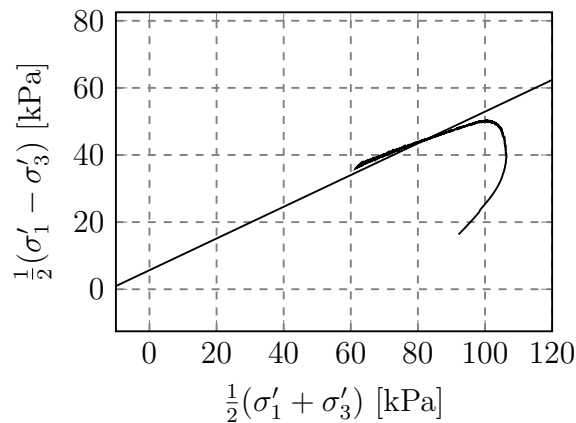
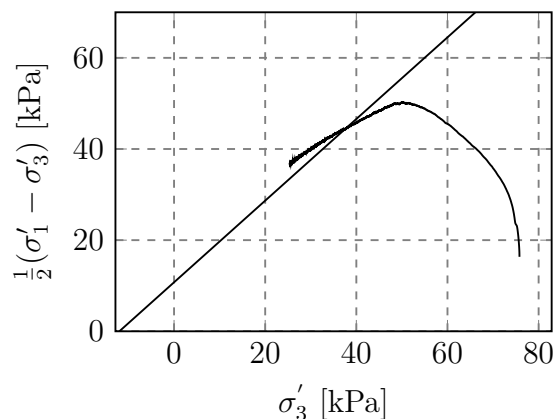
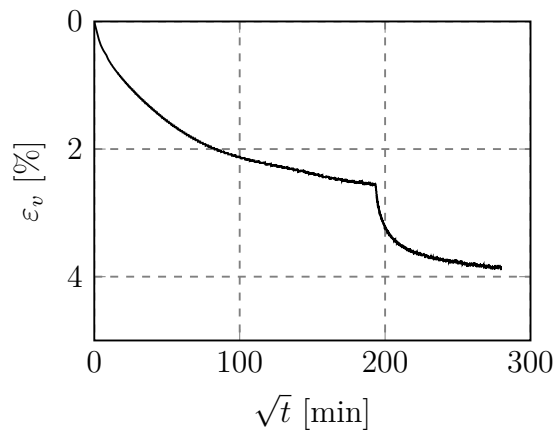


Figure I.16: Presentation of CAUc-results from depth 11.53 m.

KPG-CIUc-0526
Flotten, Trondheim
54 mm sample

Depth	5.26 m
Sampling date	23.02.17
Opening date	16.03.17
Testing date	20.03.17
Vertical strain rate	2 %/hr
σ'_{v0}	49.4 kPa
w	49.0 %
γ	17.0 kN/m ³
u	32.6 kPa
ΔV	2.81 cm ³
ε_{vol}	1.2 %
Operator	KPG

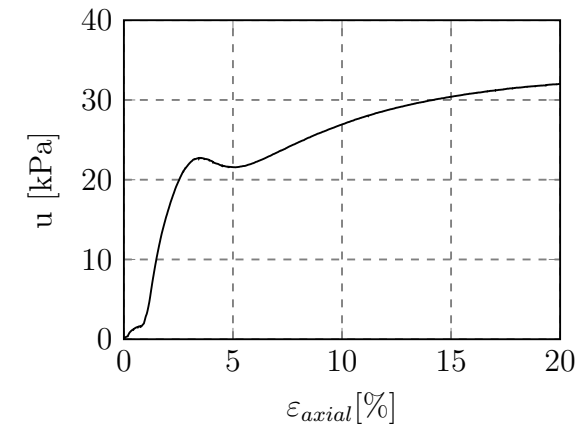
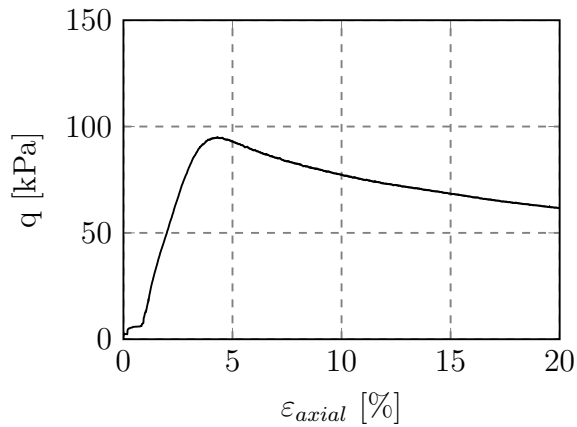
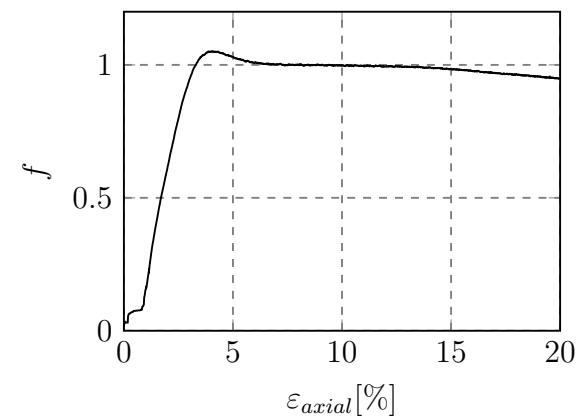
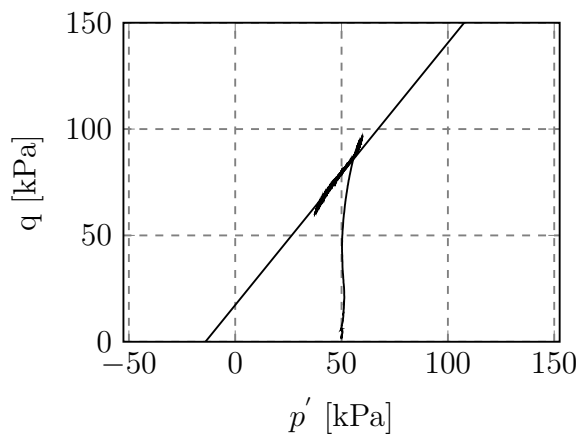
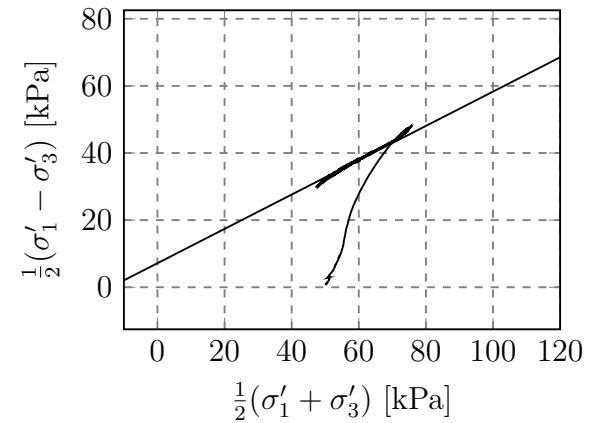
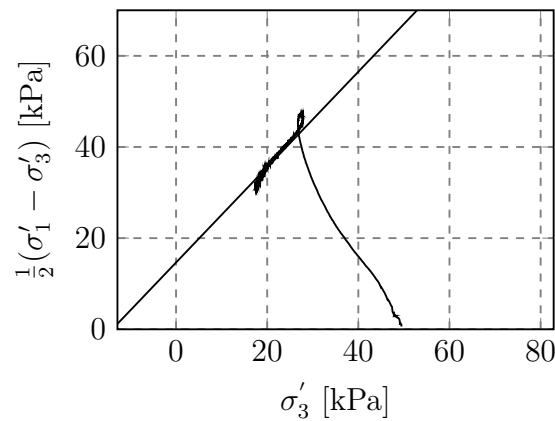
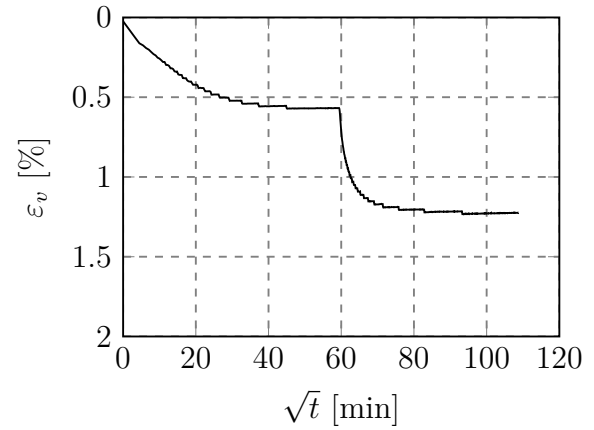


Figure I.17: Presentation of CIUc-results from depth 5.26 m.

KPG-CIUc-0540
Flotten, Trondheim
54 mm sample

Depth	5.40 m
Sampling date	25.01.17
Opening date	02.02.17
Testing date	16.02.17
Vertical strain rate	3 %/hr
σ'_{v0}	46.5 kPa
w	49.0 %
γ	17.0 kN/m ³
u	34 kPa
ΔV	2.83 cm ³
ε_{vol}	1.2 %
Operator	KPG

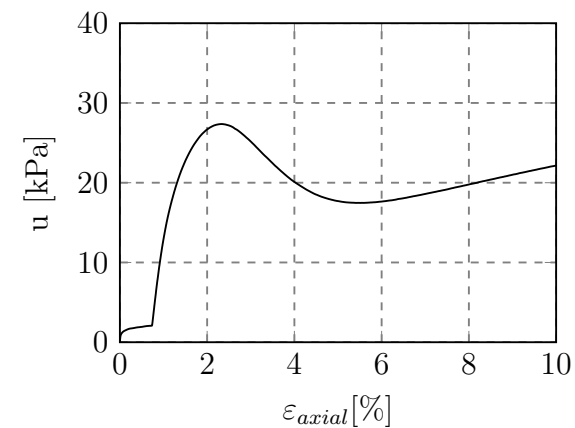
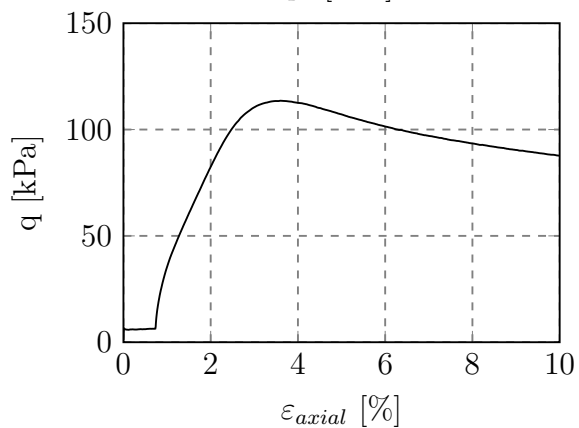
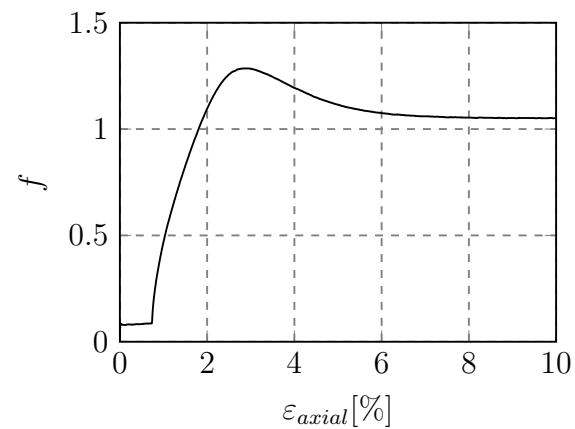
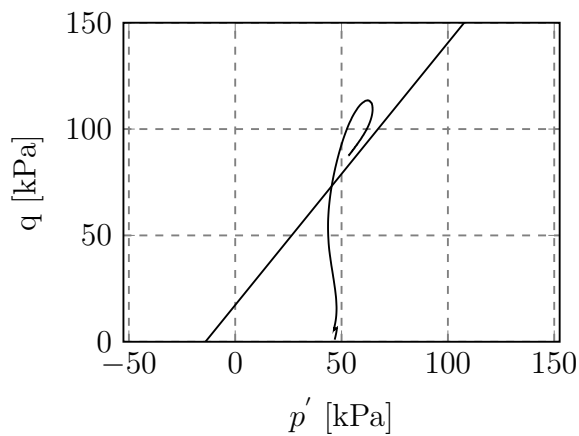
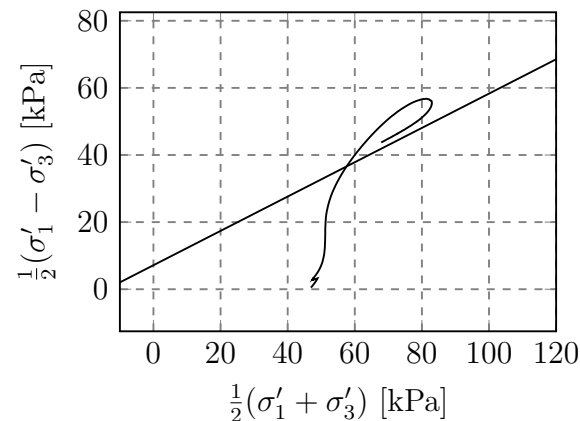
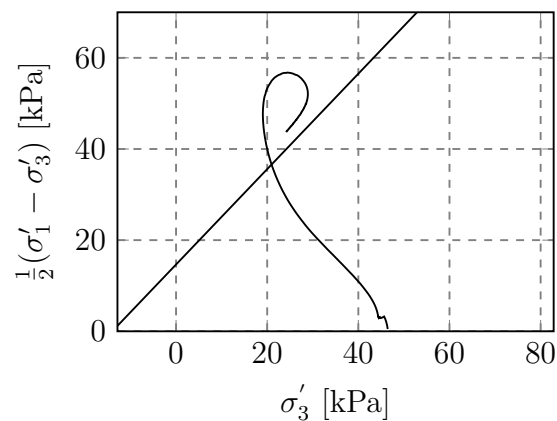
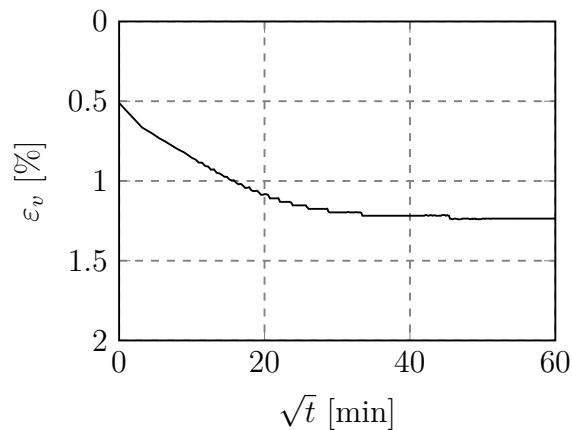


Figure I.18: Presentation of CIUc-results from depth 5.40 m. Please note that this specimen is from the borehole 54MM_1.

KPG-CIUc-0626
Flotten, Trondheim
54 mm sample

Depth	6.26 m
Sampling date	23.03.17
Opening date	27.03.17
Testing date	28.03.17
Vertical strain rate	2 %/hr
σ'_{v0}	55.3 kPa
w	49.7 %
γ	17.6 kN/m ³
u	42.6 kPa
ΔV	18.47 cm ³
ε_{vol}	8.1 %
Operator	KPG

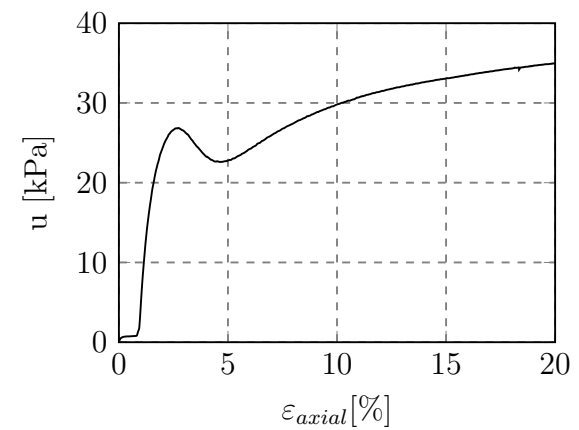
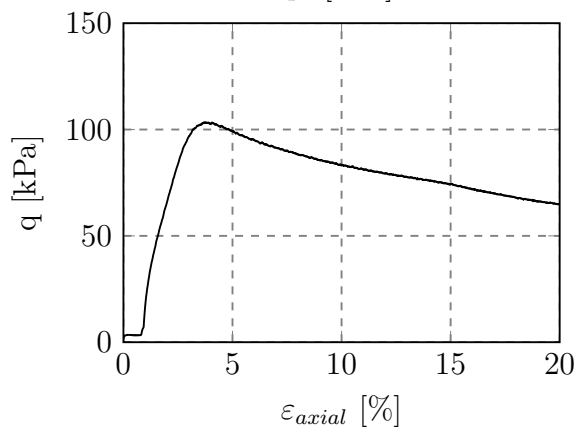
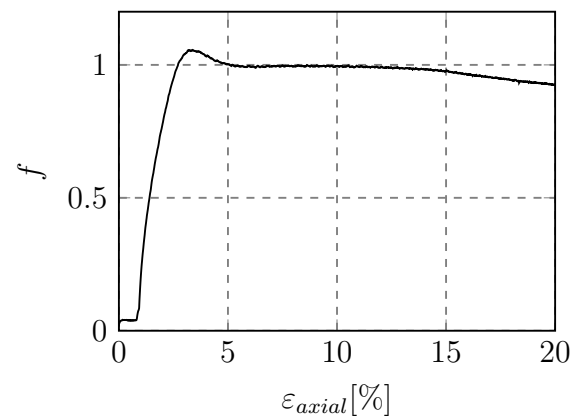
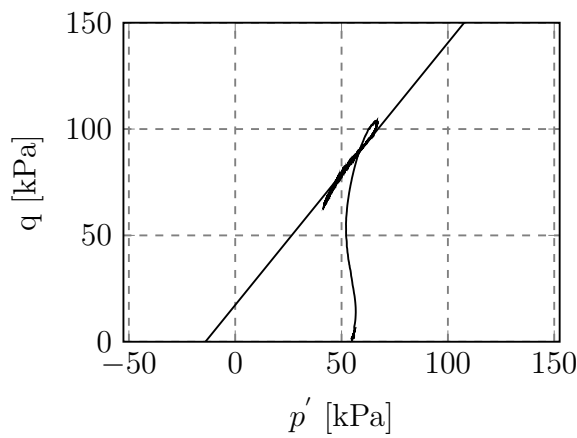
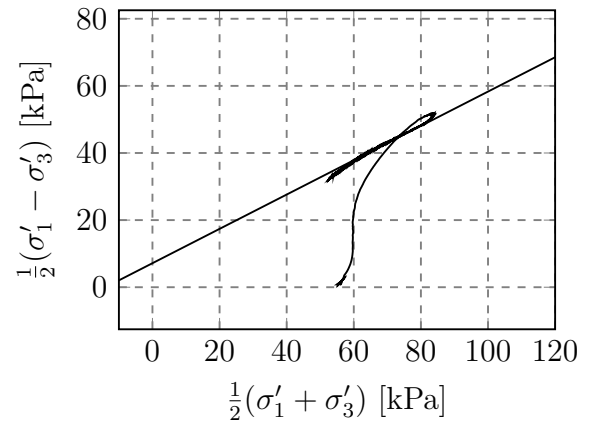
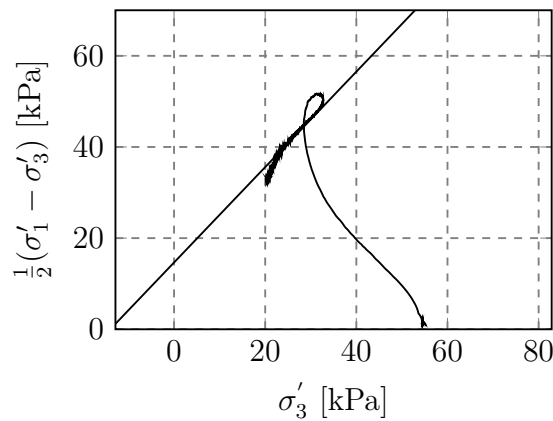
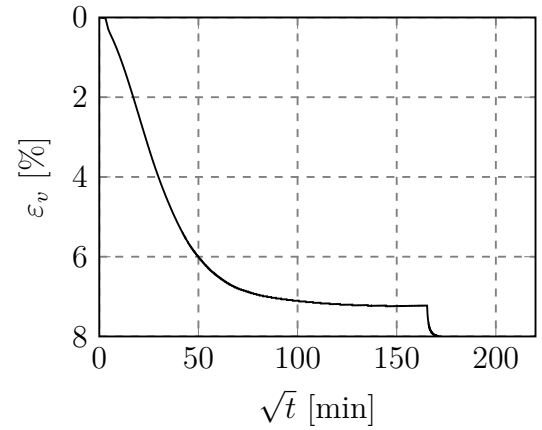


Figure I.19: Presentation of CIUc-results from depth 6.26 m.

KPG-CIUc-0726
Flotten, Trondheim
54 mm sample

Depth	7.26 m
Sampling date	23.03.17
Opening date	03.04.17
Testing date	04.04.17
Vertical strain rate	2 %/hr
σ'_{v0}	56.4 kPa
w	39.5 %
γ	17.4 kN/m ³
u	52.6 kPa
ΔV	4.16 cm ³
ϵ_{vol}	1.8 %
Operator	KPG

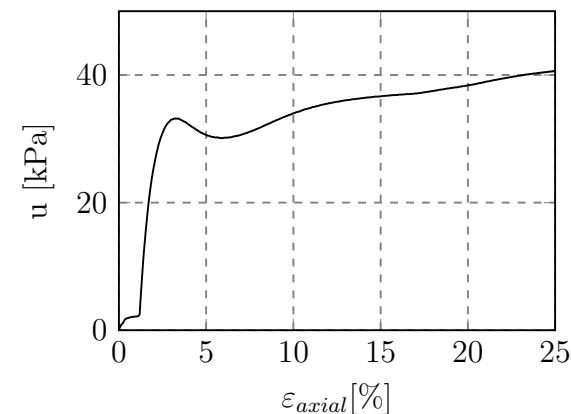
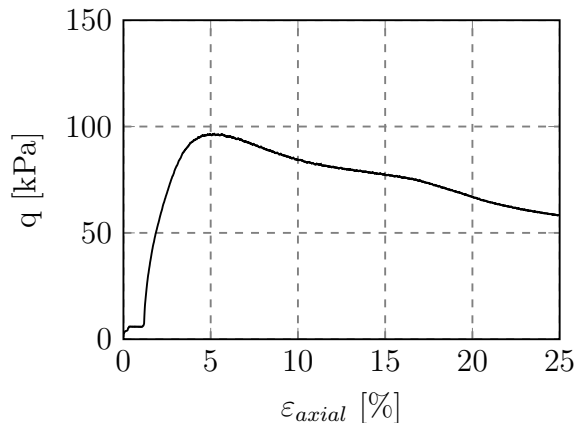
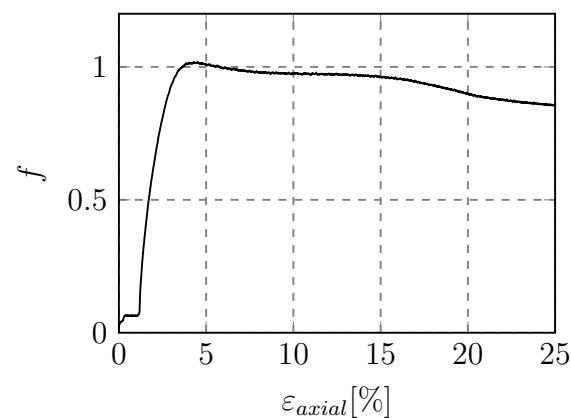
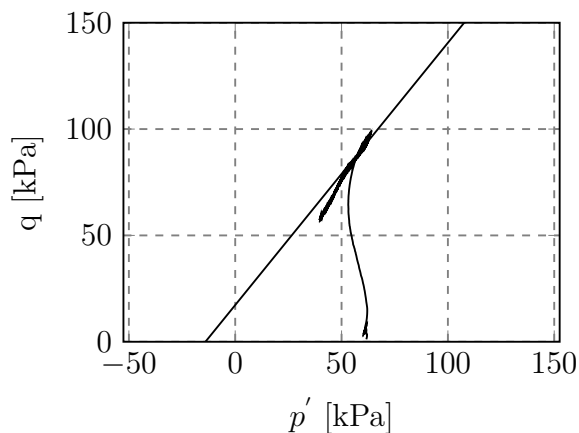
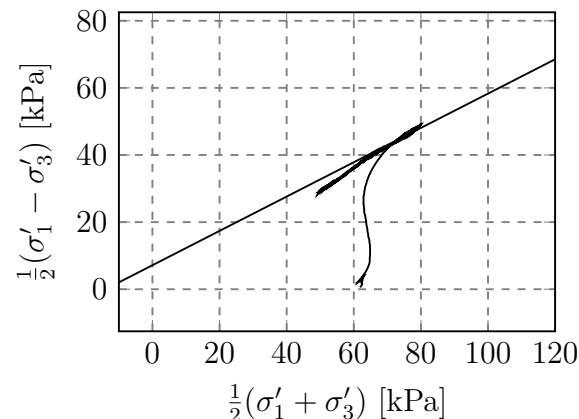
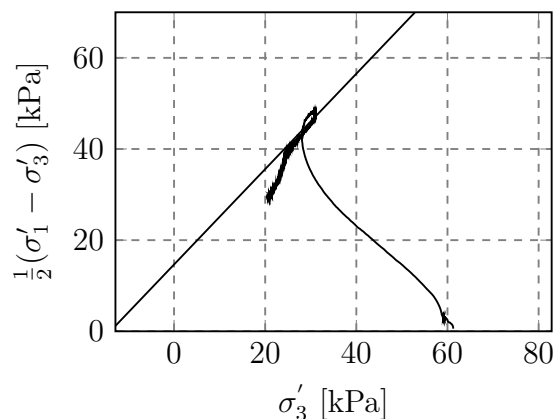
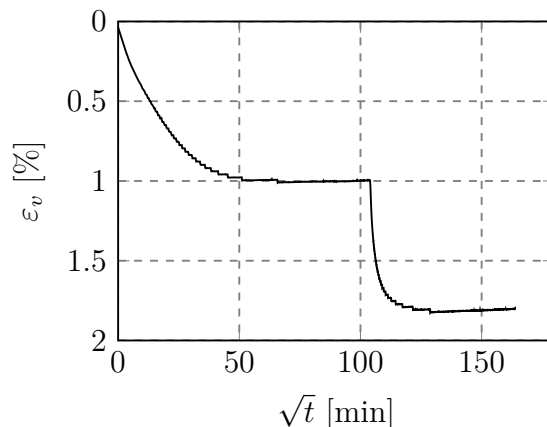


Figure I.20: Presentation of CIUc-results from depth 7.26 m.

KPG-CIUc-0926
Flotten, Trondheim
54 mm sample

Depth	9.26 m
Sampling date	07.04.17
Opening date	18.04.17
Testing date	20.04.17
Vertical strain rate	1.2 %/hr
σ'_{v0}	74.5 kPa
w	44.4 %
γ	17.1 kN/m ³
u	72.6 kPa
ΔV	9.63 cm ³
ε_{vol}	4.2 %
Operator	KPG

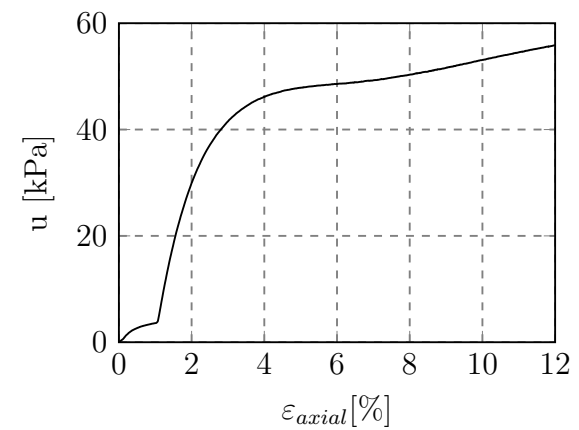
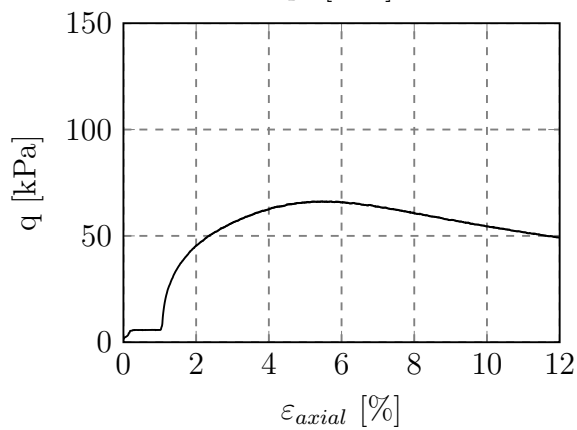
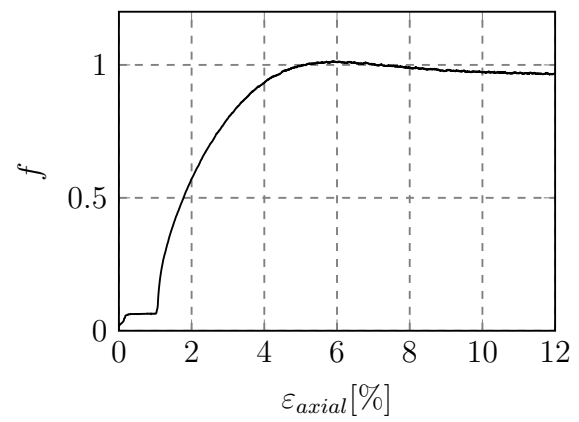
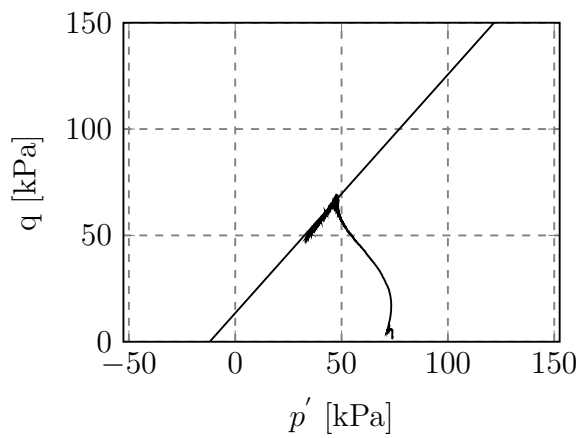
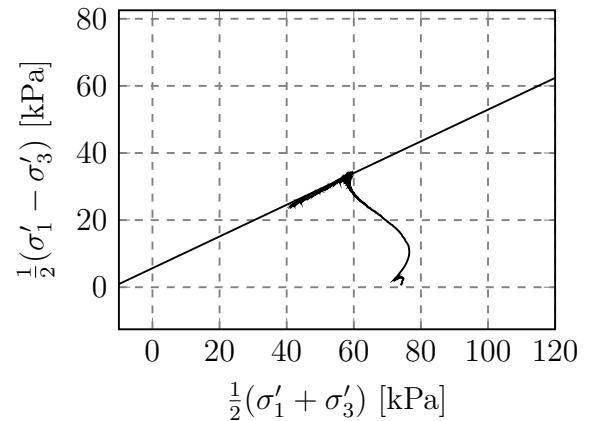
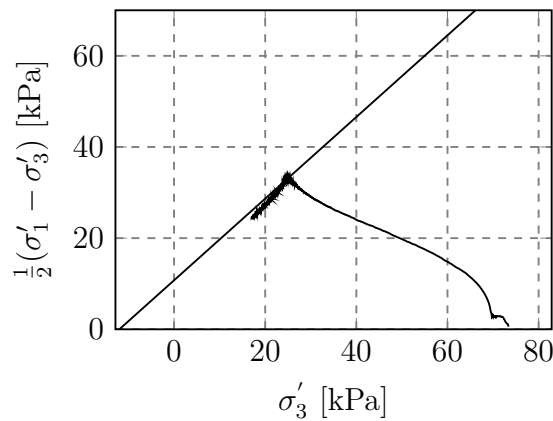
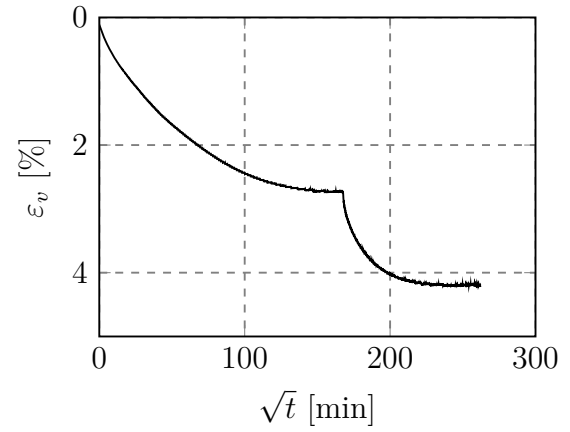


Figure I.21: Presentation of CIUc-results from depth 9.26 m.

KPG-CIUc-1026
Flotten, Trondheim
54 mm sample

Depth	10.26 m
Sampling date	26.04.17
Opening date	27.04.17
Testing date	28.04.17
Vertical strain rate	1.2 %/hr
σ'_{v0}	89.0 kPa
w	50.8 %
γ	17.5 kN/m ³
u	82.6 kPa
ΔV	9.84 cm ³
ε_{vol}	4.3 %
Operator	KPG

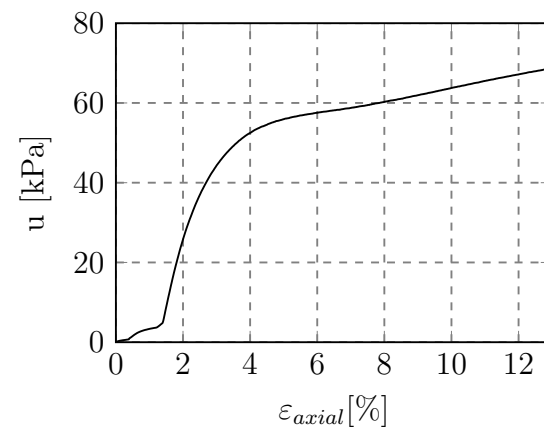
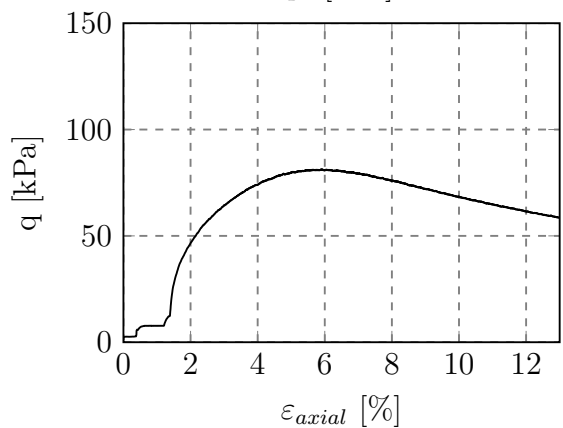
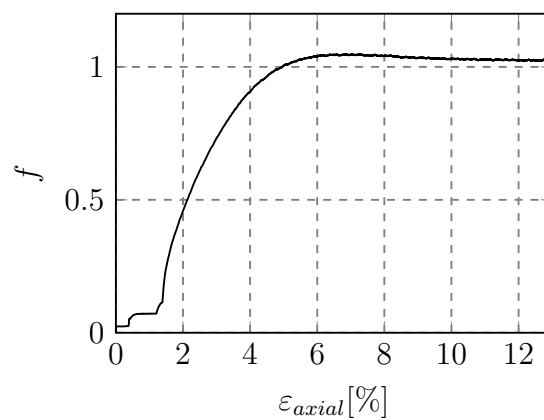
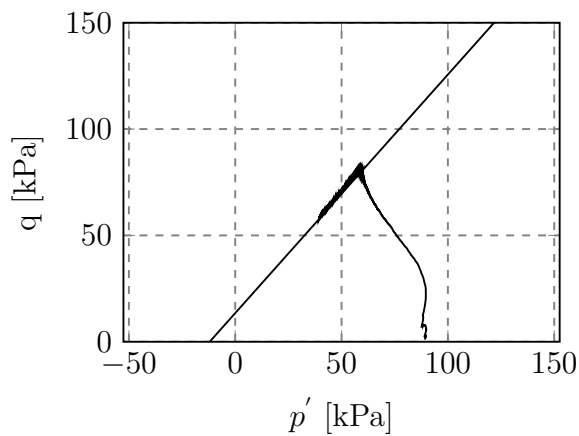
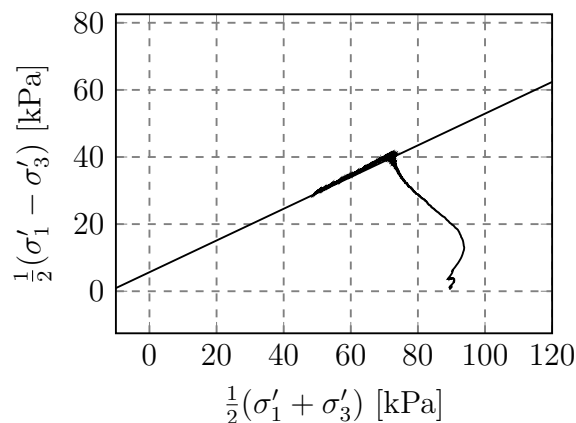
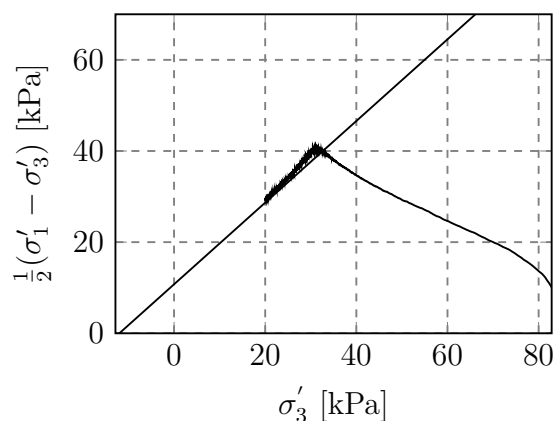
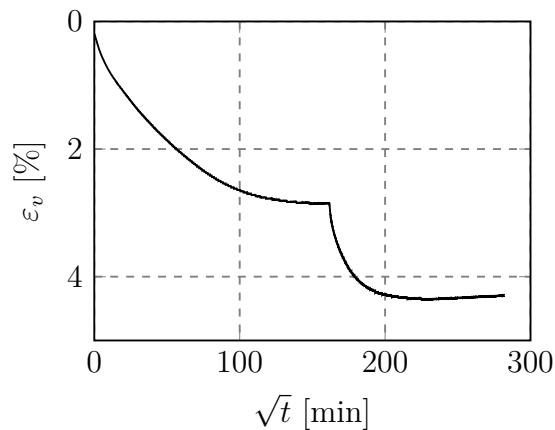


Figure I.22: Presentation of CIUc-results from depth 10.26 m.

KPG-CIUc-1142
Flotten, Trondheim
54 mm sample

Depth	11.42 m
Sampling date	26.04.17
Opening date	01.05.17
Testing date	01.05.17
Vertical strain rate	1.2 %/hr
σ'_{v0}	86.0 kPa
w	33.8 %
γ	17.2 kN/m ³
u	94.2 kPa
ΔV	8.95 cm ³
ϵ_{vol}	3.9 %
Operator	KPG

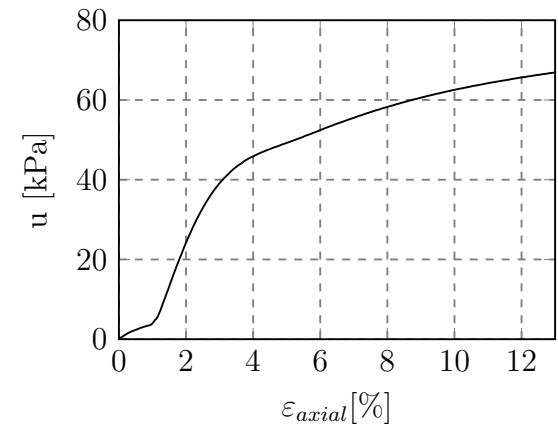
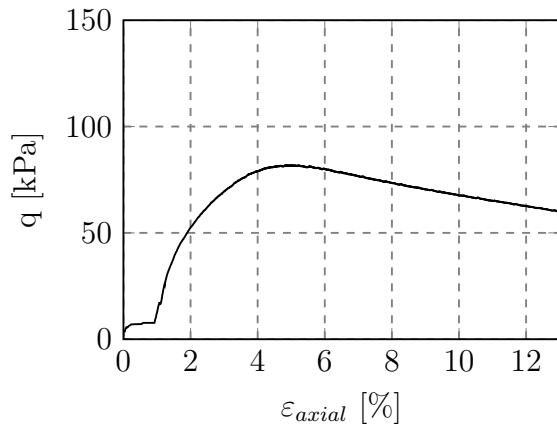
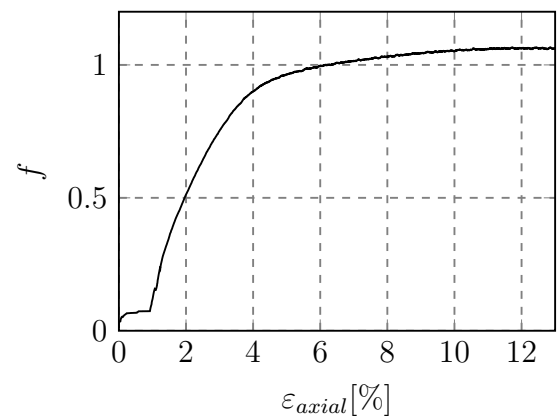
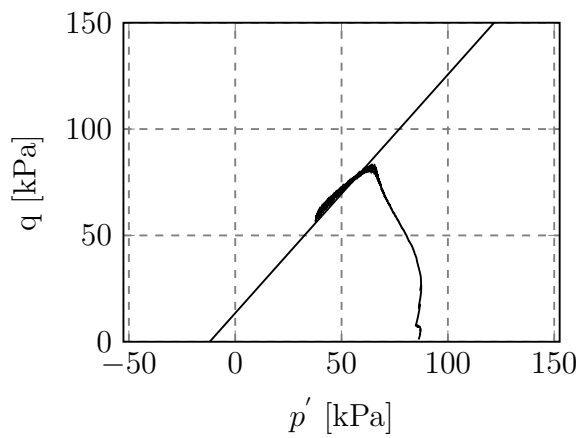
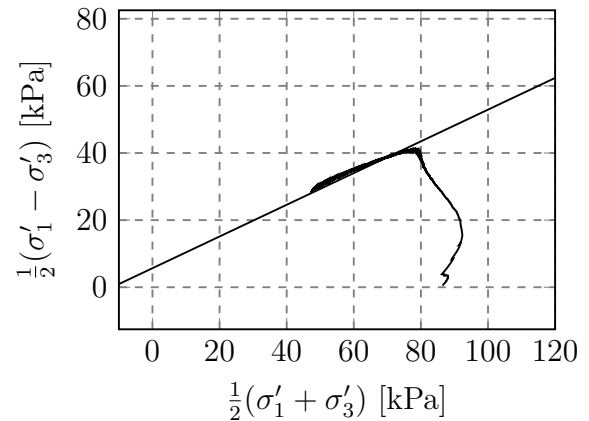
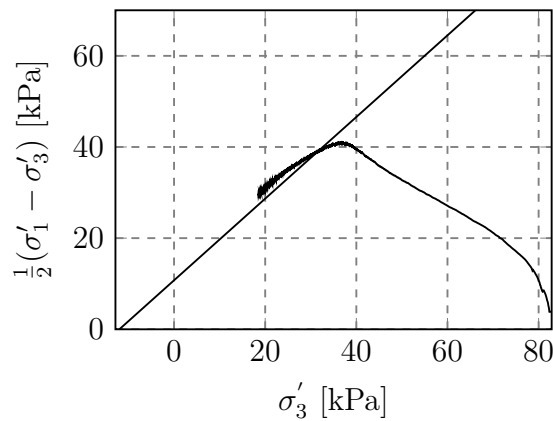
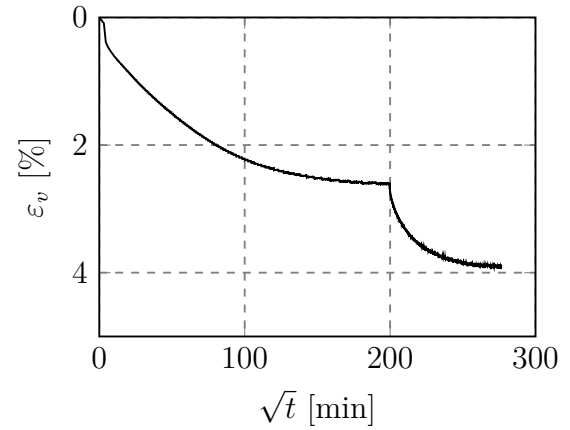


Figure I.23: Presentation of CIUc-results from depth 11.42 m.

Appendix J

Oedotriaxial Test

This appendix contains the test results from the first oedotriaxial test. The specimen tested was retrieved from the borehole 54MM_K0, see Appendix A.

Similar to the oedometer and triaxial appendix, key information regarding the test is given in the table above the group of plots. First, the depth; sampling, opening and testing dates as well as the water content of the test specimen are presented. The water content presented for the test was determined based on adjacent clay when trimming the test specimen. The value of γ presented was estimated based on the weight and approximate volume of the test specimen.

Oedotriaxial test
Flotten, Trondheim
54 mm sample

Depth	9.2 m
Sampling date	23.02.17
Opening date	01.03.17
Testing date	02.03.17
Vertical strain rate	-
w	48 %
γ	18.1 kN/m ³
K'_0	-
ΔV	-
ε_v	-
Operator	AnL & CSO

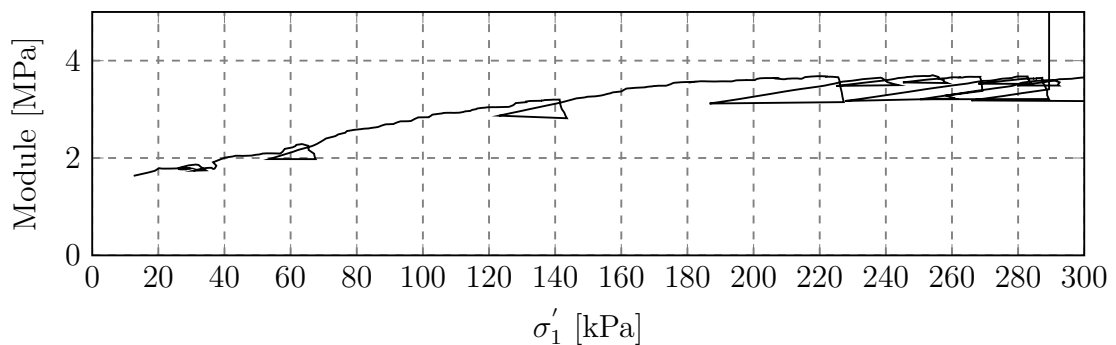
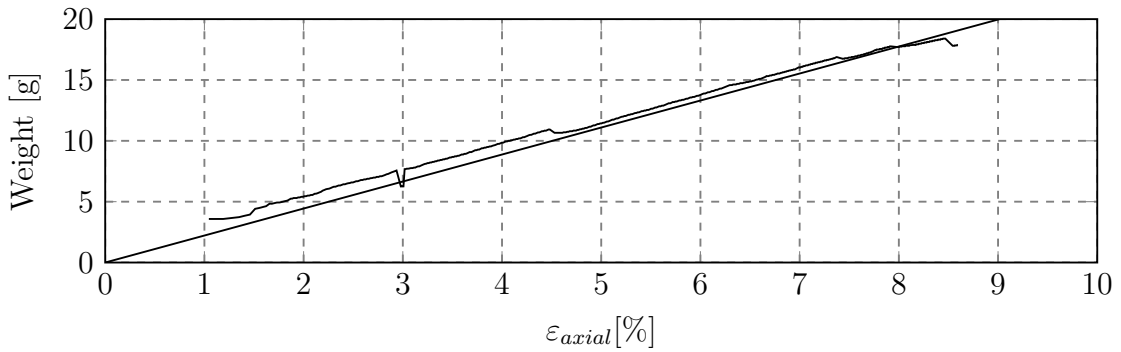
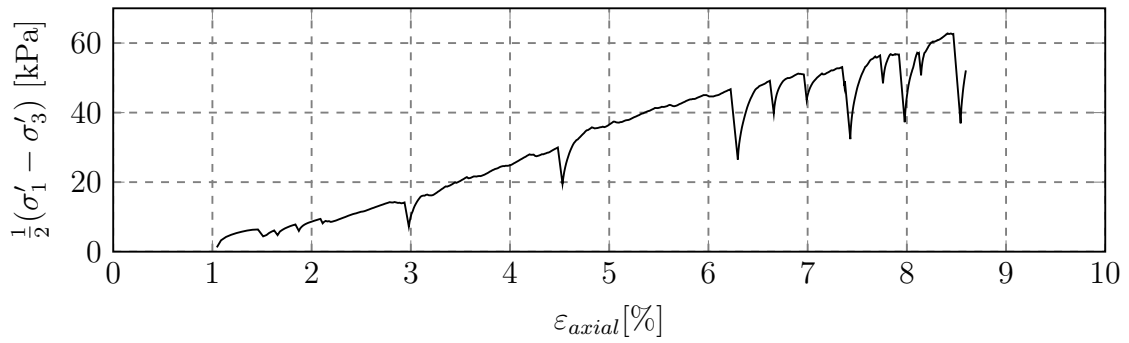
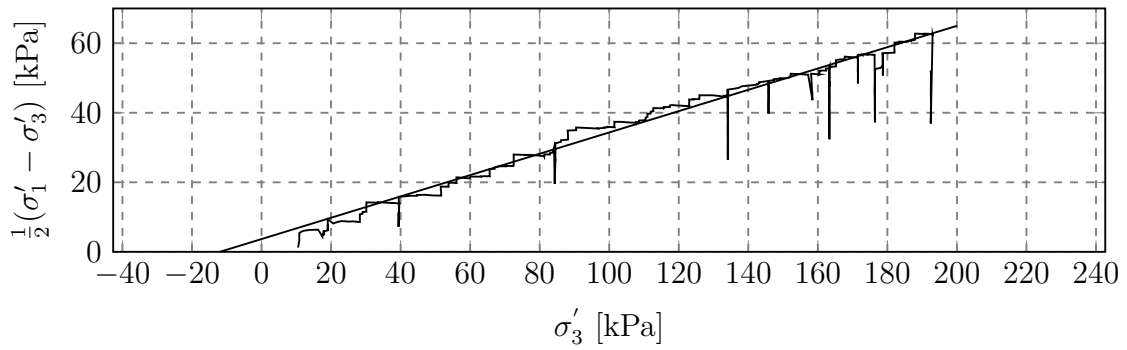
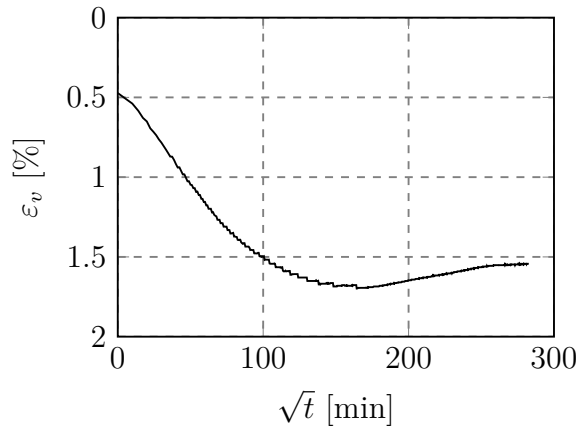


Figure J.1: Presentation of oedotriaxial results from depth 9.2 m.